INELASTIC NEUTRON SCATTERING BY ADSORBED MOLECULES AND CATALYSTS.

P. H. GAMLEN
St Johns College
Oxford

Hilary 1978



INDEX

ABSTRACT

CHAPTER 1 - INTRODUCTION

1.1 - Directions in Surface Science
1.2 - Applications of Neutron Scattering to Surface Studies
1.3 - Previous work employing Neutron Scattering Techniques
1.4 - Intention of this work

CHAPTER 2 - THE EFFECTS OF SURFACE POTENTIAL PERIODICITY

2.1 - Introduction
2.2 - Previous experimental observations on surface potential periodicity
2.3 - Previous calculations
2.4 - The HOPSCOTCH calculation
2.5 - Conclusions

CHAPTER 3 - INTRODUCTION TO THE PRINCIPLES OF NEUTRON SCATTERING THEORY

3.1 - The Scattering Cross Section
3.2 - Correlation functions and neutron scattering
3.3 - Scattering Laws for simple systems
3.4 - The total Scattering Law
3.5 - Experimental measurement of $S^{INC}(\kappa,w)$ by neutron scattering
3.6 - Scattering Laws for Adsorbed Molecules
3.7 - Application of the method to diffusion on surfaces
3.8 - Scattering Laws for possible admolecule dynamics
3.9 - Quantitative treatments
3.10 - The Importance of Quasi elastic scattering
3.11 - Summary
3.12 - Simulation of the scattering laws for adsorbed molecules by the ORIANA and ORJUMP programs

CHAPTER 4 - EXPERIMENTAL

4.1 - Instrumentation
4.2 - Data Handling
4.3 - Preparation and containment of samples
4.4 - Recommendations for future experimental designs
4.5 - Sample preparation for the neutron experiment
4.6 - Determination of surface concentrations by neutron transmission measurements

CHAPTER 5 - ADSORPTION ON GRAPHON

5.1 - Graphon
5.2 - Adsorbed methane
5.3 - Adsorbed ethylene
5.4 - Adsorbed ammonia

CHAPTER 6 - ABSORPTION ON LA-Y ZEOLITE

6.1 - Molecular sieves as absorbents
6.2 - Neutron scattering from La-Y
6.3 - Absorption of methane on La-Y

CHAPTER 7 - INELASTIC NEUTRON SCATTERING FROM SIMPLE MOLECULES ABSORBED ON CATALYST SURFACES

7.1 - Introduction
7.2 - The Sorption of Formic Acid on La-Y zeolite and on γ-alumina
7.3 - The Sorption of CH_2Cl_2 and CH_3CN on La-Y zeolite
7.4 - The Sorption of hydrogen and methane on La-Y zeolite
7.5 - Summary

REFERENCES

ABSTRACT

ACKNOWLEDGEMENTS

Abstract

The possibilities of applying cold neutron scattering to the study of sorbed molecules are discussed. Atom-atom pair calculations have been carried out for the interaction of methane and hydrogen molecules with the basal plane of graphite and the results used as a guide to the best scattering law for the sorbed molecule dynamics. As the sorbents used are powders, a method of averaging the two dimensional scattering law over three dimensions has been developed.

Neutron time of flight spectra were obtained for methane, ethylene and ammonia adsorbed on Graphon. For the surface coverages studied, 0.6-0.2, methane appears to change from a two dimensional Fickian liquid, to an unidentified phase at the lower surface coverage. The data for ethylene at around one monolayer approaches the two dimensional liquid model, but at higher surface coverages there are significant deviations.

Whilst methane and ethylene appear to wet the Graphon surface, ammonia does not seem to do so. The spectra for ammonia show a liquid phase characterised by a diffusion coefficient and activation energy for diffusion, 2.4 kcals/mole, close to those measured for bulk ammonia. A solid phase is observed at lower temperatures.

Neutron time of flight spectra were obtained for methane absorbed in a lanthanum exchanged Y type zeolite. The spectra show that the methane has lost translational motion but retained rotational freedom. A vibration frequency of 19±1 cm^{-1} is observed and this is ascribed to a vibration of the methane molecule within the cavity.

The sorption of simple molecules on catalytically active surfaces was investigated by beryllium filter spectroscopy. A range of interactions was discovered, varying from the gas like sorption of hydrogen and methane on La-Y, to the dissociative sorption of formic acid on γ alumina. Intermediate behaviour was observed when dichloro-methane and acetonitrile were sorbed on La-Y.

LIST OF SYMBOLS

A_{ij}	Constant of Inductive attraction for interactions between the ith & jth atoms
A1, A2, A3	Scaling factors in the calculation of scattered neutron intensity
B	Rotational constant
B_{ij}	Constant of short range repulsive forces between the ith and jth atoms
BEF	Beryllium Filter Spectrometer
b_i	Neutron scattering length for the ith nucleus
$^nC_{ij}$	Attractive dispersion force constants for interactions between the ith & jth atoms
D	Hydrodynamic diffusion coefficient
D_{2D}	Two dimensional hydrodynamic diffusion coefficient
D_r	Rotational diffusion coefficient
E_A	Activation energy for diffusion
$\Delta E_{jj'}$	Energy of the transition between rotational energy levels J and J´
FWHM	Full Width at Half Maximum
$G^{CL}(r,t)$	Distinct correlation function for the system in the classical limit
$G_S^{CL}(r,t)$	Self correlation function for the system in the classical limit
$G_S^{\phi}(r,t)$	The self correlation function for a 2D system inclined at an arbitrary angle ϕ to κ, the momentum transfer vector
$G(\Omega,\Omega_o, t-t')$	Rotational correlation function
I_o, I	Incident and scattered neutron intensity
$I_n(y)$	Modified or hyperbolic Bersel function of order n
$I_S(\kappa,t)$	The Intermediate Scattering function
$j_n^2(x)$	Spherical Bessel function or order n

K	Bond force constant
k_o, k	Initial and final neutron wave vectors
M	Multiple scattering scaling parameter
$P_J(T)$	Boltzmann population factor at temperature T^0K
$P(\kappa)$	The single particle neutron interference function
Q_{ADS}	Differential heat of adsorption at zero surface coverage
QEP	Quasielastic Peak
Q(X-Y)	Length increment of X-Y bond
q(X-H)	Length increment of X-H bond
R_o	Radius of gyration
r_e	Equilibrium separation of admolecule and adsorbent
r_{ij}	The separation of the ith & jth atoms
$S(\alpha,\beta)$	Reduced scattering law

$$\alpha = \frac{\hbar^2\kappa^2}{2mk_BT} \qquad \beta = \frac{\hbar\omega}{k_BT}$$

$S_{COH}(\kappa,\omega)$ $S_{INC}(\kappa,\omega)$	Coherent and incoherent scattering laws for the system
$S^{\phi}_{TRANS}(\kappa,\omega)$	The translational scattering law for a 2D system inclined at an arbitrary angle ϕ to κ, the momentum transfer vector
TOF	Neutron Time of Flight Spectrometer
$\langle u \rangle$, $\bar{u}$	Root mean square amplitude of vibration
V(t)	Velocity at time t
V(r)	The neutron-nucleus interaction potential, approximated to the Fermi psuedo potential
$\langle \ldots\ldots \rangle_T$	The thermal average of the transition probability

α(HXH)	Increment of HXH bond angle
β	$1/k_B T$ Where k_B is the Boltzmann constant and T the absolute temperature
β(YXH)	Increment of YXH bond angle
γ(XYZ)	Increment of XYZ bond angle
ε_τ	Efficiency of the neutron detector for a neutron with a time of flight τ
θ	Angle through which the neutron has been scattered
θ	Surface coverage
κ	Momentum transfer during a scattering event
λ	Neutron Wavelength
μ	Moment of Inertia
$\phi(z)$	Potential energy at point z above the surface
ρ_{CH}	Angle of rotation of a bond relative to the plane through the other two bonds
σ_i	Scattering cross section for the ith nucleus = $\frac{4\pi b_i^2 M^2}{(M+m)^2}$

Where M = molecular mass and m = neutron mass

τ	Surface residence time or Pressure in torr as appropriat
ν_n	The n th fundamental vibration frequency
χ	Increment of the angle determining the mutal positions of two parts of a molecule
$\omega_{\frac{J}{O}}$	Fundamental frequency of the vibration of the admolecule perpendicular to the adsorbent surface
$\omega(t)$	The width function = $\int_0^t \int_{0^-}^{t_1} dt_1 dt_2 \langle \nu_k(t_2)\nu_k(t_1)\rangle$

CHAPTER 1: INTRODUCTION

1.1. Directions in Surface Science

There are two facets to surface science. They can be broadly described as the complementary studies of interfaces and interfacial phenomena. The former is seeking to characterise the chemical and physical properties of an interface. To describe what happens to bulk properties such as crystal structure and magnetisation at that finite limit and to quantify these changes in terms of the atomic or molecular properties of the entities constituting the bulk matter.

In constrast the study of interfacial phenomena looks at the region formed between two phases in contact (whether of the same or different matter) where the properties of the species in that volume of space differ from bulk properties of the individual phases present. Depending on the phases in contact the interfacial region may extend over a few molecular diameters, as for example in the physisorption of non polar molecules on a solid surface, or possibly over several hundred atomic diameters as in the epitaxial growth of one crystal upon another. Generally the forces in one bulk phase will be stronger than the bulk forces in the second phase with the result that the first phase is less perturbed by the presence of the second phase and can be said to form a surface for the sorption of the second phase. In the sorption of gases onto solid surfaces the perturbation of the solid by the gas molecules is usually extremely small, whereas a fraction of the molecules comprising the gas phase are substantially influenced by the solid. The problem thus simplifies to finding an adequate description of the interface of the gas with the solid. The interface of the solid with the gas can be taken in the majority of cases as unaltered from the interface between the solid and vacuum. The situation can be considerably more complex, if for example the interface to be described is that between

the different solid phases that make up a nonstoichiometric compound such as titanium oxide.

This Thesis is concerned with interfacial phenomena and in particular with the sorption of gases on solids;how the molecular properties of a sorbate can be modified by the periodic potential of a sorbent and the closeness of other sorbate molecules; together with the consequences of these changes on the properties of the interfacial region formed between the gas and the solid. Because the perturbation of the solid by the gas is small the interfacial region is regarded as being only the sorbed layer of gas molecules. The solid surface is nonetheless critical in determining the properties of the sorbed layer through the balance of sorbent-sorbate and sorbate-sorbate interactions, and the geometrical requirements of the surface and the gas molecule.

It is an area of science that has seen a notable growth in knowledge during recent years. In part the growth can be attributed to the development and application to the problem of a wide range of physical techniques(1). Particularly physical techniques that probe at the molecular level and so avoid the ambiguities that can result from studying macroscopic properties such as pressure and heat changes (2). The surface specificity and high sensitivity of the particle scattering methods, Ultra violet (1e) and X-ray Photoelectron Spectroscopy (1f), Auger Electron Spectroscopy (1g), Secondary Ion Mass Spectrometry (1h) and Low Energy Electron Diffraction (1i), have enabled the identification of sorbed species (3), studies of the bonding between the sorbate and the sorbent (4), determination of the spatial arrangement of sorbate atoms with respect to the sorbent surface atoms (5) and the characterisation of changes in the solid/gas interface (6). The contribution of these techniques has been greatest in the regime of chemisorption where the interaction between

the gas molecules and the solid surface is strong enough to lead to electronic rearrangements in the interfacial region. Very often the information obtained by any one method is not complete in itself but must be taken alongside the results from other methods and other experiments in order to get a full description of the interfacial system. Neutron scattering is similarly a physical technique sensitive to the microscopic rather than the macroscopic It offers the possibility of studying new sorption systems and providing new information on those previously studied.

There is considerable interest in studying sorbed molecules from the point of view of any changes brought about by the reduction in dimensionality that occurs on going from a bulk phase to an essentially two dimensional surface layer (7). The question raised is whether a two dimensional system can maintain order over macroscopic distances. For example crystal structure is positional order, magnetism is long range spin order and superconductivity is ordered momentum states. Calculations have suggested that a two dimensional system can only have long range order at absolute zero (8). The two dimensional vibrational and rotational density of states has a greater number of low frequency modes than the corresponding three dimensional density of states. At temperatures above absolute zero these low frequency states are populated and the resulting vibrations destroy any long range order in the system. The mono-molecular sorbed layer is the closest approach possible to a two dimensional system on which to test the theories. Ideally the absorbent should have a homogeneous surface with an adsorption potential that is isotropic and structureless in the plane of the surface and with a sharply defined energy minimum perpendicular to the surface. The recently developed adsorbent 'Grafoil', an exfoliatedgraphite (9) comes close to satisfying these requirements.

Measurement of adsorption isotherms (10) and heat capacities has shown that these pseudo two dimensional systems can show gas and liquid phases and quite often more than one solid phase. Figure 1.1 shows the adsorption isotherms for krypton on exfoliated graphite (10). The similarity to PV isotherms for three dimensional gases is clear, and the existence of corresponding solid liquid and gaseous phases in the two dimensional adlayer is strongly suggested. Diffraction measurements have given further evidence for the long range positional order in the sorbed layer (11). As far as testing theories of two dimensional systems go the inference must be that the graphite/krypton adsorption potential is sufficiently periodic across the carbon basal plane to impose order on the krypton adlayer and so remove the true two dimensionality. Nonetheless the occurrence of these adlayer phases and the parameters which control their formation and properties are of great relevance to the description of the interface and interfacial phenomena. It is a topic which the work described in this thesis has taken up and explored using the technique of cold neutron scattering.

FIGURE 1,1

A TWO DIMENSIONAL PHASE DIAGRAM

Isotherms for Krypton adsorbed on exfoliated graphite (10)

(i) 77,3 to (ii) 90,9 °K

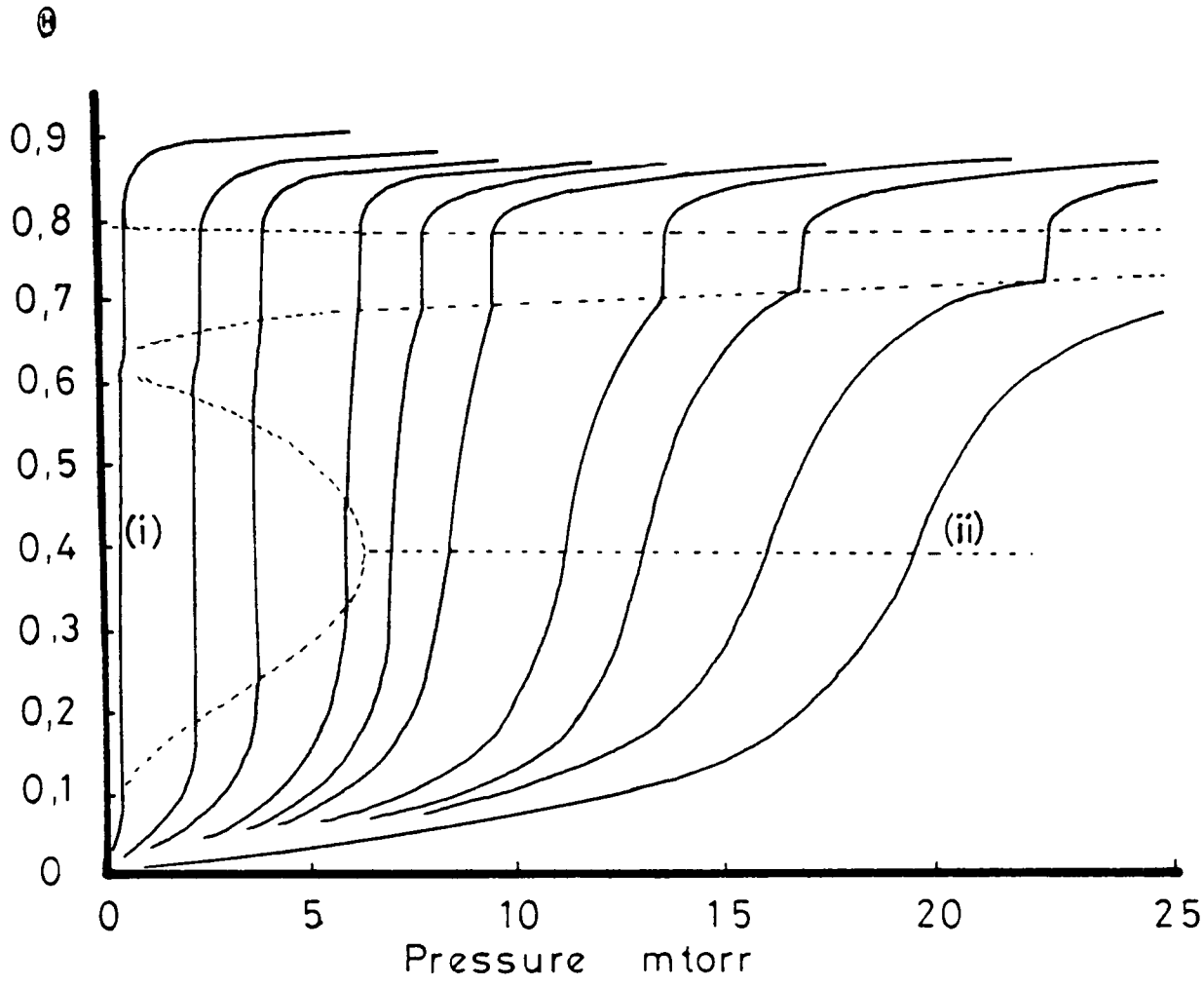

Isotherms for CO_2 near the critical point

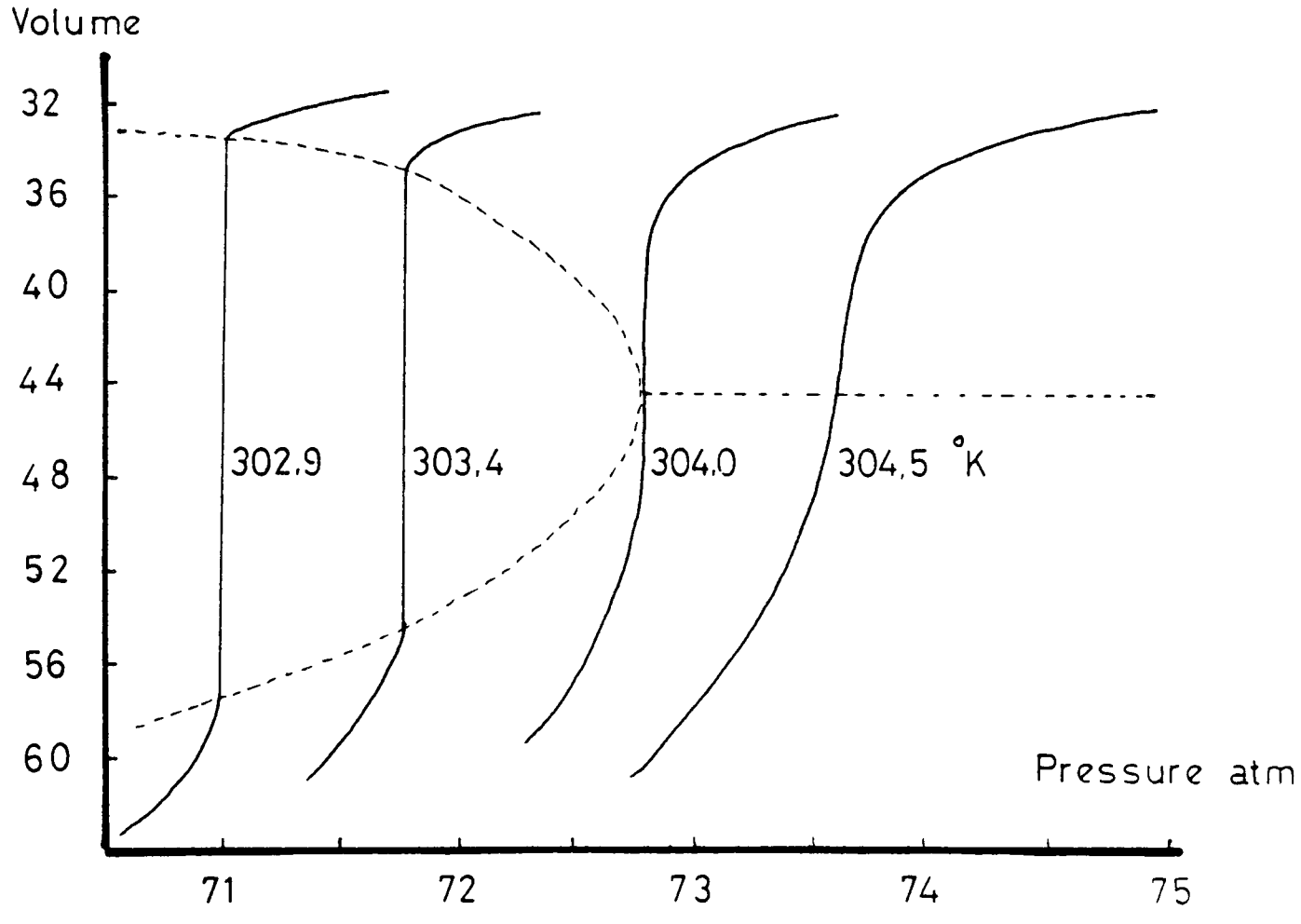

1.2 Application of Neutron Scattering to Surface Studies

1.2.1. The Advantages and limitations of the neutron method

The interaction of neutrons with matter is weak, and as a consequence the method is not intrinsically a surface probe. This is indirect contrast to other particle scattering methods where the interaction is very strong e.g. XPS, Auger or SIMS. The difficulty can be overcome to some extent by use of the cross section weighting in the scattering law expression. By choosing an adsorbent of low cross section and adsorbing molecules with very high scattering cross sections the observed scattered neutron spectrum will be dominated by the scattering from the molecules at the surface.

From a chosen neutron experiment the information obtained falls into three general categories:-

1) Coherent Inelastic and Elastic cross sections reflect the structure and dynamical properties of condensed phases (12)

2) Incoherent Inelastic scattering characterises the density of states for the system and is in many ways similar to conventional optical spectroscopy. (13)

3) Incoherent quasi elastic scattering gives information on the intermediate time scale process of diffusive motion (14)

So when applied to studying surface species one might anticipate that the neutron method would be

1) complementary to LEED and ARPS in investigating the structure of the condensed adsorbate phase (15)

2) Complementary to IR, Raman and UV spectroscopy in identifying species on the surface (16)

3) Able to extend NMR relaxtion measurements of mass transport on the surface to shorter observation times (17)

The information that the neutron method should be capable of uniquely accessing is

4) The vibrations of the adsorbed molecule with respect to the surface atoms, and, if the adsorbate is very strongly bound to the adsorbent, then also the vibrations of the admolecule-surface atom cluster with respect to the bulk material. There is no strong coupling mechanism whereby such a vibration could give intensity in the optical spectrum

5) The adsorbate-adsorbate forces through the measurement of the lattice dynamics of the condensed adsorbate phase. The large, controllable momentum transfer available in a neutron scattering event makes measurement of dispersion relations over the complete Brillouin zone possible.

6) The microscopic nature of the surface diffusion. The characteristic time scale of observation with neutrons (10^{-13}- 10^{-8} s), is much shorter than NMR (10^{-9}- 10^{-6} s), and so jump, rotational and translational diffusion should be readily untangled. The pressure drop methods (18) conventionally used to give surface diffusion coefficients are macroscopic measurements and very sensitive to the physical make up of the sample, and intrinsically unable to provide such detailed insight.

The neutron method has other advantages for surface work. Because of the non-electromagnetic origin of the neutron selection rules (19) one can investigate both physisorbed and chemisorbed molecules. Optical spectroscopy methods in attempting to improve signal to noise ratios, generally study molecules with marked polar characters e.g. CO, NO, Amines. This has the result that there is now a permanent dipole-induced dipole contribution to the total interaction energy and the molecule is strongly bound to the surface. As a result of the choice of probe molecule for maximum signal, the observation is thus limited to chemisorbed systems.

The energy of the incident neutron is low, typically 4 meV. There is no damage to the surface or break up of the adsorbed layer.

This is a problem with most other particle beam techniques, e.g. LEED and SIMS. Since the interaction of neutrons with matter is weak it is not necessary to have the high vacuum conditions needed for electron beams and the system can be studied by netron beams with high vapour pressures of adsorbates present, e.g. several atmospheres. Equally sample changers operating at temperatures from 1°K to 1500°K can be used routinely.

As mentioned above the neutron method observes molecular motion on the microscopic level and so is not affected by surface defects and grain boundaries which often render tracer and pressure drop measurements of surface diffusion unreproducible.

Naturally enough there are limitations to the use of neutrons for surface studies.

1) Because the neutron interaction is weak, the technique is inherently insensitive. One has got round this to some extent by using moderate surface area adsorbents and high scattering adsorbates. However it is unlikely that the method will ever be extended to measurements on single crystal surfaces, simply on a concentration of adsorbate argument. A single crystal has generally 10^{15} sites cm^{-2}. The powdered adsorbents used in this work have between 10^{20} and 10^{21} sites cm^{-2}. It also means that if the surface is heterogeneous one will only obtain an average picture. This problem could be overcome to some extent if the surface area is large and the distribution of adsorption sites is not continuous but widely separated in energy. Then selective dosing of the surface with low scattering deuterium or perfluoro analogues would enable one to study a narrower range of sites when the hydrogenous probe adsorbate is admitted.

Another consequence of the insensitivity and the need to make use of cross section weighting is that one has no information on the states of the adsorbent surface atoms. With techniques that are intrinsically surface probes one has a double handle on the adsorption

process, e.g. with UPS one can monitor changes in the adsorbent surface electronic states alongside changes in the adsorbate molecular orbital energies (20). If there is any neutron scattering from the adsorbent then it will be dominated by the bulk properties of the material and surface effects will be minimal unless the adsorbent is extremely finely divided (21).

2) There is still a large lag between the real behaviour of the systems being investigated by neutron scattering and the degree of sophistication of the theoretical models available to describe the systems. Only for simple systems (22) can an exact calculation of the scattering law be performed. Complicating factors likely to arise when one considers modelling adsorbed molecules are:-

a) Coupling of translational and rotational motion. Generally separability is assumed in order that the total correlation function can be written as a product of functions for the translational and the rotational processes.

b) The marked anharmonicity of the adsorption potential.

c) The effects of quantum mechancial tunnelling between surface sites and between different orientations with respect to the surface.

d) The contribution of the vibrations of the adsorbent surface atoms to the motion of the adsorbed molecule.

It is evident that neutron scattering has a contribution to make in the field of surface science but as is always the case with any technique it should not be used in isolation and the systems to which it is applied should be chosen with care.

1.3 Previous work employing Neutron Scattering Techniques

1.3.1. Structure and dynamics of adsorbed phases

The advent of grafoil (9a), a carbon adsorbent with high surface area and preferred orientation of the basal plane has opened the way for coherent scattering studies. The presence of the preferred orientation means that the sample can be oriented with the momentum transfer vector parallel to the c direction of the adsorbent, and the normally strong coherent effects due to the structure and dynamics of the carbon lattice in this direction are absent.

Studies are being made of N_2 (23), Ar^{36} (24), and D_2 (25) adsorbed on grafoil. Characteristic two dimensional diffraction patterns have been observed from the adsorbed layers in all cases. Nitrogen appears to show two solid phases. At just below monolayer coverage in registry with the surface - at just above the monolayer compressed out of registry, though there is some dispute that the changes in the diffraction pattern observed, could also be explained by a tilting of the molecules in the first layer (26), rather than a change in number density. A liquid phase is observed at higher temperatures. Following the diffraction pattern as a function of surface coverage and temperature has led to a determination of the two dimensional phase diagram for adsorbed nitrogen.

In contrast adsorbed ^{36}Ar shows only one solid phase, out of registry with the surface, and a liquid phase. Deuterium has only one solid phase, in registry, and no liquid phase within the range of temperatures and surface coverages so far studied.

In the case of adsorbed ^{36}Ar it has proved possible to see coherent inelastic excitations and so measure the phonon dispersion curves for this two dimensional solid. The results for the phonon eigen vectors and eigen frequencies are in good agreement with those calculated from a nearest neighbour Born Von-Karman analysis of a

triangular lattice. A Leonard Jones (6-12) potential is used to describe the Argon-Argon interactions and it is found that the substrate interaction can be neglected, at least for the in plane modes, at high surface coverages and low temperatures.

1.3.2 Spectroscopy of adsorbed species

M Nielsen et al (27) have observed the J=0-1 rotational transition of molecular hydrogen adsorbed on grafoil. The transition is not split by the Stark effect as might be expected if there is a strong electric field gradient at the carbon surface. The transition disappears at 40°K when it is thought that a solid to gas transition takes place on the surface, and the translational motion broadens the peak so much as to make it undetectable. There is no evidence for transitions due to vibrations of the adsorbed H_2 with respect to the surface. The reason for this is not clear.

Stockmeyer et al (28) have studied the vibrations of hydrogen chemisorbed on Raney Nickel. They find that dissociative adsorption takes place and that the hydrogen atom is bound to only one nickel atom. This is shown by the inelastic scattering which strongly reflects the lattice frequencies of bulk nickel. Vibrations of adsorbed hydrogen atoms with respect to the nickel atom are also evident and their preliminary data suggested that there could be two different adsorption sites. Further experiments on a high performance instrument, IN1(BE) at ILL, (29), have confirmed this observation and also picked up the second harmonics of the vibrations.

The work of J. White and coworkers (30), and C.J. Wright (31) has been with adsorbent-adsorbate systems in the intermediate binding energy range, 10-40 kcals/mole. J. White (30) and R. Anderson (32) have looked at the vibrations of small molecules such as methanol, ammonia and water in Y type zeolites. They find that the lattice modes of the zeolite appear to be emphasised, suggesting once again that the adsorbed molecule is quite strongly bound to the surface. C.J. Wright

has looked at the specific interaction of ethylene and acetylene with silver cations in Y type zeolites. The spectra can be interpreted in terms of hindered rotations of the adsorbed π systems at the cation, and the potential well for this motion evaluated.

1.3.3. Diffusive motions of adsorbates

Stockmeyer's experimental set-up (28) for the Raney Nickel experiments enabled the observation of quasi elastic as well as inelastic scattering. They were unable to observe any broadening of the former feature and conclude, not surprisingly, that the diffusion coefficient of the hydrogen atoms on the surface must be less than 5×10^{-7} cm^2 sec^{-1}.

Anderson (32) studied the diffusion of water in molecular sieves. He showed how mobility increased as the pore filling increased, the adsorbate apparently changing from surface bound at low coverages and restricted to the interior of pores, to pockets of bulk liquid free to move between cavities at high surface coverages.

The work of Todireanu (33) and Verdan (34) must be regarded with caution in view of the limitations of their neutron scattering apparatus; the poorly characterised nature of the activated charcoal used as an adsorbent in both cases and the crudeness of the model chosen to interpret the observations.

It seems likely that a transition from a gas-like to a liquid-like phase was found for acetylene adsorbed on carbon, and possibly for ethylene. Hydrogen and methane were considered to be gas like on the surface down to the lower limit of measurements at $78^{o}K$.

1.4 Intention of this work

The experiments reported in this thesis are primarily concerned with incoherent scattering measurements, that is the study of diffusive motions, and the vibrational and rotational densities of states of adsorbed molecules.

A summary of the experiments that will be discussed is given in Table 1.1.

The choice of adsorbent-adsorbate systems was made with several points in mind.

A) From the neutron scattering point of view:-

1) Adsorbents should have low cross sections and so be as transparent to the neutrons as possible.

2) Adsorbent surface areas should be as high as possible whilst still retaining energetic homogeneity.

3) Adsorbates should have as high a cross section as possible so as to increase the "spot lighting" effect. This means almost exclusively hydrogenous materials.

4) Adsorbate molecules should be fairly small and symmetric in order to simplify the calculation and interpretation of the scattered neutron spectra.

B) From the surface chemistry point of view:-

1) The zeolites and carbons are two extremes of adsorbent. The carbons have planar, homogeneous surfaces with generally small adsorption potential energies. Zeolites on the other hand are curved, porous surfaces with appreciable, specific energies of interaction. In some cases there is the possibility of chemical reaction between adsorbate and adsorbent.

2) The adsorbates show a gradation of strength, and types of intermolecular interactions in their condensed phases. The importance of lateral interactions may then be studied by an evaluation of the adsorbate dynamics and phase transitions as a function of temperature and coverage.

3) All these systems have been studied by conventional techniques such as isotherm and calorimetric methods, and quite often magnetic resonance studies. This means that the systems are well characterised and this information can be used to optimise the neutron scattering experiment e.g. to select critical surface coverage and temperature regimes for study.

Table 1.1

Summary of Experiments Performed

ADSORBENT	ADSORBATE	SURFACE COVERAGE	TEMPERATURE °K	EXPERIMENT
Graphon	-	-	298	TOF/CES/INS
Graphon	Methane	0.58	115	TOF
		0.52	127	
		0.43	140	
		0.42	148	
		0.30	162	
		0.23	176	
Graphon	Ethylene	2.10	175	TOF
		1.80	185	
		1.30	195	
		1.10	204	
		1.00	215	
		0.80	235	
Graphon	Ammonia	1.05	145	TOF
		1.02	155	
		1.08	168	
		1.19	176	
		1.21	186	
		1.72	199	
		1.82	223	
		1.00	242	
		0.70	249	
		0.65	254	
		0.27	261	
		NUMBER OF MOLECULES PER CAVITY		
La-Y	-		298	TOF/CES/INS
La-Y	Methane	1.40	160	TOF
		1.32	190	
		1.11	213	
		0.58	245	
		0.25	295	

Table 1.1 continued

La-Y	Methane	≃ 4-8	80	INS
	Methane	≃ 0.5-1	298	INS
La-Y	Hydrogen	≃ 5-10	80	INS
		<< 1	298	INS
La-Y	Dichloromethane	≃ 19	80	INS
La-Y	Methylcyanide	≃ 15	80	INS
		≃ 5	298	INS
La-Y	Formic Acid	≃ 20	80	INS
γ-AL_2O_3	Formic Acid	θ=2.0	80	INS

Experiment - TOF Time of flight spectrum

- CES Coherent Elastic scattering study

- INS Inelastic neutron scattering study

CHAPTER 2

The effect of surface potential periodicity on adsorption energies and adsorbate dynamics

2.1 Introduction

When a gas is in equilibrium with a solid there are forces between gas atoms and the surface atoms of the solid.

The interaction is more favourable than for the interaction between the gas atoms themselves, at that pressure, and this leads to a localisation of a fraction of the gas phase atoms at the surface of the solid. This is the phenomenon of adsorption. The value of this fraction and its variation as a function of the pressure and temperature of the system, together with the equilibrium position that the adsorbed molecule takes up with respect to the surface are a consequence of the strength of this interaction relative to the thermal energy.

Two extremes can be envisaged

1) The interaction is very strong and a chemical bond is formed between adsorbate and adsorbent atoms. This leads to an electronic rearrangement and implies a definite orientation of the adsorbate molecule with respect to the surface atoms.

2) The interaction is weak and the perturbation of the adsorbate electronic configuration is slight. The separation of the adsorbate and the surface plane is larger than the case above and the adsorbate may have no preferred orientation with respect to the surface atoms.

The second case is referred to as physisorption and is regarded as a necessary precursor to case 1), chemisorption (35).

It is the aim of this thesis to provide information on

adsorbate dynamics using cold neutron spectroscopy. The direct analysis of an observed scattered neutron spectrum is difficult. The usual starting point in an interpretation is to make an estimate or model for the potential energy surfaces in which the scattering centre is moving. A solution to the equations of motion on the model energy surface is found and the expected neutron spectrum constructed for comparison with the observed data.

The forces between the adsorbent and adsorbate are various and depend upon the electronic configurations of the constituents. There will be strong, specific interactions, such as electron exchange, electrostatic forces, dipolar and higher multipole interactions. Here the influence of the surface periodicity is very evident. The nature of such an interaction is also highly dependent on the adsorbate/adsorbent system chosen. The weaker forces of physisorption originate in London dispersion forces (36), and the quantifying parameters should be transferrable between similar adsorbate/adsorbent systems.

Even in the instance of a weak adsorbate - adsorbent interaction the surface will not appear featureless to the adsorbed molecule. The periodicity of the surface atoms can be regarded as imposing energy barriers to the translations and rotations of the adsorbate molecule. The critical feature is the ratio of these barriers to the thermal energy, $(^1/\beta)$, of the adsorbate.

As the barrier to translation increases so one would expect the motion of the adsorbate to progress from

a) Free translation - gas like

to b) Continuous diffusion - liquid like

to c) Jump diffusion

to d) Localised - surface crystallisation

Increasing the barriers to rotation gives rise to a similar sequence, commencing with

a) Free rotation

b) Rotational diffusion

becoming c) Hindered rotation

and eventually

d) No rotational motion other than torsions and librations.

So far the consideration has been of a single molecule interacting with the surface and the barriers are a consequence of the adsorbate - adsorbent interaction alone. As the surface coverage increases so the adsorbate - adsorbate forces become more important, the barriers alter, and the adsorbate dynamics may change significantly. This is when rotational diffusion might become a more appropriate description.

In order to systematise the approach to adsorption phenomena on the basis of possible electronic interactions Kiselev (37) has proposed a general classification scheme for adsorbates and adsorbents. This is given in Table 2.1. The systems investigated in this work are shown in their respective groups.

Table 2.1 Classification of Adsorbents & Adsorbates

A) Adsorbents

Group	Characteristics	Example
1	Non specific, not carrying on their surfaces, active functional groups, or electron donor or acceptor groups	Graphon
2	Specific with concentrated positive charges exposed on the surface	La-Y
3	Specific with concentrated negative charges exposed on the surface	None in this work

B) Adsorbates

Group	Characteristics	Examples
A	Spherically symmetric with only σ bonds	CH_4, H_2
B	Electron density located on the periphery of groups of atoms such as π bonds or lone pairs	C_2H_4, NH_3 CH_2Cl_2
C	Positive charge located on the periphery	None in this work
D	Both positive and negative charges on the periphery	None in this work

(After Avgul and Kiselev (47))

2.2 Previous experimental observations on surface potential periodicity

W. Steele and R. Karl (38) have carried out heat capacity measurements as a function of temperature for the adsorption of neon, argon, xenon and krypton on graphon. They observed anomalies which by analysis of the temperature of the maximum and the shape of the anomaly they consider to arise from passage through a two dimensional critical region. If the adsorbed rare gas atoms are freely translating on the surface then the ratio of the two dimensional to the three dimensional critical temperature should be a constant for the series of gases. This is not the case for neon and they conclude that the surface potential barrier to translation is large enough in this case to prevent free translation. The calculations of A. Myers and J. Prausnitz (39) support this view.

Y. Nardon and Y. Larher (40), used the same adsorbates, but by choosing a series of layer like halides were able to study the effect of varying the adsorbent surface periodicity, and adsorbate - adsorbent interaction. They demonstrated the effect of the surface periodicity both on the translational motion and the structure of the monolayer formed. The structure of the condensed monolayer is a consequence of the balance between the adsorbent - adsorbate and adsorbate - adsorbate forces. Where the barriers to translation and approach of the adsorbed molecules are large, eg. for Kr on $CdCl_2$ and $NiCl_2$, then the structure adopted is an expanded (III) plane of the fcc solid adsorbate. Examples where the adsorbate - adsorbate interactions are dominant and give rise to crystalline clusters even at submonolayer coverages were discovered in a LEED investigation of physisorption by J. Lander and J. Morrison (5).

The importance of adsorbate mobility and its relation to the periodicity of the surface potential is underlined in the elegant

experiments of M. Bretz and coworkers (86). They have conducted heat capacity and isotherm measurements for ^3He, ^4He and Ne adsorbed on exfoliated graphite. They are able to show that there is a wealth of two dimensional phases possible for adsorbed helium. With increasing surface coverage they observe a progression down the following series of phases:-

1) A lattice gas

to 2) A two dimensional gas

to 3) A two dimensional dense gas or fermi liquid

to 4) A two dimensional liquid

to finally

5) A two dimensional solid phase

The evidence for barriers to rotational motion of an adsorbed molecule is less well characterized. The calculations of A Myers and J. Prausnitz (39) indicate that for small diatomic and spherical top molecules adsorbed on graphon, the loss in rotational entropy on adsorption is of the order of 5%. If the adsorbate is large and nonspherical, e.g. benzene, then the decrease may be as high as 30%. NMR relaxation measurements are potentially very powerful for investigating hindered rotation on surfaces (Id). The experiments of J. Riehl and K. Koch (41) are indicative of a barrier to rotation about an axis parallel to the surface for methane adsorbed on graphon, but free rotation about an axis perpendicular to the surface. Their results and calculations will be discussed in more detail in the next section. J. K. Thompson et al. (42) have used a similar technique for studying the motion of benzene adsorbed on graphite. Their results show that rotation about the six fold axis for the molecule is considerably less hindered than about any other molecular axis.

The adsorption of molecules in molecular sieves, where the

barriers to rotation might be expected to be much larger than for a carbon surface, has received much attention. Experiments are complicated by the heterogeneity of the surface and the presence of paramagnetic impurities. As might be expected water adsorbed on porous supports shows hindered rotation about all axes (43), benzene on silica gel has effectively free rotation about the sixfold axis but no rotation about any other axes (44), and sulphur hexafluoride adsorbed on a synthetic faujasite has complete rotational freedom (45). In contrast to this last observation, an IR study of a similar spherical top molecule, methane, adsorbed on porous glass, by N. Shephard and D. Yates (46a), suggests that the adsorbed methane has lost either two or three rotational degrees of freedom.

Measurements of the second moments of the NMR signals for CH_4 and CF_4 adsorbed on rutile (46) show that there is present one type of CF_4 molecule on the surface with hindered rotation, and most probably a similar circumstance exists for adsorbed methane.

2.3 Previous Calculations

The prime aim of previous calculations has been to determine the energy of interaction between an adsorbate and surface, in terms of fundamental properties such as polarisabilities and magnetic susceptibilities. Generally the calculation is performed for an isolated molecule on the surface and the value of the potential energy so obtained should equate with the experimental heat of adsorption extrapolated to zero surface coverage, with due allowance for the zero point energy. With an expression for the adsorption potential and taking account of adsorbate - adsorbate forces one can derive a partition function for the adsorbate and so predict isotherm forms, heats and entropies of adsorption. The range and applicability of these calculations have been reviewed by N. Avgul and A. Kiselev (47),

S. Ross and J. Oliver (48), M. Dubinin et al (49). Such calculations are only successful for low surface coverages, breaking down when the lateral interactions are very strong and wholly inapplicable to multilayer adsorption. The approaches of B. Ninham (50) and C. Anderson (51), who treat the problem as one of forces between slabs of differing dielectric seem to offer more hope of success in this particular regime.

Because of the complexity of the calculations, assumptions must be made and this leads to a loss of information about the system. Two classes of assumption recur in all calculations.

1) The equilibrium separation of the adsorbate centre of gravity and the centre of gravity of the uppermost adsorbent atoms is not known, but is yet a vital parameter. For example in the Leonard Jones potential used by R. M. Barrer (52) it comes in as Z

$$\phi(\bar{z}) = -C \sum_{ij} \left[\frac{1}{2r_{ij}^{6}} - \frac{\bar{z}^{6}}{r_{ij}^{12}} \right] \qquad (2,1)$$

or in the calculations of Avgul et al (53) when $\bar{z}$ must be fixed in order that the repulsion constant B_i can be determined

$$\phi(\bar{z}) = {}^{1}C_{ij} \sum_{ij} r^{-6}(\bar{z}) - {}^{2}C_{ij} \sum_{ij} r^{-8}(\bar{z})$$

$$- {}^{3}C_{ij} \sum_{ij} r^{-10}(\bar{z}) - A_{ij} \sum_{ij} r^{-6}(\bar{z})$$

$$+ B_i \sum_{ij} \exp\left\{\frac{-r_{ij}}{p_{ij}}\right\} \qquad (2.2)$$

The ${}^{n}C_{ij}$'s are the attractive dispersion force constants for interactions between the i and j atoms. As with A_{ij}, the constant of inductive attraction, these constants are calculable from polarizabilities and magnetic susceptibilities using Kirkwood and Mullers relationship(54).

Since the equilibrium separation, $\bar{z}$, is not known and not readily calculated, it has been usual to assume that its value is given as the sum of half the relevant lattice spacing of the adsorbent, graphite in this instance, and half the intermolecular separation of the bulk solid adsorbate.

2) Usually the shape and structure of the adsorbate is suppressed and the molecule regarded as a sphere, with the polarizability and susceptibility of a hypothetical rare gas atom of a similar radius. In the calculations of Crowell et al (55) and Ninham[50] and Anderson[51], a further assumption is made that the surface itself is a continuous dielectric. As a result the only information available is the adsorption potential energy. If a structured surface is considered then the barriers to translation are accessible but there is no way of estimating rotational energy barriers.

Some of the results of these calculations which are relevant to this work are summarised in Tables 2.2 and 2.5 together with the experimental values.

Recently two calculations have been published (41) (56) whose intention has been to determine these rotational barriers, specifically for the case of CH_4 on graphon. J. Riehl and K. Koch[41] used a potential of the form

$$\phi(\bar{z}) = \sum_{i=I}^{4} A \left\{ \frac{1}{5} \left(\frac{r}{\bar{z}_i} \right)^{10} - \left(\frac{r}{\bar{z}_i} \right)^{4} \right\} \qquad (2.3)$$

The dispersion forces are assumed to be at the centre of each carbon-hydrogen bond in methane. $\bar{z}$ is the separation of the ith bond and the carbon surface. As in previous calculations $\bar{z}$ has to be fixed so that the centre of gravity of the CH_4 molecule is 3.8 Å above the surface, i.e. the sum of half the interlayer spacing of graphite (3.4 Å) and half the intermolecular spacing of bulk solid methane

(4.3 Å). A stable tripod configuration over the centre of a carbon hexagon was assumed to be the most favourable position, and the value of A adjusted to set the value of ϕ (z) equal to the heat of adsorption at zero coverage.

The results of this calculation together with those of Avgul et al (56) are shown in Table 2.2. The poor agreement between these two calculations together with the uncertainty in the assumptions required provided the stimulus for undertaking a calculation with the same objective in mind but using a slightly different approach to the potential.

2.4 The HOPSCOTCH Calculation (57)

A technique of calculation known as the atom-atom pair potential (AAPP) approach has been developed by A. Kitaigorodskii (58), D. Williams (59) and G. Pawley (60), amongst others. It has proved particularly successful for the setting up of force fields in simple molecular crystals.

As its name implies the method regards the total potential energy of the system as the sum of the energies of all atom pairwise interactions. The attractive part of the potential is derived from London dispersion forces and the repulsive part is described by the Born-Mayer exponent. It is known as a Buckingham potential (61).

$$\phi(r) = \sum_{ij} \left\{ - A_{ij}/r_{ij}^{6} + B_{ij} \exp(-C_{ij} r_{ij}) \right\} \qquad (2.4)$$

The parameters A,B and C are obtained from a condensation of thermodynamic, structural and spectroscopic data (59) (62). They should be transferrable parameters but in practice can only be used with confidence amongst the simple hydrocarbon systems (63)(64). The assumptions behind the AAPP approach are as follows

1) That the molecule is rigid. This is only true if the highest lattice frequency is much less than the lowest intermolecular frequency.

2) That the system possesses no kinetic energy. At room temperature root mean square amplitudes, <u>, of thermal vibration are of the order of 0.2 Å.

3) That interactions are pairwise and there are no third body interactions.

4) That there are no special electrostatic effects, e.g. hydrogen bonding, quadrupole moments which will affect the transferability of the parameters.

Such a method of calculation seems to have merit for the determination of the adsorption potential for hydrocarbons. Molecular geometry and surface periodicity are retained and the potential can be determined for continuous variations of:-

1) The height of the adsorbate molecule above the surface. Thus the equilibrium separation can be calculated and does not have to be assumed.

2) The position of the adsorbate molecule centre of gravity with respect to the surface atoms.

3) The orientation of the adsorbate atoms with respect to the surface atoms.

Consequently it should be possible to obtain the heat of adsorption at zero surface coverage, 1), the barriers to translation, 2), and the barriers to rotation, 3). Indeed such a type of calculation has recently been published (65) concerned with the orientation of long chain hydrocarbons on a graphon surface. The results for methane are shown in Table 2.2.

In the HOPSCOTCH calculation the summation was evaluated over

forty carbon atoms representing a graphite surface. Twenty four of these atoms made up the first layer, sixteen the second layer, 3.4 Å below the first. The hexagon side length was taken from the x-ray diffraction data (66) to be 1.42 Å. The coordinate system is shown in Figure 2.1.

The values of the parameters A, B and C were taken from J. Twistleton's (67) work on polyethylene.

carbon-carbon

A_{cc} 568 Kcals mol^{-1} Å^6 B_{cc} 83630 Kcals mol^{-1} C_{cc} 3.60 Å^{-1}

carbon-Hydrogen

A_{CH} 125 Kcals mol^{-1} Å^6 B_{CH} 8766 Kcals mol^{-1} C_{CH} 3.67 Å^{-1}

Calculations were carried out for hydrogen, methane and ethylene adsorbed on graphite. The results are summarised in the Tables and Figures following.

It should be stressed that these calculations of activation barriers via potential energies are for an isolated molecule and do not attempt to allow for perturbations to these barriers that may arise from the following circumstances.

1) Adsorbate-adsorbate interactions. These are generally attractive for simple molecular systems and will tend to increase the barriers.

2) The dynamics of the adsorbent surface atoms. This coupling is not expected to be a problem in physisorption where the strength of the interaction between the adsorbate and adsorbent is very much less than the forces binding an adsorbent surface atom into the bulk material (68).

3) For these light molecules and low energy barriers, quantum mechanical tunnelling could be present. The work of W.Press et al (69) indicates that this is unlikely for the case of

FIGURE 2.1

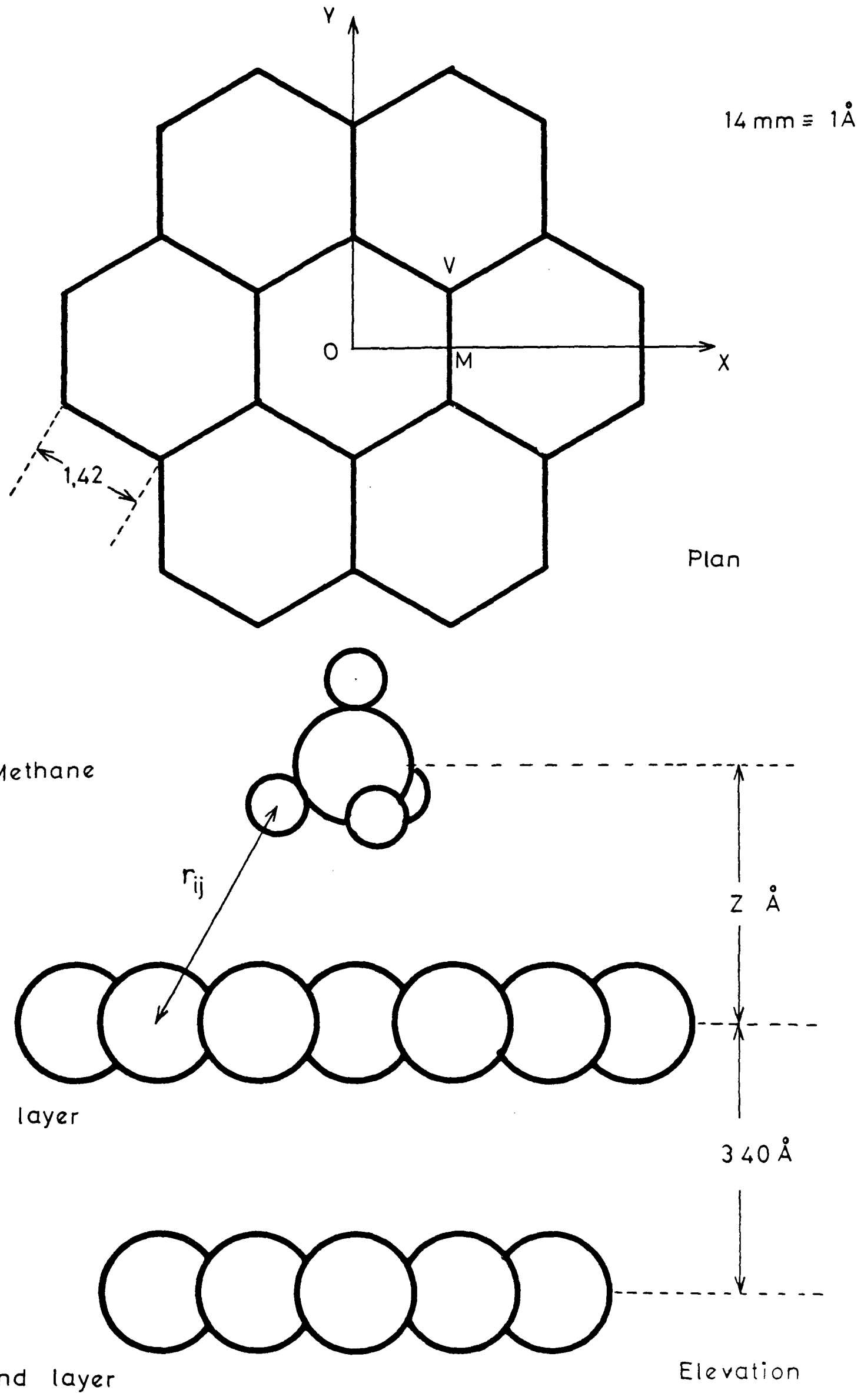
Y
V
O
M
X
1,42
14 mm ≡ 1Å
Plan
Methane
r_{ij}
Z Å
First layer
3 40 Å
Second layer
Elevation

adsorbed methane.

2.5 Conclusions

2.5.1. Methane adsorbed on graphon

The values of the adsorption potential calculated in this fashion are in good agreement with previous calculations and the measured limiting value of the heat of adsorption (neglecting the zero point energy). The surprising feature is the very much shorter surface / adsorbate separation found. The work of M. Lal and D. Spencer (65) also produces a smaller value of $\bar{z}$ than that assumed in the other methods cited above.

Taking the second differential of the potential curve at the equilibrium separation gives the force constant and hence the fundamental vibration frequency for the well.

$$K = \left\{\frac{\partial^2(\phi(r))}{\partial r^2}\right\}_{r = re} \qquad (2.5)$$

$$V = \frac{1}{2\pi}\sqrt{\frac{K}{\mu}} \qquad (2.6)$$

The values calculated by HOPSCOTCH agree well with those predicted by S. Ross and J. Oliver.

	HOPSCOTCH	R ⁄ O
K dynes cm^{-1}	7.39×10^3	6.056×10^3
W_o^1 cm^{-1}	88	80

The values of the barriers determined are smaller than previous work had suggested. The relative values of the barriers are comparable and the good agreement for the total potential gives credibility to the figures produced.

The first six rotational levels of the methane molecule occur at approximately 0, 10, 30, 60, 100 and 150 cm^{-1} ($B \simeq 5 cm^{-1}$)

The barrier to translation is $84 cm^{-1}$, to rotation about an axis parallel to the surface $158 cm^{-1}$ and about

an axis perpendicular to the surface, $85cm^{-1}$.

One can conclude that over the temperature range of the experiments, 180-115 ^{o}K ($kT = 168 - 107cm^{-1}$), the adsorbed methane has free rotation about the $\bar{z}$ axis, nearly free translation and slightly hindered rotation about axes parallel to the surface.

Table 2.2 METHANE

Characterisation of the adsorption potential minimum and comparison with previous calculations

Stable tripod configuration

Energies in kcals mole^{-1}

Most favourable rotational orientation 1

Position of centre of gravity at		O (0,0)	M (1.23,0)	V (1.23,0.71)
1) Equilibrium distance of the molecule from the surface.				
a) Ross and Oliver	(48)	3.78		
b) Avgul et al	(56)	3.78		
c) Crowell and Steele	(55)	3.56		
d) Lal and Spencer	(65)	3.40		
e) Riehl and Koch	(41)	3.80		
HOPSCOTCH				
f) One layer of 24 atoms		3.30	3.30	3.40
g) Two layers, total 40 atoms		3.30	3.30	3.40
2) Minimum potential energy of the adsorbed methane, Kcalsmole^{-1}				
a) Differential heat of adsorption				
(H) = 0	(70)	2.92		
	(71)	3.03		
b) Ross and Oliver		-2.520		
c) Avgul et al		-2.740		
d) Crowell and Steele		-2.560		
e) Lal and Spencer		-3.00		
f) Riehl and Koch		-3.00		

HOPSCOTCH	O (0,0)	M (1.23,0)	V (1.23,0.71)
g) Two layers of 40 atoms			
r_e = 3.30 Å	-2.971	-2.745	-2.717
r_e = 3.60 Å	-2.626		
r_e = 3.80 Å	-2.258		

FIGURE 2,2

METHANE

U_{max} = - 2,971 Kcals/mole

Z_{eqm} = 3,30 Å

Stable tripod

Position 0 (0,0)

Orientation 1

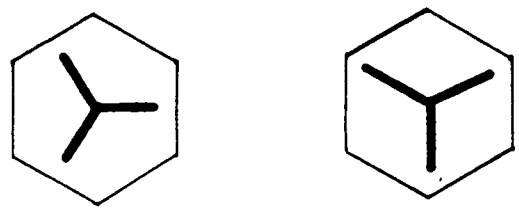

1 2

Table 2.3 METHANE

Contributions to the total potential energy

	O (0,0)	M (1.23,0)	V (1.23,0.71)
1) Contributions to the total potential assuming only the first layer is important			
a) Of the first six surface atoms	-1.162	-0.934	-1.041
% of the total potential	40.9	35.5	39.6
b) Of the first twelve surface atoms	-2.002	-1.699	-1.745
% of the total potential	70.4	64.5	66.3
2) Improvement on considering a second layer of carbon atoms	-0.129	-0.112	-0.086
% of the total potential	4.3	4.1	3.2
3) Contribution to the potential energy at the minimum by			
a) The carbon atom	-1.216	-1.066	-1.132
% of the total potential	42.8	40.5	43.0
b) The uppermost hydrogen	-0.152	-0.146	-0.135
% of the total potential	5.3	5.5	5.1
3) The lower hydrogens	-1.475	-1.4209	-1.364
% of the total potential	51.9	54.0	51.9

Using only one layer of carbon atoms.

Energies in kcals mole^{-1}

Table 2.4 METHANE

Barriers to translation and rotation

1) Translation

Potential at centre of hexagon, position O		-2.971
Potential at midpoint of hexagon side, position M		-2.745
Potential at vertex of hexagon, position V		-2.717
Minimum barrier	226 cals $mole^{-1}$	
Maximum barrier	254 cals $mole^{-1}$	
Average barrier	240 cals $mole^{-1}$	

2) Rotation

Molecule at the centre of the hexagon, position O

	HOPSCOTCH	R ‡ K(41)	AVL(56)
a) Molecule in stable tripod configuration - Orientation 1	-2.971	-4.00	-3.00
- Orientation 2	-2.947		
b) Molecule with an S_4 axis perpendicular to the surface	-2.790	-3.600	-2.750
c) Molecule in unstable tripod configuration	-2.520	-2.500	-2.320
Barrier to rotation between configurations a) and b)	0.180	0.250	0.400
Barrier to rotation about the z axis, a1 to a2	0.024		
Barrier to rotation about the x or y axis, a) to c)	0.450	0.680	1.500

Energies in kcals $mole^{-1}$

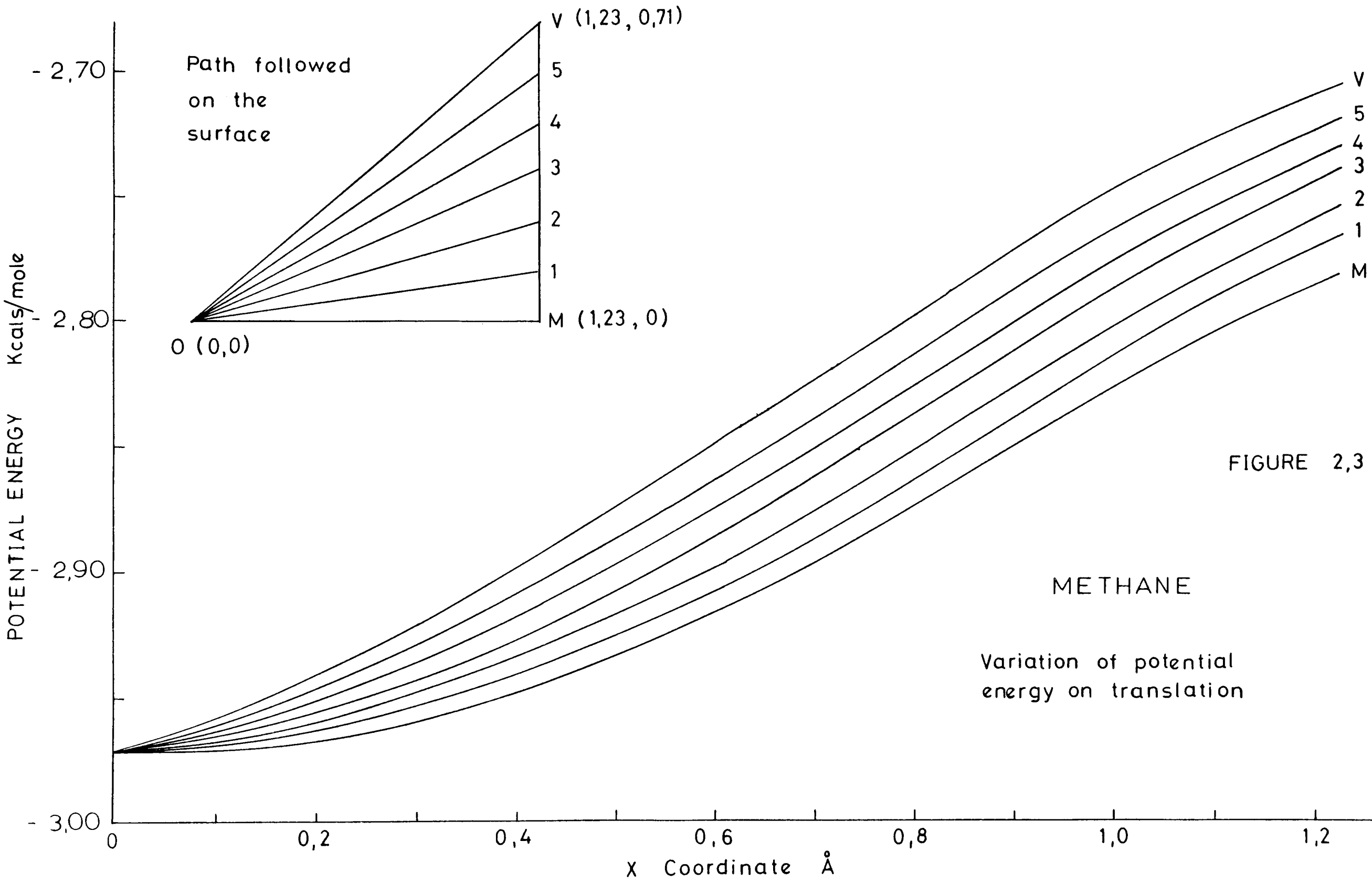
V (1,23 , 0,71)
5
4
3
2
1
M (1,23 , 0)
0 (0,0)
Path followed
on the
surface
V
5
4
3
2
1
M
- 2,70
- 2,80
- 2,90
- 3,00
POTENTIAL ENERGY Kcals/mole
0
0,2
0,4
0,6
0,8
1,0
1,2
X Coordinate Å
METHANE
Variation of potential
energy on translation

FIGURE 2,3

2.5.2 Hydrogen adsorbed on graphon

The agreement between the calculated and measured heat of adsorption is fair. Again the surface-adsorbate separation is found to be smaller than generally assumed. The barrier to translation is close to that calculated by Barrer (52).

The values of the force constant and vibration frequency perpendicular to the surface do not agree well with Ross and Olivers calculation.

	HOPSCOTCH	K ‡ P	R ‡ O
K dynes cm^{-1}	3.17×10^3	3.57×10^3	1.28×10^4
W $\frac{1}{o}$ cm^{-1}	163	173	330

Another unusual feature is that the most favourable position for the hydrogen molecule is not directly over the centre of a carbon hexagon, but displaced off centre by about 0.5 Å. This is due to the small size of the hydrogen molecule relative to the dimensions of the carbon hexagon.

2.5.3 Ethylene adsorbed on graphon

No results are given for this molecule. It proved impossible to calculate a potential energy comparable with the heat of adsorption at zero coverage. The value for ethylene in the centre of the carbon hexagon in orientation 1 was calculated as 7.15 kcals $mole^{-1}$. The observed value is 4.5 kcals $mole^{-1}$. This breakdown of the calculation is believed to arise from the non transferability of the A, B and C parameters to a system with $p\pi$ interactions.

Table 2.5 HYDROGEN

A) Characterisation of the adsorption potential

Position of centre of gravity at:-	O (0,0)	M (1.23,0)	V (1.23,0.71)
Flat configuration, most favourable rotational orientation.			
1) Equilibrium distance of molecule from surface, Å	3.6	3.6	3.6
a) Barrer (52)			
b) Kiselev ‡ Poshkus (160)	2.9	2.9	2.9
HOPSCOTCH			
c) Two layers of 40 atoms	2.9	2.9	2.9
2) Minimum potential energy of the hydrogen molecule			
a) Differential heat of adsorption, Θ = 0, kcals, mole^{-1}			
Barrer (52)	0.90		
Constabaris et al (71)	1.293		
b) Barrer	1.155		0.976
c) Kiselev and Poshkus	1.456		
d) Constabaris et al	0.956		
HOPSCOTCH			
e) Two layers of 40 atoms	-1.111	-1.085	-1.062
Most favourable position (0.5, 0.14)		-1.212	
3) Potential energy of the hydrogen molecule in an upright orientation at (0.5, 0.14, 3.1)		-0.962	

Energies in kcals mole^{-1}

FIGURE 2,4

HYDROGEN

U_{max} = - 1,111 Kcals/mole

Z_{eqm} = 2,90 Å

Flat

Position O (0,0)

Orientation 2

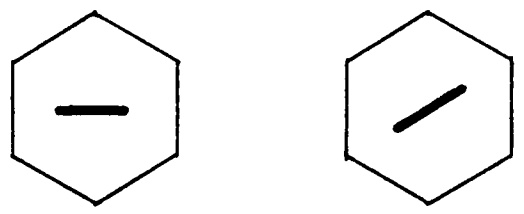

1 2

B) Barriers to translation and rotation

	HOPSCOTCH	Barrer	Kiselev et al
Minimum barrier to translation	0.127		
Maximum barrier to translation	0.150		
Average barrier to translation	0.138	0.179	
Barrier to rotation about the x or y axes	0.250		0.220
Barrier to rotation about the z axis	0.022		

Energies in Kcals mole^{-1}

FIGURE 2,5

HYDROGEN

Variation of potential energy on translation

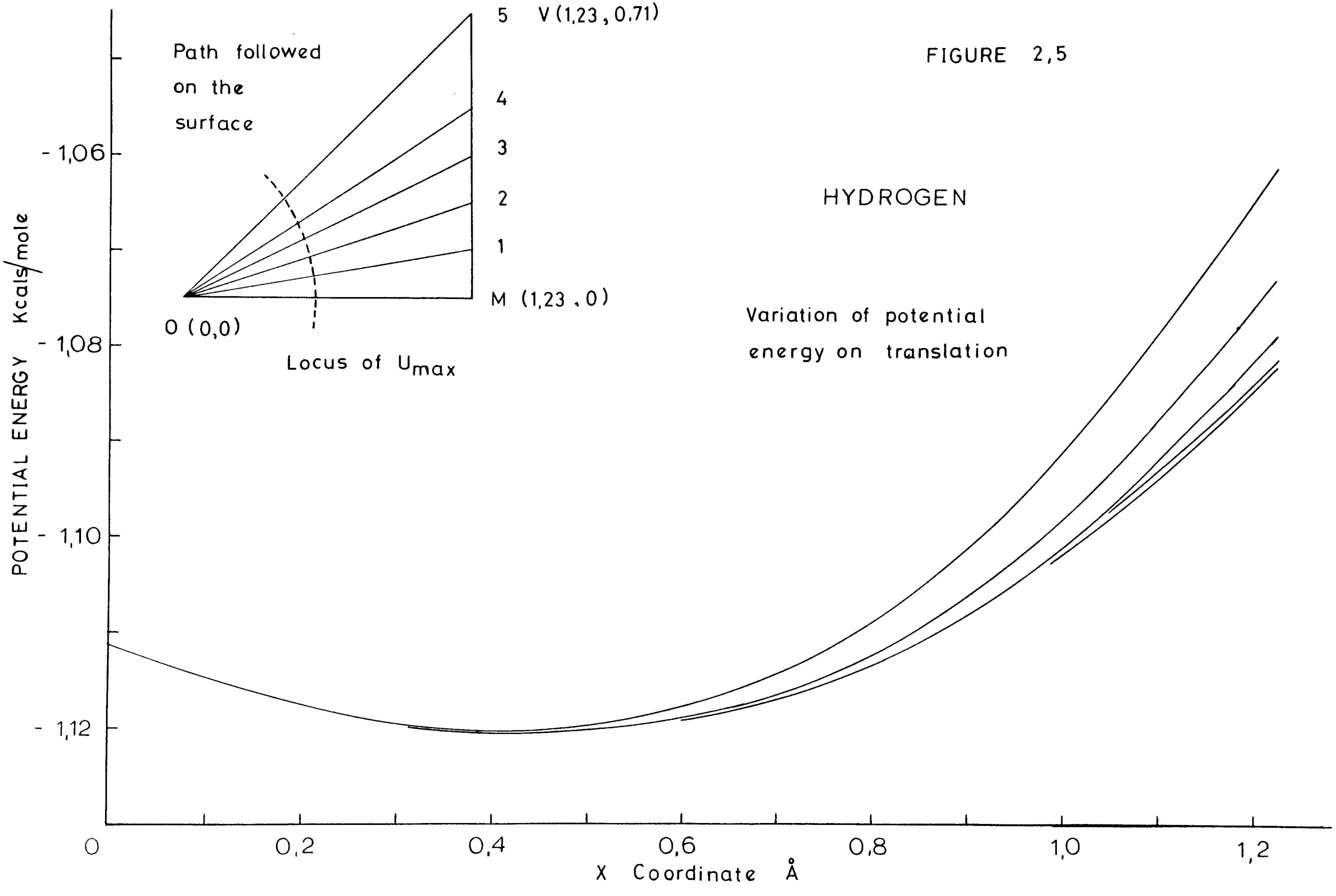

CHAPTER 3

Introduction to the Principles of Neutron Scattering Theory

The purpose of this section is to demonstrate the origin of the various terms used in the interpretation of the scattered neutron data, and to indicate the limitations of the various possible approaches. For a detailed theoretical treatment see references (72). The exposition here is largely based upon (72d).

The Scattering Cross Section

The neutron is regarded as a plane wave

$$\psi(r) = \exp(ik_o r) \tag{3.1}$$

where k_o is the wave vector of the neutron. The probability of a scattering process taking place when the neutron wave vector changes from k_o to k, at a constant energy E, is given by the square of the matrix element.

$$\rho^{E}_{k_o - k} = \frac{1}{L^6} \frac{2\pi}{\hbar} \rho_k^{(E)} \left| \langle k/V/k_o \rangle \right|^2 \tag{3.2}$$

where L is the size of the space required for normalisation

$\rho_k^{(E)}$ is the density of final scattering states per unit energy range.

$$\rho_k^{(E)} = \left(\frac{L}{2\pi}\right)^3 \frac{mk}{\hbar^2} \, d\Omega \tag{3.3}$$

$d\Omega$ is an element of solid angle.

To express this probability as a cross section requires normalisation to the incident flux, $= \frac{\hbar k_o}{mL^3}$

thus

$$\frac{d\sigma}{d\Omega}\Big|_E = \frac{k}{k_o} \left(\frac{m}{2\pi\hbar^2}\right)^2 \left| \langle k/V/k_o \rangle \right|^2 \tag{3.4}$$

If there is also the possibility of an energy change as well as a momentum transfer, then this is expressed in the double differential cross section as

$$\frac{d^2\sigma}{d\Omega d\varepsilon} = \frac{k}{k_o} \left(\frac{m}{2\pi\hbar^2}\right)^2 \sum_{\sigma\lambda} \rho_\sigma \rho_\lambda \sum_{\sigma'\lambda'} |\langle k\sigma'\lambda' |V| k_o\sigma\lambda\rangle|^2$$

$$\times \quad \delta(\hbar\omega + E_\lambda - E_{\lambda'}) \qquad (3.5)$$

Here the first differential cross section is averaged over all initial states, summed over all final states, for both the scattering nuclei and the neutron spin states.

σ, σ' are the initial and final neutron spin states

λ , λ' are the initial and final states of the scattering nuclei

ρ_σ, ρ_λ are the probabilities of occupation of the states σ and λ.

E_λ, $E_{\lambda'}$ are the energies of the initial and final states. The form of the interaction potential, V, is taken to be the Fermi psuedo potential.

$$V(r) = \frac{2\pi\hbar^2}{m} \sum_i b_i \, \delta(r - R_i) \qquad (3.6)$$

which is a point like potential, as the interaction is assumed to involve infinite forces acting over very short distances.

R_i is the position vector of the i th nucleus

b_i the scattering length of the i th nucleus

r the neutron position vector.

Thus on substituting for V, and dropping the spin labels, assuming, as will be the case for all experiments in this work that the incident neutron beam is unpolarised

$$\frac{d^2\sigma}{d\Omega d\varepsilon} = \frac{k}{k_o} \sum_{\lambda\lambda'} \rho_\lambda |\langle\lambda'| \sum_i b_i \exp(i\kappa R_i) |\lambda\rangle|^2 \, \delta(\hbar w + E\lambda - E\lambda') \qquad (3.7)$$

where $\kappa = k - k_o$, the momentum transfer during the scattering event.

If the eigenstates and eigenvalues of the scattering system are known then this expression for the double differential cross section can be evaluated exactly. This is not generally the case and a more fruitful approach is by the correlation function formalism developed originally by Van Hove (73).

3.2 Correlation Functions and Neutron Scattering

Expanding the energy conservation delta function of equation 3.7 as an exponential, and introducing H, the Hamiltonian of the scattering system for which E_λ and $E_{\lambda'}$ are eigenvalues, gives

$$\frac{d^2\sigma}{d\Omega d\varepsilon} = \frac{k}{k_o} \frac{1}{2\pi\hbar} \int_{-\infty}^{\infty} dt \exp(-iwt) \sum_{\lambda\lambda'} \rho_\lambda$$

$$x \langle\lambda| \sum_i b_i^* \exp(-i\kappa R_i) |\lambda'\rangle$$

$$x \langle\lambda'| \sum_{i'} b_{i'} \exp\left(\frac{iHt}{\hbar}\right) \exp(i\kappa R_{i'}) \exp\left(\frac{-iHt}{\hbar}\right) |\lambda\rangle \qquad (3.8)$$

Transferring the time dependence to the position operators and performing the sum over final states gives

$$\frac{d^2\sigma}{d\Omega d\varepsilon} = \frac{k}{k_o} \frac{1}{2\pi\hbar} \int_{-\infty}^{\infty} dt \exp(-iwt) \sum_{ii'} \overline{b_i^* b_{i'}} \qquad (3.9)$$

$$x \langle \exp\left[-i\kappa R_i(o)\right] \exp\left[i\kappa R_{i'}(t)\right] \rangle_T$$

where $\langle \ldots\ldots \rangle_T$ denotes the thermal average

$\sum_\lambda \rho_\lambda \langle\lambda| \ldots |\lambda'\rangle$

It is clear from the form of this expression that the scattering can be regarded as the interference arising from a wave scattered by a stationary centre at R_i and a retarded wave scattered from a moving centre at $R_{i'}$.

$\overline{b_i^* b_i} = |\overline{b}|^2$ for $i \neq i'$ incoherent scattering

$= |\overline{b}|^2$ for $i = i'$ coherent scattering

$$\frac{d^2\sigma}{d\Omega d\varepsilon} = \frac{k}{k_o} \frac{1}{2\pi\hbar} \int_{-\infty}^{\infty} dt\, e^{iwt} \left\{ \overline{b_i}^2 \sum_{ii'} \langle e^{i\kappa R_i(o)} e^{i\kappa R_{i'}(t)} \rangle_T \right.$$

$$\left. + (\overline{b_i^2} - \overline{b_i}^2) \sum_i \langle e^{-i\kappa Ri(o)} e^{i\kappa Rj(t)} \rangle_T \right\} \qquad (3.10)$$

and the separation into incoherent and coherent cross sections is now evident.

$$\frac{d^2\sigma}{d\Omega d\varepsilon}\Big|_{TOTAL} = \frac{d^2\sigma}{d\Omega d\varepsilon}COH + \frac{d^2\sigma}{d\Omega d\varepsilon}INC \tag{3.11}$$

Equation 3.10 can be rewritten in terms of the correlation functions $G_\kappa(r,t)$

$$\frac{d^2\sigma}{d\Omega d\varepsilon} = \frac{Nk}{k_o}\frac{1}{2\pi\hbar}\int_{-\infty}^{\infty} dt e^{-iwt}\sum_r e^{i\kappa r}\left\{\frac{\overline{2}}{b_i}G(r,t)+\overline{(b_i^2} - \frac{\overline{2}}{b_i})G_s(r,t)\right\} \tag{3.12}$$

where by definition

$$N\sum_r G(r,t)e^{i\kappa r} = \sum_{ii'} <e^{-i\kappa R_i(o)}e^{i\kappa R_{i'}(t)}>_T$$

$$N\sum_r G_s(r,t)e^{i\kappa r} = \sum_i <e^{-i\kappa R_i(o)}e^{i\kappa R_i(t)}>_T$$

$G(r,t)$ and $G_s(r,t)$ are referred to as the Van Hove correlation functions. They have a quantum mechanical basis and are complex quantities. The real part of the function describing the spatial and temporal dependence of density fluctuations within the target and the imaginary component describing the dissipation of that fluctuation. In the classical limit of long times, these correlation functions are real quantities and the position operators commute.

$$G^{CL}(r,t) = \frac{1}{N}\sum_{ii'}\delta(r + R_i(o) - R_{i'}(t)) \tag{3.13}$$

$$G_s^{CL}(r,t) = \frac{1}{N}\sum_i \delta(r + R_i(o) - R_i(t)) \tag{3.14}$$

These are known as the distinct and self correlation functions respectively, and are directly related to the coherent and incoherent cross sections

$$\begin{aligned}\frac{d^2\sigma}{d\Omega d\varepsilon} &= \frac{d^2\sigma}{d\Omega d\varepsilon}COH + \frac{d^2\sigma}{d\Omega d\varepsilon}INC \\ &= \frac{Nk}{k_o}\frac{\overline{b}^{\,2}}{2\pi\hbar}\int_{-\infty}^{\infty}\int drdt\ \exp(i[\kappa r - wt])G(r,t) \\ &+ \frac{Nk}{k_o}\frac{(\overline{b^2} - \overline{b}^{\,2})}{2\pi\hbar}\int_{-\infty}^{\infty}\int drdt\ \exp(i[\kappa r - wt])G_s(r,t)\end{aligned} \tag{3.15}$$

These space time fourier transforms of the pair correlation functions are generally written as scattering laws in the transform domain

$$\frac{d^2\sigma}{d\Omega d\varepsilon} = \frac{Nk}{k_o} \overline{b}^2 S_{COH}(\kappa,w) + \frac{Nk}{k_o} (\overline{b^2} - \overline{b}^2) S_{INC}(\kappa,w) \qquad (3.16)$$

A correlation function G(r,t) and its transform S(κ,w) are reflections of the dynamics of the sample system and wholly independent of the technique, in this instance neutron scattering, used to probe the sample properties. All spectroscopic techniques operate in limited regions of (κ,w) space. Since the transform integral takes place between the limits of $+\infty$ and $-\infty$ it is generally not possible to transform the observed spectral response directly and obtain the total correlation function for the target system. The region of typical conditions for the incident neutron is shown in fig 3.1.

The usual procedure is thus to assume a form for G(r,t) for the target system, calculate an S(κ,w) for the regime being investigated and then compare this with the actual function measured on the spectrometer.

3.3 Scattering Laws for Simple Systems

Considering a generalised system where there is translational, rotational and vibrational motion, the position operator R_i can be written as

$$R_i(t) = r(t) + d_i(t) + u_i(t) \qquad (3.17)$$

where r is the radius vector of the centre of mass of the molecule

d_i is the equilibrium position of the ith nucleus relative to the centre of mass

u_i is the displacement of the ith nucleus from the equilibrium position.

If one assumes that the various motions are uncoupled one can write the total wave function for the system as a product of the wave functions for the individual motions

$$\psi_{TOT} = \psi_{TRANS}\, \psi_{ROT}\, \psi_{VIB} \qquad (3.18)$$

FIGURE 3,1

$S(\chi,\omega)$ SPACE ACCESSIBLE IN A

NEUTRON SCATTERING EVENT

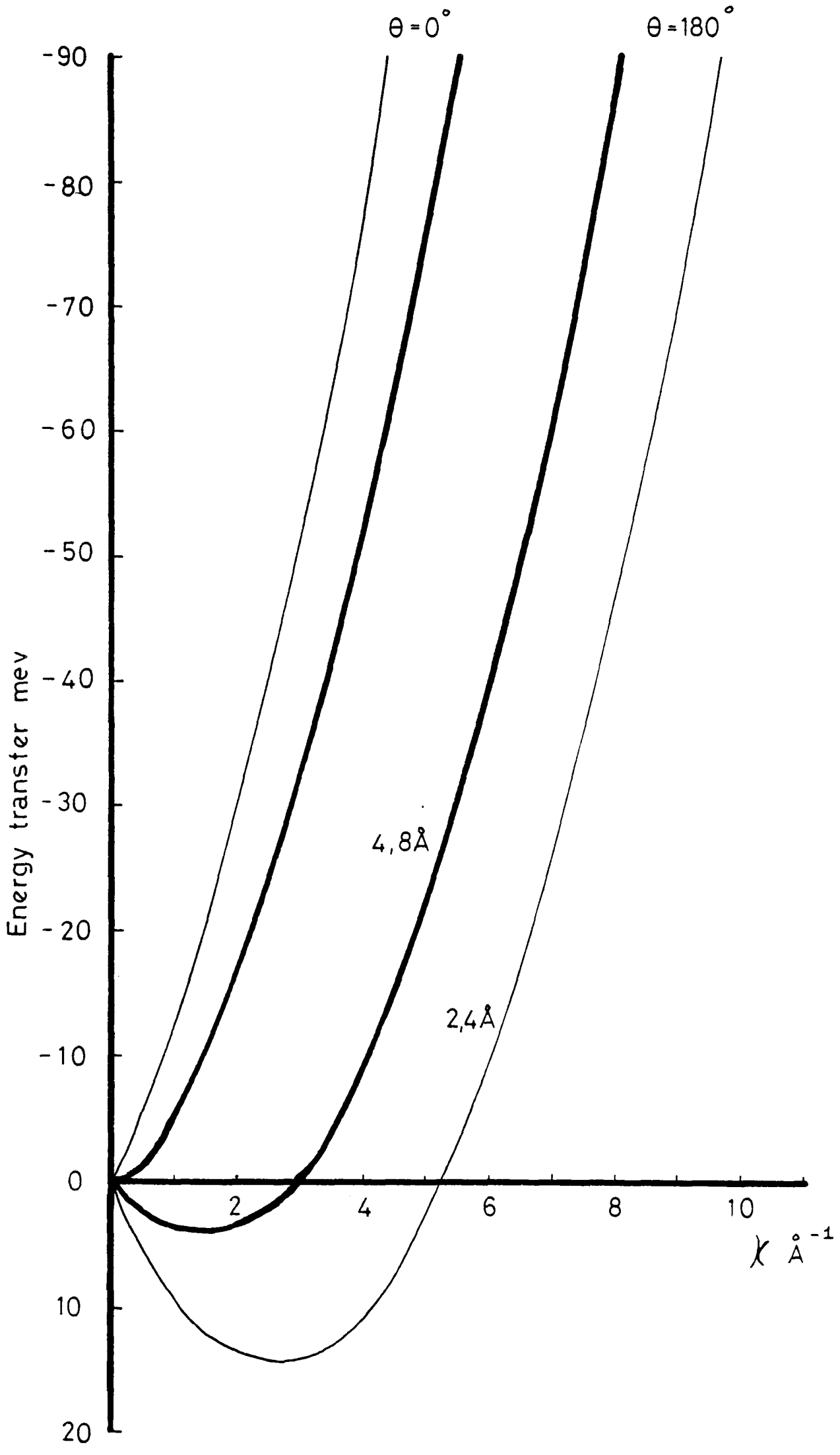

Whilst the operator r(t) commutes with $d_i(t)$ and $u_i(t)$, the latter pair do not themselves commute at different times. This lack of commutation is most evident at long collision times when the vector u_i will have rotated due to molecular motion. Nonetheless, it is usual to make the approximation that for small collision times, $d_i(t)$ and $u_i(t)$ commute and there is no vibration-rotation interaction.

The total scattering law can then be written, (22), as

$$S(\kappa,w) = \frac{1}{2\pi\hbar N}\int_{-\infty}^{\infty} dt\ \exp(-iwt)\sum_{ii'} \langle \exp(-i\kappa r_i(o))\exp(i\kappa r_{i'}(t))\rangle_T$$
$$x\ \langle \exp(-i\kappa d_i(o))\exp(i\kappa d_{i'}(t))\rangle_T$$
$$x\ \langle \exp(-i\kappa u_i(o))\exp(i\kappa u_{i'}(t))\rangle_T \qquad (3.19)$$

Fourier transforming a series of products leads to a convolution of the functions. The total scattering law for any system can thus be regarded, to a fair approximation, as a convolution of the scattering laws for the individual types of motion.

$$S_{TOT}(\kappa,w) = \frac{1}{2\pi\hbar N} S_{TRANS}(\kappa,w) * S_{ROT}(\kappa,w) * S_{VIB}(\kappa,w) \qquad (3.20)$$

where the symbol * denotes a convolution.

3.3.1 The Vibrational Scattering Law

Suppose that the scattering system is a single nucleus bound in an isotropic harmonic potential. It is required to evaluate

$$S_{VIB}(\kappa,w) = \int_{-\infty}^{\infty} dt\ \exp(-iwt)\ \langle \exp(-i\kappa u(o))\exp(i\kappa u(t))\rangle_T \qquad (3.21)$$

As the well is isotropic

$$\langle \exp(-i\kappa u(o))\exp(i\kappa u(t))\rangle_T = \prod \langle \exp(-i\kappa_\alpha u_\alpha(o))\exp(i\kappa_\alpha u_\alpha(t))\rangle_T$$
$$\alpha = x,\ y,\ z \qquad (3.22)$$

The Hamiltonian for the linear case is

$$H_l = \frac{1}{2m}\rho x^2 + \frac{Mw_o^2}{2} x^2 \qquad (3.23)$$

and has eigenvalues

$$E_n = \hbar w_o(n + \tfrac{1}{2}) \quad n = 0,\ 1,\ 2\ \ldots\ldots \qquad (3.24)$$

where w_o is the fundamental vibration frequency.

Employing Bose operators (74), a and a^+, to express the position and momentum operators

$$x = \left(\frac{\hbar}{2Mw_o}\right)^{\frac{1}{2}} (a + a^+) \tag{3.25}$$

$$\rho = -i \left(\frac{M\hbar w_o}{2}\right)^{\frac{1}{2}} (a - a^+) \tag{3.26}$$

reduces the Hamiltonian to

$$H_1 = \hbar w_o \ (a^+a + \tfrac{1}{2}) \tag{3.27}$$

Going from the equation of motion for the operators a and a+ one can write the development of the position operator with time as follows

$$x(t) = \left(\frac{\hbar}{2Mw_o}\right)^{\frac{1}{2}} \ (a \exp(-iw_o t) + a^+ \exp(iw_o t) \tag{3.28}$$

Using Bloch's identity, (22), one arrives at the following expression for the correlation function.

$$\begin{aligned} &\langle \exp(-i\kappa_x x(o)) \exp(i\kappa_x x(t)) \rangle_T \\ &= \exp\left\{-\frac{\hbar^2\kappa^2}{2Mw_o} \coth\left[\frac{\hbar w_o \beta}{2}\right]\right\} \exp\left[\frac{\hbar^2\kappa^2}{2Mw_o} \operatorname{cosech}\left(\frac{\hbar w_o \beta}{2}\right)\right. \\ &\left. x \left(\exp\left\{iw_o t + \frac{\hbar w_o \beta}{2}\right\} + \exp\left\{-iw_o t - \frac{\hbar w_o \beta}{2}\right\}\right)\right] \end{aligned} \tag{3.29}$$

This expression can be further simplified, before carrying out the time Fourier integral, by noting that

$$\exp\left\{\tfrac{1}{2}y(t + t^{-1})\right\} = \sum_{-\infty}^{\infty} t^n I_n(y) \tag{3.30}$$

and substituting in this modified Bessel function $I_n(y)$

Thus finally

$$S(\kappa, w) = \exp\left\{\frac{-\hbar\kappa^2}{2Mw_o} \coth\left(\frac{\hbar w_o \beta}{2}\right)\right\} \exp\left(\frac{\hbar w \beta}{2}\right) \sum_{-\infty}^{\infty} \delta(\hbar w - n\hbar w_o) I_n(y) \tag{3.31}$$

where

$$y = \frac{\hbar\kappa^2}{2Mw_o} \operatorname{cosech}\left(\frac{\hbar w_o \beta}{2}\right)$$

One can see that the scattering surface for a simple harmonic oscillator is made up of a series of delta functions centred at multiples of the transition energy and whose intensity is governed by the product

$$\exp\left(\frac{-\hbar\kappa^2}{2Mw_o}\right) \coth\left(\frac{\hbar w_o \beta}{2}\right) \sum_n I_n\left(\frac{\hbar\kappa^2}{2Mw_o}\right) \operatorname{cosech}\left(\frac{\hbar w_o \beta}{2}\right) \tag{3.32}$$

A diagrammatic representation of this is given in figure 3.2.

FIGURE 3,2

SCATTERING SURFACE FOR A HARMONIC OSCILLATOR

$$S_{VIB}(x,\omega) = Exp\left(-\frac{\hbar x^2}{2m\omega_0}\coth\left[\frac{\hbar\omega_0\beta}{2}\right]\right)\sum_n I_n\left(\frac{\hbar x^2}{2m\omega_0}\,\mathrm{cosech}\left[\frac{\hbar\omega_0\beta}{2}\right]\right)\delta(\hbar\omega - n\hbar\omega_0)$$

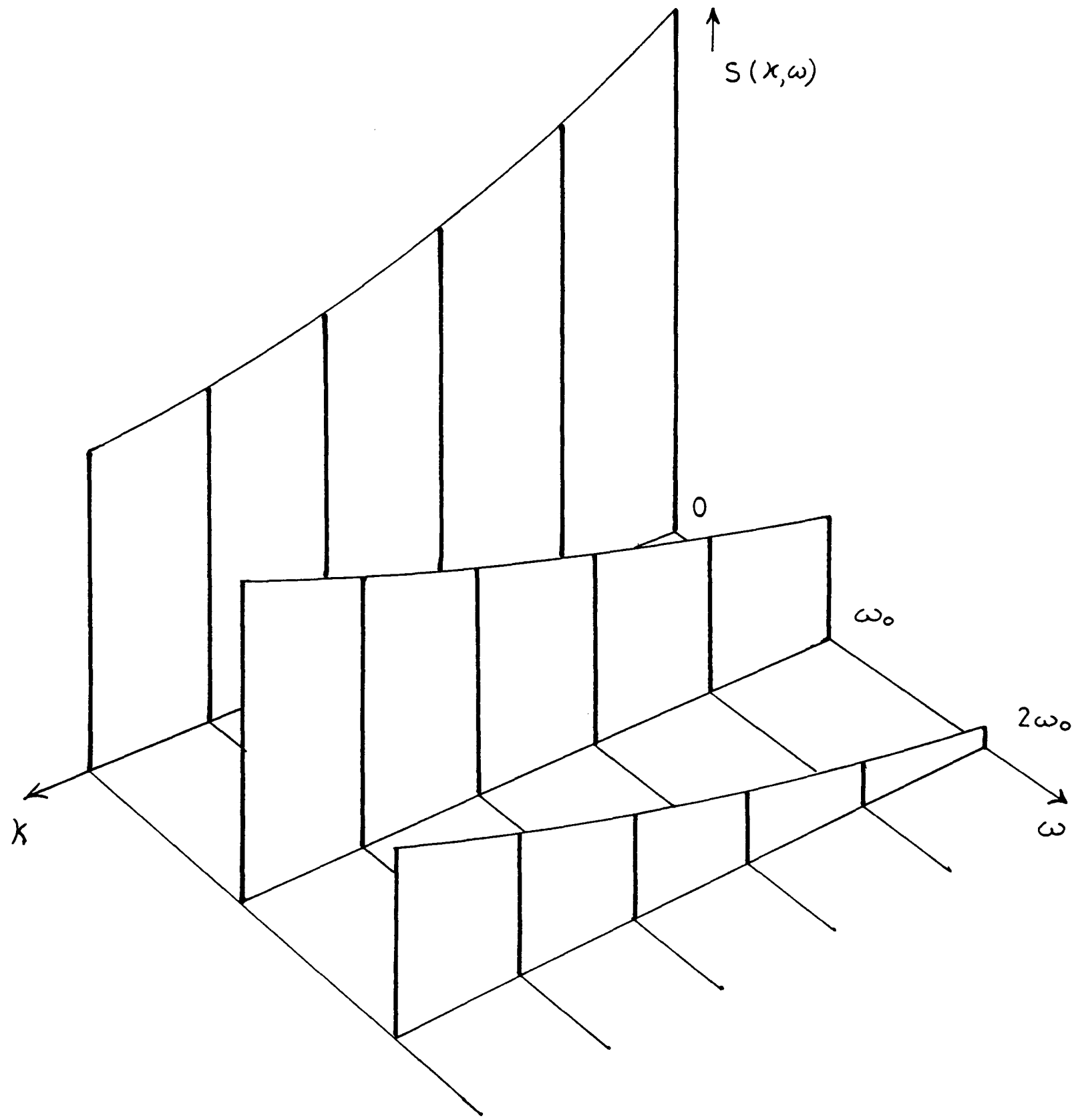

3.3.2 The Rotational Scattering Law

If the rotations of the molecule are free, uncoupled to any other motions, and the molecule itself possesses a high degree of symmetry, then it is possible to calculate the rotational motion exactly. Such a situation only exists for the gas phases of such simple molecules as CH_4, NH_3 and $HC\ell$. Should the rotational motion be at all hindered then the calculation of the correlation function is extremely complex and it is necessary to adopt one of the approximate treatments which seems most suited for the system under consideration.

One of the more general approaches is by the use of rotational correlation functions defined in an analagous fashion to the Van Hove correlation functions. Thus $G(\Omega,\Omega_o,t-t')\ d\Omega$, is the probability of finding the orientation of a molecule in a solid angle element $d\Omega$ at a time t, given that the orientation was centred at Ω_o at a time t'. If it is assumed that the classical description holds, and the rotational motion is isotropic, then $G(\Omega,\ \Omega_o,t)$ can be expanded in spherical harmonics. Hence the scattering law is expressed as

$$S_{ROT}(\kappa,w) = \sum_{\ell=0}^{\infty} (2\ell + 1)\ j_\ell^2(\kappa r)\frac{1}{2\pi}\int_{-\infty}^{\infty} dt\ \exp(-iwt)F_\ell(t) \qquad (3.33)$$

The spatial dependence is expressed in the spherical bessel function and the time development in the expansion coefficients $F_\ell(t)$.

$$F_\ell(t) = \int d\Omega P_\ell\left[\cos(\beta(t)\right] G(\Omega,\Omega_o,t) \equiv \langle \rho_\ell \cos(\beta(t)) \rangle_T \qquad (3.34)$$

Where $\beta(t)$ is the angle through which an internal position vector of the molecule rotates in a time interval t

P_ℓ is a Legendre polynomial

If this molecular axis performs random motion then the correlation function will decay to zero at long times, and only $F_o = 1$ remains.

The scattering law becomes

$$S_{ROT}(\kappa,w) = j_o^2(\kappa r)\delta(w) + \sum_{\ell=1} (2\ell + 1) j_\ell^2(\kappa r) \tilde{F}_\ell(w) \qquad (3.35)$$

$\tilde{F}_\ell(w)$ is the transformed function $F_\ell(t)$

One of the major experimental problems of neutron scattering is separating the contribution of these two components $\delta(w)$ and $\tilde{F}_\ell(w)$ in a measured neutron spectrum.(14)

If the rotational motion is dynamically independent and unhindered, $F_\ell(t)$ takes a simple form

$$F(t) = \sum_{J^1 = |J-\ell|}^{J+\ell} \frac{1}{2\ell + 1}\left[\frac{2J^1 + 1}{2J + 1}\right] P_J(T)\exp(iw_{JJ^1}t) \qquad (3.36)$$

where $P_J(T)$ is the Boltzman population factor

$E = \hbar w_{JJ^1} = E_J - E_{J^1}$ is the rotational transition energy.

Fourier transformation gives rise to an energy conservation delta function in the rotational scattering law

$$S_{ROT}(\kappa,w) = \sum_{\ell=0}^{\infty} \sum_{J^1 = (J-\ell)}^{J+\ell} \frac{(2J^1 + 1)}{(2J + 1)\ (2\ell + 1)} P_J(T) j_\ell^2(\kappa r)\delta(\hbar w - n\hbar w_{JJ'}) \qquad (3.37)$$

In an analagous fashion to the previous section it can be seen that the scattering surface for the spherical top rotor consists of a series of delta functions located now at the energies of the rotational transitions. Their intensities are governed by the product of a population factor and a κ dependent spherical Bessel function. The scattering surface is represented diagrammatically in figure 3.3.

If, on the other hand, the orientational auto correlation function satisfies a diffusion equation

$$D_r \Delta_\Omega G(\Omega,\Omega_o,t) = \partial G(\Omega,\Omega_o,t)/\partial t \qquad (3.38)$$

where Δ_Ω is the Laplacian for the rotations and D_r the rotational diffusion coefficient. Thus

$$F_\ell(t) = \exp(-\ell(\ell + 1)\ D_r t) \qquad (3.39)$$

and the $\tilde{F}_\ell(w)$ are lorentzian, the scattering law being a sum of an infinite number of lorentzians.

FIGURE 3,3

SCATTERING SURFACE FOR A SPHERICAL TOP ROTATOR

$$S_{ROT}(\chi,\omega) = \sum_{\ell=0}^{\infty} \sum_{J'=J-\ell}^{J+\ell} \frac{2J'+1}{(2J+1)(2\ell+1)} P_J(T)\, j_\ell^2(\chi_r)\, \delta(\hbar\omega - n\hbar\omega_{JJ'})$$

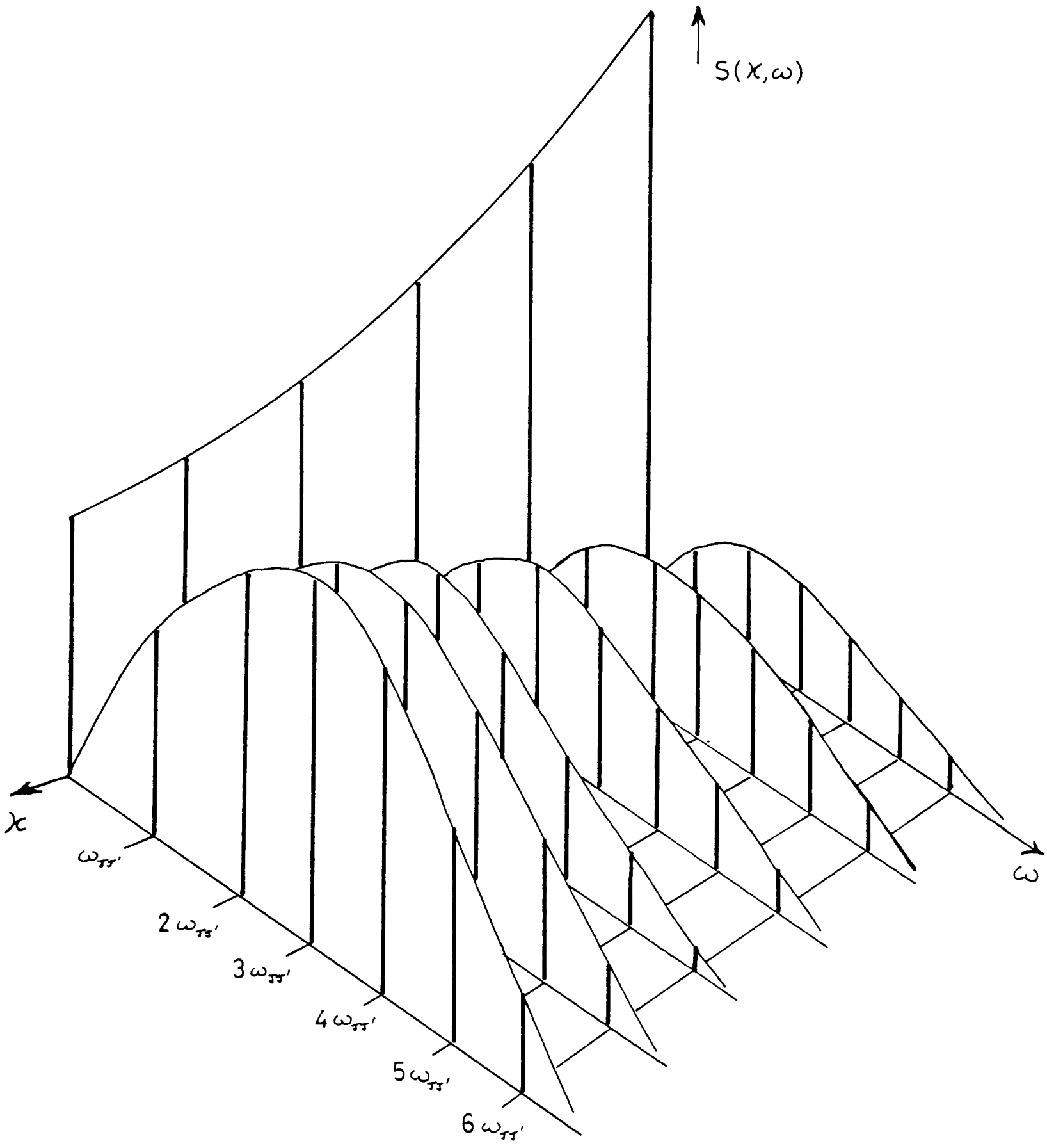

3.3.3 The Translational Scattering Law

In the limiting examples of an ideal gas, a harmonic oscillator, diffusion in a simple liquid at long times, or in all cases when the interaction time is very short (i.e., large incident neutron energies) the correlation function for centre of mass motion is gaussian

$$G_s(r,t) = \left[\frac{1}{4\pi\gamma(t)}\right]^{-3/2} \exp\left\{\frac{-r^2}{4\gamma(t)}\right\} \tag{3.40}$$

For a classical system $\gamma(t)$ is the mean square displacement of the particle from the origin after time t. For a monatomic gas

$$\gamma(t) = \frac{V^2t^2}{2}$$

$$V = \left(\frac{2}{M\beta}\right)^{\frac{1}{2}}$$

hence

$$G_s(r,t) = \left(\frac{\beta M}{2\Pi t^2}\right)^{3/2} \exp\left(\frac{-\beta M r^2}{2t^2}\right) \tag{3.41}$$

which on transforming gives

$$S^{GAS}_{TRANS}(\kappa,w) = \left(\frac{\beta M}{2\pi\hbar^2\kappa^2}\right)^{\frac{1}{2}} \exp\left[\frac{-\beta M}{2\hbar^2\kappa^2}\left(\hbar w - \frac{\hbar^2\kappa^2}{2M}\right)\right] \tag{3.42}$$

For a given value of κ, this is a gaussian function centred at an energy of $\left(\frac{\hbar^2\kappa^2}{2M}\right)$, the so called "recoil energy" of the system. In the case of neutron scattering from a gas there is a true elastic peak only for $\kappa = o$. As κ increases so the gaussian moves to larger energy transfers and its width increases steadily. A diagrammatic representation of the scattering surface for a monatomic gas is given in figure 3.4.

In a simple liquid

$$\gamma(t) = \frac{1}{3}\int_o^{t'} dt\langle\vec{V}(o).\vec{V}(t)\rangle \tag{3.43}$$

and at long times, the velocity autocorrelation function for a simple liquid is directly related to the diffusion coefficient

$$\gamma(t) = \frac{1}{3}\int_o^{t'} dt\langle\vec{V}(o).\vec{V}(t)\rangle = D$$

FIGURE 3,4

SCATTERING SURFACE FOR A MONATOMIC GAS

$$S^{GAS}(\kappa,\omega) = \left(\frac{\beta M}{2\pi\hbar^2\kappa^2}\right)^{1/2} \exp\left(\frac{-\beta M}{2\hbar^2\kappa^2}\left[\hbar\omega - \frac{\hbar^2\kappa^2}{2M}\right]\right)$$

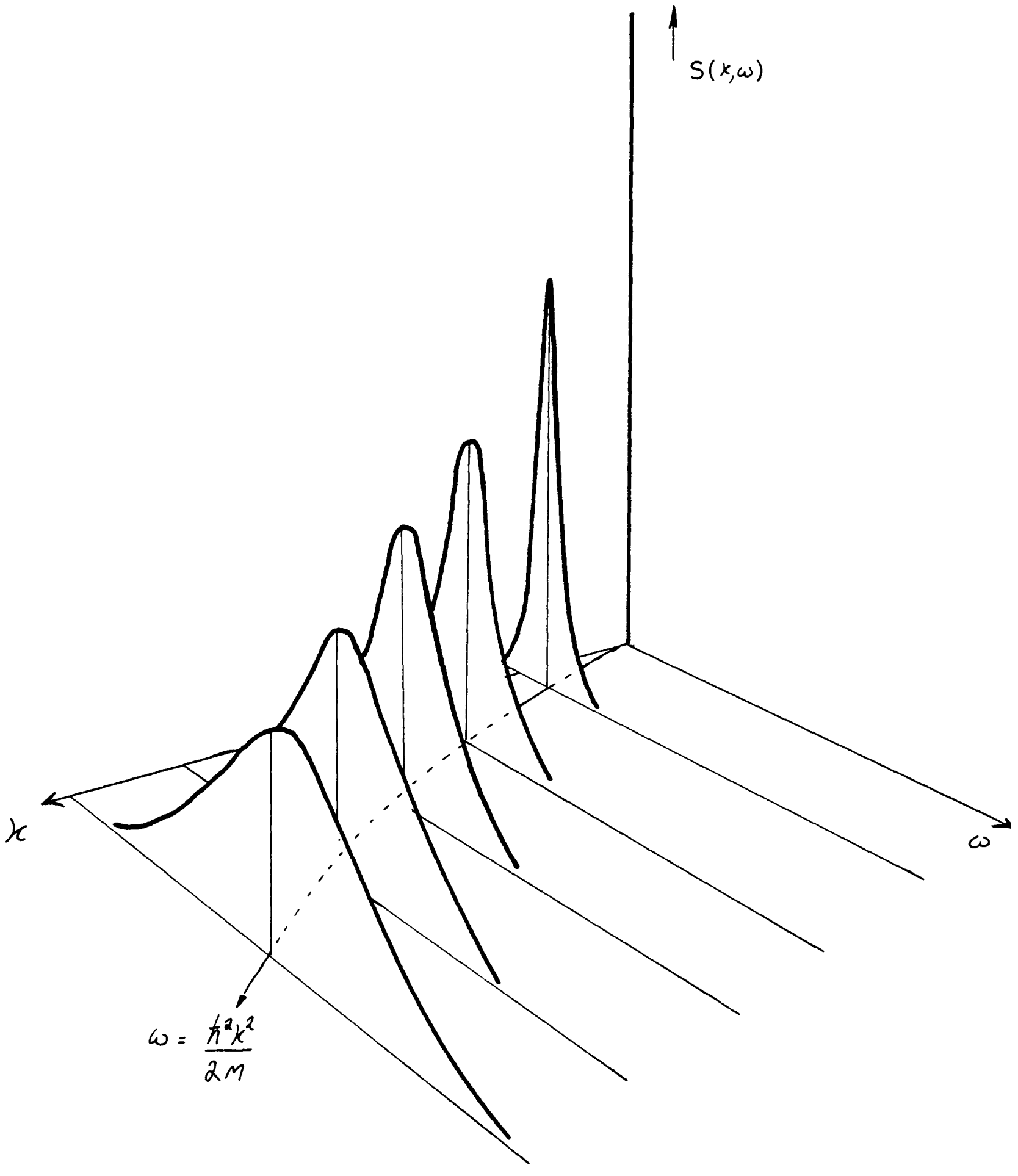

Hence

$$S^{LIQ}_{TRANS}(\kappa,w) = \int_{-\infty}^{\infty}\int dr\ dt\ \exp(i[\kappa r - wt])\left[\frac{1}{4\pi Dt}\right]^{3/2}\ \exp\left[\frac{-r^2}{4Dt}\right] \tag{3.44}$$

$$S^{LIQ}_{TRANS}(\kappa,w) = \frac{\pi}{2}\ \frac{D\kappa^2}{[D\kappa^2]^2 + w^2} \tag{3.45}$$

The scattering surface is now lorentzian in w at a given κ, and the width of this lorentzian goes as $D\kappa^2$. The scattering surface is shown diagrammatically in figure 3.5.

3.4 The Total Scattering Law

As discussed earlier the total scattering law can be treated approximately as a convolution of the scattering laws for the "individual" motions. As examples of this, consider the forms of the scattering laws for gaseous and liquid methane as derived by (76), (77), and (78), (79).

3.4.1. Gaseous Methane

The total cross section is made up of the scattering from the hydrogen and carbon nuclei independently.

$$\frac{d^2\sigma}{d\Omega d\epsilon} = \frac{k}{k_o}\left\{4\bar{A}_{HH}\ S^{HH}(\kappa,w) + A_{CC}\ S^{CC}(\kappa,w)\right\} \tag{3.46}$$

where

$$A_{ii'} = b_i^{COH} b_{i'}^{COH} + \delta nn'(a_i^{INC}\ a_{i'}^{INC}) \tag{3.47}$$

Since $4\ A_{HH} >> A_{CC}$ it is a reasonable approximation to consider only the incoherent scattering by the protons. The incoherent scattering law for gaseous CH_4 according to Griffing (76) is:-

$$S^{HH}(\kappa,w) = \frac{1}{2\pi\hbar}\ \exp(-\kappa^2\gamma_{HH})\left(\frac{2\pi M\beta}{\kappa^2}\right)^{\frac{1}{2}} \sum_{JJ'} P_{J(T)}$$
$$x\ \exp\left\{-\left[\frac{\hbar^2\kappa^2}{2M} + \Delta E_{JJ'} - \hbar w\right]^2 \Big/ \frac{2\hbar^2\kappa^2}{M\beta}\right\}$$
$$x\ (2J+1)(2J'+1) \sum_{\ell=|J-J'|}^{J+J'} j_\ell^2(\kappa r) \tag{3.48}$$

FIGURE 3,5

SCATTERING SURFACE FOR FICKIAN DIFFUSION

$$S(\kappa,\omega) = \frac{\pi}{2}\frac{D\kappa^2}{[D\kappa^2]^2+\omega^2}$$

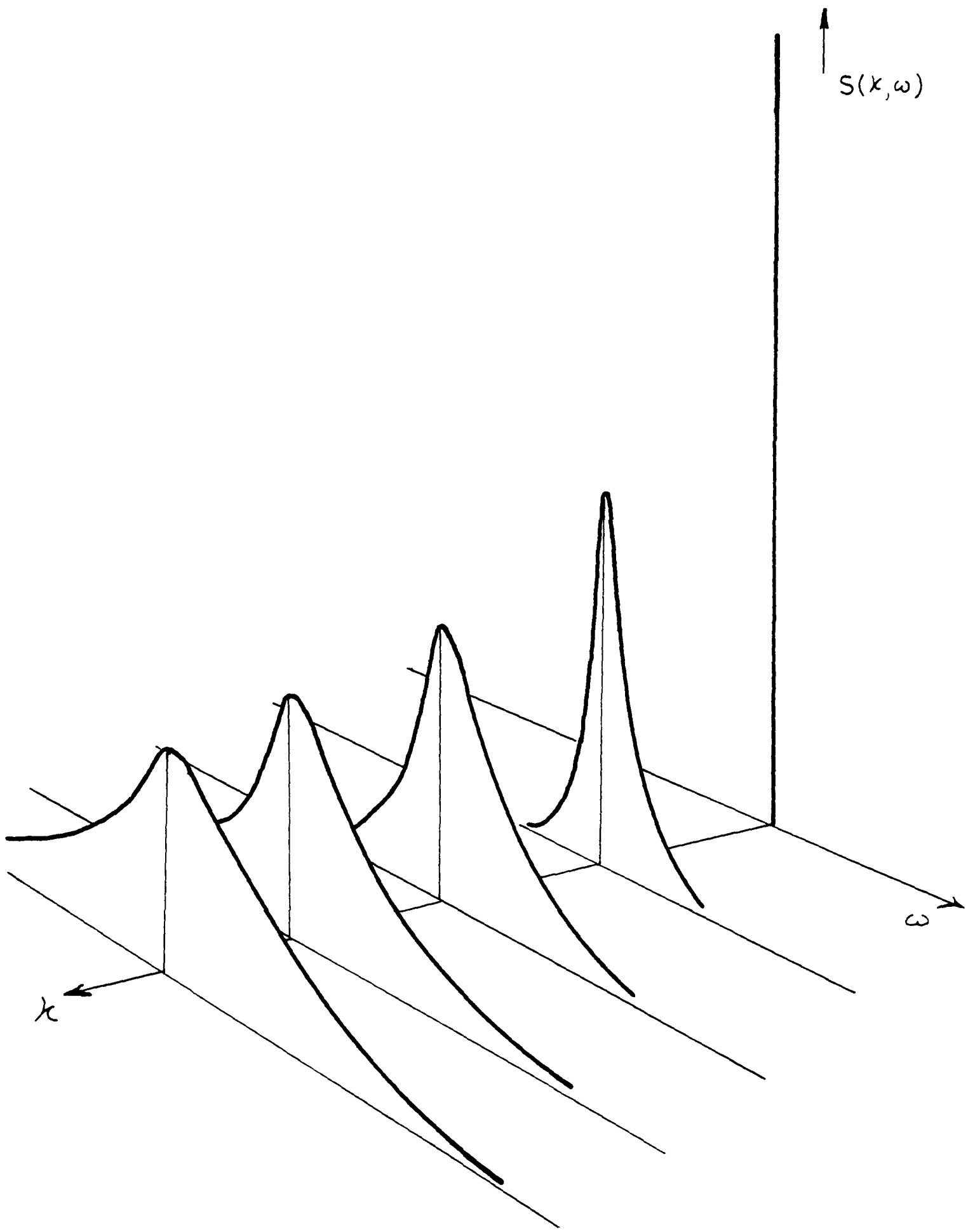

where $P_J(T)$ is the Boltzmann population factor

$$P_J(T) = \frac{\exp\left[-BJ(J+1)\beta\right]}{\sum_J (2J+1)^2 \exp(-BJ(J+1)\beta)}$$

B is the rotational constant $= \frac{\hbar^2}{2Mr^2}$

$\Delta E_{JJ'} = BJ'(J'+1) - BJ(J+1)$ the energy of the rotational transition.

The total scattering surface is constructed from the individual motion as follows. Each rotational transition contributes a delta function at multiples of $\Delta E_{JJ'}$. These delta functions are then convoluted with the gaussian scattering law for the centre of mass motion. Because of the recoil energy, $\frac{\hbar^2\kappa^2}{2M'}$, the $J = J'$ transition, (the "elastic" peak), occurs at increasingly bigger energy transfers as κ increases. The first vibrational transition of CH_4 comes at a relatively high energy, 900 cm^{-1}, and the contribution from the vibrational scattering law appears only as the Debye Waller term, $e^{-\kappa^2\gamma_{HH}}$. Because of the large width of the gaussian centre of mass scattering law, the discrete rotational transitions are no longer evident and merge into a rotational envelope.

3.4.2 Liquid Methane

The simplest approach as developed by (76) and (78)has a form very similar to that for the gaseous state. Now instead of a gaussian centre of mass scattering law there is a lorentzian function convoluted with each rotational transition, and no recoil energy term.

$$S^{HH}(\kappa,w) = \frac{1}{2\pi\hbar} \exp(-\kappa^2\gamma^*_{HH}) \sum_{JJ'} \left\{ \frac{2D\kappa^2}{\left[D\kappa^2\right]^2 + \left[\frac{\Delta E_{JJ'} - \hbar w}{\hbar}\right]^2} \right\}$$

$$\times \exp(\left[\Delta E_{JJ'} - \hbar w\right]2\beta)(2J+1)(2J'+1)P_J(T)$$

$$\times \sum_{\ell = |J-J'|}^{J+J'} j_\ell^2(\kappa r) \qquad (3.49)$$

Where D is the diffusion coefficient for the centre of mass of the methane molecule.

The width of each lorentzian centred at $n\Delta E_{JJ'}$ is controlled by this diffusion coefficient, $\delta E = 2D\kappa^2$ and so whether any rotational transitions remain as discrete entities depends largely on the value of D.

If the rotational motion was at all hindered then the delta functions would be replaced by, for example, lorentzians in the case of classical rotational diffusion. Convolution with the centre of mass scattering law will produce a broad continuous function analagous to the rotational envelope present with gaseous methane. The lack of inelastic singularities in the experimentally observed scattering law for liquid methane is taken to indicate that the rotational motion is hindered to some degree (80).

3.5 Experimental Measurement of $S^{INC}(\kappa,w)$ by Neutron Scattering

It is pertinent at this stage to discuss some of the features of an experimental observation of a scattering law using a neutron spectrometer.

1) The measured scattering law is a convolution of the machine resolution function and the true total scattering law. This will lead to a broadening and blurring of all features in the scattering law and alter the (κ,w) development of those features. The consequence of this is discussed in detail in section 3.9.3.

2) The measurements reported in this thesis were performed on time of flight instruments, where the scattered neutron energy is analysed by its time of arrival, and its momentum by the angle of scattering. Consequently the observation is of $w^2S(\kappa,w)$, not $S(\kappa,w)$, though this is readily corrected. More importantly, a time of flight spectrum is not at constant κ, but on a parabolic cut through (κ,w) space as shown in figures 3.1 and 5.2. The consequences of this are two fold.

A) Before a vibrational density of states can be extracted from the inelastic scattering, the data must be extrapolated to zero momentum transfer. The method of Egalstaff (81) is often used as an approximate way of achieving this, and his approach forms the basis of the FLORENCE program in the ROUNDABOUT suite (82).

B) With increasing momentum transfer one is moving towards shorter collision times and the limit of "free" particle scattering. Since the total scattering law is a convolution of the individual scattering laws, any singularity due to vibrational or rotational transitions occurring at energies greater than about 200 cm^{-1} on a time of flight machine will have an intrinsic width of approximately $(\frac{\hbar^2\kappa^2}{2M\beta})^{\frac{1}{2}}$. This width is the width of the centre of mass scattering law gaussian for the κ value corresponding to the energy of that transition, not the κ value for the elastic peak which, because of the parabolic cut in (κ,w) space, is always much less. The most successful approach to inelastic analysis by time of flight methods seems to be to work in the low κ regime, i.e. using large incident neutron energies and very small angles of scatter.

Some examples of the simulated time of flight spectra for gaseous and liquid methane are shown in figures 3.6 and 3.7. These were calculated using the program CARLY (57) and CHARLOTTE (83).

FIGURE 3,6

CARLY SIMULATIONS OF THE TIME OF FLIGHT SPECTRA FROM A GASEOUS SPHERICAL TOP.

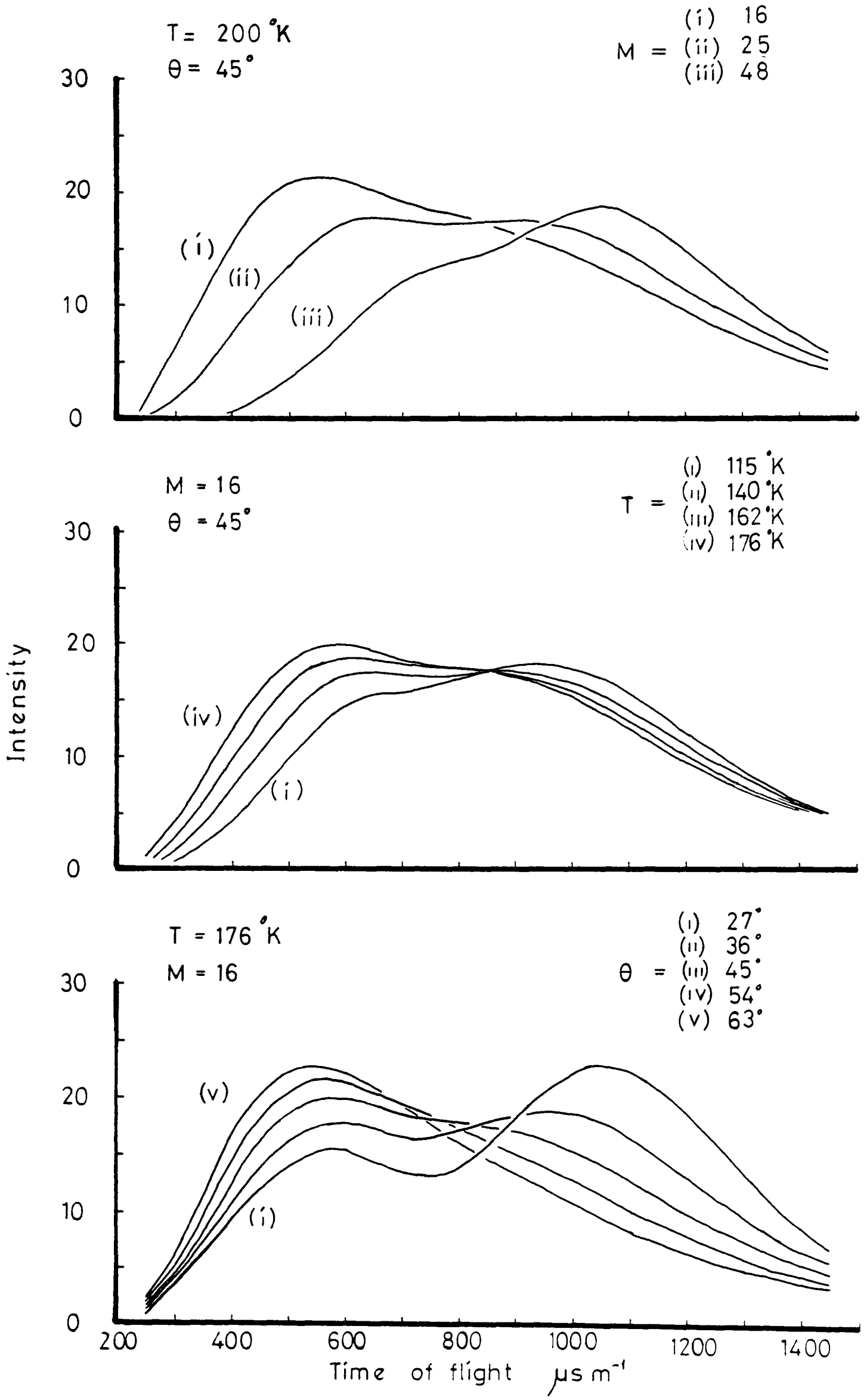

FIGURE 3,7

SIMULATED TIME OF FLIGHT SPECTRA – LIQUID CH_4

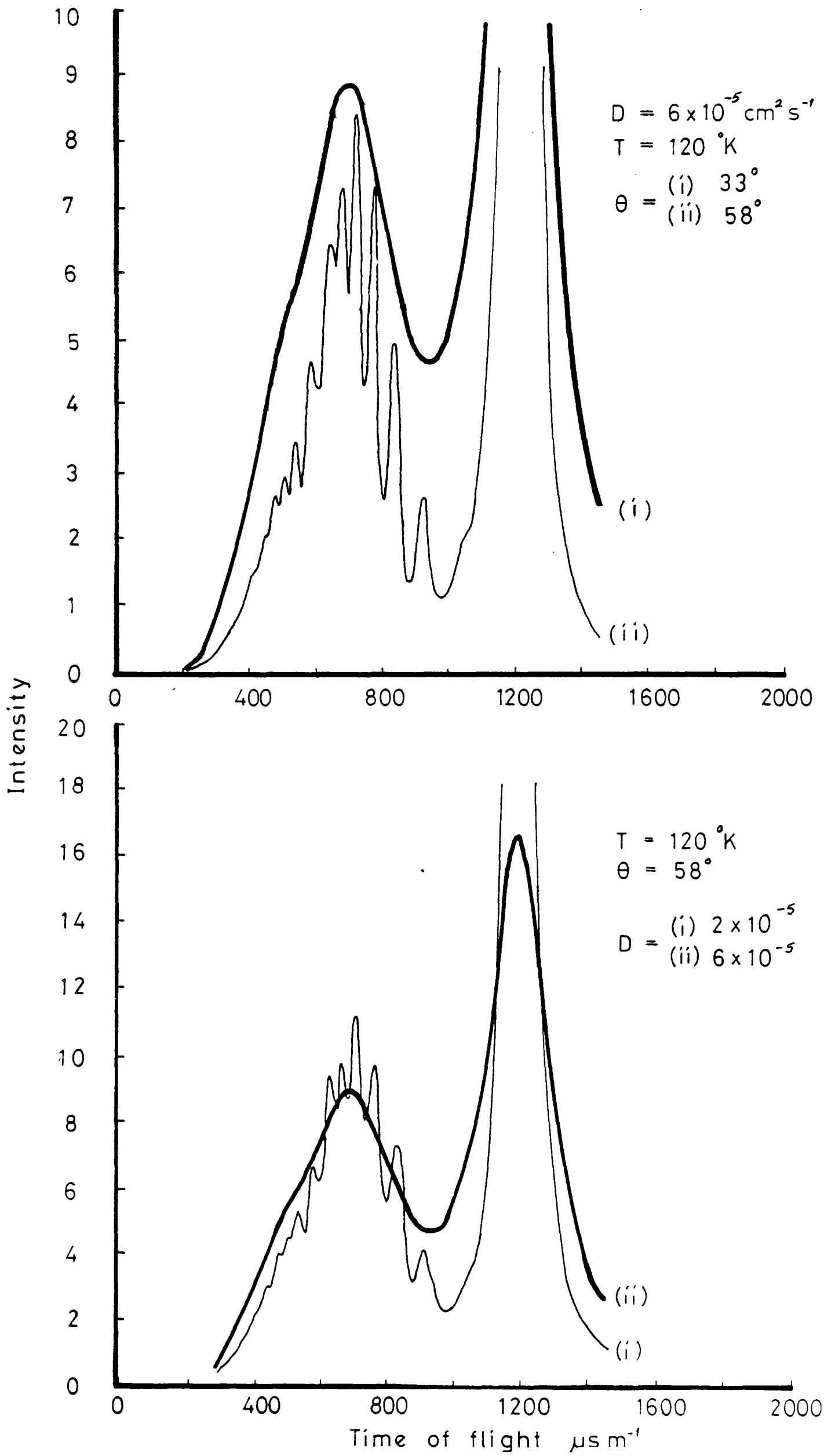

3.6 Scattering Laws for Adsorbed Molecules

3.6.1 Introduction

The problem has two aspects.

1) What are the likely dynamics of an adsorbed molecule and what is the most suitable correlation function to be used?

2) How will the polycrystallinity, i.e., the directional disorder of the adsorbent, affect the observed neutron spectra?

At present there is no continuity of interpretation amongst workers in this field, and the situation leaves much to be desired Todireanu (33) analysing the quasi elastic scattering for ethylene adsorbed on carbon does not specify explicitly the formulae used but it seems from the context that he has treated the scattering as arising from a continuous, isotropic system. The scattering law for a simple liquid adsorbate phase was taken to be Lorentzian and the broadening of the quasi elastic peak due to diffusion was assumed to go as $\Delta E = 2\hbar D_{2D}\kappa^2$. This is equivalent to the assumption that averaging an observation of the dynamics of a particle on a surface, over all possible orientations of that surface, produces a scattered neutron spectrum identical with the spectrum of that molecule in its equivalent bulk phase. This cannot be the case.

Verdan (34) has also taken the view that the correlation function for the two dimensional motion is the same as the correlation function for isotropic three dimensional motion. He does however consider the disorder of the adsorbent and concludes that this leads to a linear scaling of the observed parameters. Thus the measured diffusion coefficient. D_{OBS}, is related to the actual two dimensional diffusion coefficient, D_{2D}, by

$$D_{OBS} = \langle D_{2D} \rangle_{\Omega} = \frac{2}{3} D_{2D} \qquad (3.50)$$

This is the averaging approach adopted by Thompson et al (42)

for the interpretation of their NMR data for the diffusion of benzene on charcoal.

Verdan also considers the possibility of a localised admolecule. Now there are vibrations of the molecule parallel and perpendicular to the surface, which on angle averaging give rise to a single frequency $< w >_{\Omega}$

$$< \frac{1}{w} >_{\Omega} = \frac{2}{3w_{11}} + \frac{1}{3w_{\perp}} \qquad (3.51)$$

Verdan was unable to see this vibration in the neutron spectrum and concludes that either the motion is markedly anharmonic, or that a wide distribution of frequencies exist. In either case this should produce a very broad feature not easily distinguished. Whilst these possibilities exist they are not the reason for the non appearance of the vibration in this case. Only in particular circumstances will the motion be detectable and this question of admolecule surface vibrations is discussed more fully in section 3.9.3.

A possible approach to the angle averaging required appears in three recent publications on neutron scattering from disordered, anisotropic system. Stockmeyer (28) has developed the method for analysing the quasi elastic scattering from hydrogen adsorbed on powdered Raney-Nickel. Leadbetter et al (84) and Dianoux et al (85) were concerned with the anisotropic motions in nematic mesophases of liquid crystals 5CB, DMBCA, and TBBA respectively. The same approach is hinted at in an earlier paper by Sköld and Nelin (86) who were studying the centre of mass jump diffusion of hydrogen in polycrystalline metals.

The steps in the general procedure are as follows.

1) To set up a correlation function for a single molecule in terms of some arbitrary orientation of the molecular axes with respect

to the direction of the momentum transfer vector.

2) Double fourier transform this correlation function to obtain a scattering law for that particular orientation of the molecule.

3) Average the scattering law thus formed over all possible orientations with respect to the momentum transfer vector to give a final scattering law for the disordered sample.

The averaging is carried out on the scattering law not $G_s^{\theta}(r,t)$ (14) (86) as it is not a question of observing the average dynamics of the system rather a matter of the technique giving an averaged observation of the dynamics of the system. The averaging procedure of Verdan is an approximation to the full integration over angle, (84), and is most suitable for the longer time scales observed by NMR. 10^{-8} - 10^{-6} sec.

3.7 Application of the method to diffusion on surfaces

Consider one raft of adsorbent material inclined at an arbitrary angle ϕ with respect to the momentum transfer vector κ. The momentum transfer can be resolved into components perpendicular and parallel to the surface of the adsorbent raft. See figure 3.8 . Motion of the molecule in a given direction may only couple to the component of the momentum transfer in that same direction. Thus motion along the surface couples to $\kappa_{||}$, and any motion perpendicular couples to $\kappa_{\perp}$.

The total scattering law for this chosen raft will be made up by convoluting the scattering laws for the translations, rotations and vibrations of the molecules in these two possible directions. The assumption is made, as before, that the motions are uncoupled.

FIGURE 3.8

COORDINATE SYSTEM

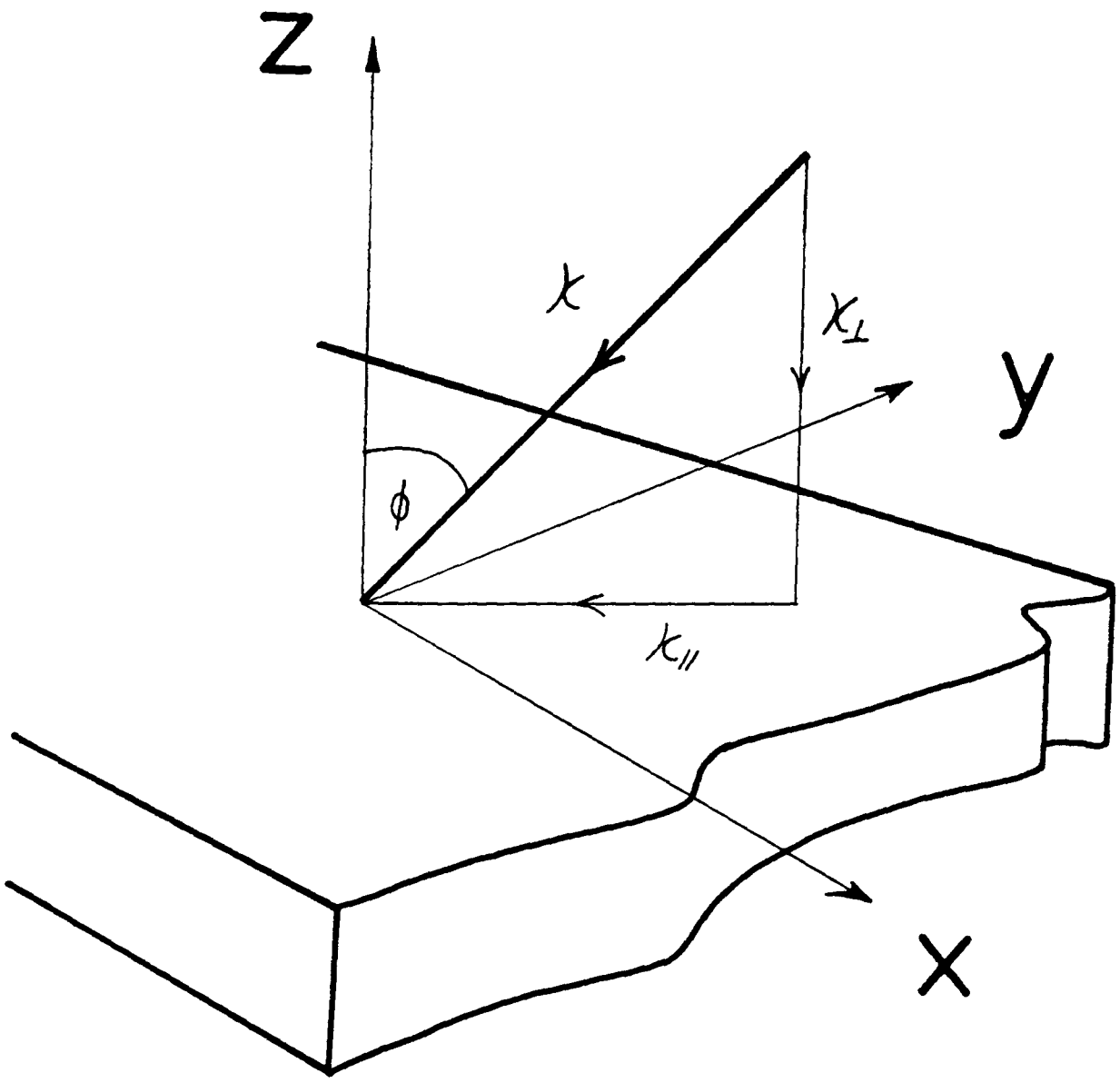

$$S^{\phi}_{TOT}(\kappa,w) = S^{\phi}_{TRANS}(\kappa_{\perp},w) * S^{\phi}_{ROT}(\kappa_{\perp},w) * S^{\phi}_{VIB}(\kappa_{\perp},w)$$

$$* S^{\phi}_{TRANS}(\kappa_{ll},w) * S^{\phi}_{ROT}(\kappa_{ll},w) * S^{\phi}_{VIB}(\kappa_{ll},w) \qquad (3.52)$$

The observed scattering law is the angle averaged value of this individual scattering law.

$$S_{TOT}(\kappa,w) = \tfrac{1}{2}\int_{0}^{\pi} \sin\phi d\phi \; S^{\phi}_{TOT}(\kappa,w) \qquad (3.53)$$

Attention must now return to the actual adsorbate/adsorbent system chosen in order to decide what are the likely kinds of motion adopted by the admolecule for a given set of conditions. Section 2.1 summarises the range of possible surface motion and section 1.2. discusses the information that neutron scattering might be expected to provide.

3.8 Scattering laws for possible admolecule dynamics

The HOPSCOTCH calculations show that the periodicity of the surface potential offers very low barriers to rotational and translational motion of the adsorbed molecule, at least for the temperature range of these experiments. In the plane of the surface the potential will be regarded as isotropic and structureless. The variation of potential perpendicular to the surface is calculated to be slow and markedly anharmonic. In view of the difficulty of quantitatively handling anharmonic vibrations, the first treatment will regard the potential as harmonic. Any deviations from this might be expected to show up as line broadening of any inelastic features present in the spectrum.

As finite surface coverages are reached so the lateral interactions of the admolecules increase and modify the dynamics.

The adlayer may show several phases, some similar to the bulk phases (see section 2.1). The first treatment will concentrate on these extremes of behaviour and investigate the two dimensional gaseous, liquid and solid phases.

The model that has been adopted has a macroscopic analogy in the bobbing for apples on Halloween night. The water in the bucket mirrors the adsorption potential. A single apple, or admolecule, may be pushed about on the surface of the water and will apin about any of its own axes with minimal hinderance. If pushed towards the bottom of the bucket the apple will perform a rapidly damped oscillation at the liquid interface. As the number of apples in the bucket increases so the translational motion decreases to nil when the first layer is filled. Adding more apples now gives a multilayer system where the quasi-crystalline character causes noticeable obstruction to spinning of the apples.

3.9 Quantitative treatments

3.9.1 Rotational scattering law

A) Methane and Ammonia

Taking into account.

1) The HOPSCOTCH results for the effect of the adsorbent on the rotation of a methane molecule on a carbon surface.

2) The experimental data on liquid and solid methane (80) (87), and liquid and solid ammonia, (88) (89) suggests that it will be a good approximation to regard the methane rotation as free, but only a fair approximation for ammonia. The rotational motion should certainly be unperturbed by the surface potential at these temperatures. Consequently one can use the standard three dimensional form of the scattering law given in equation 3.48 for methane and in reference (90) for ammonia. For methane this should be applicable to the gaseous, liquid and solid phases. For ammonia it will hold

for the gas phase, will be poor for the liquid phase and is unlikely to hold for the solid phase in view of hydrogen bonding.

B) Ethylene

No quantitative treatment exists at present to calculate the rotational scattering law for such an asymmetric molecule as ethylene. The situation is further confused in this instance by the presence of the surface. The planarity and geometry of the ethylene molecule make it quite energetically favourable for the molecule to lie flat on the surface with large barriers to rotation about axes parallel to the surface (91). In the solid phase rotational motion would be expected to be severely hindered.

Even in the case of the spherical top, methane, the calculation of the total 3D scattering law by convolution with the rotational scattering law is not trivial. In the CHARLOTTE program the following saving steps are taken.

1) The Bessel function series is truncated at j_{20}

2) Initial rotational states are limited to 15

3) Final rotational states are limited to 200

Even with these restrictions it is still only feasible to simulate a time of flight spectrum for a few selected angles of scatter, and extremely expensive in computer time to calculate any appreciable amount of the $S(\kappa,w)$ surface for a given set of operating conditions.

3.9.2 Translational scattering law

The adlayer is not strictly two dimensional as it is possible to move in a direction perpendicular to the surface. Large centre of mass movements in this direction correspond to desorption and a return to the gas phase for the admolecule. If the rate of desorption is very fast compared with the neutron observation time scale, then the scattered neutron spectrum will reflect the properties of the

unadsorbed molecule. The surface residence time can be estimated using the equation

$$\tau \simeq 10^{-13} \exp\left(\frac{Q}{k_B T}\right) \qquad (3.54)$$

derived by de Boer (35a). Q is the heat of adsorption. Table 3.1 gives the values so calculated for the systems studied in this work. As the neutron observation time scale is typically 10^{-11} to 10^{-12} secs, these residence times are seen to be generally three orders of magnitude longer. One can feel confident that the neutrons will be scattered from the adsorbed layer and not the desorbed molecules. Motion in the $\hat{z}$ direction will be restricted to small centre of mass oscillations and will only contribute via the vibrational scattering law. The process of jump diffusion whereby an admolecule may be "partially desorbed" and then readsorbed on a new surface site will be treated as motion in the xy plane.

Consider now the motion of the admolecule parallel to the surface. As has been mentioned earlier attention will be focused on gaseous, liquid and solid adlayers and the scattering laws. $S_x^{\phi}(\kappa,w)$ will be taken to be the same as the scattering laws for the corresponding three dimensional motion. Regarding the adsorption potential as structureless means that one is discarding the subtle ramifications of the surface that lead to lattice gases and Fermi liquids (26) at very low temperatures.

The process of jump diffusion might be expected to be important for the quasi-solid which will exist close to monolayer coverage. If there is a crystalline structure to the adlayer then there will be a definite jump geometry. If order is low then jump direction will be unimportant though it is reasonable to suppose that a well defined average jump length might exist.

Table 3.1

Surface Residence Times for Adsorbed Molecules

ADSORBENT	ADSORBATE	QADS kcal/mole	TEMPERATURE ^{o}K	τ x 10^{-9} secs.
Graphon	Methane	3.0	115	52.71
			127	15.18
			140	5.01
			148	2.79
			162	1.15
			176	0.55
Graphon	Ethylene	4.5	175	43.69
			185	21.64
			195	11.53
			204	6.89
			215	3.90
			235	1.59
Graphon	Ammonia	6.0	223	79.72
			242	27.43
			249	19.29
			254	15.18
			261	11.02

Q_{ADS} Isosteric Heat of Adsorption kcals/mole

$\tau \simeq 10^{-13} * \exp (Q_{ADS}/RT)$ see (35a)

$\tau_{NEUTRON} \simeq 10^{-11} - 10^{-13}$ secs.

3.9.3 Vibrational Scattering Law

As mentioned in section 3.3.1 vibrations contribute delta function intensity at multiples of $\hbar w$, where w is the fundamental vibration frequency. The intramolecular vibrations of these molecules are all relatively high energies, typically around 900-1000 cm^{-1}. Most of the molecules will be in their ground vibrational states at the temperatures used and the chief contribution they will make to the total scattering law is via a "Debye Waller" factor for these zero point motions. Using the Einstein model of the oscillator to derive an expression for u^2 in $\exp(-\kappa^2 u^2)$ gives, (22)

$$u^2 = \left\{ \frac{\exp(-\hbar w\beta)}{1 - \exp(-\hbar w\beta)} + \tfrac{1}{2} \right\} \frac{\hbar}{4\pi m w} \qquad (3.55)$$

The values of u^2 at $200^{o}K$ for chosen values of w are given below, together with the value of $\exp(-\kappa^2 u^2)$ for $\kappa^2 = 1.0 A^{0-2}$

w cm^{-1}	u^2 A^{o2}	$\exp(-\kappa^2 u^2)$
1000	0.0084	0.992
900	0.0094	0.991
800	0.0106	0.989
700	0,0122	0.988
600	0.0144	0.986

The effect of the intramolecular vibrations is thus seen to be virtually zero and they will be ignored.

3.9.4 Vibrations of the admolecule with respect to the surface

There are however, intermolecular vibrations, or more strictly vibrations of the admolecule with respect to the surface. As mentioned previously these are low frequency modes, generally less than 100 cm^{-1}. In the ideal case of a narrow distribution of harmonic motions these vibrations will contribute delta function intensities centred at multiples of $\hbar w_{\perp}$ and hw_{11} to be convoluted with

the other scattering laws. Whether there will be distinct peaks visible for such vibrations in the scattered neutron spectrum depends primarily on the form of the scattering law with which they are being convoluted. If the scattering law is for a gaseous molecule, or a liquid molecule with a large diffusion coefficient, then the inelastic feature may be so broadened as to be invisible. As the translational motion decreases and the adlayer "solidifies" so the possibility of picking up the vibrations of the admolecule with respect to the surface improves, since the convoluting scattering law is becoming more sharp. As an example of this figure 3.9 shows the simulated time of flight spectra for gaseous methane and 'solid' methane on a surface. These spectra represent the $w^2\ S^{\phi}_{TOT}\ (\kappa,w)$ for a single raft of adsorbent and are not yet angle averaged. They were obtained by convoluting the form of the three dimensional scattering law with the scattering law for a one dimensional harmonic oscillator, and then folding with the instrument resolution function for that energy window as documented by Harriman (92). The example of 'solid' methane is purely hypothetical and bears no relation to the true spectrum of solid CH_4. The spectrum was obtained from the spectrum of liquid methane by setting the diffusion coefficient very small so that the line broadening effects due to centre of mass motion are negligable in comparision to the machine resolution broadening. The intensity distribution in the inelastic region is that for the same temperature, $176^{o}K$, and the same angle of scatter, 45°, as the gas spectrum. It does at least serve to illustrate, that as the scattering laws to be convoluted sharpen up, so there is a much better possibility of observing the vibration frequencies of an adsorbed molecule with respect to the surface. There would seem to be little hope of making this measurement with any precision when the adsorbate possesses appreciable surface mobility.

FIGURE 3,9

OBSERVATION OF ADMOLECULE/SURFACE VIBRATION

Effect on the total scattering law of convolution with a broad translational scattering law

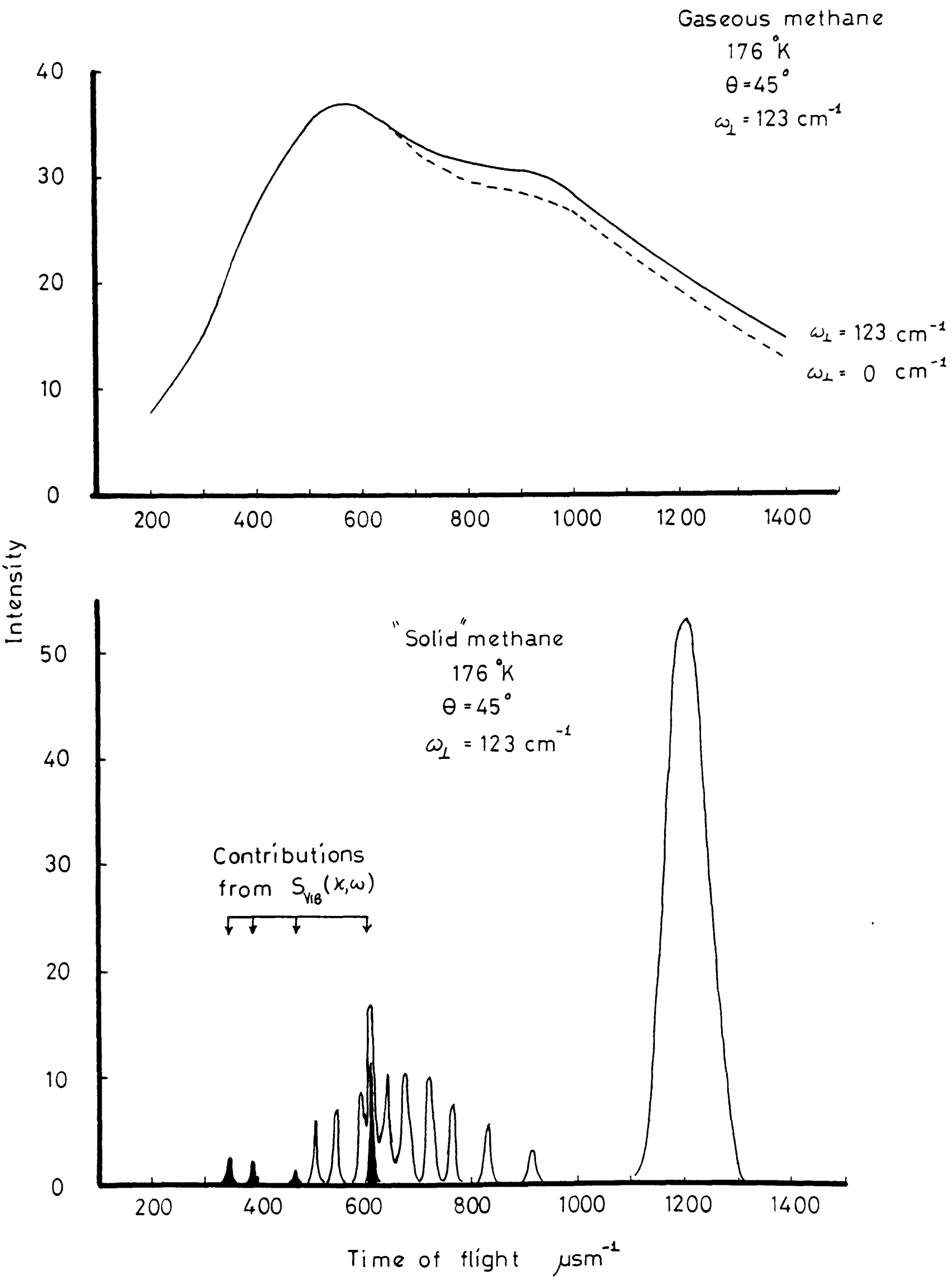

The broadening of an inelastic feature due to the centre of mass motion of the admolecule is most likely the reason why Verdan was unable to pick up a surface-admolecule vibration since he was working in a region of high surface mobility for the admolecule. It is also a plausible explanation of the disappearance of the $J = 0 \rightarrow 1$ transition of hydrogen molecules adsorbed on carbon at $40^{o}K$, as observed in the neutron scattering experiments of Nielsen (27). The result suggests that there is a phase change at $40^{o}K$ and the 'solid' adlayer of H_2 goes over to a phase of high mobility. The expected delta function intensity is then so broad as to be undetectable.

Whilst it may prove impossible to detect any inelastic features due to these surface-admolecule vibrations, there is nonetheless some information on this motion accessible from the "Debye Waller" factor for the quasi elastic peak. As the sample is polycrystalline only a single averaged frequency is applicable and the Debye Waller factor will be a consequence of both parallel and perpendicular vibrations.

Using Verdan's approach

$$< \frac{1}{w} >_{\Omega} = \frac{2}{3w_{11}} + \frac{1}{3w_{\perp}} \qquad (3.51)$$

If the admolecule can be treated as an einstein oscillator then

$$u^2 = \left\{ \frac{\exp(-\hbar < w >_{\Omega} \beta)}{1 - \exp(-\hbar < w >_{\Omega} \beta)} + \tfrac{1}{2} \right\} \frac{\hbar}{4\pi m < w >_{\Omega}} \qquad (3.56)$$

The einstein model might be expected to be most suitable for low surface coverages when the lateral interactions are small. As surface coverage and adatom interactions increase then it may be better to go over to a Debye model for the frequency spectrum, where $< w >_{\Omega}$ is now the maximum possible frequency. In which case

$$u^2 = \frac{3}{4} \left\{ \frac{1}{\beta \pi^2 m (< w >_{\Omega})^2} \right\} \qquad (3.57)$$

3.0 The Importance of the Quasi-elastic Scattering

It is clear that generally the quasi-elastic neutron scattering contains most of the desired information about the dynamics of the adsorbed molecule. The momentum transfer dependence of the shape of this feature should ideally enable

1) A distinction between different phases of the adlayer.

2) Determination of the mechanism of the centre of mass motion.

3) Depending on the appropriate model, an elucidation of the parameters.

a) Diffusion coefficient

b) Jump length

c) Jump Geometry

d) Site residence times.

The variation of the quasi-elastic peak intensity with momentum transfer reflects the admolecule-surface vibrations. These properties can be followed as a function of

1) Temperature - giving activation energies for motion

2) Surface coverage - to determine the effect of adatom-adatom interactions and their consequence for phase transitions.

3) Adatom type - when information on the role of the surface potential itself should be forthcoming.

If attention is to be focussed on the quasi elastic peak then it is necessary to inquire what the relative contribution from the inelastic scattering will be in this region. Is it reasonable to

a) Neglect the inelastic scattering?

b) Treat it as a background to be subtracted?

c) Or must it be included in a full scale calculation of $S(\kappa,w)$ for comparison with the actual data?

Consider the example of methane for which a relatively simple

calculation is possible. The intensity of a transition from the Jth to the jth level is proportional to

$$(2J + 1)(2j + 1) \exp(-B_j(j + 1)\beta) \sum_{|j-J|}^{j+J} j_n^2 (\kappa r) \qquad (3.58)$$

Table 3.2 gives the values of this expression for various possible combinations of j and J, and three different values of (κr) corresponding to angles of scatter of 27°, 45° and 90° for 6H, $\lambda_o = 4.8$ Å. The results are summarised in figure 3.10. The following points are evident.

1) Only terms where J = j or J = j ± 1 are significant as the rise in the terms of the Bessel function higher than j_2 is quite slow for the range of κ available.

2) The ratio of intensities of these two components is small for small κ but as the angle of scatter increases so the inelastic intensity increases to equal importance with the elastic peak.

The ease of separation of these components is dependent on their relative heights, and this intensity ratio reflects the relative areas, so the problem is not as bad as the graph suggests.

At 200^oK the most intense inelastic feature is the 6-5 transition. In this simple model for liquid CH_4 any inelastic feature has the same shape as the quasi elastic peak, that is lorentzian with a full width at half maximum given by $\Delta E = 2\hbar D\kappa^2$. Consequently in this case the ratio of the heights is the ratio of the areas, and the height of this 6-5 component can be taken as the height of the total inelastic component. This ratio as a function of (κr) is shown in figure 3.10. Even by a value $\kappa r = 3.0$ the ratio is not greater than 0.2. With the spectrometer configuration used in this work the maximum κr value is 1.85 when the ratio is approximately 0.075, so that it should be a good approximation to extract the

FIGURE 3,10

RELATIVE INTENSITIES OF THE ELASTIC AND INELASTIC COMPONENTS

$$T = (2J+1)(2J'+1)\exp\left(-BJ'(J'+1)/k_BT\right)\sum_{|J'-J|}^{J'+J} j_n^2(Kr)$$

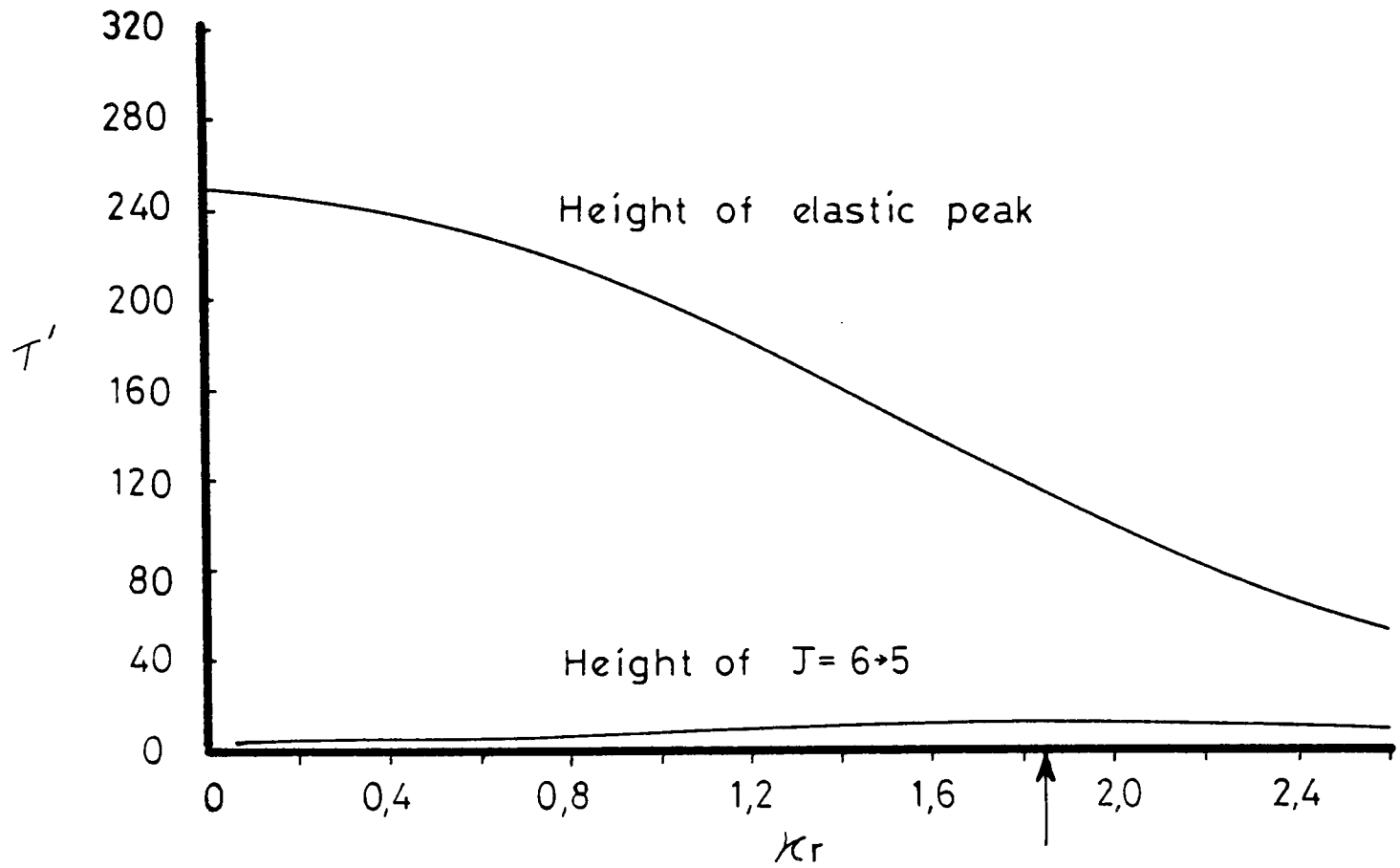

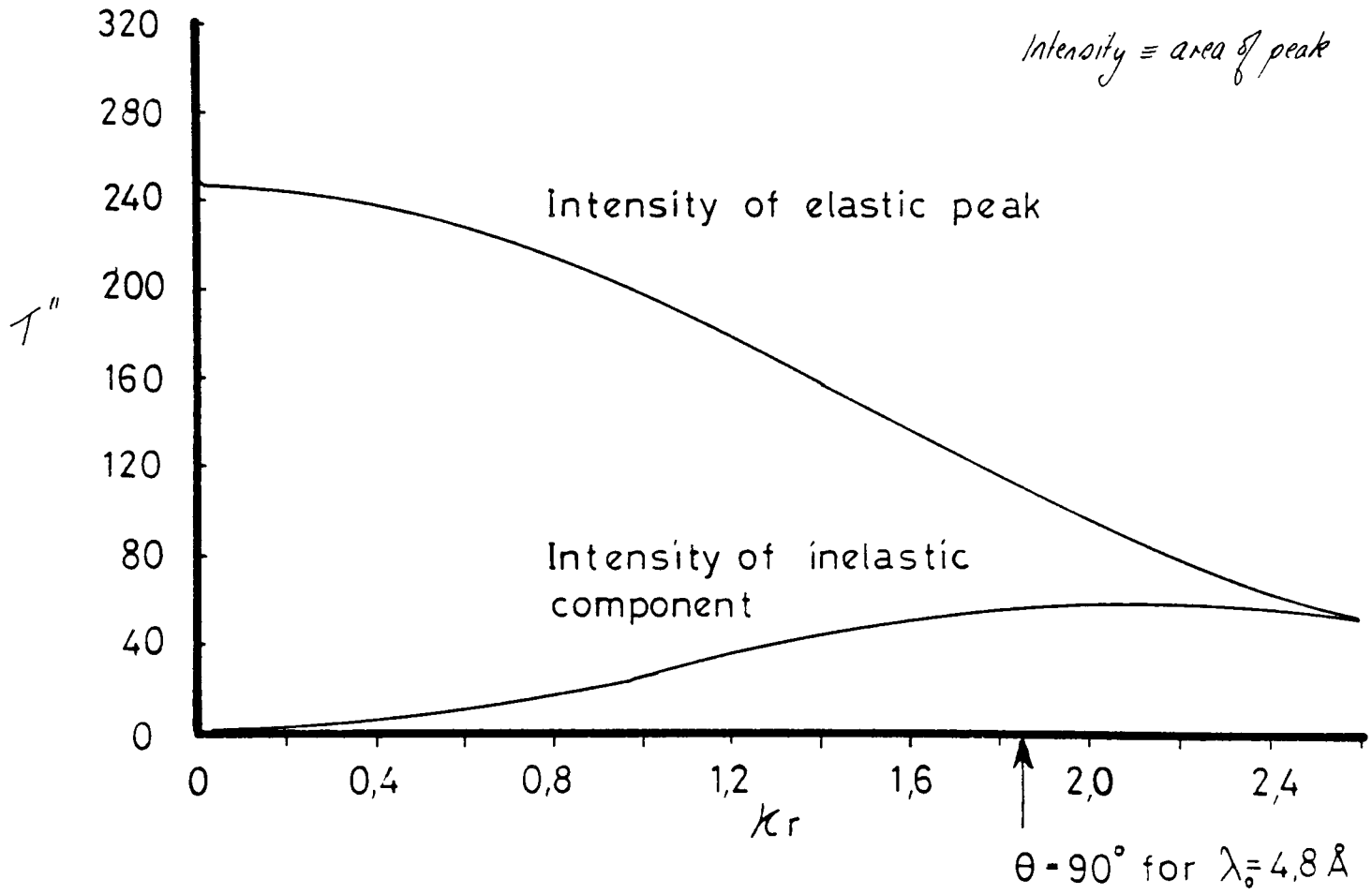

inelastic scattering from the quasi elastic scattering by subtracting a small flat background.

Since an observed spectrum contains background due to multiple scattering and machine 'noise' as well as the inelastic scattering, it is often uncertain at what level to draw the background. To rephrase the question slightly, what is the smallest energy window which will completely encompass the quasi elastic scattering?

A lorentzian curve has decayed away to 1% of its maximum height by 5 full widths at half maximum from the origin. A gaussian lacks such pronounced wings and is down to 1% by 2 full widths at half maximum from the origin. A Voigt profile falls somewhere in between these values depending naturally enough on the gaussian fraction. The policy followed in this thesis has been to go out from the origin to five full widths at half maximum of the Voigt profile and take the level at this point as the background level.

This discussion applied to $S(\kappa,w)$. The rotational envelope will be very visible in the time of flight spectrum (76)(79) since here one is observing the function $w^2S(\kappa,w)$.

3.11 Summary

The following models for the dynamics of the adsorbed molecule will be investigated.

1) A two dimensional gas possessing free translation in the xy plane. Translation in the $\hat{z}$ direction will be replaced by a harmonic vibration with the frequency as found by HOPSCOTCH.

2) A two dimensional liquid. As in 1) motion in the $\hat{z}$ direction will be assumed to be simple harmonic. In the xy plane translational motion will be governed by Fick's Law and quantified by a macroscopic diffusion coefficient D.

Table 3.2 Intensities of Rotational Transitions in Neutron Scattering for Methane

$$T = (2J + 1)(2j + 1)\exp(-Bj(j + 1)/k_B T) \sum_{|j - J|}^{j + J} j_n^2(\kappa r)$$

r_{CH} in CH_4 = 1.06 Å

κr	$j_0^2(\kappa r)$	$j_1^2(\kappa r)$	$j_2^2(\kappa r)$
0.6	0.886	0.037	0.001
1.0	0.708	0.091	0.004
1.9	0.248	0.187	0.034

Values of spherical bessel functions, for orders 0, 1, & 2 and various arguments, κr.

J = j

κr	0	1	2	3	4	5	6	7	8	9	10	TOTAL
0.6												231.247
1.0	0.708	6.688	16.068	25.333	31.329	32.562	29.428	23.578	16.950	11.020	6.517	200.181
1.9												109.000

J = j + 1

κr	1	2	3	4	5	6	7	8	9	10	11	12	13	14	TOTAL
0.6															11.666
1.0	0.273	1.269	2.560	3.713	4.368	4.392	3.879	3.056	2.169	1.397	0.819	0.440	0.217	0.098	28.650
0.9															58.950

Values of T for J, j and various arguments, κr.

Sum of all T values for J, j significant

3) A two dimensional solid. Any centre of mass motion will only be possible by jump diffusion. Three possibilities will be considered.

a) Jumping in a square lattice

b) Jumping in a triangular lattice

c) Jumping in random directions but with fixed jump length.

Only the quasi elastic scattering will be considered in any quantitative analysis attempted. All the dynamical information, except for any perturbations of rotational motion, will be contained in the κ dependence of the shape and intensity of the observed quasi elastic peak.

3.12 Simulation of the Scattering Laws for adsorbed molecules by the ORIANA and ORJUMP programs

The ORIANA and ORJUMP programs (57) were written to calculate the scattering laws for the three models described above and also to perform the numerical integration of equation 3.53. The total scattering law so obtained can then be convoluted with the desired machine resolution function and compared directly with the observed $S(\kappa,w)$.

One difficulty arises in performing the numerical integration. The value of $S^{\phi}(\kappa,o)$ goes to ∞ as $\phi \to o,\pi$, and this necessitates care in the computation. The trend to infinity is not disturbing in terms of the physical reality of the system, as the integral is a product with $\sin\phi$ and goes to zero as $\phi \to o,\pi$. To avoid problems with computational logic the integration was carried out between the limits $\frac{\pi}{50}$ (3.6^{o}) and $\frac{49\pi}{50}$ (176.4^{o}), closer approaches to the limits contributing negligably to the final value of the integral.

3.12.1 INPUT to the programs

1) ORIANA

The following parameters must be provided for the program IOPT

Flag for the model required

IOPT = 0 3D liquid
= 1 2D liquid
= 2 3D gas
= 3 2D gas
} scattering laws will be calculated

I CONV Flag for option on convolution with a desired machine resolution

= 0 YES
= 1 NO

RESLN The FWHM of the machine resolution gaussian in μeV

KA KB The initial and final values of the momentum transfer vector to be stepped over.

DD The diffusion coefficients for the liquid options

TEMP The temperature of the sample in ^{o}K

UU The value of u in the Debye Waller factor exp $(-\kappa^2 u^2)$

AMASS The atomic weight of the scattering centre.

2) ORJUMP

The ICONV, RESLN, KA, KB, UU, parameters are all common to this program. IOPT, DD, TEMP, AMASS are redundant and the following parameters must be provided instead.

IOPT Flag for the model required

= 0 Cubic lattice
= 1 Triangular lattice
= 3 Square lattice
= 4 3D random jump
= 5 2D random jump
} Scattering laws for jump diffusion in these geometrics will be calculated

ALEN The jump distance in $\mathring{A}$

TOR The site residence time in seconds.

3,12,2 OUTPUT from the programs

1) A list of the input parameters

2) The values of $S(\kappa,w)$ for a series of selected κ values over a range of ± 2400 μeV in steps of 100 μeV or 20 μeV as requested.

3) The shape of the peak is then characterised by a list of full widths at various fractional heights. The height and area of the peak for each κ value are also output.

4) A line printer graph of $S(\kappa,w)$ vs E in μeV.

3.12.3 Operation of the program

The expressions evaluated are as follows

1) 3D Liquid

$$S(\kappa,w) = \frac{1}{\pi} \frac{D\kappa^2}{(D\kappa^2)^2 + w^2} \exp(-\kappa^2 u^2) \qquad (3,59)$$

2) 2D Liquid

$$S(\kappa,w) = \frac{1}{2\pi} \int_0^{\pi} \sin\phi d\phi \frac{D(\kappa \sin\phi)^2}{\left[D(\kappa \sin\phi)^2\right]^2 + w^2} \exp(-\left[\kappa \sin\phi\right]^2 u^2)$$

(3.60)

3) 3D Gas

$$S(\kappa,w) = \left[\frac{\beta M}{2\pi\hbar^2\kappa^2}\right]^{\frac{1}{2}} \exp\left\{\frac{-\beta M}{2\hbar^2\kappa^2}\left[\hbar w - \frac{\hbar^2\kappa^2}{2M}\right]^2\right\} \qquad (3.61)$$

4) 2D Gas

$$S(\kappa,w) = \frac{1}{2} \int_0^{\pi} \sin\phi\, d\phi \left(\frac{\beta M}{2\pi\hbar^2(\kappa \sin\phi)^2}\right)^{\frac{1}{2}} \exp\left\{\frac{-\beta M}{2\hbar^2(\kappa \sin\phi)^2}\left(\hbar w - \frac{\hbar^2(\kappa \sin\phi)^2}{2M}\right)^2\right\}$$

(3.62)

5) Jump Diffusion in three dimensions

$$S(\kappa,w) = \frac{1}{\pi} \frac{f(\kappa)}{f(\kappa)^2 + w^2} \exp(-\kappa^2 u^2) \qquad (3.63)$$

where for

a) simple cubic lattice

$$f(\kappa) = \frac{1}{3\tau} \left(3 - \cos(\kappa_x \alpha) - \cos(\kappa_y \alpha) - \cos(\kappa_z \alpha)\right) \tag{3.64}$$

b) close packed lattice

$$f(\kappa) = \frac{1}{3\tau} \left(1 - \cos\left(\frac{\kappa_x \alpha}{\sqrt{3}}\right) \cos\left(\frac{\kappa_y \alpha}{\sqrt{3}}\right) \cos\left(\frac{\kappa_z \alpha}{\sqrt{3}}\right)\right. \tag{3.65}$$

c) 3D random jump

$$f(\kappa) = \frac{1}{\tau} \left(1 - \frac{\sin(\kappa l)}{\kappa l}\right) \tag{3.66}$$

6) Jump diffusion in two dimensions

$$S(\kappa,w) = \tfrac{1}{2} \int_0^{\pi} \sin\phi d\phi \frac{f(\kappa)}{f(\kappa)^2 + w^2} \exp(-\kappa^2 \sin^2\phi u^2) \tag{3.67}$$

where for

a) Polycrystalline square lattice

$$f(\kappa) = \frac{1}{2\tau} \left(2 - \cos(\kappa_x \alpha) - \cos(\kappa_y \alpha)\right) \tag{3.68}$$

b) Polycrystalline triangular lattice

$$f(\kappa) = \frac{1}{2\tau} \left(1 - \cos\left(\frac{\kappa_x \alpha}{\sqrt{3}}\right) \cos\left(\frac{\kappa_y \alpha}{\sqrt{3}}\right)\right) \tag{3.69}$$

c) Polycrystalline 2D random jump

$$f(\kappa) = \frac{1}{\tau} \left(1 - \sin(\lceil \kappa \sin\phi \rceil 1)}{\lceil \kappa \sin\phi \rceil 1}\right) \tag{3.70}$$

where κ_x, κ_y and κ_z are the components of κ

l is the jump length and τ the site residence time

3.12.4 Scattering Laws for Jump Diffusion

The forms of the scattering laws for gases and liquids have been discussed in previous sections. The scattering law for jump diffusion in these simple geometries was first formulated by Chudley and Elliott (93) and has been much developed in its application to the dynamics of interstitial hydrogen (94). The underlying assumptions in this treatment are as follows

1) The system possesses local lattice-like structure

2) The scattering centre will perform many oscillations between jumps.

3) The site residence time is much longer than the jump time

4) The oscillatory and diffusion motion are uncorrelated.

The first three assumptions are likely to be acceptable for an adlayer close to monolayer coverage. Item 4) is a common assumption throughout the correlation function approach to neutron scattering and its applicability has been discussed in section 3.3. It is not expected to be any worse an assumption for two dimensional phases than for bulk systems.

Whilst lorentzian in shape the behaviour of the scattering law with κ for jump diffusion is quite different to that for a liquid. The periodicity of the scattering centres motion in real space is reflected in a periodic variation of the scattering law with κ. The amount of broadening is determined by the residence time τ and the occurrance of maxima and minima in the broadening in determined by the jump length, α, and the jump geometry, through the trigonometric form of $f(\kappa)$. Thus for jump diffusion in a cubic lattice, minimum broadening occurs when

$$\cos(\kappa_x \alpha) = \cos(\kappa_y \alpha) = \cos(\kappa_z \alpha) = 1$$

$$\text{i.e.} \quad \kappa\alpha = 0, 2\pi, 4\pi \quad \text{etc.}$$

Figures 3.11 to 3.12 give the results of these calculations for illustrative systems. The data is summarised, in this instance, as a plot of fractional height in the (κ,w) plane of the S(κ,w) surface. In effect a contour representation of the surface. A quasi elastic peak as measured at a given angle on a time of flight machine is a cut at close to constant κ through this surface.

3.12.5 Discussion

Figure 3.14 shows how the dependence of the quasi elastic peak width on κ^2 ceases to be linear when the sample scattering law is convoluted with the machine resolution function and a Voigt profile results. The following discussion will concentrate on a comparison between the convoluted scattering law predictions.

Figure 3.14 compares the form of S(κ,w) for a 3D liquid and a 3D averaged 2D liquid of the same diffusion coefficient. The comparison is also made in section 4.2.3. as an example of the problems of deconvolution techniques in quasi elastic peak analysis. The immediate observation is that the 3D averaged 2D scattering law is much sharper than that of the 3D system and that the development of the function with increasing κ is primarily in the wings of the function. The difference can be seen more clearly on the log-log plot in Figure 3.13, which is a replot of the unconvoluted scattering law where the intensity coordinate is expressed as a fraction of the maximum intensity, and the energy coordinate as a fraction of the full width at half maximum (113). The corresponding curve for a gaussian and a lorentzian is also shown, any such type of function lying on the same generic curve when expressed in the reduced coordinate system. A Voigt profile would fall between the extremes of gaussian and lorentzian behaviour. The greater sharpness of the scattering law for a 3D averaged 2D liquid is quite clear as are the very broad wings of the function.

Figure 3,11

3D Fickian Liquid , $D = 2 \times 10^{-5}\ cm^2\ s^{-1}$

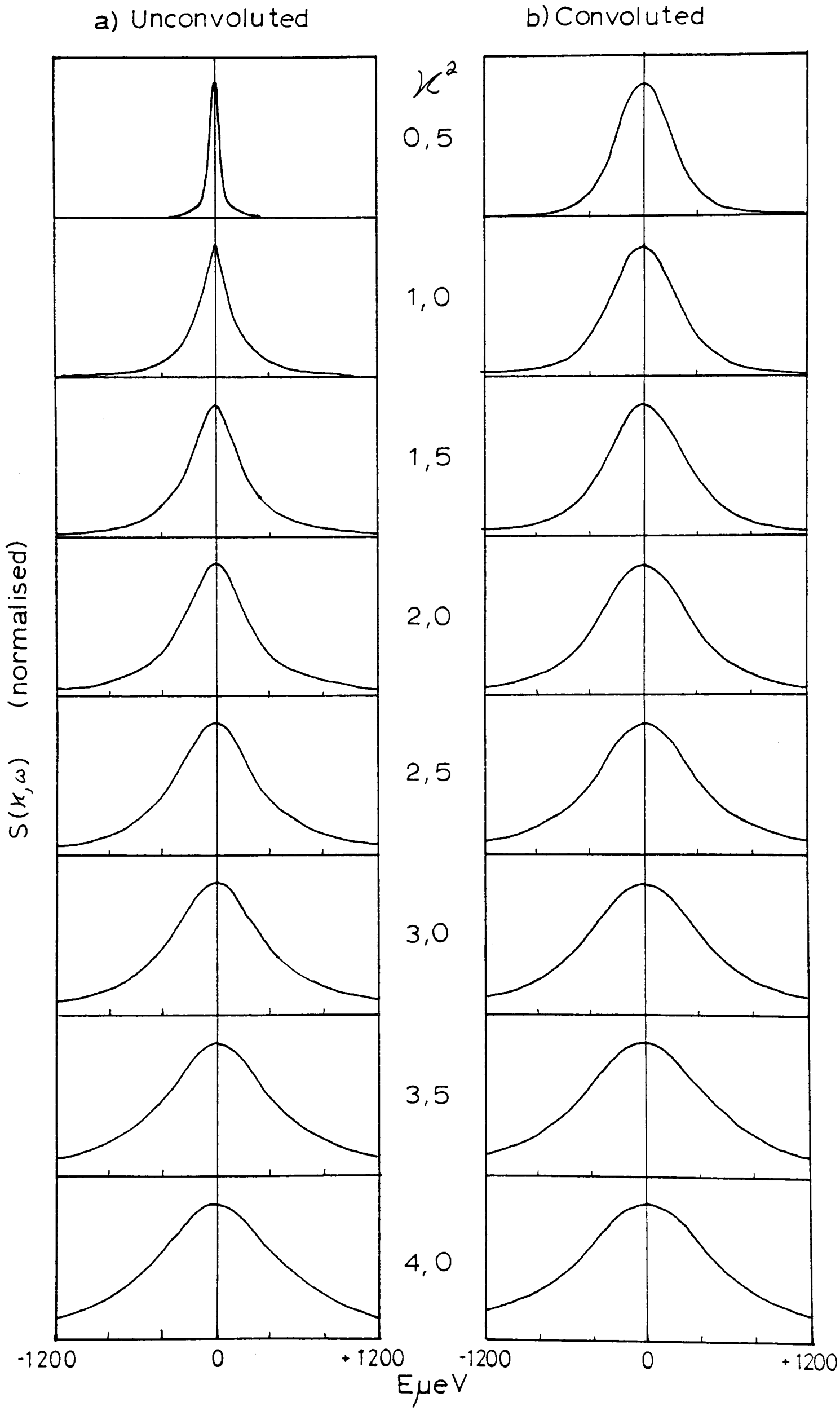

Figure 3,12

2D Fickian Liquid , $D = 2 \times 10^{-5}\ cm^2\ s^{-1}$

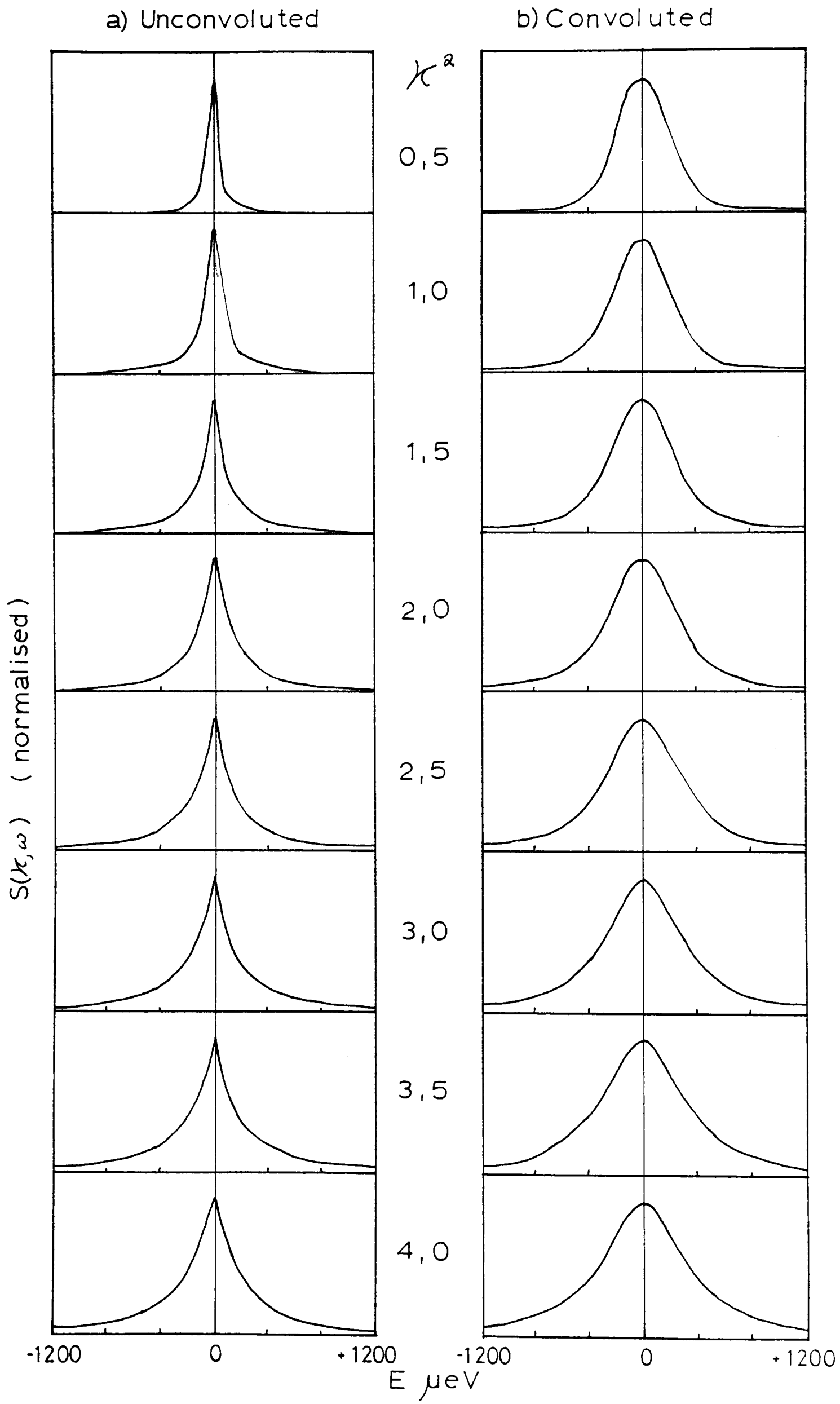

FIGURE 3,13

COMPARISON OF FUNCTION SHAPES

(i) Gaussian
(ii) Lorentzian
(iii) Averaged $S(k,\omega)$ for a 2D liquid, $D = 9 \times 10^{-5}\ cm^2\ s^{-1}$, $k^2 = 1,0\ Å^{-2}$
(iv) As for (iii), $k^2 = 2,0\ Å^{-2}$

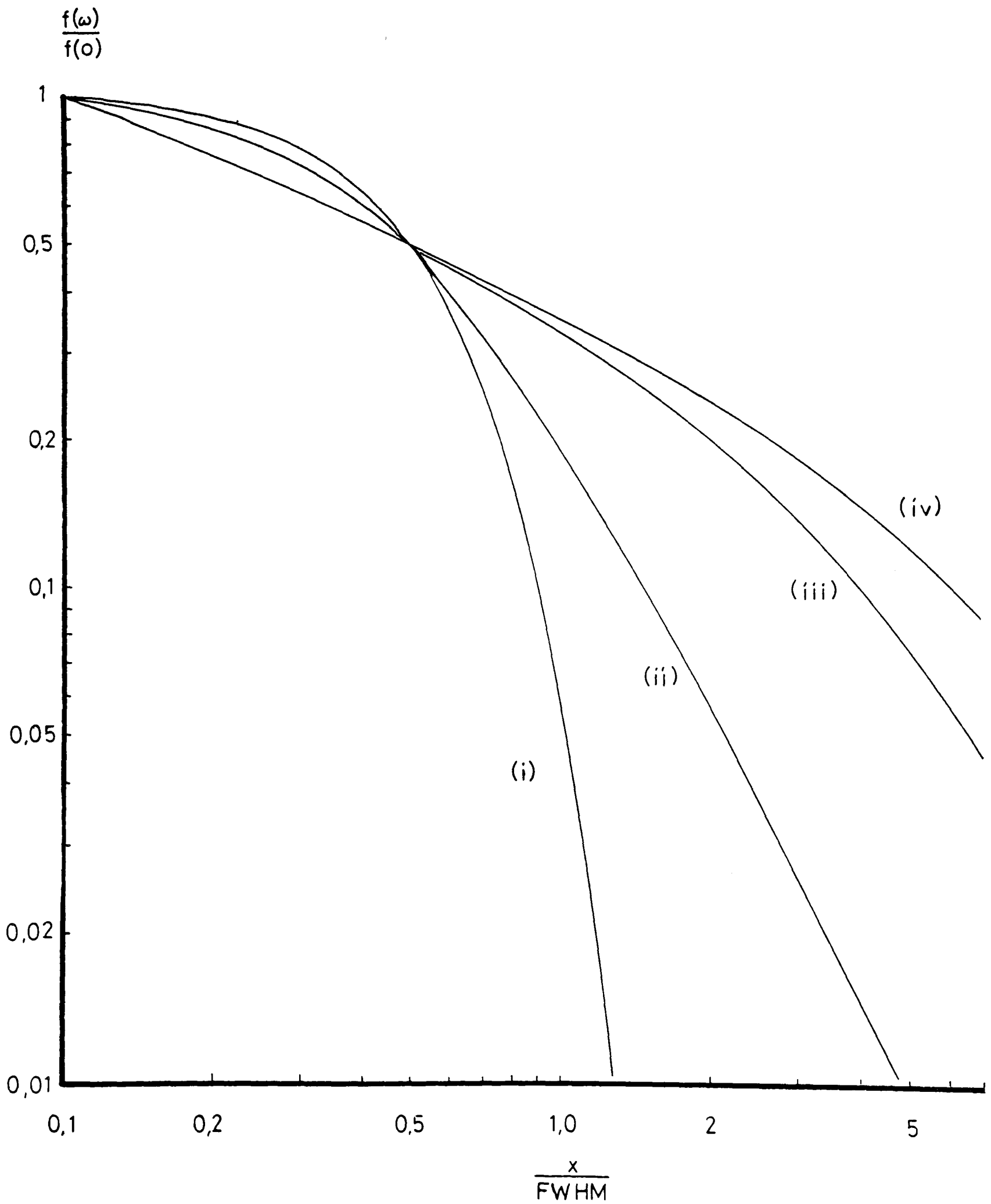

In the case of the scattering law for a gas the contrast between the 3D $S(\kappa,w)$ and the 3D averaged 2D $S(\kappa,w)$ is even more marked. See Figure 3.15. Again the 3D averaged scattering law is sharper but more important the maximum intensity remains located at $w = o$. For a 3D gas the recoil of the scattering nuclei causes the "quasi elastic" peak to shift into the inelastic region as κ increases. With the random 2D gas this recoil shift shows up as an asymetry in $S(\kappa,w)$ which develops with κ^2 in a similar fashion to the 3D gas scattering.

The sharpness of $S(\kappa,w)$ for the 3D averaged 2D motion can be understood by reference to the width function, $w(t)$, (95) characterising the self correlation function $G_s(r,t)$ for the adsorbed molecule.

$$G_s(r,t) = \int \exp\left\{-i\kappa r\right\} I_s(\kappa,t)\,d\kappa$$

$$= \int_t \exp\left\{-i\kappa r\right\}\exp\left\{-\kappa^2 w(t)\right\}\,d\kappa \qquad (3.71)$$

$$w(t) = \int_o^t dt_1 \int_o^{t_1} dt_2 \langle \vec{v}_K(t_2).\vec{v}_K(t_1)\rangle \qquad (3.72)$$

The two extremes of behaviour can be envisaged, $w(t)$, or loosely speaking the probability of finding the scattering centre within a chosen volume element can either go to zero or stay finite within the time interval considered. If the particle has sufficient mobility to move out of the volume element, e.g. a 3D liquid or a 3D gas, then $w(t)$ goes to zero and the transform $S(\kappa,w)$broadens and eventually becomes flat at large κ's. Conversely for a solid there is always a finite probability of finding the scattering centre within the volume element and the transform $S(\kappa,o)$ is a delta function. The adsorbed molecule falls into the latter class as however mobile it is in the x and y directions, it is always at a fixed point in the z direction and cannot recoil through the adsorbent surface.

FIGURE 3,14

$S(x,\omega)$ SURFACES FOR LIQUIDS WITH $D = 9 \times 10^{-5} cm^2 s^{-1}$
Convoluted with a machine resolution of 430 μev

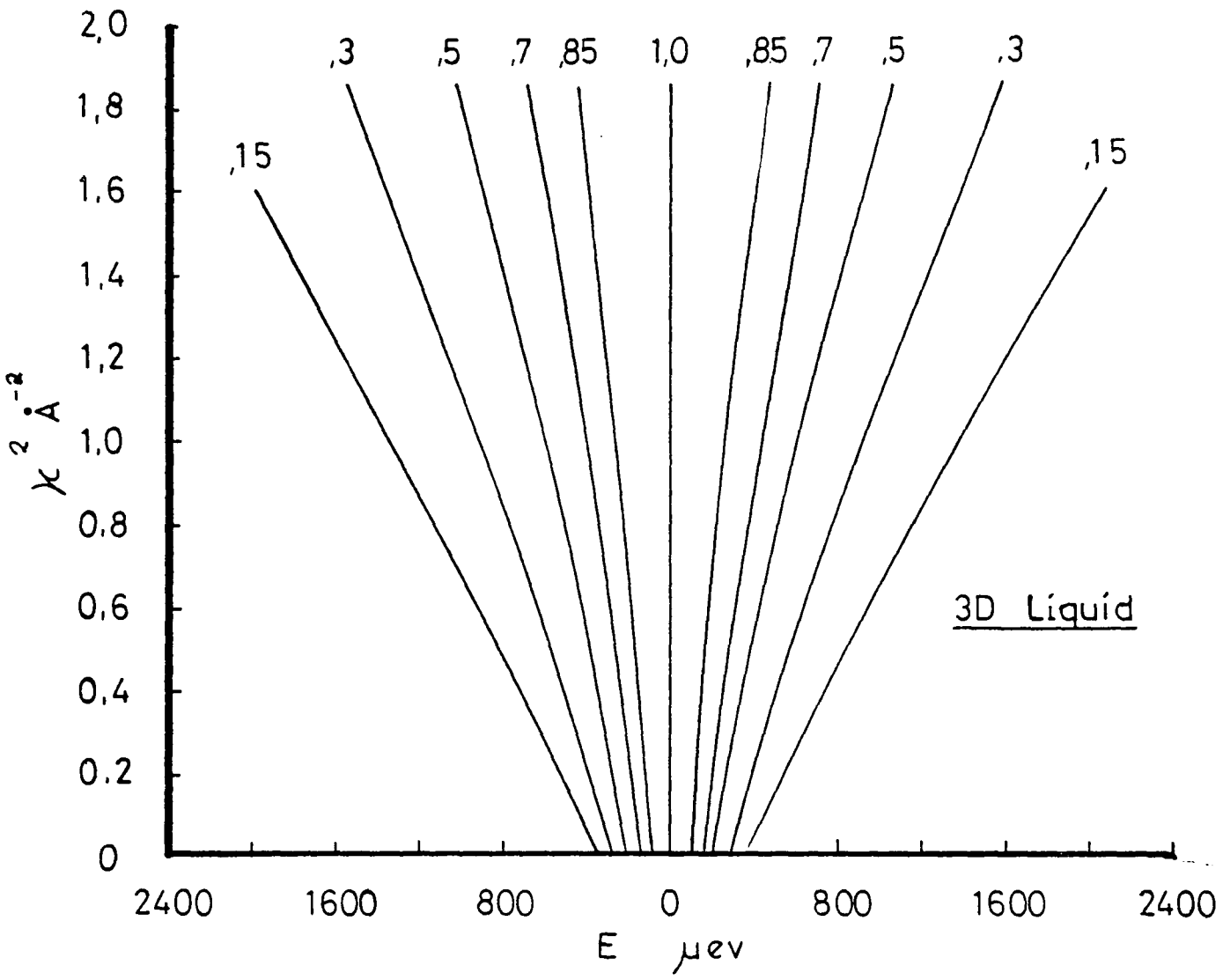

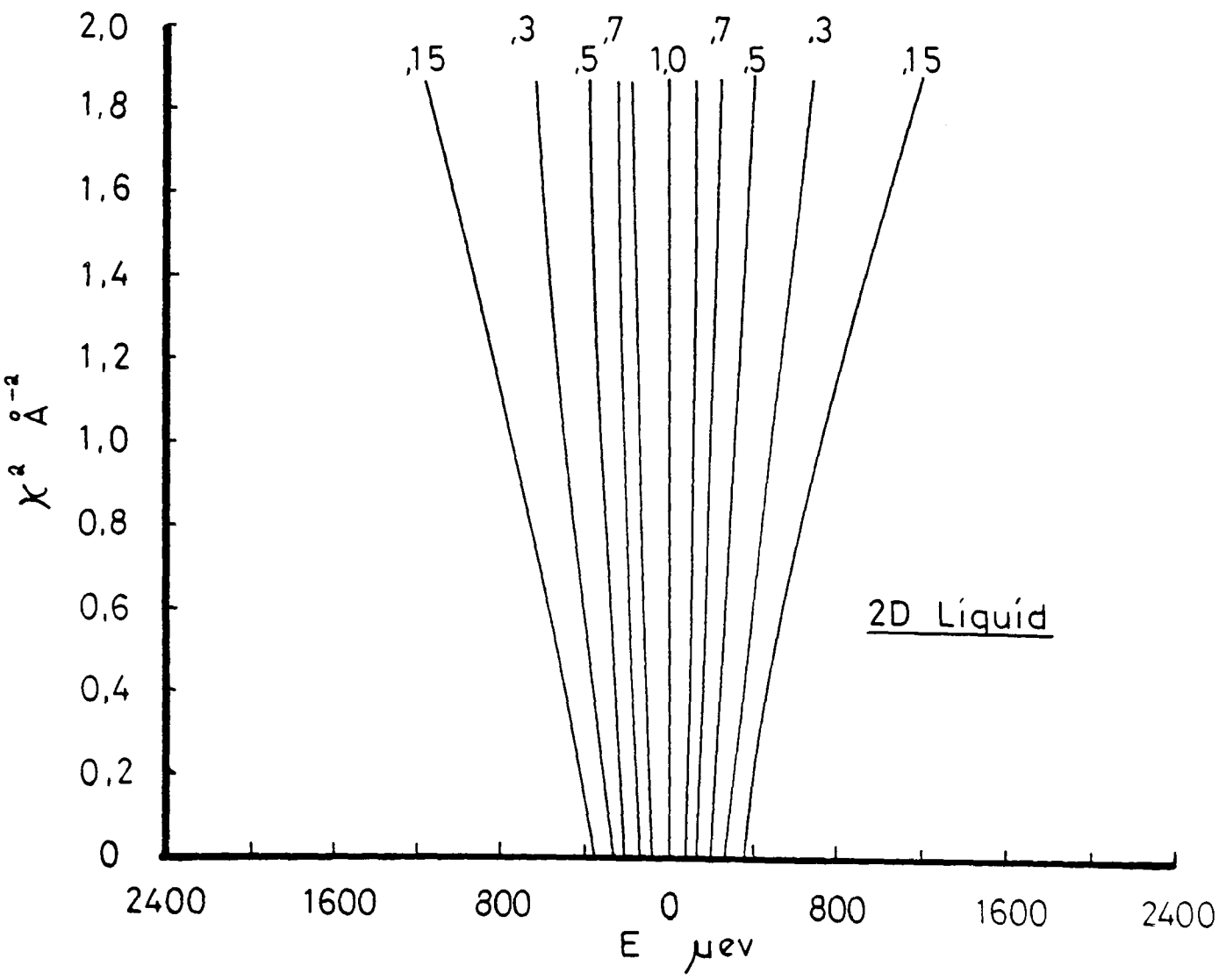

FIGURE 3,15

$S(k,\omega)$ SURFACES FOR M=16 GASES , T=176°K
Convoluted with a machine resolution of 430 μev

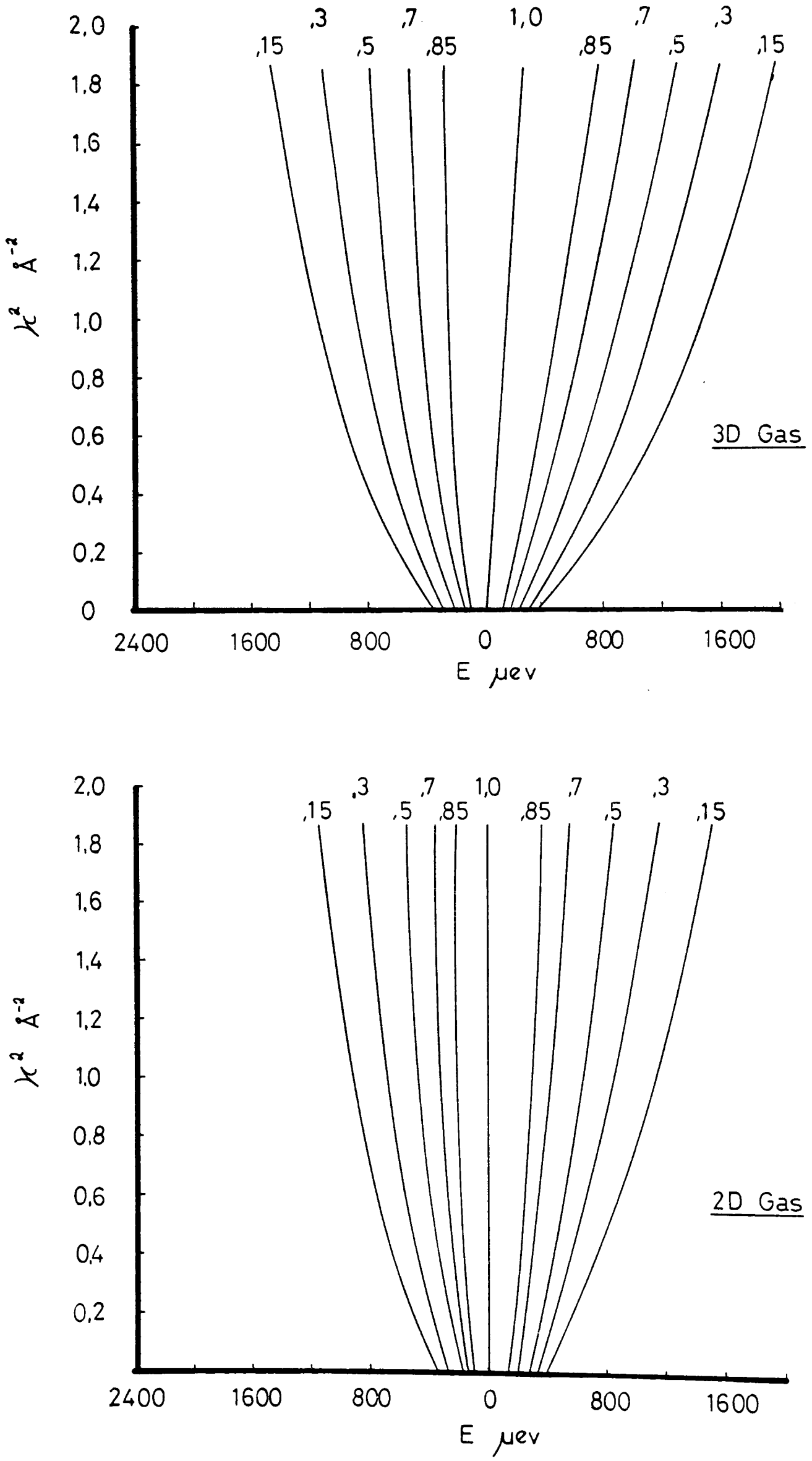

The averaging procedure modifies the expected scattering law for a particle jump diffusing, altering the shape of $S(\kappa,w)$ and the momentum transference dependence of that shape fluctuation.

CHAPTER 4: EXPERIMENTAL

4.1 Instrumentation

The neutron spectrometers used in this investigation fall into three general categories.

1) Solely elastic scattering instruments - powder diffraction and low angle scattering.

2) Inelastic spectrometers with large energy transfers, $100 < E < 1000\ cm^{-1}$.

3) Inelastic spectrometers with small energy transfers.

4.1.1 Elastic Scattering Instruments

In all cases experiments on these machines were aimed at characterising the adsorbents rather than the adsorbate behaviour.

The BADGER machine on the DIDO reactor at AERE Harwell is a conventional powder diffractometer (96) with a single detector moving in a horizontal plane. The use of the machine is described in (97) and its specification given in (98). The D1B instrument on the High Flux Reactor at the Institut Laue-Langevin, Grenoble, France, is a logical development of this simple design. Instead of a single counter there is a 400 unit multi counter mounted in the horizontal plane and covering an arc of 80°. This is not a high resolution machine but its particular attraction is the rapidity of data collection. With this feature it is possible to perform kinetic experiments, study phase changes directly, or analyse unstable samples, collecting the information over large regions of reciprocal space simultaneously.

The experiments that were performed on this machine were of a trial nature to test the instrument performance rather than to take advantage of the fast data collection times. The machine specification and description are given in (99).

The purpose behind these measurements was twofold. Firstly to investigate the macroscopic structure of the powders from the

broadening of the diffraction peaks and secondly, and perhaps more important, to determine accurately at what points in momentum space coherent effects from the adsorbent are manifested. Coherent elastic scattering from adsorbents swamps the weak incoherent scattering from the adsorbate rendering subtraction impossible. Wherever feasible one should work in a region of momentum space before the first singularity in the structure factor of the adsorbent. If this has a large lattice spacing eg. La-Y, then the first peak in the structure factor comes at a low κ value and this approach is not possible. In this case it is necessary to select an incident neutron energy such that with a given counter configuration the observations are made at κ values between those corresponding to the adsorbent diffraction peaks. The feature is discussed further in the sections on the individual adsorbents.

Complementary information on the macroscopic properties of these powdered adsorbents can be obtained from small angle neutron scattering. These experiments were done on the D11 instrument at the ILL . This is a high performance machine employing a two dimensional multidetector, 64 x 64 cm^2 comprising 4096 elements. The incident wavelength is obtained with a helical velocity selector and can vary from 6 to 20 $\mathring{A}$. The scan through momentum space is further extended by the ability to place the detector at distances varying from 66 cms to 80 metres behind the sample. The use of this machine is described in (100) and its specification given in (101).

4.1.2 Inelastic Spectrometers with large energy transfers

The intention of carrying out measurements of transitions in the energy range 200 - 1200 cm^{-1} was firstly to see if there were any perturbations of the internal molecular modes of the adsorbate brought about by interactions with the adsorbent.

Secondly if a crystalline lattice is formed by the adsorbate then the observation of external molecular modes will give the site

symmetry, and if accurate intensity measurements are possible then intermolecular force constants are calculable (102).

Neutron scattering spectroscopy in this energy range can be carried out with a down scattering filter machine. The design and operation of the beryllium filter machine (BEF) on the PLUTO reactor at AERE Harwell on which all such measurements were made, are described in (103). The use of this machine in a variety of investigations has been reported in (104).

4.1.3 Inelastic Spectrometers with small energy transfers

These experiments were performed on the 6H and 4H5 time of flight spectrometers (TOF) on the DIDO reactor at AERE Harwell.

In contrast to the diffraction instruments which measure $S(\kappa)$ i.e. $\int_{-\infty}^{\infty} d\omega\, S(\kappa,w)$, and the BEF which takes a single cut through $S(\kappa,w)$ space, the time of flight machines take a series of paraboloid cuts through $S(\kappa,w)$ space, the limits of which are determined by the incident neutron energy and the disposition of the scattered neutron counters. (105). Because of this such machines extend the inelastic measurements possible with the BEF to very low energy transfers, $< 100\ cm^{-1}$, but more importantly can be used to monitor the properties of $S(\kappa,w)$ around $w = o$, the so-called quasi elastic peak region, where the effect of diffusive processes is manifested.

The design, operation and specifications of the 6H and 4H5 spectrometers are given in (106). In these preliminary experiments no especial advantage was taken of the cold source on 4H5 to go to longer neutron wavelengths and so improve the quasi elastic peak resolution. Both TOF machines were used with similar operating parameters.

4.2 Data Handling

4.2.1 Elastic scattering spectrometers

The output from these machines consists of the number of

neutrons scattered through a particular angle by the sample, for a given flux of neutrons incident on that sample. Since the experiments only required the determining of peak widths and positions, corrections to obtain accurate intensities were not applied. In all cases it was felt to be sufficient to take the raw data, subtract a suitably scaled set of blank data, and obtain the required parameters from the residue.

On the single detector BADGER machines this is a straight forward process once an accurate calibration of the machine zero angle has been made with a standard nickel sample. Such a calibration is also necessary for D1B but the use of a multi detector counter on this machine does produce another difficulty. The detectors consist of a pair of wires, 0.1 mm in diameter, 5 mm apart, at a potential of 3KV in an atmosphere of ^{3}He gas at a pressure of 4 atms. There are 400 such detectors over the whole arc. Ideally each pair should respond to the arrival of a neutron within its vicinity independently of its neighbours. In fact this is not the case and it is necessary to run a vanadium standard. This is a completely incoherent scatterer giving rise in principle to a flat background. The observed diffraction pattern is then scaled to the actual vanadium pattern. This is carried out automatically, the incoming sample raw data being collected in a multichannel analyser, transferred to filestore on the NICOLE computer and there manipulated with standard programs. The corrected data is output to the teletype at the instrument as the experiment progresses.

The D11 low angle scattering machine also requires such a calibration but lacks the facility for automatic processing. A vanadium standard was run during the sequence of experiments, and the sample data scaled accordingly by hand.

4.2.2 Inelastic spectrometers with large energy transfers

A critical approach to the use of the BEF for molecular spectroscopy requires the answer to two questions.

1) At what energy in the 42 cm^{-1} neutron filter energy window is the maximum scattered intensity and how is it peaked? i.e. What is the resolution function of the instrument?

2) What is the resolving power of the machine and how is this a function of the energy of the transitions being scanned?

The work of B Haywood et al. (107) was felt to be incomplete in view of the better incident beam collimation now available (0.6^{o} as opposed to 1.2^{o}), and the observation of systematic deviations in the determination of transition frequencies compared with the optical data, at energies below those that (107) were concerned with. It has been found by P. Gamlen et al (103) that the resolution function of the instrument is asymmetric and this asymmetry is related to the take off angle from the monochromator crystal and hence to the value of the energy being scanned. The displacement correction so calculated agreed with that of Haywood in the limit of large take off angles, i.e. large energy transfers. A plot of this energy dependent displacement correction is given in figure 4.1. Spectra taken on the BEF are presented with a constant 25 cm^{-1} displacement. Quoted values of transition energies have been fully corrected using figure 4.1.

It must be borne in mind that the BEF does not measure a density of states either at constant or zero momentum transfer. The energy and κ values are linked and their form is shown in figure 4.2. The consequence of this is twofold.

1) The width of any transition is directly related to κ as

$$\Delta E \quad \alpha \quad \frac{\hbar^2\kappa^2}{2M\beta} \qquad (4.1)$$

FIGURE 4,1

BERYLLIUM FILTER DISPLACEMENT CORRECTION FACTOR



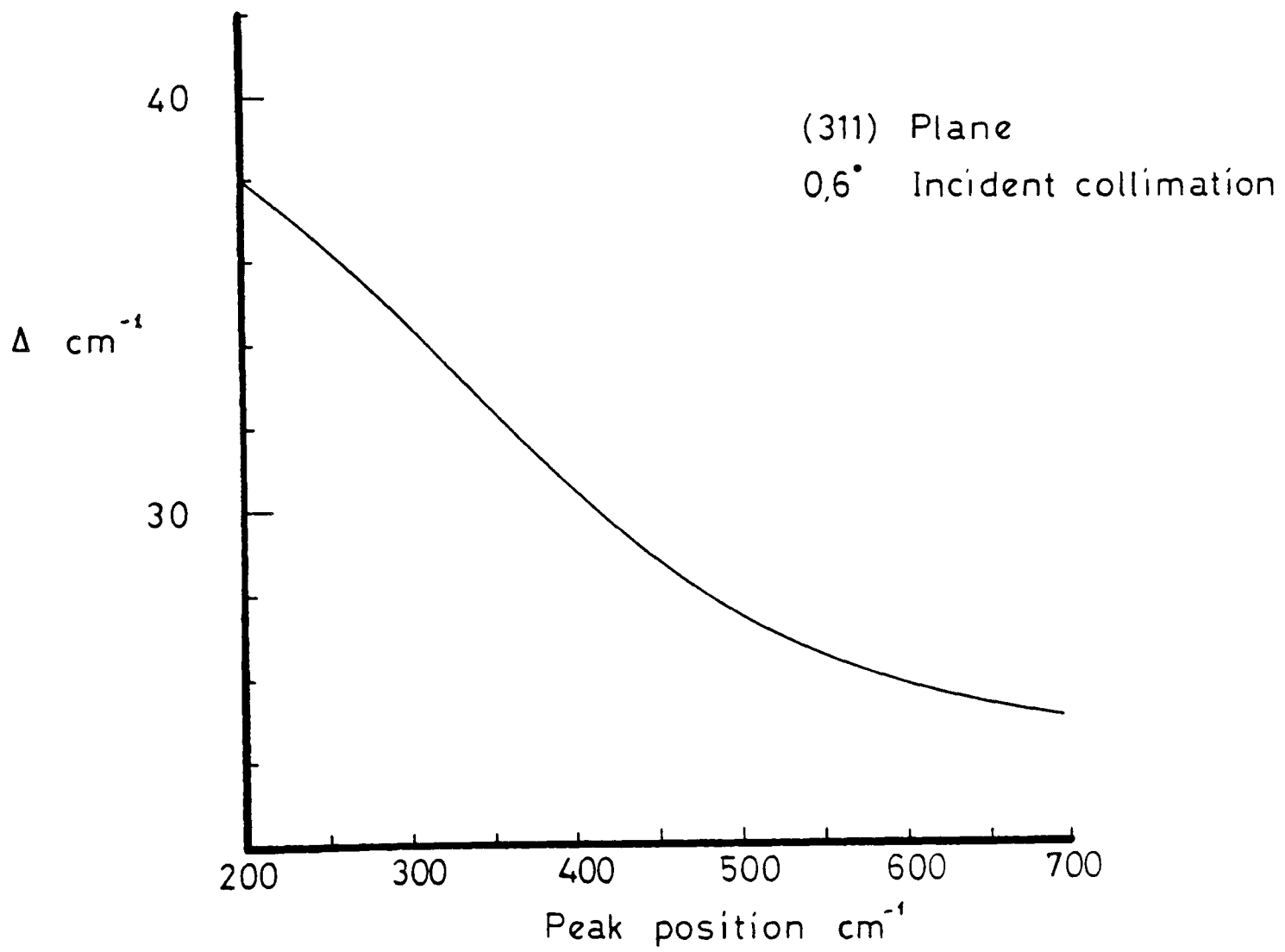

FIGURE 4;2

BERYLLIUM FILTER - (E, κ) RELATION

$$\kappa^2 = \frac{2m}{\hbar^2}\left\{E_i + E_f - 2\sqrt{E_i E_f}\cos\alpha\right\}$$

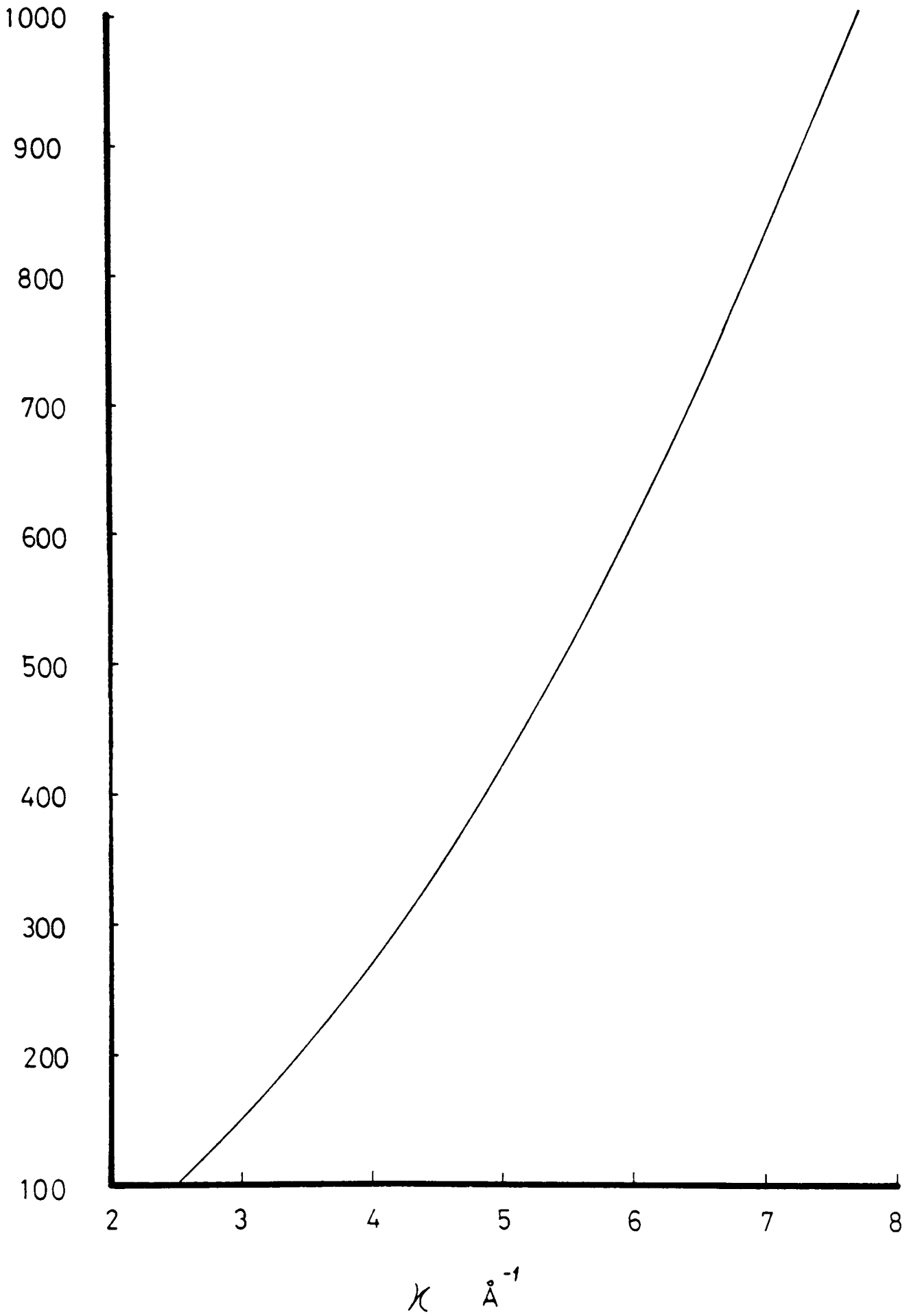

The background due to the multiphonon contribution will also increase with κ. The combination of these effects will tend to smear out the higher energy transitions (108). No calculation of multiphonon effects have been done for the spectra shown in this thesis.

2) The significant momentum transfer is, however, an advantage in one respect in that at large κ values one will be operating in the free particle limit (109). The neutron wavelength is much smaller than interatomic distances, so the scattering cross section applicable is now that for the unbound atom. Coherently scattering nuclei that might be expected to be unsuitable for such an experiment are in practice capable of giving good intensity because of this feature.

4.2.3 Time of flight instruments

The raw data from an experiment consists of the number of neutrons detected at each counter in a given timing channel over the chosen time period of the experiment. This raw data is collected on magnetic tape and reduced by the program suite at the RHEL NBRU (82). The treatment is a three step process. The first operation, PRESCAT, is to characterise the instrument configuration from the vanadium standard scatterer and the monitor peaks. This step is independent of the User and his sample. It provides the User with fundamental parameters such as the incident time of flight, total detected counts at any given angle, the centre of gravity of the elastic peak for each angle, the time zero channel, the total flux incident on the specimens.

The next two steps, CIRCA and ROUNDABOUT, are wholly dependent on the User and the sample in question. With the machine configuration characteristics obtained from the first step one can then normalise the raw data, correct it for counter efficiencies,

subtract a chosen blank and then convert the corrected time of flight spectrum into a scattering law. The third step is to select an initial analysis procedure, either for this scattering law or the corrected counts. For example it is possible

a) To invoke routines to fit the time of flight spectrum and report any singularities

b) Analyse the quasi elastic peak reporting peak areas and widths.

c) Or extrapolate $S(\kappa,w)$ to give $S(o,w)$ and hence construct $g(w)$, the density of states.

The two basic equations of this analysis are as follows.

A) Calculation of corrected counts

$$Yc = \left\{ \frac{A_1 \, C_{IN}}{V_{IN}} - \frac{A_2 \, C_{OUT}}{V_{OUT}} \right\} \frac{N\sigma_V}{N\sigma_S} \frac{1}{\delta\tau} \frac{1}{A_3} \frac{\varepsilon\tau o}{\varepsilon\tau} \qquad (4.2)$$

C_{IN} and C_{OUT} are respectively the raw counts for the sample and the blank in a given time channel corresponding to a time of flight τ.

V_{IN} and V_{OUT} are the vanadium normalising counts for the sample and the blank.

$N\sigma_V$ and $N\sigma_S$ are the percentage scatter of the vanadium standard and the sample respectively.

A_3 is a scaling factor to compensate for the absorption of neutrons by the vanadium.

$\delta\tau$ is the time of flight increment for each channel.

$\frac{\varepsilon\tau o}{\varepsilon\tau}$ is the counter efficiency correction term. Note that normalisation to vanadium gives an absolute value to the cross section at the zero energy transfer point. So that $Yc = Y$ at τ_o.

A_1 and A_2 are scaling factors between the sample and the blank with respect to the vanadium. Normally the value of A_1 is given by $\frac{M1VAN}{M1SAM}$ where M1VAN is the total neutron flux on the vanadium and M1SAM is the total neutron flux on the sample. A_2 is calculated similarily.

However in the kind of experiments performed here two other factors have to be taken into account.

1) In all cases except when an aluminium foil sachet was used, the percentage scatter from the sample can was significant. This necessitated using exactly the same sample can and adsorbent as a blank. The usual procedure for running a blank spectrum was to pump out the adsorbate at room temperature after the sample runs were complete. In this way no scaling for different amount of adsorbent between blank and sample runs was necessary, and another possible source of error eliminated.

2) The sample consists of an adsorbent, adsorbate and sample can. The blank comprises both the adsorbent and can. If the adsorbent and adsorbate both have appreciable percentage scatter, then the adsorbent in the sample run will be scattering less than the same adsorbent in the blank run. This occurs because the adsorbate scattering has attenuated the beam. Correction factors based on the calculations of C Carlile (110) were employed. Some representative values are shown in table 4.1. One can see that for high adsorbate scattering the corrections are large, and if not employed one would be subtracting 30% more than the blank required.

B) Calculation of the Scattering Law

$$S(\alpha,\beta) = Yc. \frac{k_B T \exp(\frac{\beta}{2}) \tau^4 10^{-16}}{m\tau_o} \qquad (4.3)$$

where $\beta = \frac{\hbar w}{k_B T}$ $\alpha = \frac{\hbar^2 K^2}{2Mk_B T}$

The scattering law observed is not however the pure scattering law for the system. It is a convolution of the scattering law and the response function of the neutron instrument. The fundamental problem of an incoherent quasi elastic scattering experiment is to unravel the scattering law for the sample, since

the resolution function of the machine is readily available from the vanadium scattering. At the present time with the machines available there exist two possible approaches:-

1) Model a feasible scattering law for the sample. Convolute it up with the machine resolution function to obtain a simulated scattering law, $M(\kappa,w)$

$$M(\kappa,w) = \int_{-\infty}^{\infty} S(\kappa,w-w^1)\ G(w)\ dw \qquad (4.4)$$

Fit this to the observed data and then manipulate the variable of the model scattering law so as to obtain the bast fit.

2) Attempt to deconvolute the scattering law directly. There are problems with both methods. The first appraoch is generally favoured. However:-

a) Only for very simple systems is it possible to set up a valid scattering law. For ease of computation it is necessary to make approximations, with the result that the possibility of a good fit to the data recedes.

b) The data is not generally good enough to give one a sensitive test of the model, and ambiguities over the parameterisation will persist.

The second method has found much favour for the analysis of neutron scattering data from liquid systems. If one assumes that the observed scattering law is a convolution of a single gaussian machine resolution function and a single lorentzian function describing the systems dynamics, the the technique of J Tudor, Davies, et al (111) is applicable (112). The errors in this method can be divided clearly into systematic and random errors. The latter are very dependent on the relative amounts of gaussian and lorentzian in the observed Voigt profile. This is dependent on the machine resolution and the time scale of the process under observation. The problem has

Table 4.1

Attenuation Factors

SURFACE COVERAGE	ANGLE OF SCATTER								
	18	27	36	45	54	63	72	81	90
Methane on Graphon									
0.58	1.1235	1.1198	1.1177	1.1171	1.1177	1.1198	1.1235	1.1294	1.1388
0.52	1.1090	1.1058	1.1040	1.1034	1.1040	1.1058	1.1090	1.1143	1.1225
0.43	1.0913	1.0886	1.0871	1.0886	1.0871	1.0886	1.0913	1.0956	1.1024
0.42	1.0877	1.0851	1.0837	1.0833	1.0837	1.0851	1.0877	1.0919	1.0984
0.30	1.0634	1.0615	1.0605	1.0602	1.0605	1.0615	1.0634	1.0664	1.0710
0.23	1.0463	1.0450	1.0442	1.0440	1.0442	1.0450	1.0463	1.0485	1.0518
Ethylene on Graphon									
2.10	1.4050	1.3916	1.3843	1.3819	1.3843	1.3916	1.4050	1.4267	1.4609
1.80	1.3341	1.3234	1.3175	1.3156	1.3175	1.3234	1.3341	1.3515	1.3789
1.30	1.2545	1.2466	1.2422	1.2408	1.2422	1.2466	1.2545	1.2673	1.2875
1.10	1.2185	1.2118	1.2081	1.2069	1.2081	1.2118	1.2185	1.2793	1.2463
1.00	1.1797	1.1742	1.1713	1.1703	1.1713	1.1742	1.1797	1.1884	1.2021
0.80	1.1532	1.1486	1.1461	1.1455	1.1461	1.1486	1.1532	1.1606	1.1722
Ammonia on Graphon									
1.00	1.1349	1.1306	1.1285	1.1277	1.1285	1.1306	1.1349	1.1416	1.1510
1.44	1.1941	1.1880	1.1850	1.1839	1.1850	1.1880	1.1941	1.2080	1.2173
1.54	1.1950	1.1900	1.1867	1.1855	1.1867	1.1900	1.1950	1.2180	1.2323
0.86	1.1160	1.1124	1.1106	1.0980	1.1106	1.1124	1.1160	1.1218	1.1299
0.55	1.0742	1.0718	1.0707	1.0702	1.0707	1.0718	1.0742	1.0779	1.0831
0.51	1.0687	1.0666	1.0655	1.0651	1.0655	1.0666	1.0687	1.0722	1.0770
0.23	1.0310	1.0301	1.0295	1.0293	1.0295	1.0301	1.0310	1.0322	1.0347

been investigated by A Taylor (113). To summarise if there is an error of α on the measurement of the full width at half maximum (FWHM) of the Voigt profile, then the error on the width of the deconvoluted lorentzian is given by

$$\delta E = \alpha A(x)$$

$$A(x) = 1 + \frac{2x^2}{y} \qquad (4.5)$$

Where x is the gaussian fraction, and y the lorentzian fraction. To put this result in perspective it is necessary to consider a possible scattering law and contrast the results of observing that process with neutron spectrometers of different resolution. The results are summarised in figure 4.3. If the system can be described by a hydrodynamic diffusion coefficient of 2×10^{-5} cm^2s^{-1} then a measurement on 4H5 in normal use will, at a κ^2 value of 1.0 A^{0-2} return a value of $(2 \pm 0.2) \times 10^{-5}$ cm^2s^{-1}, but IN5 (114) at the same κ^2 value will return a value of $(2 \pm 0.05) \times 10^{-5}$ cm^2s^{-1}. This is assuming an initial measurement error on the half width of 3% in both cases.

These random errors are of course errors from experiments performed with ideal machines, with ideal data analysis on the simplest possible dynamical system. There are two sources of systematic error that make the use of deconvolution methods extremely suspect.

A) Backgrounds

The parameters used to characterise a Voigt profile are sensitive in varying degrees to the level of background assigned. If there is appreciable broadening then the decay of intensity with energy in the wings of the function is slow. A wrong background will have a marked effect on the area but lesser effects on the height and widths measured for the peak. Ambiguity in the size of the background has two sources.

FIGURE 4,3

GAUSS LORENTZ DECONVOLUTION ERRORS

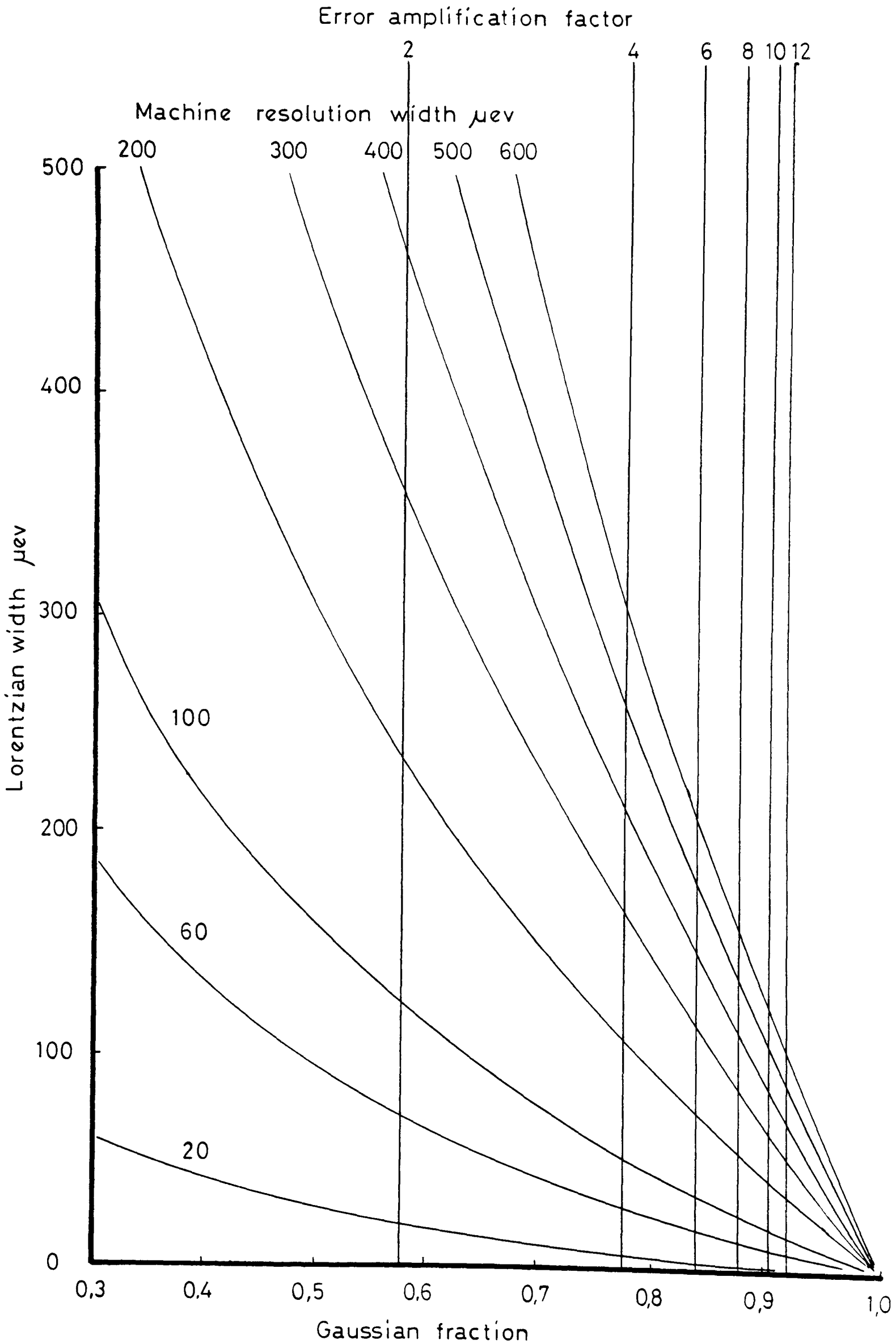

1) Definition of the energy range that is quasi elastic. The ROUNDABOUT Program, DYLAN, used for quasi elastic peak analysis selects an energy window to view $M(\kappa,w)$ through by determining the rate of change of slope with energy of the curve it has fitted through the experimental data. When this rate has fallen to a small value it assumes that the background level has been reached and draws either a flat background or fits a background to a polynomial of a degree selected by the User. When the broadening is large and the counting statistics poor, DYLAN may conclude that it has reached the background when in fact the function still persists.

The effect of this on the deconvolution procedure is shown in figure 3.11. The scattering law for a three dimensional liquid undergoing Fick's Law diffusion with a diffusion coefficient of $2 \times 10^{-5} cm^2\ s^{-1}$ was calculated and then convoluted with a gaussian machine resolution of 400 μeV FWHM.

$$S(\kappa,w) = \frac{1}{\pi} \frac{D\kappa^2}{(D\kappa^2)^2 + w^2} \qquad (4.6)$$

$$M(\kappa,w) = S(\kappa,w) * \exp\left\{-\frac{(w-w^1)^2}{2(150)^2}\right\} \qquad (4.7)$$

The results are presented for a constant energy window of ± 1200 μeV. It is quite evident that even by $\kappa^2 = 1.0$ Å^{-2} $M(\kappa,w)$ has not decayed to zero within this energy window. Taking the apparent background will give systematically low values for the parameters of the Voigt profile. The discrepancy will increase rapidly with κ^2. This discrepancy is given below expressed as a percentage of the expected area, width or height.

κ^2	0.5	1.0	1.5	2.0	2.5	3.0	3.5	4.0	
Area	0	13.9	22.7	32.9	41.3	48.0	55.1	62.8	%
Width	0	1.8	4.5	5.3	9.1	12.0	13.7	12.5	%
Height	0	2.7	3.9	5.6	9.1	12.2	16.0	20.0	%

FIGURE 4,4

DECONVOLUTION ARTIFACTS (I)

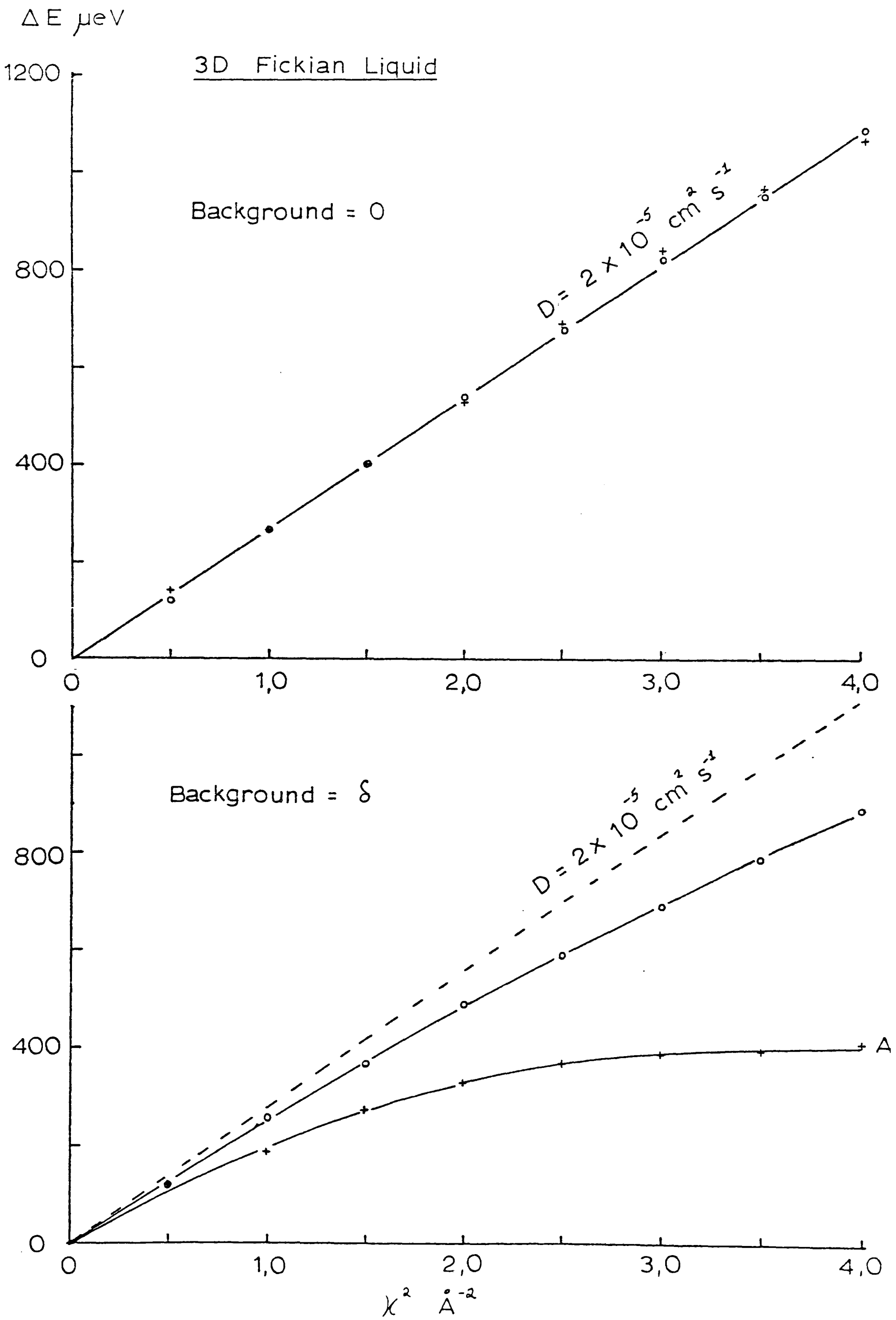

The consequence of this error is to

1) Cause the plot of deconvoluted half widths to drop below the true value

2) Cause the plot to curve over at large κ^2

3) Separate out the Area and Table (112) methods the former saturating much faster with κ^2.

The results of using DECONVOX on this data is shown in figure 4.4 for the real and apparent (δ) backgrounds. The choice of a constant energy window is perhaps an exaggeration of the effects caused by a misalignment of DYLAN. However it demonstrates the deviations that will be manifested by such a misalignment.

2) Inelastic contributions to the quasi elastic region.

This problem has been investigated by P Brier et al (115) who emphasise that a separation into quasi elastic and inelastic components is generally arbitrary, and that with the parameterisation necessary ambiguity of interpretation is introduced. In their approach to the neutron scattering from dichloromethane they favour the prediction of the quasi elastic and near elastic features from a knowledge of the intermediate scattering function, $I(\kappa,t)$, available from IR and Raman data. For the systems dealt with in this thesis such detailed information is not available and in most cases this has necessitated the approach of separating the low energy scattering into quasi and near elastic scattering. The loss of precision with such a method is felt to be compensated for by the gain in tractability of the results.

Another contribution to 'inelastic' scattering in the quasi elastic region may come from multiple scattering. This problem has been investigated by M Johnson (116). It is a κ dependent contribution and most prominent in the low angle counters, arising as it does from a self convolution of the scattered neutron spectrum which is

most peaked for small κ's. Though total percentage scattering was kept low in these experiments an attempt was made to estimate the effects of multiple scattering by interpolation from (116). Table 4.2 shows the values of $\frac{J_1 + J_2}{J_1}$, the ratio of the sum of the first and second scatter to the first scattering, as a function of energy. The factor was used as a multiplier applied to the calculated model scattering law for comparison with the observed data.

B) Non-lorentzian $S(\kappa,w)$

The whole basis of the deconvolution procedure is that one has a Voigt profile resulting from the convolution of a gaussian and a lorentzian function. It is quite possible for the scattering law of the sample to be non-lorentzian, either because of the nature of the system's dynamics, or because one is measuring a nominally lorentzian $S(\kappa,w)$ at large κ^2 where the scattering law is going over to the gaussian form of the free particle scattering.

The results of attempting to carry out a deconvolution on a particularly interesting non-voigt profile are shown in figure 4.5. The scattering law was generated for a system diffusing in two dimensions according to Fick's law, and this anisotropic diffusion then averaged over three dimensions. Examples of such systems could be intercalate diffusion in polycrystalline laminates (117), diffusion in liquid crystals (85), and diffusion of adsorbates on powdered adsorbents (28). The question of this orientational averaging is dealt with in detail in section 3.11.

The scattering law is now given by

$$S(\kappa,w) = \frac{1}{2\pi} \int_0^{\pi} \sin\theta \, d\theta \, \frac{D\kappa^2 \sin^2\theta}{(D\kappa^2\sin^2\theta)^2 + w^2} \qquad (4.8)$$

Table 4.2

Multiple Scattering Corrections

$$S^{2D}_{OBS}(\kappa,w) = M \times S^{2D}_{CALC}(\kappa,w)$$

Incident wavelength 4.8 Å

Total Scattering 10%

Angles of Scatter 18°, 27°

EμeV	0	100	200	300	400	500	600	700	800	900	1000	1100	1200
$\frac{J_1+J_2}{J_1}$	1.014	1.080	1.100	1.277	1.500	1.600	1.817	2.000	2.200	2.405	2.600	2.750	2.870

Angles of Scatter 36°, 45°, 54°

EμeV	0	100	200	300	400	500	600	700	800	900	1000	1100	1200
$\frac{J_1+J_2}{J_1}$	1.025	1.035	1.075	1.082	1.100	1.170	1.201	1.250	1.280	1.333	1.360	1.410	1.432

FIGURE 4,5

DECONVOLUTION ARTIFACTS (II)

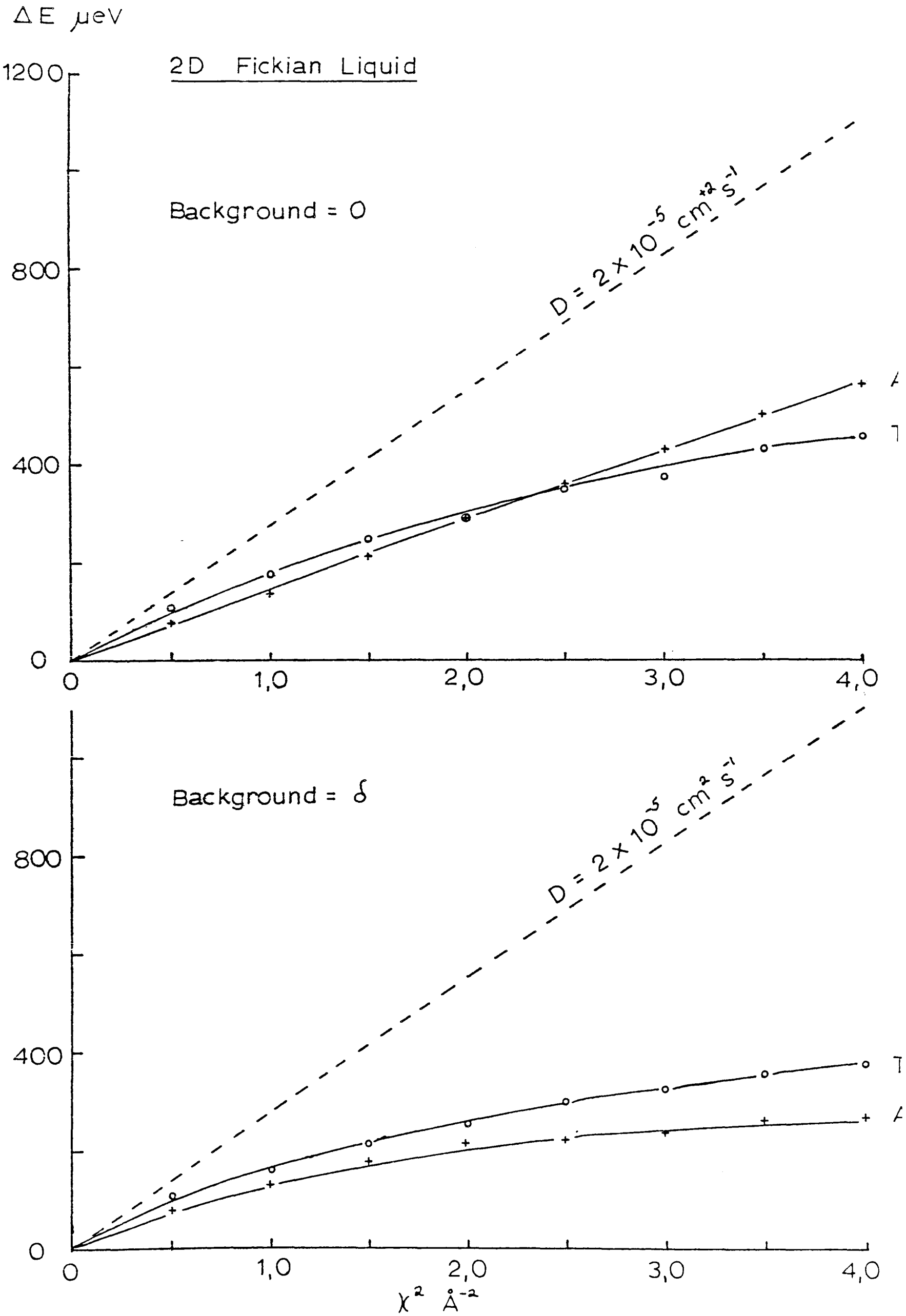

The integral has been evaluated numerically for the case where the two dimensional diffusion coefficient is 2×10^{-5} cm^2sec^{-3}. Figure 3.12 shows the convoluted and unconvoluted scattering laws. The shape is certainly non lorentzian, but treating the profile as a Voigt and taking the heights, areas and widths as normal gives the broadening plots in figure 4.5. No useful information can be obtained by such an approach, and certainly nothing can be inferred as to the mechanism of the diffusive behaviour.

To summarise then:-

1) Deconvolution will only work for systems whose dynamics give rise to a lorentzian scattering law.

2) Deconvolution cannot give any information on what kind of dynamical process is giving rise to a non lorentzian line shape.

3) Precise, quantitative values for diffusion coefficients are only forthcoming if background levels are low and can be accurately assessed.

The policy adopted in this thesis will be to use deconvolution as a cursory probe, but to rely on convoluting up a parameterised model scattering law, and to fit this to the experimental results.

4.3 Preparation and containment of samples

One of the major difficulties ofthis work was designing a sample can that would satisfy the requirements of the neutron instrument and yet be useful for surface science studies.

The ideal sample can for a neutron scattering experiment would possess the following characteristics.

1) Low total cross section. It should neither contribute intensity to the final spectrum nor remove intensity by absorption of neutrons.

2) Sufficient mechanical strength to hold the sample, be it solid, liquid or gaseous, in a planar configuration of uniform thickness.

3) Good thermal conductivity. Heating and cooling of samples is effected by a cryofurnace block on which the sample is mounted. A good thermal contact is required for rapid temperature equilibration across the sample.

4) Vacuum integrity. The region surrounding the sample can is often evacuated, either to reduce scatter by the air in the sample region, or to prevent ice formation or can oxidation during cryofurnace operation.

5) Inertness. The sample can should not react with the sample.

The multipurpose can used on the time of flight machines at Harwell are made of N3(5% Mg) Magnesium aluminium alloy with windows of the order of Imm and less thickness. The can is made in two halves and vacuum sealing is achieved either by rubber or silicone 'O' rings for samples at or around room temperature, or with indium 'O' rings for cryogenic operations. Such sample cans give generally 1 - 2% scatter and it is always necessary to run a blank can for subtraction from the observed spectrum.

The requirements on the adsorbent-adsorbate environment are as follows:-

1) The adsorbent when being outgassed must experience vacuum of $< 10^{-6}$ torr and temperatures ranging from 600 to 1100°K depending on the adsorbent.

2) The adsorbent should be presented wherever possible as a flat bed of large area and shallow depth. This assists the speed and completeness of outgassing, as the slow process of inter particle mass transport is then not a limiting step.

3) Accurate dosing of the adsorbent with the adsorbate and retention of that dose for periods greater than the equilibration time must be possible.

These restrictions mean that adsorption experiments are generally performed in pyrex or silica glass apparatus.

Pyrex glass is unsuitable for neutron experiments as it contains large amounts of strongly absorbing boron nuclei. Silica glass is suitable if the thickness is not greater than 1mm. A pair of 1mm silica glass plates give about 4% scatter. Unfortunately when this thin the silica glass is not strong enough to withstand repeated heatings and high pressure differentials. There is a further problem in that obtaining a good thermal contact with the cooling block is not possible as the glass cell cannot be easily clamped down.

The Beryllium filter instrument is less stringent in its requirements than the time of flight configuration. The sample is held at a fixed temperature in a liquid nitrogen cryostat and thermal contact with the walls of the inner jacket of the cryostat is via an atmosphere of dry helium gas. This type of instrument measures the cross section/amplitude weighted density of states of the sample. Silica glass gives a low intensity of scatter with weak, broad peaks (118). A blank spectrum can be accurately subtracted. As a result the sample could be prepared and the spectrum obtained using the same silica glass apparatus. This is shown in figure 4.7 and its use described in section 4.5.2.

For the time of flight experiments a single piece magnalloy can was designed and built. Its special features are a single, large diameter inlet port, one piece construction with no 'O' rings, and a sample thickness of 2 mm. See figure 4.8. Such a can is only a minor modification on standard Harwell cans and adequately satisfies the requirements of the neutron method.

The low temperature of outgassing for graphon meant that it could be outgassed in the magnalloy can directly. Sample dosing was

FIGURE 4,6

EXPERIMENTAL ARRANGEMENT FOR BEF SPECTROSCOPY OF ADSORBED MOLECULES

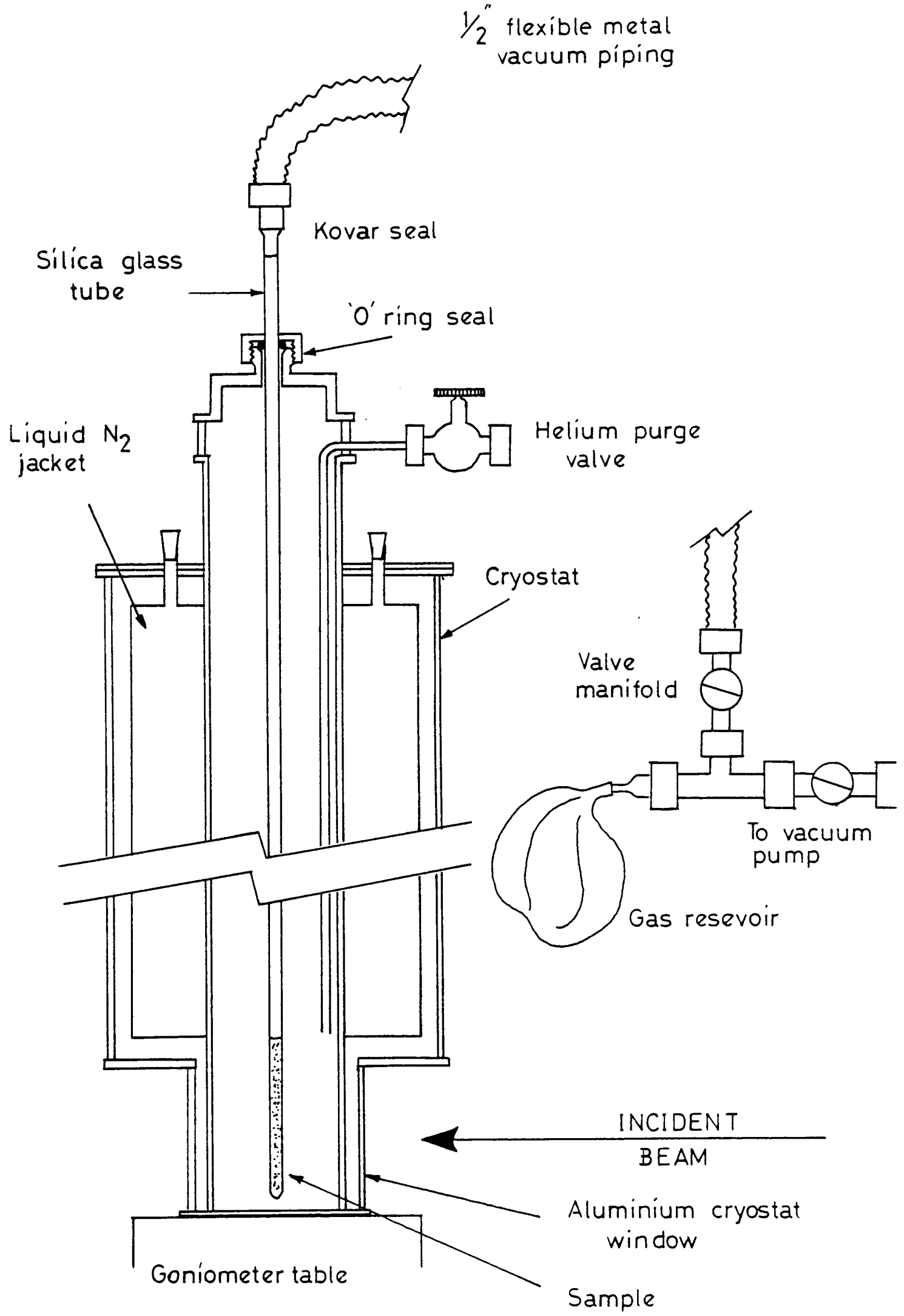

Not to scale

FIGURE 4,7

SAMPLE CAN FOR STUDIES OF ADSORBED MOLECULES BY TOF SPECTROSCOPY.

Plan

Scale 1:1

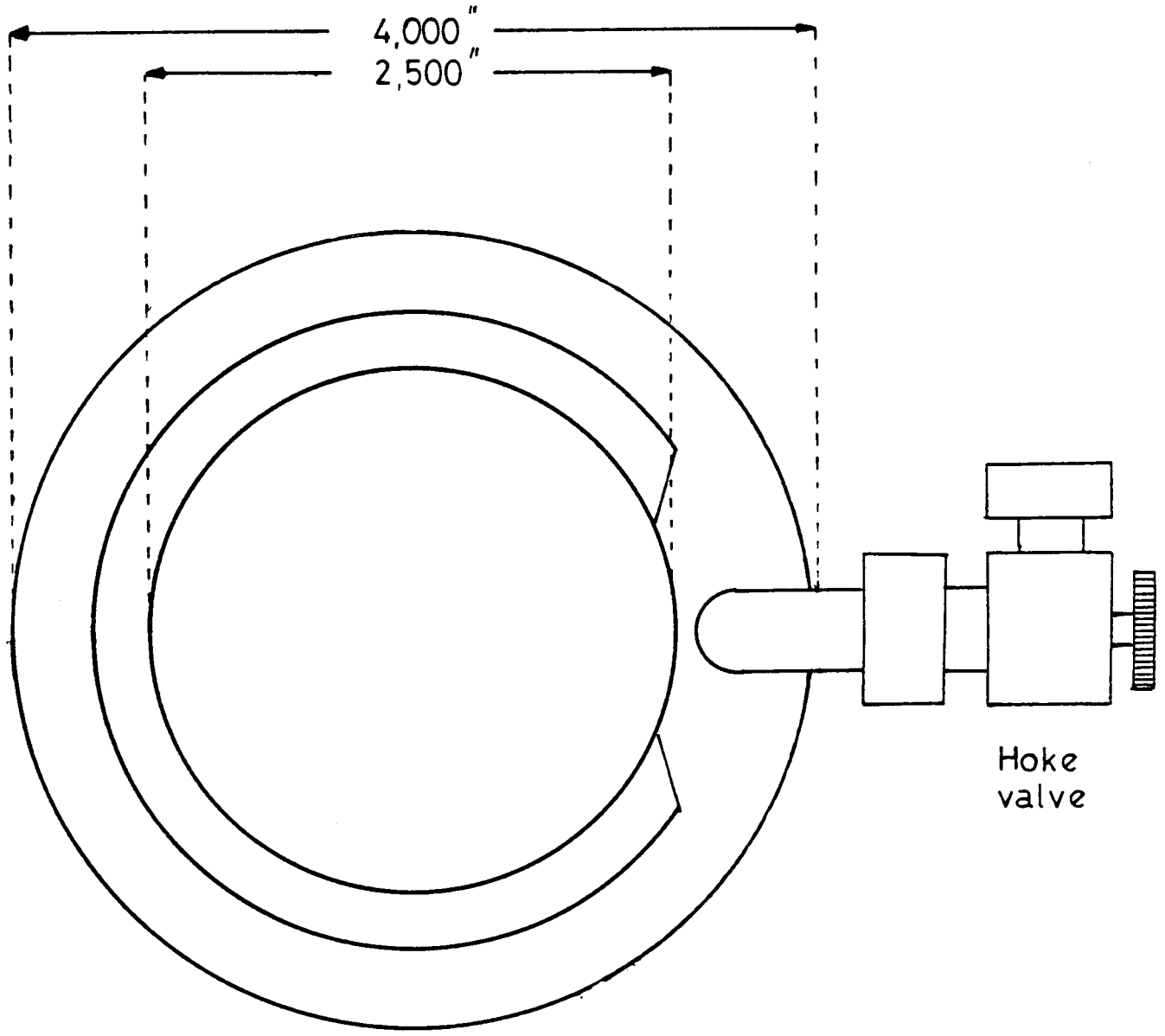

Elevation

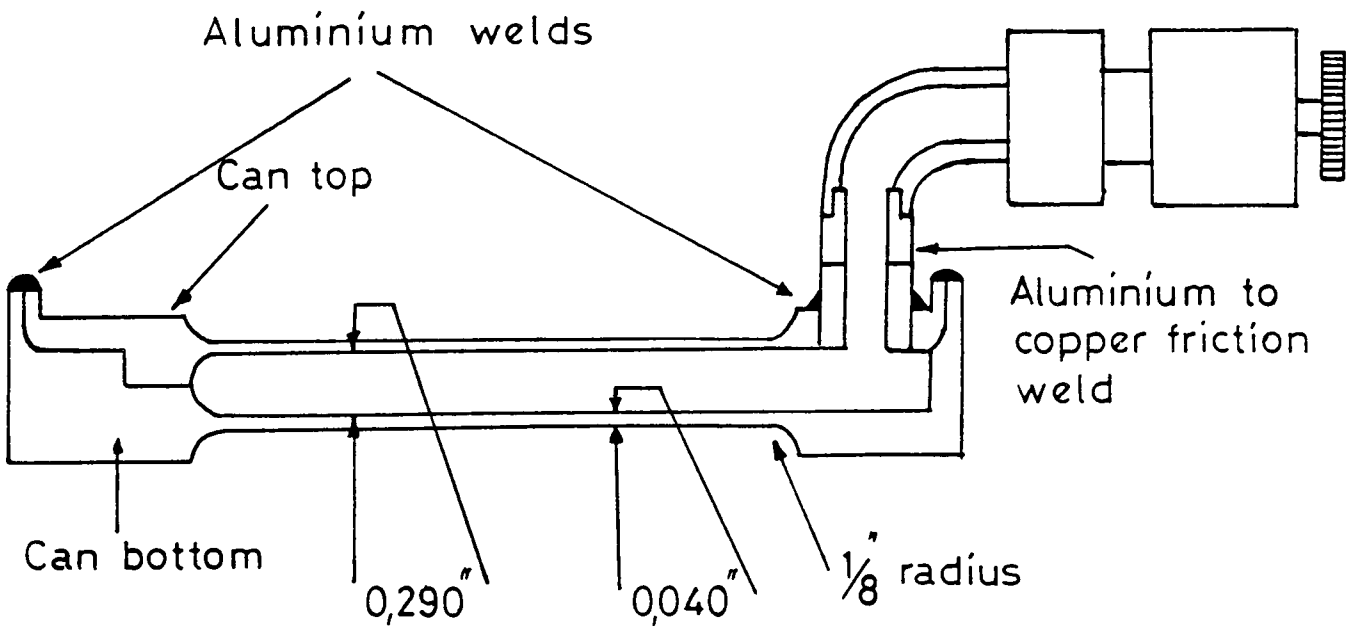

carried out by connecting an external gas line into the sample can as described in (119) and shown in figure 4.9. A problem was encountered with vacuum integrity. The magnalloy used for the can construction is cut from a rolled bar of the metal. The centre of the can window corresponds to the longitudinal axis of the bar. Over a region of about 1mm diameter at this point the metal is not homogeneous and often shows slight porosity. A slow leak could be detected on both cans using a helium-mass spectrometer leak detector. The leak rate, though slow, was sufficient to cause a noticeable change in the adsorbate concentration in the sample can over the period of a week or so during which spectra were being recorded. For this reason gas dosing was always via a large gas balloon at atmospheric pressure. In this way a constant pressure of adsorbate could be maintained over the sample for long periods of time.

The La-Y system required a totally different approach as the outgassing temperature is much higher. The same magnalloy was used to hold the sample when recording the neutron spectrum but the sample was outgassed in an attached silica bulb and shaken into this can when dosed and cooled. The system is shown in figure 4.10. This approach is not very satisfactory and has several disadvantages.

1) The dimensions of the sample changes place severe restrictions on the size of the outgassing bulb which doubles as a gas resevoir for dosing with adsorbate. It means also that a blank cannot be run at the same time as the sample since one of the sample changers positions is taken up with the glass ware.

2) The glass apparatus is fragile and clamping the can to the cryofurnace block caused the connecting line to fracture on several occasions. More important, the glass to metal kovar seal cannot withstand low temperatures or frequent temperature cycling. This was again the cause of several vacuum failures and limited the lowest temperature accessible to 160°K.

FIGURE 4,8

GAS INLET SYSTEM TO SAMPLE CAN

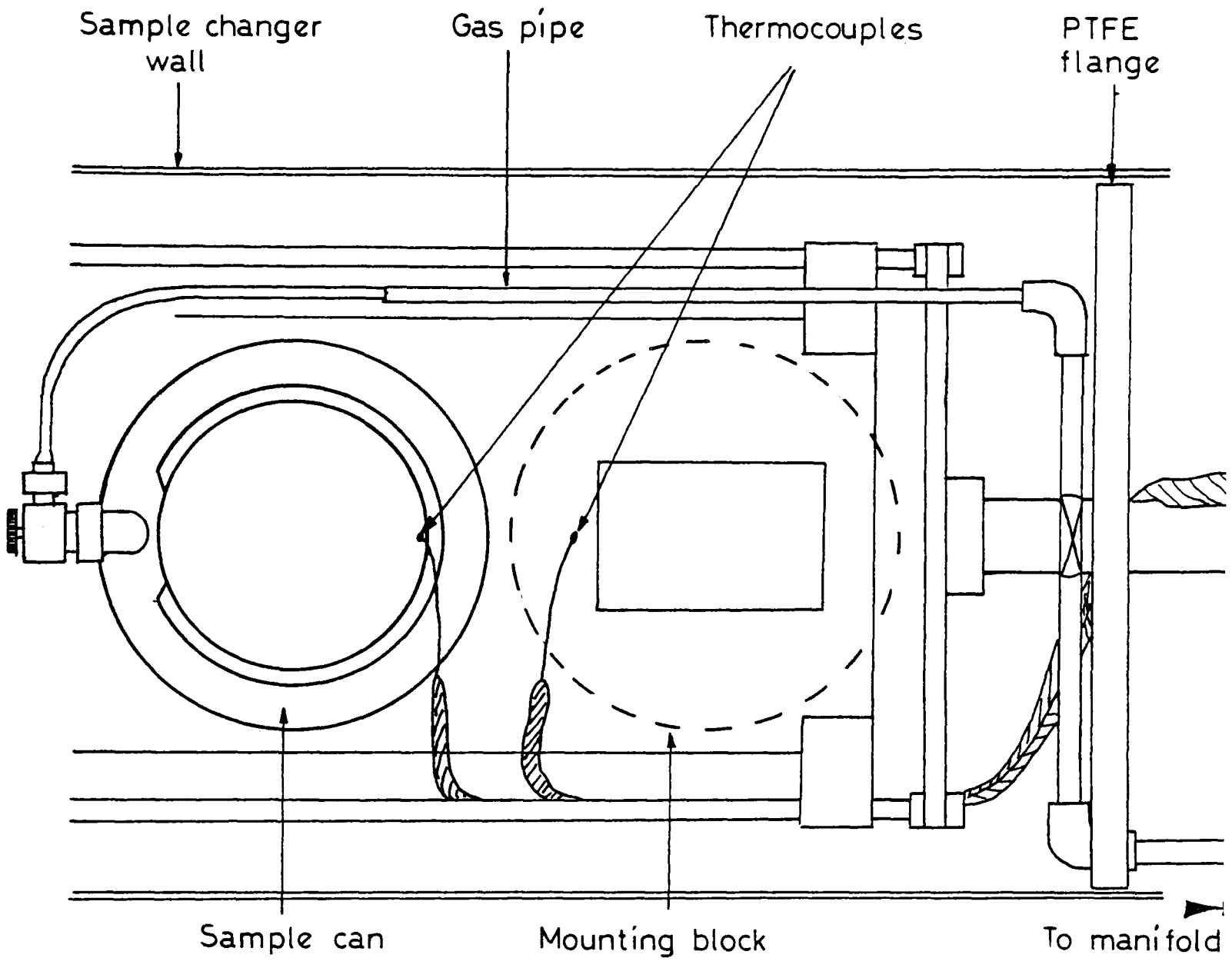

MANIFOLD

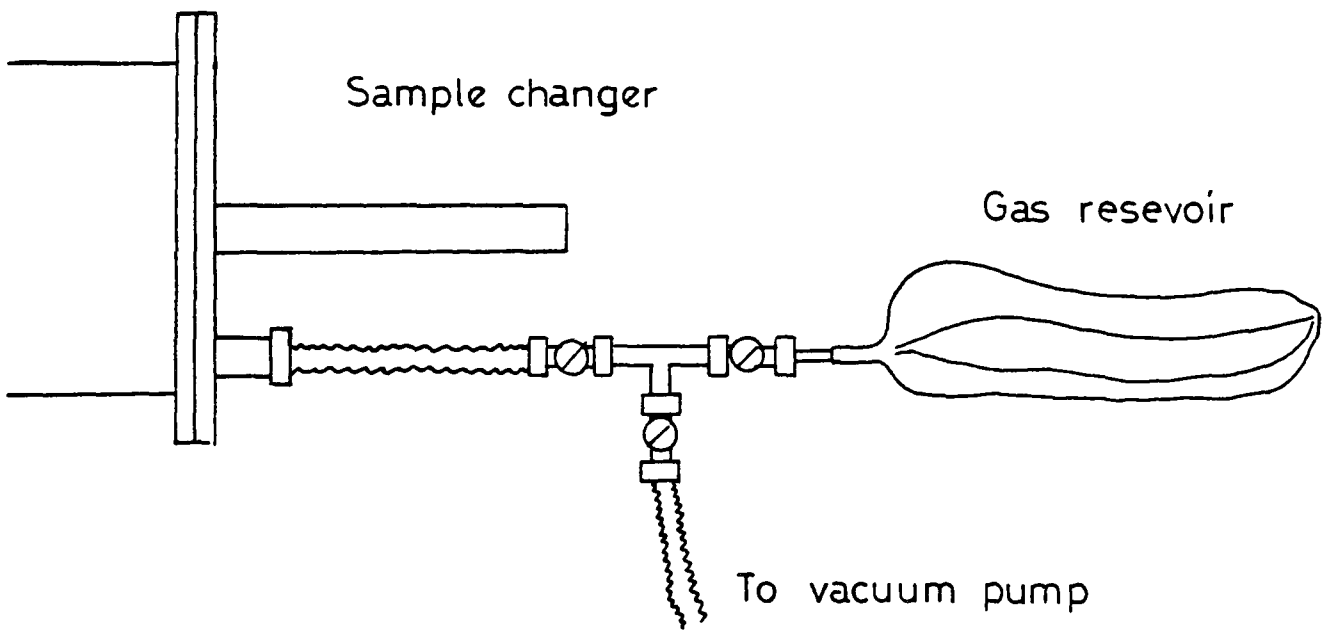

FIGURE 4,9

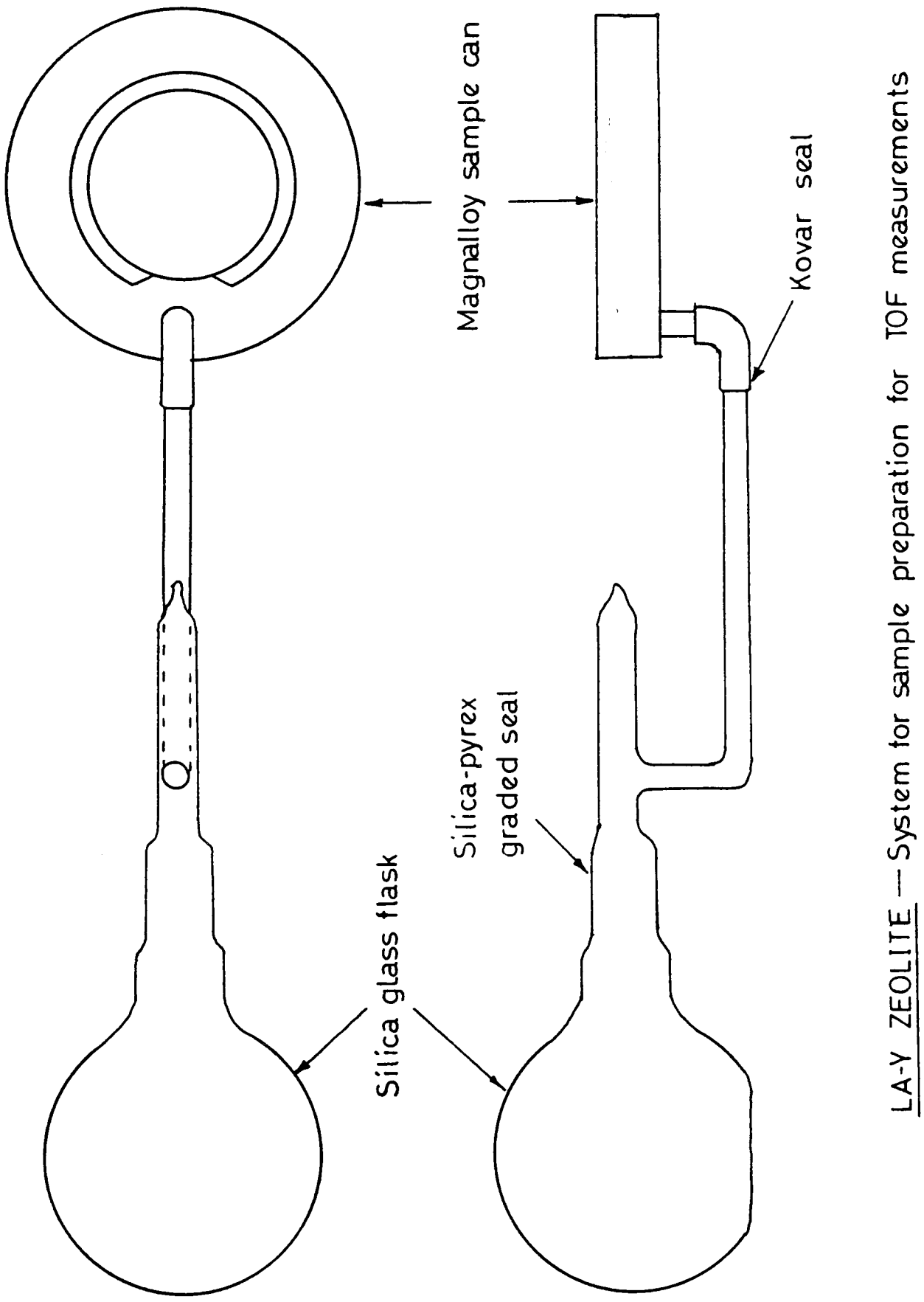

LA-Y ZEOLITE — System for sample preparation for TOF measurements

3) Outgassed zeolites develop surface electrostatic charges. The adsorbent does not stick to metals or silica glass but does however adhere strongly to the interconnecting links of pyrex glass. This made the transfer of adsorbent after outgassing quite difficult as the tube blocked easily.

4) Because of these transfer problems one cannot be certain of getting all of the sample into the area of the neutron beam. This means that estimating surface concentrations by transmission measurements is subject to very large errors.

4.4 Recommendations for future experimental designs

With these factors in mind the following recommendations can be made for future can design in surface studies employing neutron scattering.

1) If the sample is not to be cooled or heated by physical contact with a cryofurnace block, a silica cell is most suitable. The sample can be outgassed in situ so there are no transfer problems. The adsorbent may be dosed beforehand and the cell sealed off, or a gas line connection may be led out of the sample changer. Two large, opposed, inlet and outlet ports are necessary for introduction of the 'wet' sample, rapid outgassing and the possibility of streaming adsorbate or reacting gases over the adsorbent.

2) If the sample is to be cooled or heated then the sample can should be of the same design as above but made in magnalloy. The chief problem is the temperature of outgassing. This can be overcome to some extent by carrying out the outgassing in the can which is itself surrounded either by a dry argon atmosphere or in vacuo, so reducing the chance of any oxide film forming on the can.

4.5 Sample Preparation for the Neutron Experiment

4.5.1 Graphon

The procedure adopted was to heat the graphon in the magnalloy can at 600-650°K on a glass vacuum line in the laboratory at Oxford for 24 to 36 hours. The final pressure over the sample was generally 10^{-5} to 10^{-6} torr. Whilst still hot the sample was isolated and then allowed to cool under an atmosphere of the required adsorbate gas. When cooled to room temperature the can was sealed, disconnected from the vacuum line and taken out to the neutron spectrometer at Harwell.

The can was clamped to the cryofurnace block in the sample changer and connected to the external gas dosing line. It was then evacuated to 10^{-4} to 10^{-5} torr, opened to the gas bag and finally opened to the sample can. The sample changer was then sealed, evacuated and cooled down to the required temperature.

4.5.2 La-Y Zeolite

One of the main features of zeolite adsorbents is the tenacity with which they retain adsorbed water. No check was available on the conditions required for outgassing as with graphon and all that could be done was to take the outgassing apparatus to the limits of its performance. In all cases the La-Y was outgassed in a silica vessel at temperatures of 970-1030°K for not less than 48 hours. The final vacuum above the sample was not greater than 10^{-5} torr.

The apparatus used for the outgassing and the subsequent adsorbate dosing procedure varied with the type of experiment being performed.

1) Inelastic measurements.

The apparatus shown in figure 4.7 was employed when carrying out experiments on the beryllium filter instrument with gaseous

adsorbates. Outgassing was done on the vacuum line at Oxford the silica tube containing the sample being mounted in a horizontal tabe furnace. This horizontal configuration was found to be necessary to avoid the 'gunshot' effect on outgassing. The evolution of gases from the zeolites on initial heating is so rapid that if the powder is close packed in a tube then a pressure differential builds up and the powder is blown explosively out of the hot section of the tube and up into the main vacuum line. If spread out horizontally with free space above the sample then this effect can be avoided.

Once outgassing was complete the sample was isolated and dosed with the adsorbate gas whilst still hot. When cooled to room temperature the extra gas bag was inflated. At the instrument the tube was inserted into the cryostat and as the temperature of the sample decreased so more adsorbate distilled over from the gas balloon. The temperature of the sample was always $80^{o}K$ so that when working with gaseous adsorbates that condense at this temperature the extra gas balloon was dispensed with. The volume of gas in the apparatus at room temperature provided a sufficiently high surface concentration at $80^{o}K$ to give an acceptable signal to noise ratio.

The apparatus used for dosing with liquid adsorbates is shown in figure 4.11. Once the adsorbent is outgassed the appratus is isolated and the required amount of liquid evaporated into the bulb from the dropping burette. The bulb is then filled with dry argon gas and transferred from the vacuum line to a dry argon glove box. Here the treated adsorbent is put into a 0.05 mm thickness aluminium foil sachet and sealed in with aluminium cement.

The sachet is compatible with the normal sample mounting arrangements on the beryllium filter and no special arrangements were necessary.

FIGURE 4,10

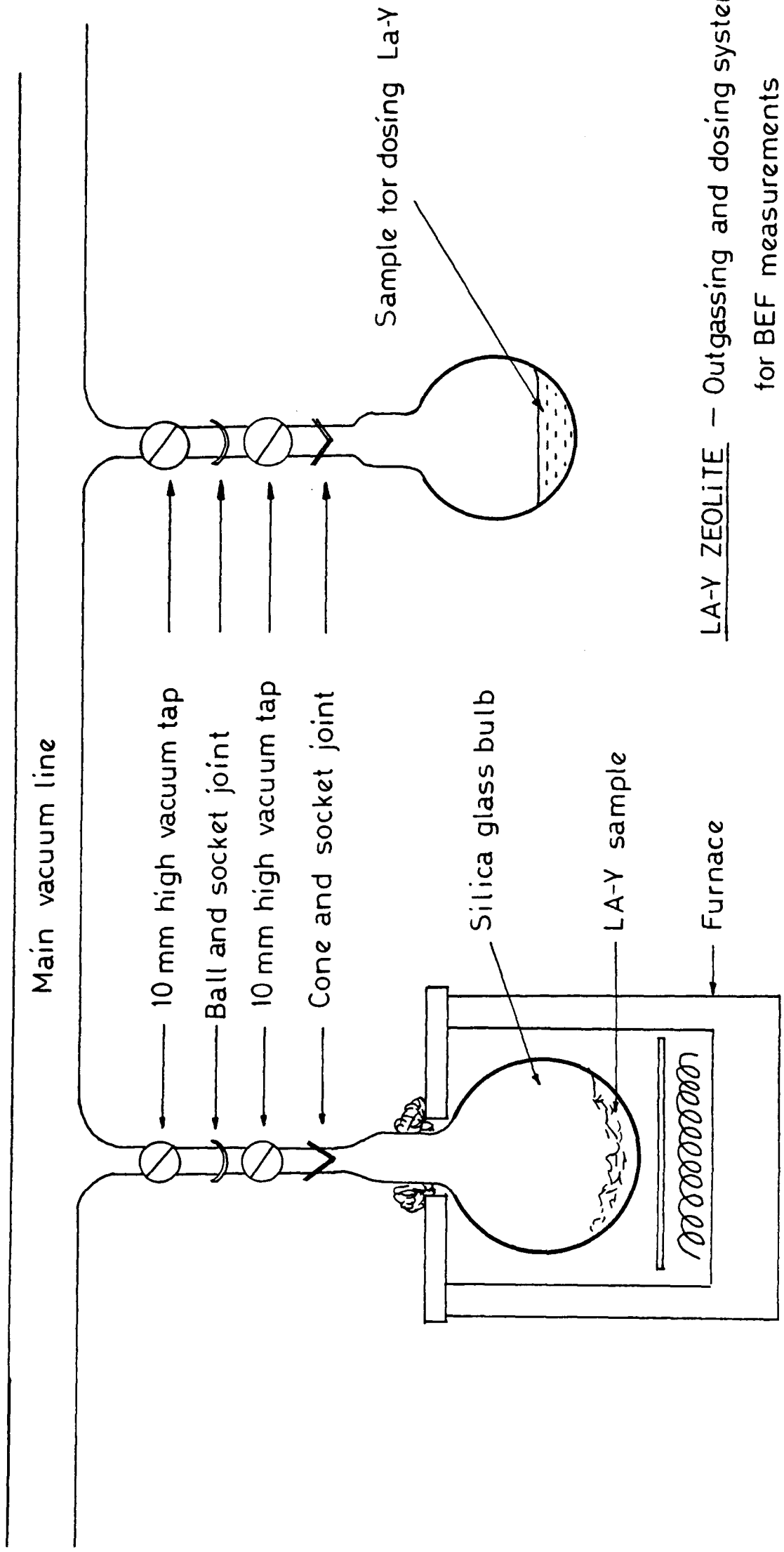

LA-Y ZEOLITE – Outgassing and dosing system for BEF measurements

2) Quasi elastic measurements

The arrangement for the time of flight experiments is shown in figure 4.10. The sample is outgassed in the silica bulb, equilibrated with the adsorbate gas as described above, and then shaken into the sample can. The limitations of this apparatus have been dealt with in section 4.3.

4.6 Determination of surface concentrations by neutron transmission measurements

At the start and end of any runs on the time of flight machines a User performs a series of two minute counts on the three monitors and the total scattered counts from the vanadium, blank and sample. This is to check that the machine is functioning correctly and that no sample has been lost. Of particular interest in this instance is the total scalars count. This gives the total counts received by all detectors at all angles in a 120 second period. By appropriate scaling to the vanadium and blank scattering it should be possible to determine the adsorbate scattering and hence concentration in the sample.

From this value one can determine the surface coverage if one knows the surface area of the adsorbent and the specific area of the adsorbate molecule. The temperature dependence of the surface coverage at a fixed pressure of adsorbate gas should enable one to make an estimate of the heat of adsorption.

Basic expression

$$\frac{I}{I_o} = \exp(-\sigma_T N x) \qquad (4.9)$$

where I is the transmitted intensity

I_o is the incident intensity

σ_T is the scattering cross section for nucleus T

x is the thickness of the sample presented to the beam

Some values of percentage scattering relevant to this work are shown in Table 4.3 below.

Table 4.3 Important values of percentage scattering

Sample	Standard Vanadium	Emty Al Can	Unadsorbed CH_4 gas in the packed can			
			180°K	160°K	140°K	120°K
Atomic Wt	51	27	16	16	16	16
Density g/cm^3	5.96	2.5	0.0010	0.0012	0.0014	0.0016
$\sigma \times 10^{-24}$ cm^2	5.13	1.5	329	329	329	329
Angle to beam	45°	45°	45°	45°	45°	45°
Thickness cm	0.1	0.2	0.2	0.2	0.2	0.2
I %	94.99	97.7	99.86	99.83	99.80	99.78
% scatter	5.01	2.3	0.14	0.17	0.20	0.22

The % scatter from the unadsorbed methane gas in the packed sample can is small enough to be neglected, but the sample can scattering is not.

4.6.1 Determination of the graphon number density and available surface area

The % scatter of the carbon blank and can = 10.02 ± 0.25.

Thus the % scatter of the carbon blank = 7.72 ± 0.25.

If M is the number of atoms of carbon per cm^2 in a sample 0.2 cm thick

$\sigma_C = 5.1$ barns

$\phi = 45°$

$$\frac{I}{I_o} = \exp(-5.1 \times 10^{-24} \times M \times 1.414)$$

so $M = 1.114 \times 10^{22}$ atoms

Thus mass of carbon per cm^2 in a sample 0.2 cm thick

$= 0.222 \pm 0.006$ gms

Assuming that the surface area is 86 m^2gm^{-1} as measured by (121), then the surface area available per cm^2 of a sample 0.2 cm thick is

$$= (0.222 \pm 0.006) \times 86\ m^2$$

$$= 19.09 \pm 0.52\ m^2$$

4.6.2 Determination of concentration parameters for adsorbates

Applying the basic equation (4.9) leads to the expressions for the surface concentrations of the adsorbate molecules shown in table 4.4. The errors on the values of these surface concentrations are calculated as follows.

1) A random counting event has a $\pm\sqrt{n}$ statistical error. The percentage scatter is usually determined by scaling to the vanadium. Typically the vanadium two minute count is of the order of 5000 and the total sample 10000 counts. So that the error is of the order of 2.5%. This error will be carried through to the calculation of the surface area of the adsorbent in the beam, and thence to the number concentration required for monolayer coverage. It will be compounded when calculating actual adsorbate concentrations from the measured adsorbate percentage scatter. So that typical errors on the surface coverage of adsorbed methane will be

$\delta\ominus$ = 48% for a 1% scatterer

$\delta\ominus$ = 10% for a 4% scatterer

The variation of surface coverage for the three adsorbates as a function of temperature, measured by the 2 minute total scalers count is shown in figure 4.12.

4.6.3 Discussion

The following qualitative conclusions are immediately obvious

1) There is an increase in the concentration of scattering centres in the beam as the temperature falls. This increase is far faster than would be expected on the basis of Charles' Law if it was

FIGURE 4,11

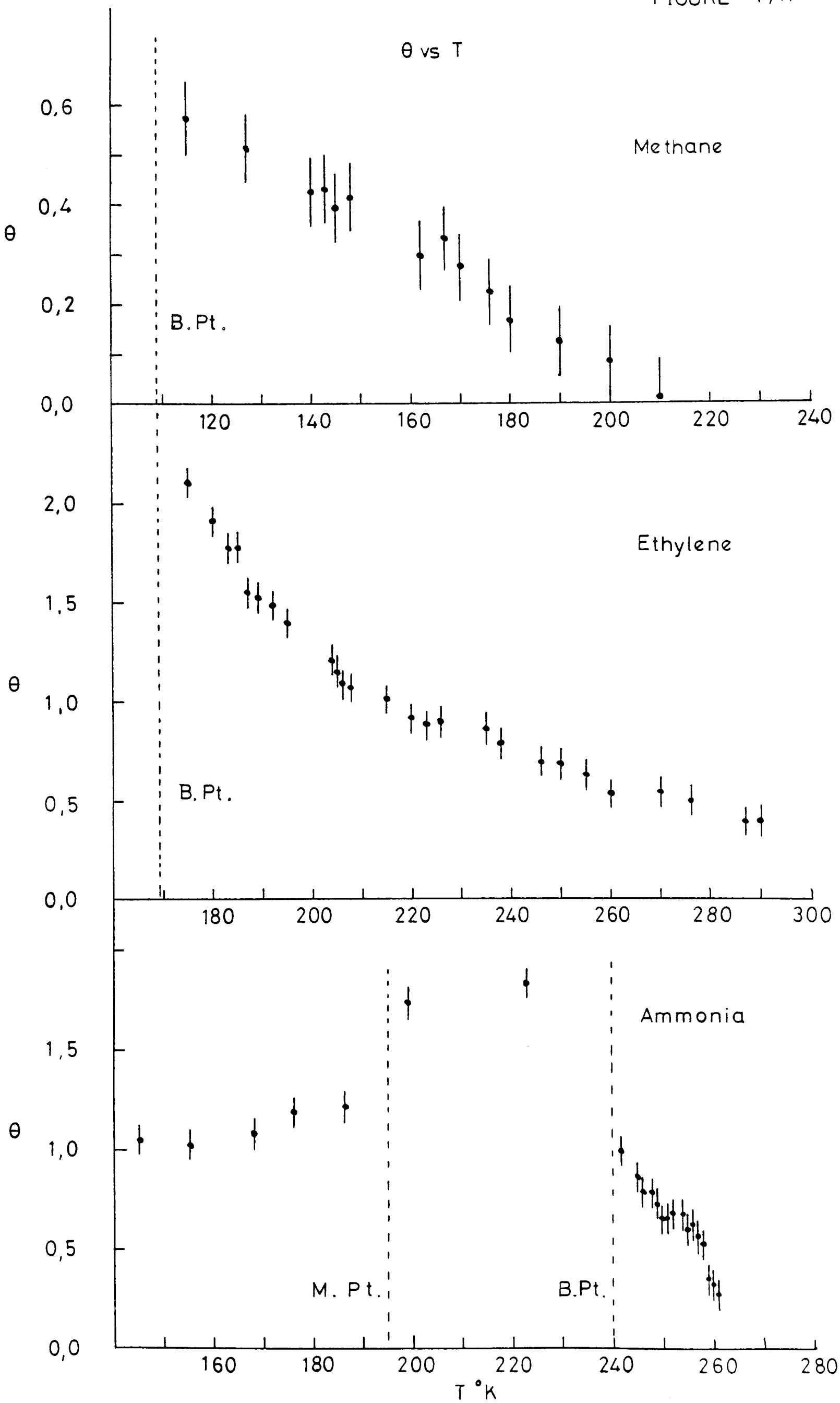
θ vs T
Methane
B.Pt.
θ
0,6
0,4
0,2
0,0
120
140
160
180
200
220
240
Ethylene
B.Pt.
2,0
1,5
1,0
0,5
0,0
180
200
220
240
260
280
300
Ammonia
M.Pt.
B.Pt.
1,5
1,0
0,5
0,0
160
180
200
220
240
260
280
T °K

Table 4.4 Surface Concentrations from Neutron Transmission Measurements

	METHANE	ETHYLENE	AMMONIA
$\sigma \times 10^{-24}$ cm^2	329	334	254
Atomic Weight	16	28	17
Specific Area Å^2	18.1	22.6	18.1
Adsorbate molecules/m^2	$\frac{[4.606 - \ln(I \pm 0.5)]}{[8.88 \pm 0.24]} \times 10^{21}$	$\frac{[4.606 - \ln(I \pm 0.5)]}{[9.02 \pm 0.24]} \times 10^{21}$	$\frac{[4.606 - \ln(I \pm 0.5)]}{[6.86 \pm 0.24]} \times 10^{21}$
Concentration μmole/m^2	$\frac{[4.606 - \ln(I \pm 0.5)]}{[5.35 \pm 0.14]} \times 10^{3}$	$\frac{[4.606 - \ln(I \pm 0.5)]}{[4.53 \pm 0.14]} \times 10^{3}$	$\frac{[4.606 - \ln(I \pm 0.5)]}{[4.13 \pm 0.14]} \times 10^{3}$
Surface coverage Ⓗ	$\frac{[4.606 - \ln(I \pm 0.5)]}{[4.91 \pm 0.13]} \times 10^{2}$	$\frac{[4.606 - \ln(I \pm 0.5)]}{[3.99 \pm 0.13]} \times 10^{2}$	$\frac{[4.606 - \ln(I \pm 0.5)]}{[3.79 \pm 0.13]} \times 10^{2}$

solely due to an increase in unadsorbed gas density as the temperature falls.

e.g. observed concentration change for CH_4 between 200°K and 115°K is approximately 6.6 times, whereas the predicted concentration change on the basis of Charles' Law would be only 1.7 times.

2) The points plotted were measured over widely differring time scales, e.g. for a run about 24 hours and when changing temperatures between runs about 5 minutes. All points fall on the same smooth curve and this curve is reversible with no hysterisis. This suggests, as would be expected, that the adsorption equilibrium is very rapidly achieved.

3) The data for the ammonia system, where a fixed quantity of ammonia was quenched onto the sample, (see section 5.4) inspire confidence in the vacuum system, there being small change in the surface concentration over a time of four days.

4.6.4 Comparison with the surface concentrations obtained from isotherm measurements

The adsorption isotherms of methane (122), ethylene (123), and ammonia (124), on graphitised carbon black adsorbents at a number of temperatures have been determined by *Kiselev* et al. In the case of methane and ethylene the adsorbent was Stirling FT (2800), surface area 12.22 m^2gm^{-1}, and for ammonia it was a Stirling MT (3000), surface area 7.65 m^2gm^{-1}.

The data is presented in tables of surface concentration per unit area of the adsorbent as a function of the reduced pressure, $P/_{Ps}$. P is the bulk gas pressure and Ps the saturated vapour pressure of the bulk gas at that temperature. The general expression for saturated vapour pressure is given in the CRC handbook (125) as

$$\log_{10} P = \left(\frac{-0.2185A}{T}\right) + B \qquad (4.10)$$

where A is the molar heat of vaporisation in cals/gmole of the substance in question

B is a constant for that system

T is the temperature in ^{o}K and P the pressure in torr.

The values of A and B used are as follows

Methane

A = 2128.8 B = 7.027729

valid over the temperature range 67 to 187°K.

Ethylene

A = 3453.7 B = 7.298306

valid from 105°K to 282°K.

Ammonia

A = 7459.6 B = 9.997400

valid from 146°K to 195°K

A* = 6001.2 B* = 8.269901

valid from 164°K to 371°K.

All experiments were performed under an atmosphere pressure of adsorbate gas, 760 mm. Table 4.5 gives the values of Ps and $P/_{Ps}$ for each system at the required temperature. Regrettably the isotherm and neutron experiments have only one temperature in common for the methane and ethylene adsorption, and none at all for the adsorption of ammonia. Only a limited comparison is thus possible. The results are shown in table 4.5.

The close agreement for the adsorption of ethylene is gratifying, but the discrepancy between the figures for methane adsorption is disturbing. Poor outgassing of the adsorbent giving rise to a lower surface area than expected is one possible source of error, though the same procedure was used for the preparation of the ethylene sample. In view of this ambiguity it

will be necessary to consider effects arising from multilayer adsorption when interpreting the scattered neutron spectra.

Table 4.5

Calculated and Observed Surface Concentrations

ADSORBATE	TEMPERATURE °K	Ps t_{orr}	P/Ps	CALCULATED *from isotherm data*		OBSERVED *from neutron data*	
				CONCN µmole m^{-2}	Ⓗ	CONCN µmole m^{-2}	Ⓗ
Methane $w_m = 18.1$ Å^2	115	961.6	0.7903	28.0	2.9	5.55	0.57
	127	2318.4	0.3278	13.5	1.4	5.00	0.51
	140	5073.2	0.1498	10.7	1.1	4.20	0.43
	148	8448.4	0.0899	10.2	1.04	4.00	0.41
	162	13200.4	0.0575	9.7	0.99	2.95	0.30
	176	24528.9	0.0313	9.4	0.96	2.15	0.22
Ethylene $w_m = 22.6$ Å^2	175	968.5	0.7847	20.0	≈2.50	17.65	2.10
	185	1656.6	0.4587	14.0	1.55	14.80	1.76
	195	2681.6	0.2834	10.0	1.13	11.75	1.40
	204	4141.6	0.1835	8.7	1.04	10.10	1.20
	215	6143.0	0.1237	8.2	0.97	8.40	1.00
	235	12220.8	0.0621	7.5	0.92	7.15	0.85
Ammonia $w_m = 18.1$ Å^2	223	254.4	3.10	-	-	18.55	1.80
	242	640.2	1.20	-	-	9.78	0.95
	249	1085.9	0.7177	-	-	7.20	0.70
	254	1280.7	0.5934	-	-	6.69	0.65
	261	1684.9	0.4510	-	-	2.86	0.27

Specification of the Adsorbates used

	Supplied by:-	Specification
1) Gases		
Hydrogen	AERE HARWELL	H_2 99.95% O_2 <20 ppm $^{v}/_{v}$
Methane		CH_4 95 - 97% O_2 0.1 - 0.2% N_2 0.2 - 0.4% CO_2 3 - 4%
Ethylene		CH_4 <1500 ppm $^{v}/_{v}$ C_2H_6 <50 ppm $^{v}/_{v}$ N_2 <50 ppm $^{v}/_{v}$ CO_2 <30 ppm $^{v}/_{v}$
Ammonia		NH_3 99.95% Anhydrous
2) Liquids		
Dichloromethane	BDH Chemicals Ltd.	Redistilled Boiling Point range 39 - 41°C
Acetonitrile		98% minimum assay by GLC Boiling Point range 80 - 82°C
Formic Acid		ANALAR Assay 89.5 - 90.5% Acetate <0.1% nonvolatile <0.002%

CHAPTER 5: ADSORPTION ON GRAPHON

5.1 GRAPHON

Lamellar carbons in one form or another have attracted much interest in the search for an adsorbent with a large, easily prepared surface, possessing an homogeneous distribution of adsorption potentials.

The types of carbon fall into four broad classes, graphites, charcoals, carbon blacks and exfoliated carbons, distinguished by the different sizes of the crystallites; the presence or absence of pores, and the size and homogeneity of the surface area. Table 5.1 compares the properties of the different classes. Graphites have large crystallites, typically La = 2000 $\mathring{A}$, L_c = 200 $\mathring{A}$ but their inhomogeneous surface of low area make them unsuitable adsorbents. Carbon blacks on the other hand have small crystallites with homogeneous surfaces of high area.

A study of adsorption phenomena must perforce commence with a characterisation of the adsorbent, in this case from two directions:-

1) Adsorption properties and surface characteristics

2) Elastic and inelastic neutron scattering

Preliminary results have been reported elsewhere (126) on the characterisation of graphon.

5.1.1 Adsorption Properties and Surface Characteristics

The sample of graphon came from the Chemistry Department at the University of Bristol (121). Surface sulphur impurities were removed by washing with dilute hydrochloric acid. The surface area was measured as 86 m^2g^{-1} by the BET isotherm method taking the specific area of a nitrogen molecule as 16 $\mathring{A}^2$.

In order to confirm the conditions required for outgassing the graphon, a simulated sample preparation was carried out on a

vacuum microbalance at AERE Harwell (127). The pressure above the sample was reduced to $\sim 10^{-4}$ τ and whilst still pumping the temperature of the sample increased in steps of about 50°. The weight of the sample when the system was a equilibrium at the chosen temperature was recorded. The resulting weight change against temperature plot is shown in figure 5.1. Run 1 is for the sample 'wet' from the atmosphere and Run 2 is for the sample equilibrated with the residual gases in the vacuum rig at 10^{-3} τ overnight. The difference in the two curves probably reflects the loss of water in run 1, which is more strongly bound than the residual gases, O_2 and N_2, adsorbed in run 2. Unfortunately due to a malfunction of the mass spectrometer at the time of the experiment this could not be checked.

From the curves it can be confirmed that outgassing the graphon requires heating to $580-680^{o}K$ under a vacuum of less than 10^{-4} τ.

The properties of the surface of carbon blacks have been studied extensively elsewhere (128). The findings can be summarised as

1) Demonstrating the reproductibility of the adsorption surface produced, viz no sintering or development of pores.

2) Confirming the high homogeneity of adsorption potentials on the basal plane, assigning any heterogeneity to exposed edge planes where carbonyl or carboxylate groups may be present.

3) Confirming the random spatial distribution of adsorption surfaces in the sample as a result of the polyhedral clustering of lamellar rafts of carbon crystallites.

5.1.2 Neutron Scattering

Per se the neutron technique is insensitive to the surface properties of the bulk sample. The characterisation of graphon

OUTGASSING OF GRAPHON

Pressure 10^{-4} τ

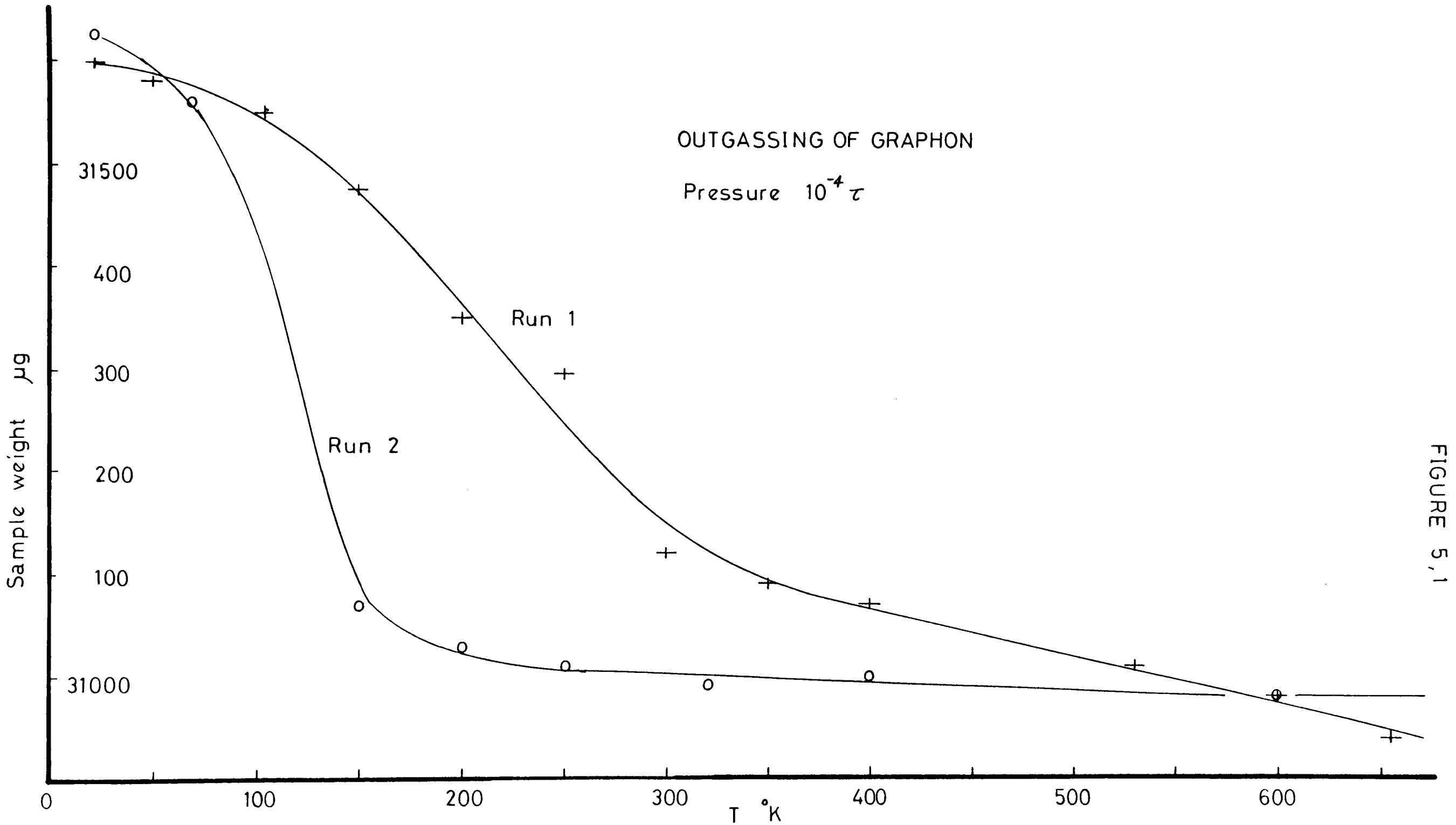

FIGURE 5,1

from the neutron point of view is rather to define the regions of (κ,w) space where bulk scattering occurs and is likely to interfere with observations of bulk scattering.

a) Elastic scattering

The neutron powder diffraction pattern for graphon has been reported previously as has the measurement of elastic peak intensities by time of flight spectroscopy (119). The results are summarised in figure 5.2 which superimposes the diffraction and time of flight data on the (κ,w) surfaces for the 6H time of flight spectrometer at wavelengths of 4.2 and 4.8 Å. The difficulties of subtracting the adsorbate spectrum from the adsorbent spectrum when coherent elastic scattering is present have been discussed in section 4.2.3. It is obviously essential to choose the machine wavelength so that the section through (κ,w) space scanned does not include any Bragg scattering from the adsorbent, whilst at the same time balancing this gain with the loss in primary beam intensity as one moves away from peak flux. For these reasons a wavelength of 4.8 Å was chosen.

The small values of La and Lc, 85 Å and 30 Å respectively (129), give rise to large broadenings of the Bragg peaks. The width of the (0002) reflection means that even using a wavelength of 4.8 Å there will be some coherent elastic scattering contributing to the elastic peak intensity in detectors at 81° and 72°. The width and asymetry of the (0002) reflection for a graphitised carbon black are due to the overlapping of diffraction peaks from graphitised and non graphitised material. In a true graphite the c spacing is about 6.76 Å and in a carbon black about 6.82 Å. With the higher resolution in X ray diffraction it is sometimes possible to assess the degree of graphitisation in a sample of carbon by the relative areas of the two (0002) peaks. It is not possible in this low resolution neutron experiment.

Table 5.1

Classes of Carbons

PROPERTY \ CARBON	PYROLYTIC GRAPHITE	EXFOLIATED GRAPHITE (GRAFOIL)	GRAPHITISED CARBON BLACKS (GRAPHON)	ACTIVATED CHARCOALS
L_A (Å)	10^3	10^2	50	50 - 500
L_C (Å)	10^2	50	30	30 - 100
POROSITY	NIL	NIL	NIL	HIGH
EDGE/BASAL RATIO	HIGH	LOW	NIL	HIGH
HOMOGENEITY	LOW	HIGH	HIGH	VERY LOW
SURFACE AREA m^2g^{-1}	< 10	< 50	< 100	< 500
PREFERRED ORIENTATION	YES	YES	NO	NO
USEFULNESS AS ADSORBENTS FOR NEUTRON SCATTERING MEASUREMENTS	NIL	GOOD Principally coherent scattering studies	GOOD Principally incoherent scattering studies	POOR Solely incoherent scattering studies

FIGURE 5,2

GRAPHON – Coherent scattering

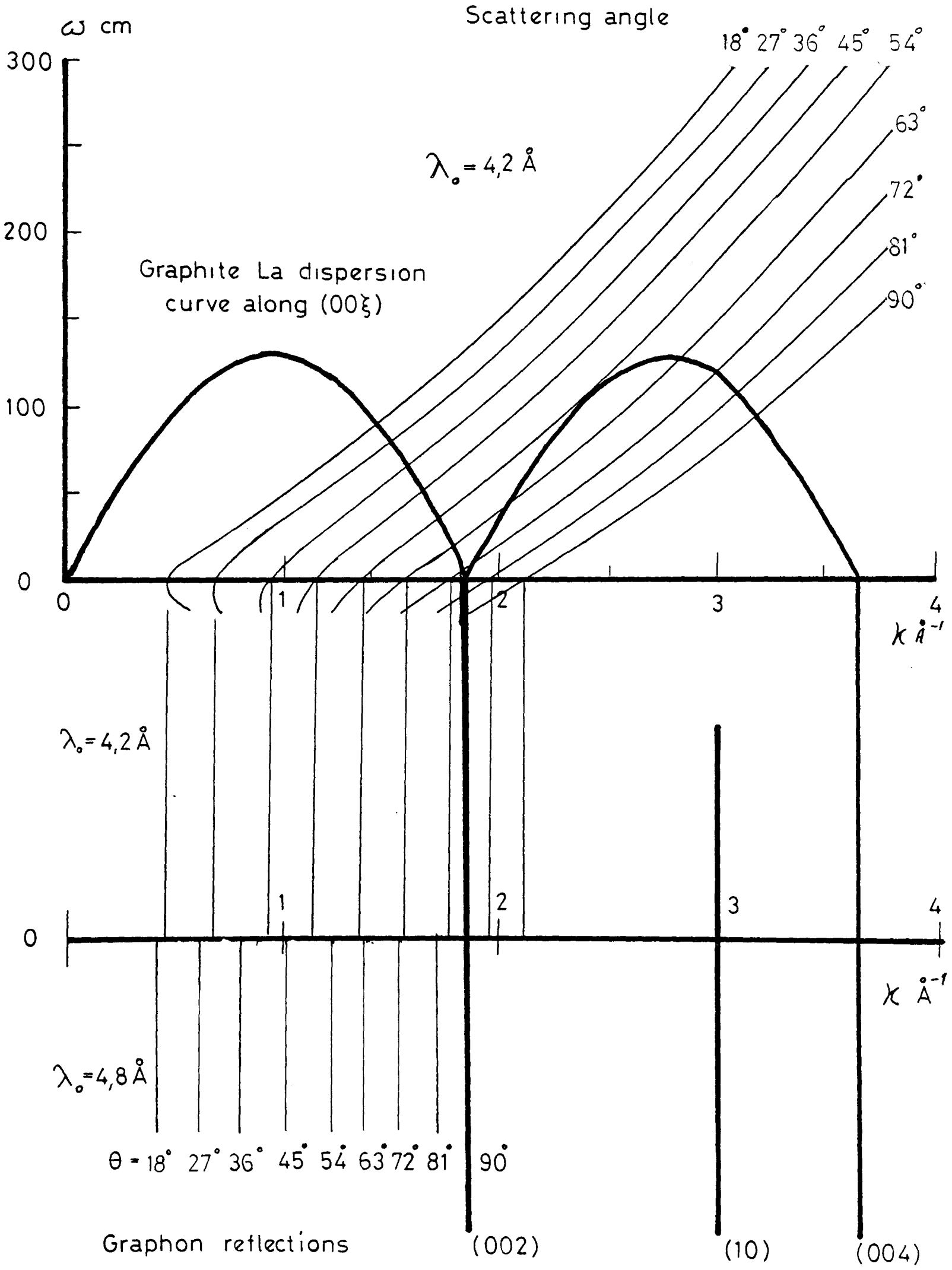

The powder diffraction pattern and the elastic peak intensities rise swiftly at small momentum transfers. The phenomenon of small angle scattering, observed both with x-rays and neutrons is due to Fresnel diffraction from regions of scattering density that are orders of magnitude larger than the wavelength of the incident radiation, in contrast to Bragg diffraction where the scattering centres are of, and separated by, comparable distances to the wavelength being used.

Measurements in this small momentum transfer range were carried out on the small angle neutron scattering spectrometer D11, at the ILL Grenoble. Two regions of reciprocal space were studied.

i) $0.01 - 0.10\ \text{Å}^{-1}$ using a sample to detector distance of 236 cms and an incident wavelength of 12 Å.

ii) $0.10 - 0.40\ \text{Å}^{-1}$ using a sample to detector distance of 66 cms and an incident wavelength of 6 Å.

The small angle scattering curve observed is shown in figure 5.3 together with the scattering from a sample of charcoal. Both samples comprised about 0.5 gms of the solid held between thin silica glass plates. The region in the beam was circular. 1 cm in diameter and 1 mm thick. Neither sample gave extensive linear regions except at very small κ. There could be two reasons for this.

1) A broad distribution of particle shapes and sizes

2) Interference scattering as the particles are not widely dispersed.

The general expression for the small angle scattering intensity is

$$\left(\frac{d\sigma}{d\Omega}\right)_{wh} = \Delta b^2_{coh}\ P(\kappa) \qquad (5.1)$$

where Δb^2_{coh} is the difference between particle scattering length density and the scattering length density of the surrounding medium, in this case air.

$P(\kappa)$ is the single particle interference function (130) and for small values of κ can be expanded as

$$P(\kappa) \simeq 1 - \frac{(\kappa R)^2}{3} + \frac{(\kappa R)^4}{60} \qquad (5.2)$$

where R is a parameter called the radium of gyration and defined as

$$R^2 = \frac{\int p(x) x^2 \, dx}{\int p(x) dx} \qquad (5.3)$$

$p(x)$ is the density of space element dx and x its distance from the centre of mass. The assumption is being made that $p(x)$ is proportional to the scattering length density within the particle.

So at very small κ values

$$\left(\frac{d\sigma}{d\Omega}\right)_{coh} \simeq \Delta b^2_{coh} \exp\left(-\frac{\kappa^2 R^2}{3}\right) \qquad (5.4)$$

From the plots in figure 5.3 the limiting slopes of the Guinier plots at $\kappa \to o$ were taken to determine the radii of gyration

For graphon $\quad Ro = 29 \pm 1$ Å

For charcoal $\quad Ro = 36 \pm 1$ Å

The values are what would have been expected given the values of La and Lc for these types of carbon.

At $\kappa^2 \simeq 5 \times 10^{-3}$ Å^{-2} a weak maximum is seen in the curve of scattered intensity for graphon. Using the full Bessel function expansion for $P(\kappa)$ suggests that this maximum corresponds to the scattering from a particle of either 130 ± 15 Å or 220 ± 20 Å diameter, depending on whether the maximum corresponds to the first

SMALL ANGLE NEUTRON SCATTERING
FROM CARBONS

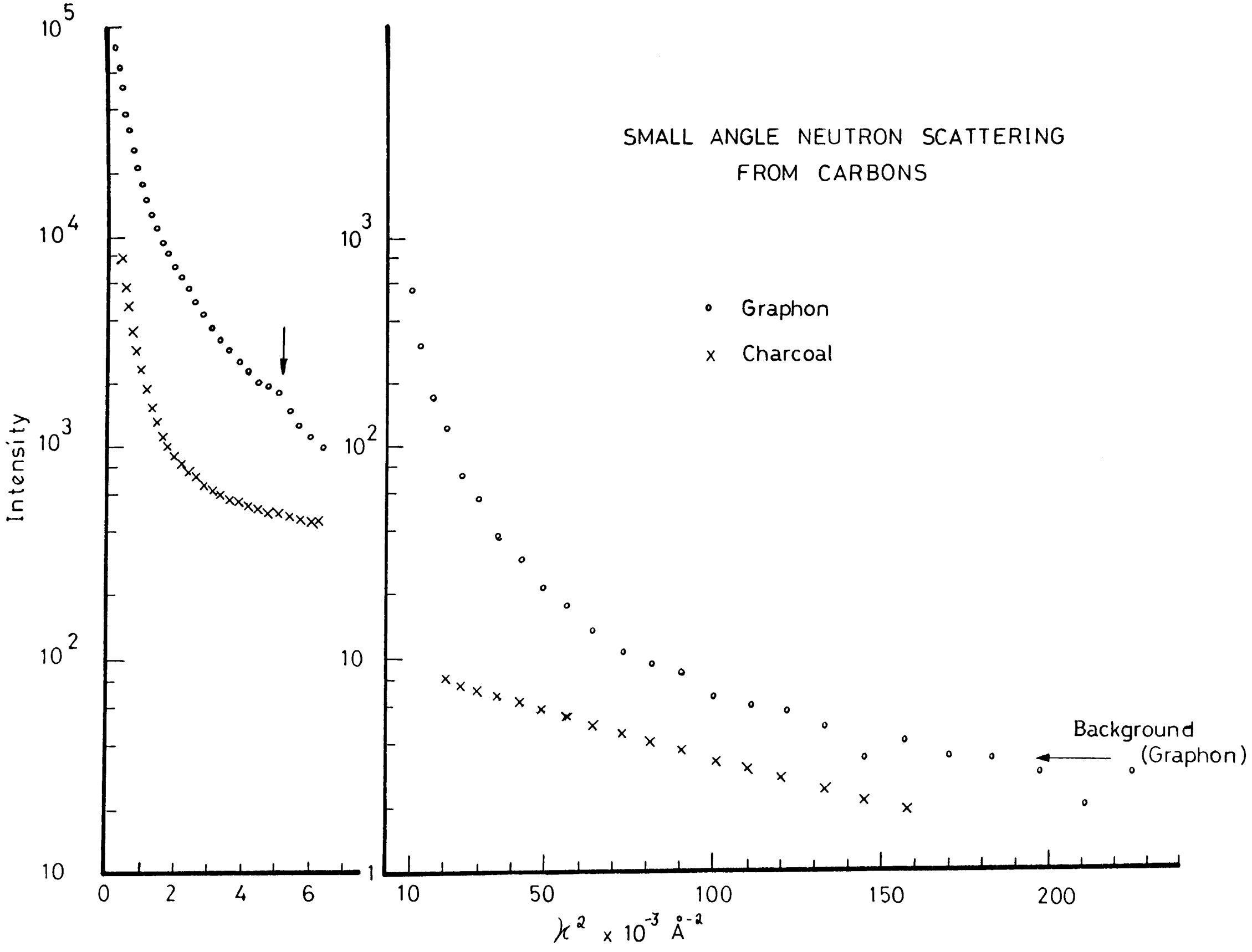

FIGURE 5.3

FIGURE 5,4

GRAPHON DISPERSION CURVE – C axis longitudinal

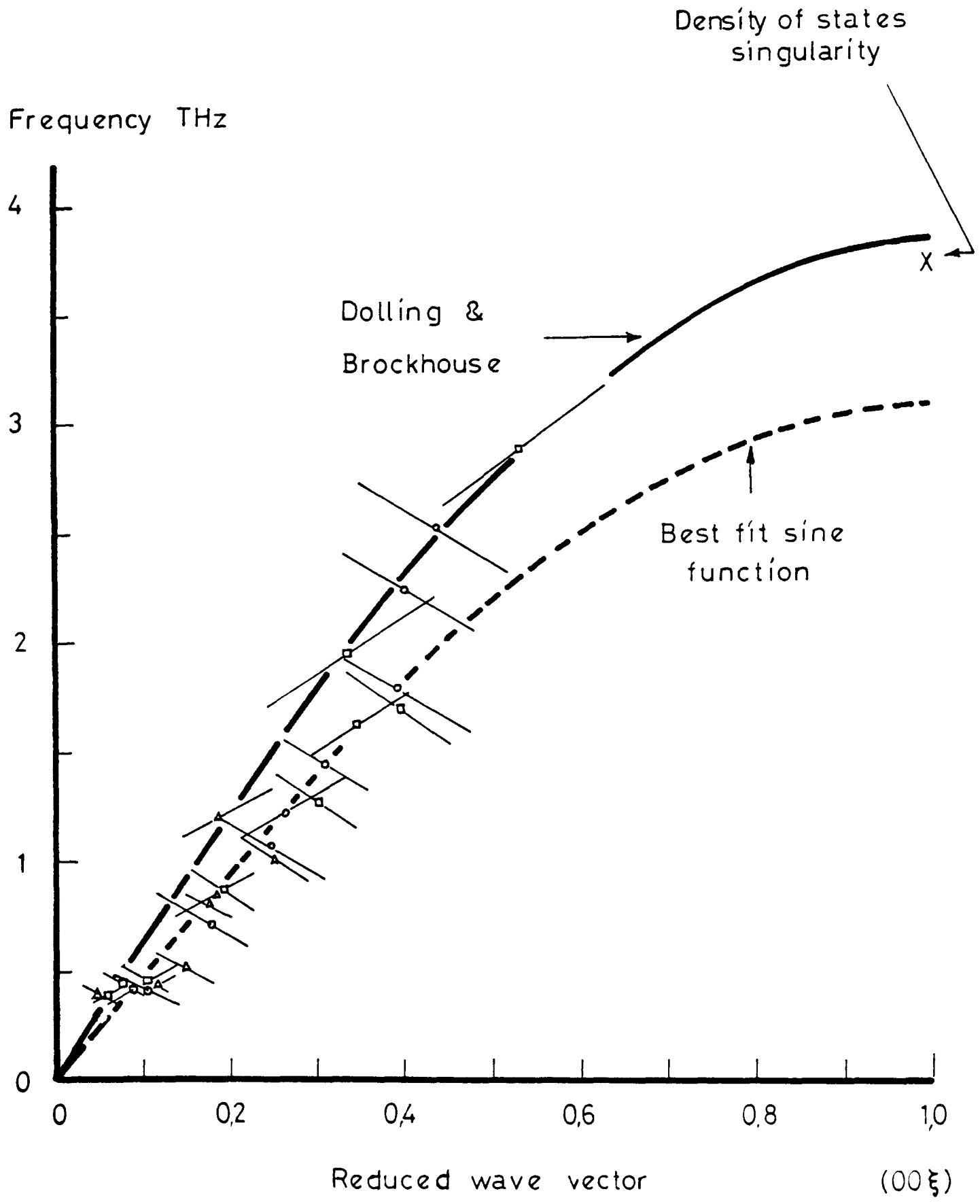

or second order scattering. Investigations of the carbon particles by electron microscopy (131) indicate that graphon particles are polyhedra composed of rafts of crystalline graphite, with an overall diameter of 250-300 $\mathring{A}$, and so confirms the second order indexing.

By the combination of conventional diffraction, small angle scattering and electron microscopy, the macroscopic structure of graphon is well determined. The large value for Ro, and the absence of a maximum in the In(I) vs κ^2 plot for charcoal are in accord with the larger crystallites and less ordered structure of the material.

b) Inelastic Scattering

Coherent inelastic excitations observed previously (132) arise from longitudinal acoustic phonons propagating in the c direction of the carbon lattice. By making measurements at a number of incident neutron wave lengths the frequencies and wave vectors of these excitations were determined and the phonon dispersion curve constructed.

The momentum transfer for the excitation is given by the angle of scatter, the incident wavelength and the energy transfer associated with the steep rise in intensity on the low frequency side of the excitation. The points plotted are taken from the half height of the steep rise, the error bars on the points extending from a quarter to three quarters height of the rise in intensity. The error bars are drawn along the cuts taken in (κ,w) space by the time of flight spectrometer. The data for a number of different scans in the second and third Brillouin zones along the c direction are shown in figure 5.4. Superimposed upon the experimental points is the dispersion curve for graphite of (133) - full line - and the best fit dispersion curve using a single force constant - dotted line. The group velocity is given by

FIGURE 5,5

FREQUENCY SPECTRA OF GRAPHITES

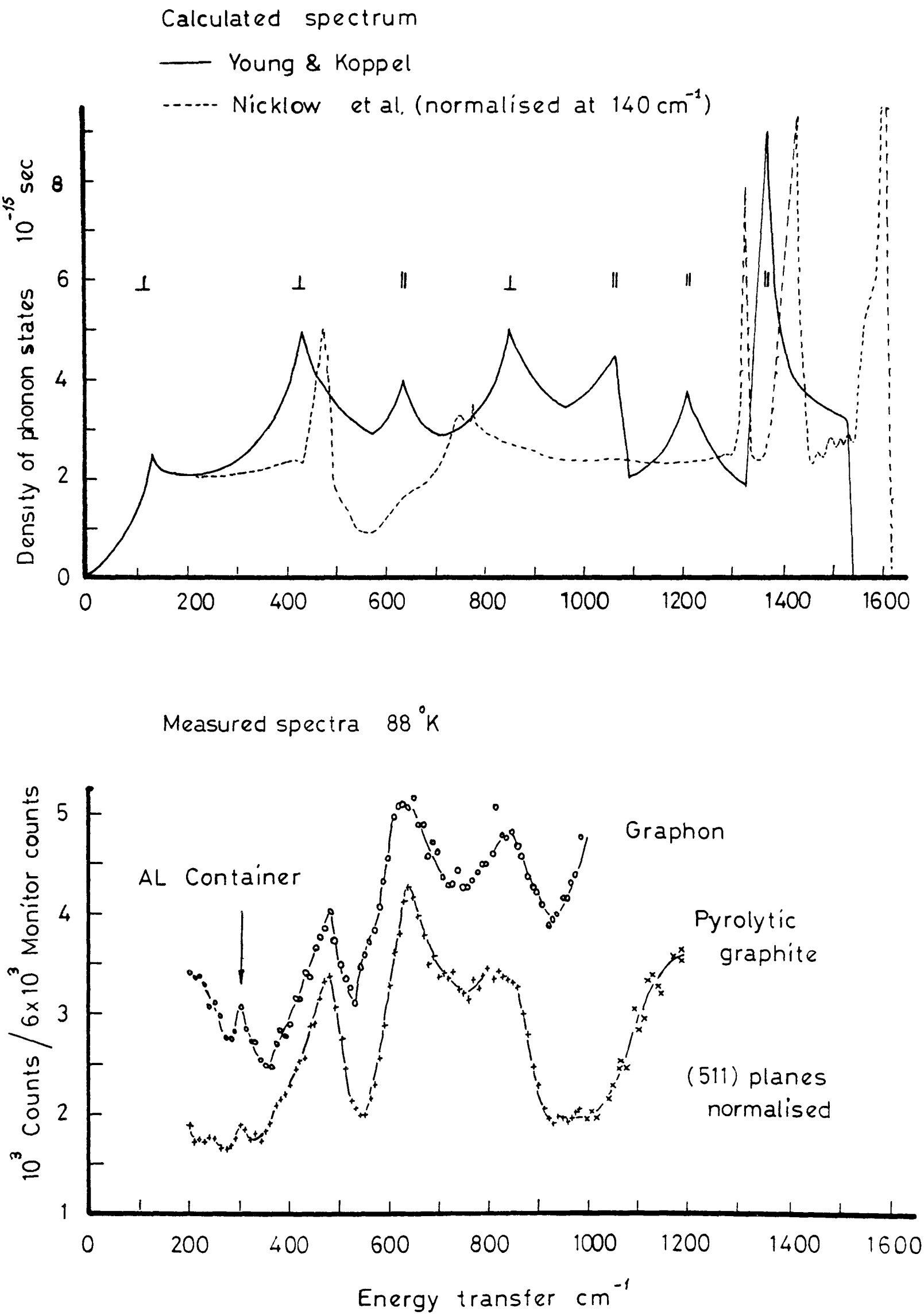

$$Vg = \frac{V}{k} \cdot 2\pi = 3.46 \times 10^5 \text{ cm sec}^{-1}$$

the force constant A1

$$A1 = Vg^2 . p = 2.70 \times 10^{11} \text{ dynes cm}^{-1}$$

and the compliance constant

$$C_{33} = \frac{A_1 \rho c^2}{8m} = 2.98 \times 10^{11} \text{ dynes cm}^{-2}$$

These values are slightly lower than the values found for graphite. With the very large error bars on the data the slope and zone edge frequency can only be defined as not more than 15% smaller than the values for pyrolytic graphite. Such a change could well be explained by the 4% larger c axis lattice parameter of graphon compared to pyrolytic graphite.

The incoherent cross section for carbon is very small. By working with large momentum transfer, i.e., small neutron wavelengths and so in the incoherent approximation (see section 4.2.2) it is nonetheless possible to observe the phonon density of states for carbon. Preliminary measurements using the time of flight spectrometer have been reported previously (126) and these measurements have since been extended to higher energies with the Beryllium filter spectrometer. The measured spectra for graphon and for pyrolytic graphite are shown in Figure 5.5. Even with large amounts of sample, 30g as opposed to the 7g used for the time of flight

flight experiments, and long counting periods the intensity of the neutrons scattered from the carbon is small, *cf* the peak for the aluminium sample holder which is undetectable at the usual counting rates. Multiphonon scattering would be expected to be appreciable from such large samples but it has been ignored in determining singularities in the density of states, as it appears as a steadily rising, continuous background with increasing momentum transfer. Also shown in figure 5.5 are the predicted densities of states from the calculations of (134) and (135). For the perpendicular modes the measurements on pyrolytic graphite agree well with the predictions of (135) rather than with other experiments (136) or theory (134). This may be due in part to differences in the sample. The only discernible difference between the densities of state for graphite and graphon are the slightly greater widths for graphon. The lack of infinite crystal boundary conditions in a microcrystalline sample could be responsible for such a difference but equally, so could different spectrometer resolutions for the differently shaped samples and no distinction is possible.

5.1.3 Conclusions

The surface area of the graphon is known and the conditions for outgassing the sample to constant weight have been defined.

The neutron measurements have shown the regions of (κ,w) space which are suitable for carrying out neutron scattering experiments from adsorbed molecules. With the limitations of resolution and intensity in the experiments performed there does not seem to be any inconsistency in treating the graphon microcrystals as if they were bulk graphon.

5.2 Adsorbed Methane

5.2.1 Results

The scattered neutron time of flight spectrum was obtained from samples of methane adsorbed on graphon at the temperatures and surface coverages shown below. The experimental arrangement (see section 4.5) was such that there was at all times a constant pressure of 1 atmosphere of methane gas above the adsorbent. Consequently temperature and surface coverage could not be varied independently.

Pressure mm Hg	Temperature ^{o}K	Ⓗ	Subtracted Counts in elastic Channel $\theta = 45^{o}$	Subtracted Counts in max. of inelastic $\theta = 45^{o}$
760	115	0.58	21891	2145
	127	0.52	20552	2128
	140	0.43	13822	2045
	148	0.42	11476	983
	162	0.30	17493	3760
	176	0.23	10618	2600

Examples of the time of flight spectra obtained are shown in figures 5.6 to 5.11. The spectrum of the adsorbate is obtained by subtraction of the appropriately normalised spectrum of graphon from the combined spectrum of graphon and adsorbed methane. Normalisation of the graphon spectrum is to the same initial neutron flux and also takes account of the attenuation of the primary beam due to the adsorbate scattering (110). Results at $\kappa^2 > 1.6$ $\overset{0-2}{A}$ have been disregarded due to the imprecision inherent in subtracting out the very large numbers of counts associated with the graphon (0002) Bragg reflection at $\kappa^2 = 1.85$ $\overset{0-2}{A}$. No corrections have been made for possible effects due to changes in the graphon small angle scattering when methane is adsorbed. Any changes are expected to be very small.

FIGURE 5,6

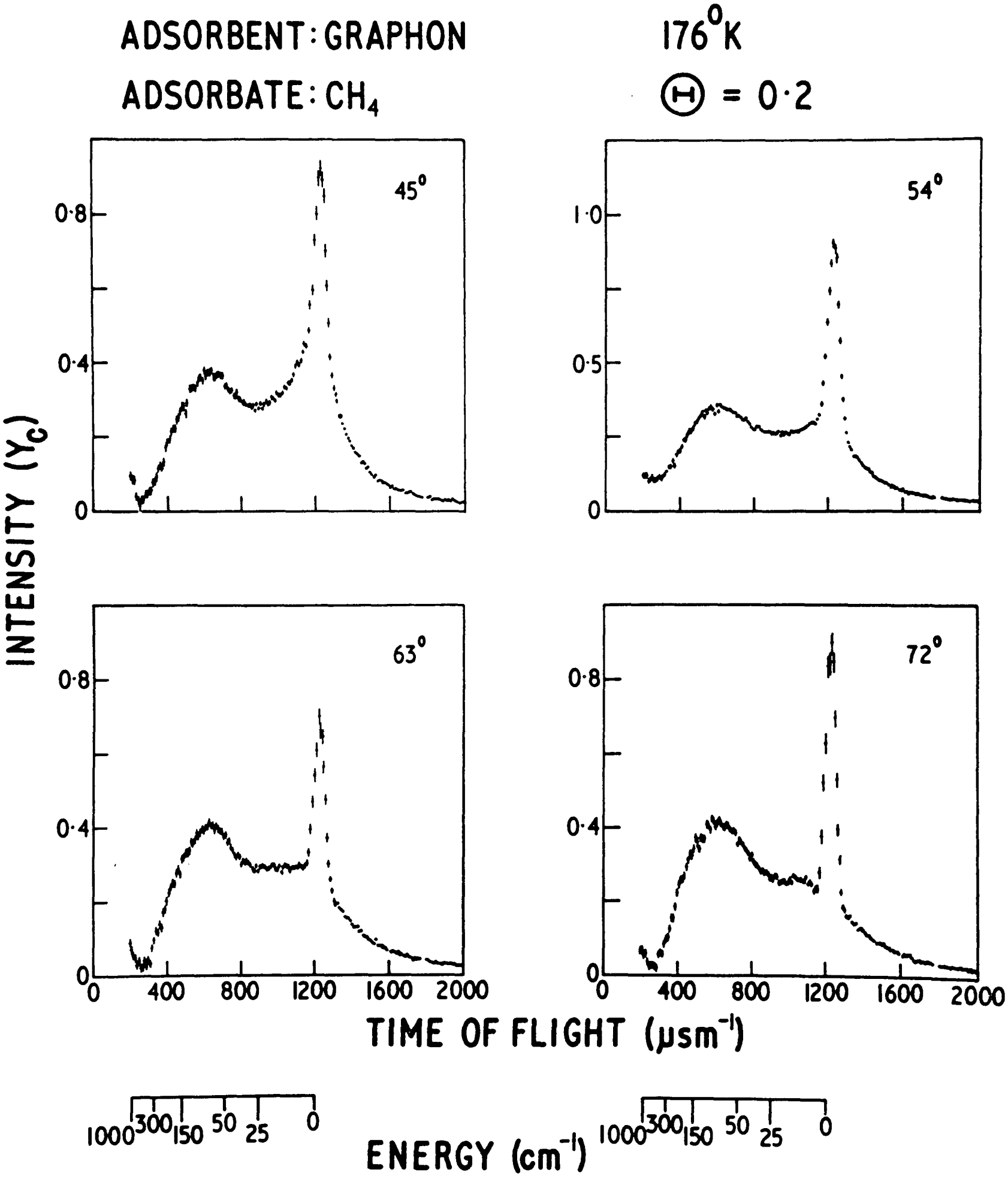
ADSORBENT: GRAPHON
ADSORBATE: CH_4
176°K
Θ = 0·2
45°
54°
63°
72°
0·8
0·4
0
1·0
0·5
400
800
1200
1600
2000
INTENSITY (Y_C)
TIME OF FLIGHT ($\mu s m^{-1}$)
1000
300
150
50
25
0
ENERGY (cm^{-1})

FIGURE 5,7

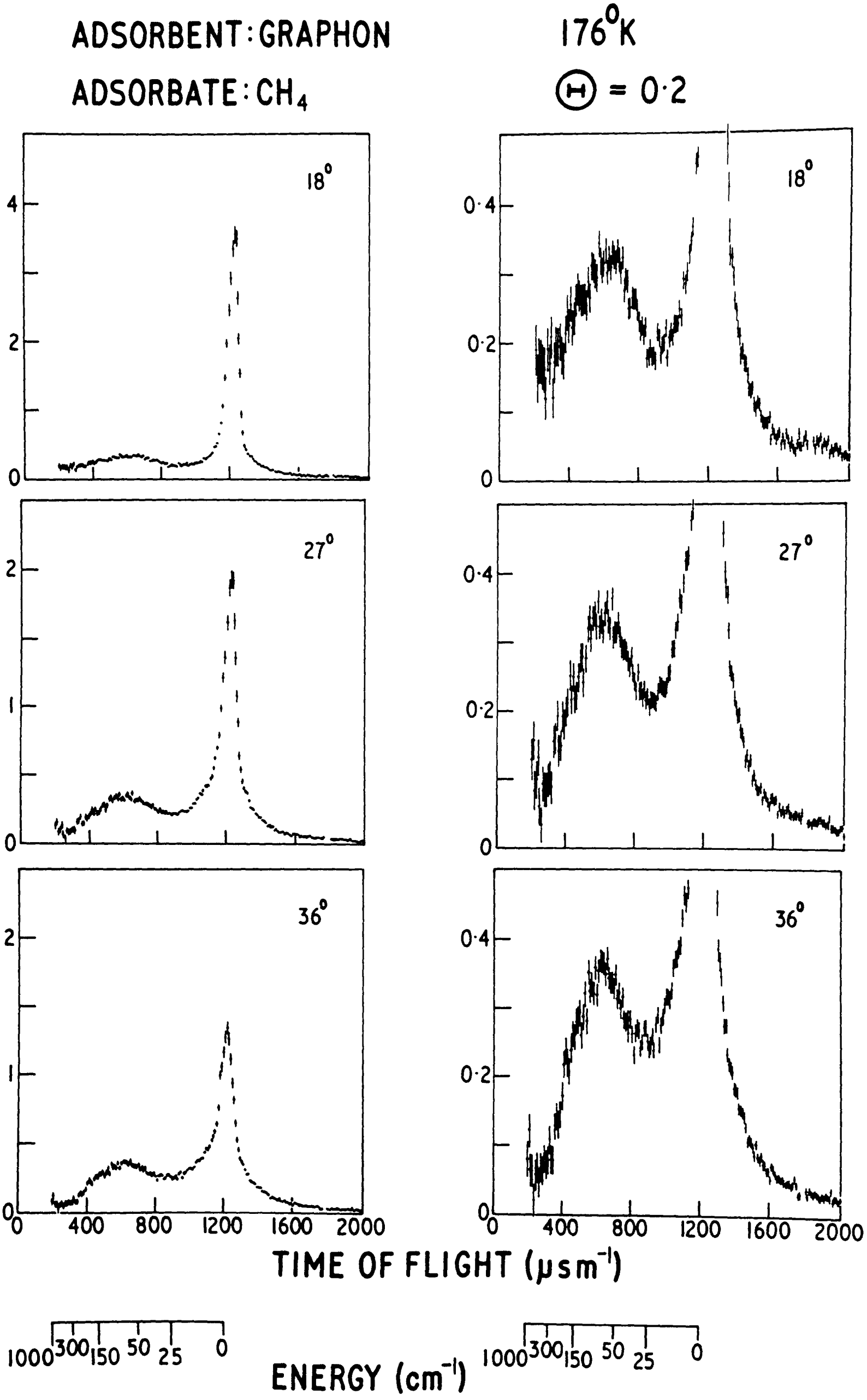
ADSORBENT: GRAPHON
ADSORBATE: CH_4
176°K
Θ = 0·2
18°
27°
36°
INTENSITY (Yc)
TIME OF FLIGHT (μsm⁻¹)
ENERGY (cm⁻¹)
0
400
800
1200
1600
2000
1000
300
150
50
25
0

FIGURE 5,8

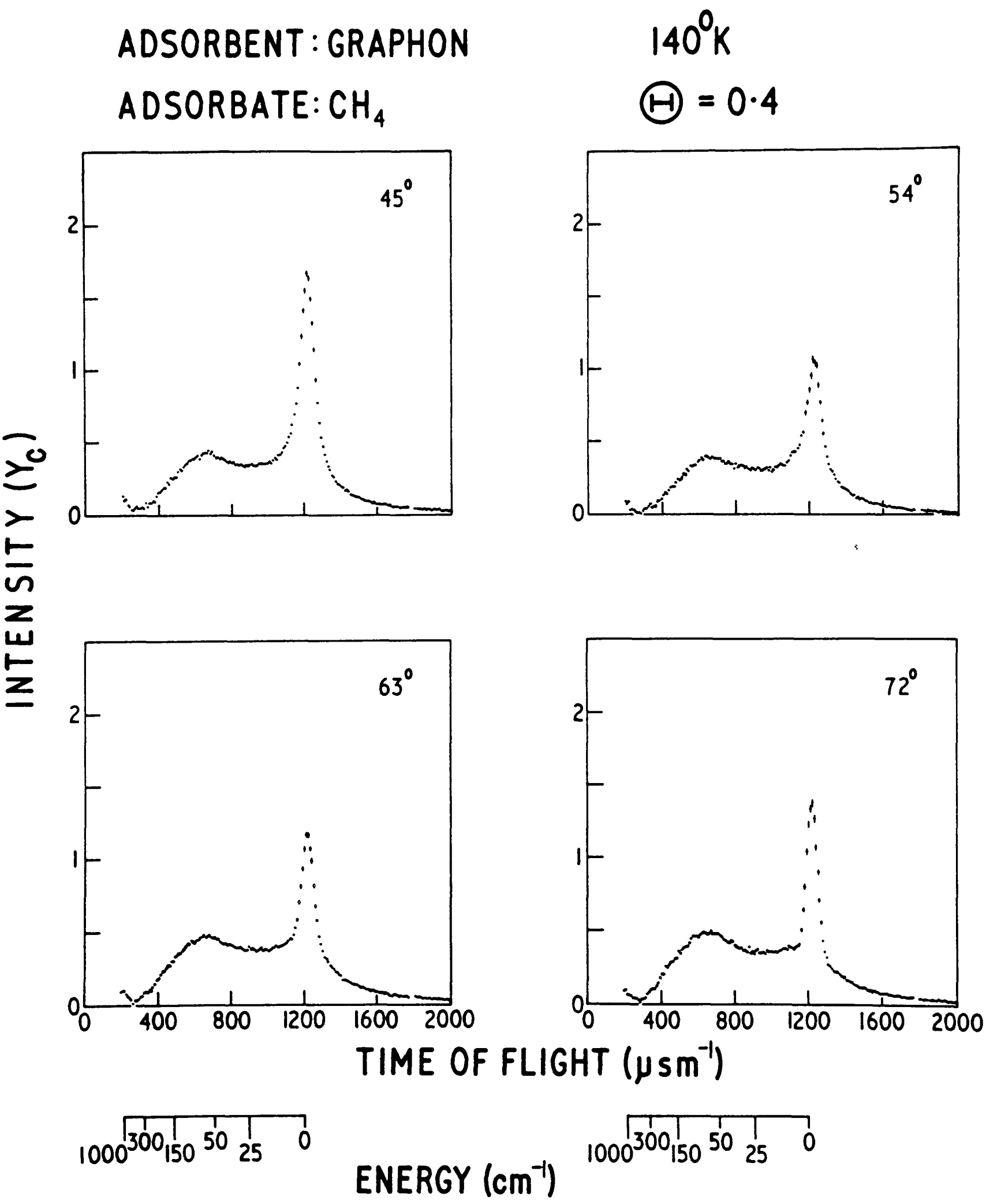
ADSORBENT : GRAPHON
ADSORBATE : CH_4
140°K
Θ = 0·4
45°
54°
63°
72°
INTENSITY (Y) (Yc)
0
1
2
0
400
800
1200
1600
2000
TIME OF FLIGHT (μsm⁻¹)
1000
300
150
50
25
0
ENERGY (cm⁻¹)

FIGURE 5.9

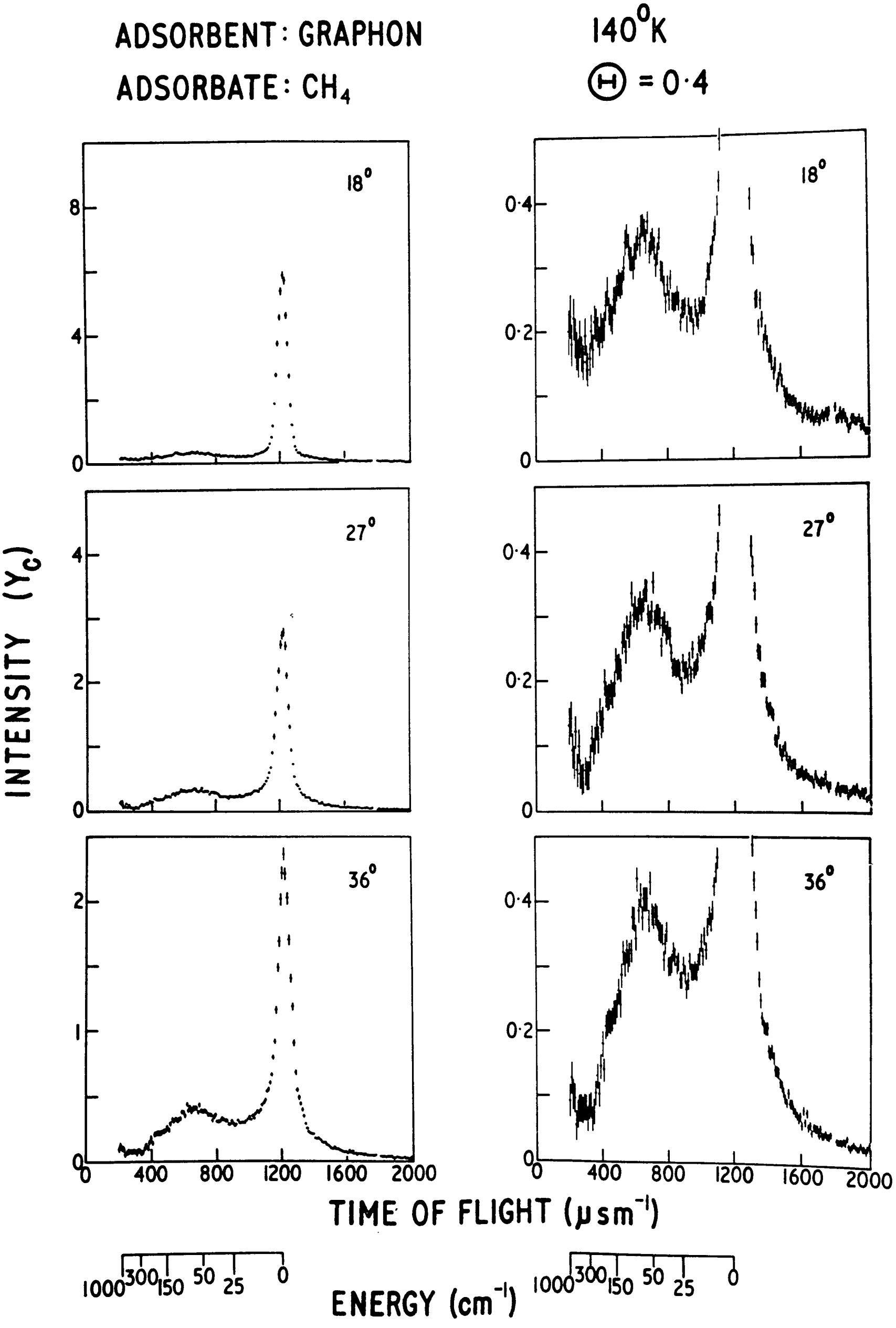
ADSORBENT: GRAPHON
ADSORBATE: CH_4
140°K
(H) = 0·4
18°
27°
36°
INTENSITY (Y_c)
TIME OF FLIGHT ($\mu s m^{-1}$)
ENERGY (cm^{-1})
1000 300 150 50 25 0
0 400 800 1200 1600 2000

FIGURE 5,10

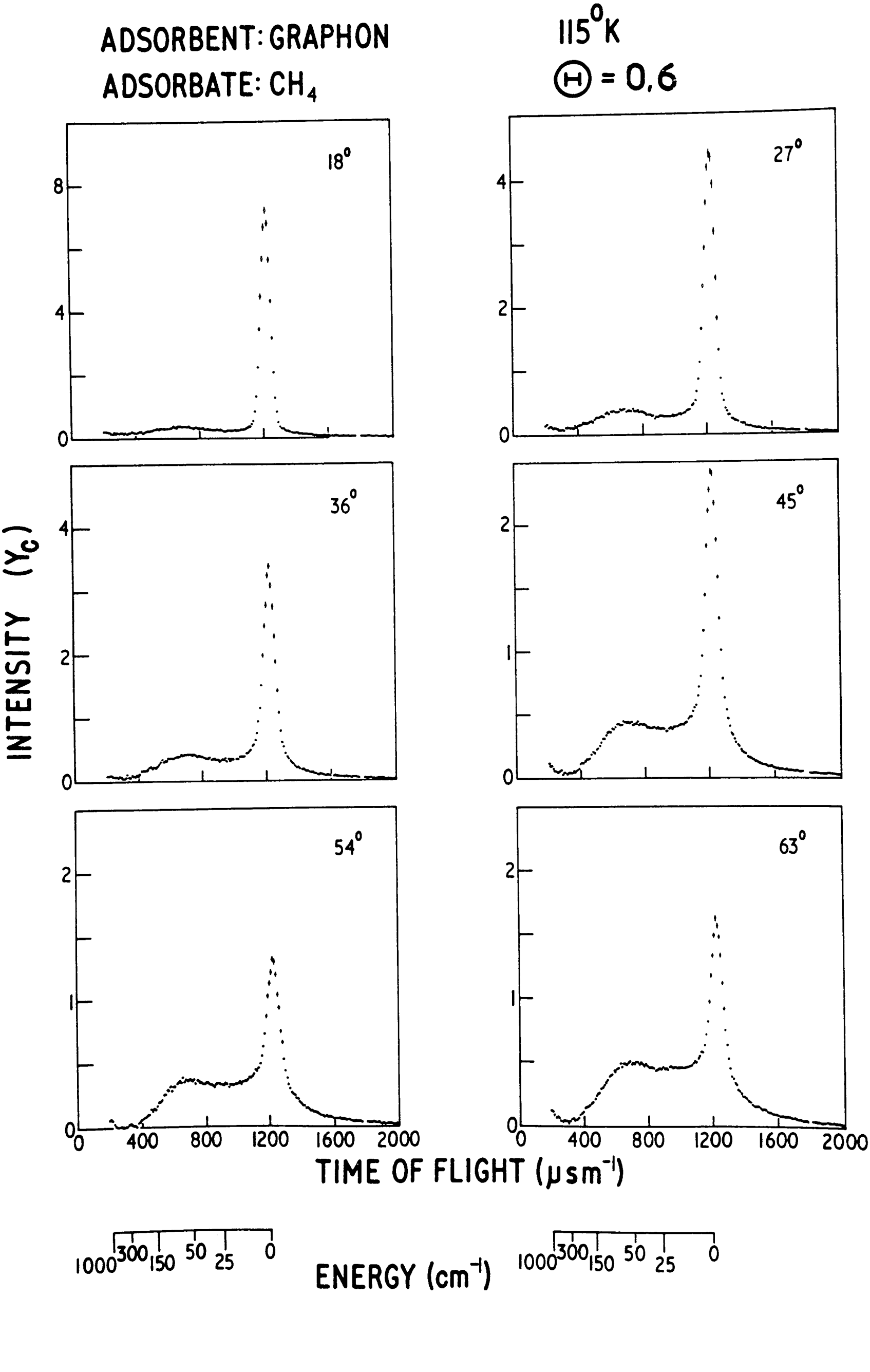
ADSORBENT: GRAPHON
ADSORBATE: CH_4
115°K
Θ = 0.6
18°
27°
36°
45°
54°
63°
INTENSITY (Yc)
TIME OF FLIGHT (μsm⁻¹)
ENERGY (cm⁻¹)
1000 300 150 50 25 0
0 400 800 1200 1600 2000

FIGURE 5,11

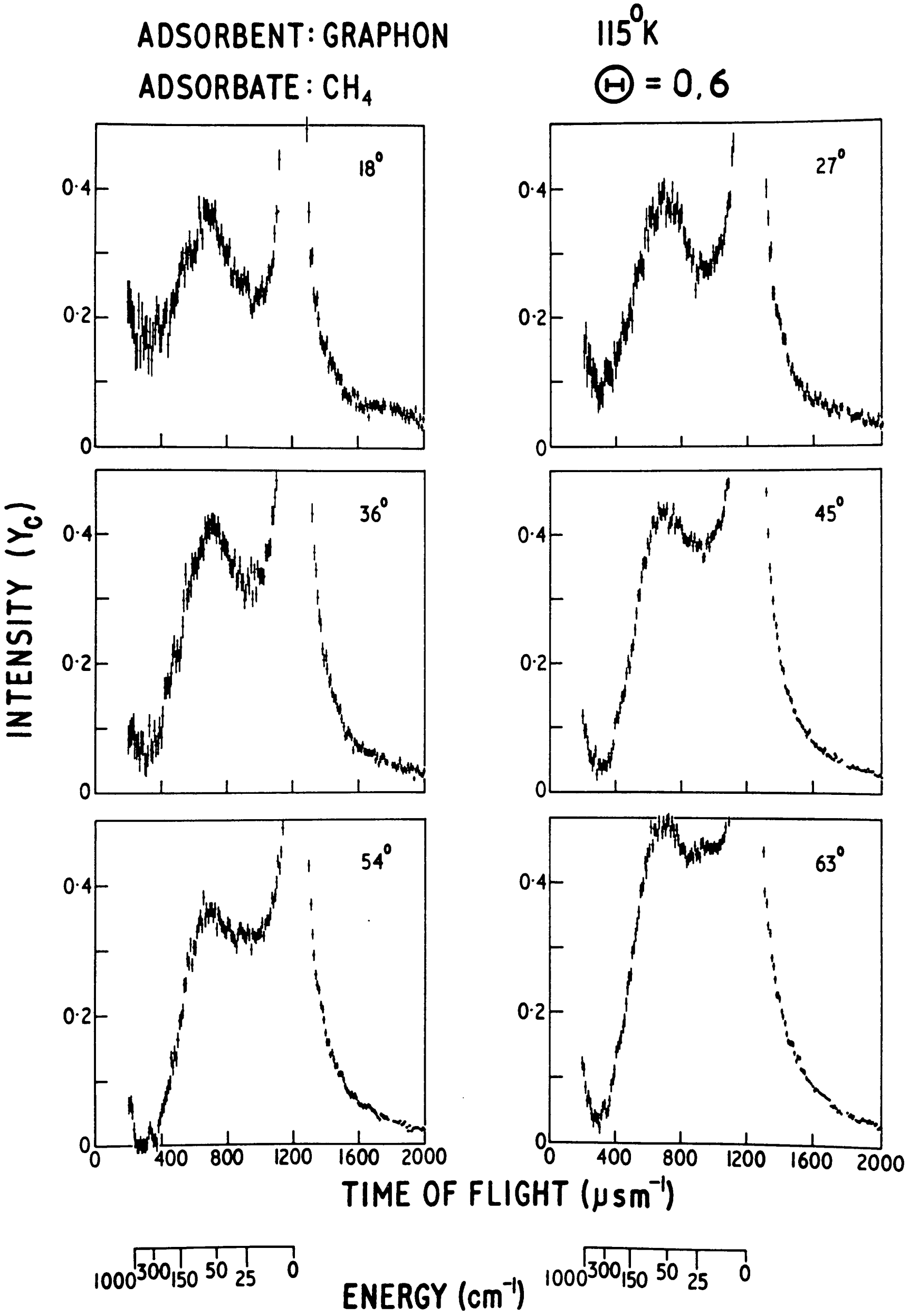
ADSORBENT: GRAPHON
ADSORBATE: CH_4
115°K
Θ = 0,6
18°
27°
36°
45°
54°
63°
0·4
0·2
0
INTENSITY (Y_c)
0
400
800
1200
1600
2000
TIME OF FLIGHT ($\mu s m^{-1}$)
1000
300
150
50
25
0
ENERGY (cm^{-1})

5.2.2 Vibrations of the adsorbed molecules with respect to the surface

As seen in previous experiments there is for all temperatures a well developed quasi elastic peak whose shape and intensity is dependent on the momentum transfer. The rotational envelope is enhanced as the time of flight spectrum is $w^2S(\kappa,w)$ and not $S(\kappa,w)$. The intensity variation of the quasi elastic peak is shown in figure 5.12. The intensity has been taken as the area under the convoluted QEP after corrections for background and multiple scattering have been made. It can be seen that the plots of log (I) vs κ^2 are close to linear and the results of each experiment can be summarised by the gradient of the plot. Figure 5.13 gives the temperature and surface coverage variation of this parameter.

Whilst the slope of the log (I) vs κ^2 plots cannot be directly related to an amplitude of vibration for the polyatomic molecule as it can for a simple harmonic oscillator, the results nonetheless suggest that the motion of the scattering nucleii is akin to the gaussian space time development of a randomly moving particle and there is no strong indication that other form factors, such as a Bessel function dependence from predominantly rotational motion, would give a better fit to the κ dependence.

There is no direct evidence in the inelastic region of the time of flight spectra for transitions associated with adsorbate/adsorbent vibrations. The total $S(\kappa,w)$ is a convolution of the scattering laws for all possible motions. Whilst the vibrational scattering law may show delta function intensity at multiples of $\hbar w_\perp$, convolution with the scattering law for rapid surface translation will produce a broad featureless scattering law where the vibrational contribution is not easily detected. (See section 3.9.3)

FIGURE 5, 12

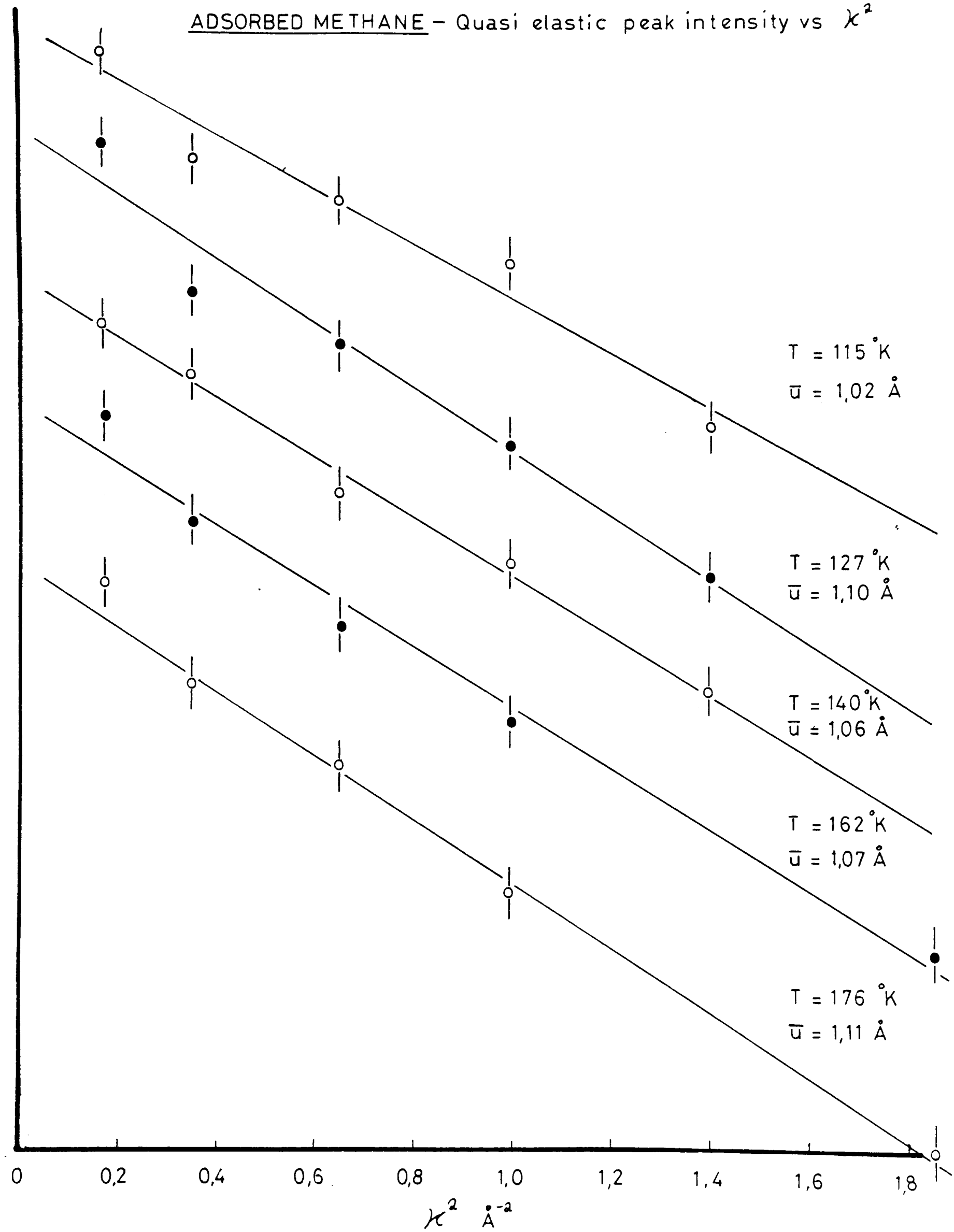
LOG(I)
ADSORBED METHANE – Quasi elastic peak intensity vs k^2
T = 115 °K
ū = 1,02 Å
T = 127 °K
ū = 1,10 Å
T = 140 °K
ū = 1,06 Å
T = 162 °K
ū = 1,07 Å
T = 176 °K
ū = 1,11 Å
0
0,2
0,4
0,6
0,8
1,0
1,2
1,4
1,6
1,8
k^2 Å^{-2}

FIGURE 5,13

ADSORBED METHANE

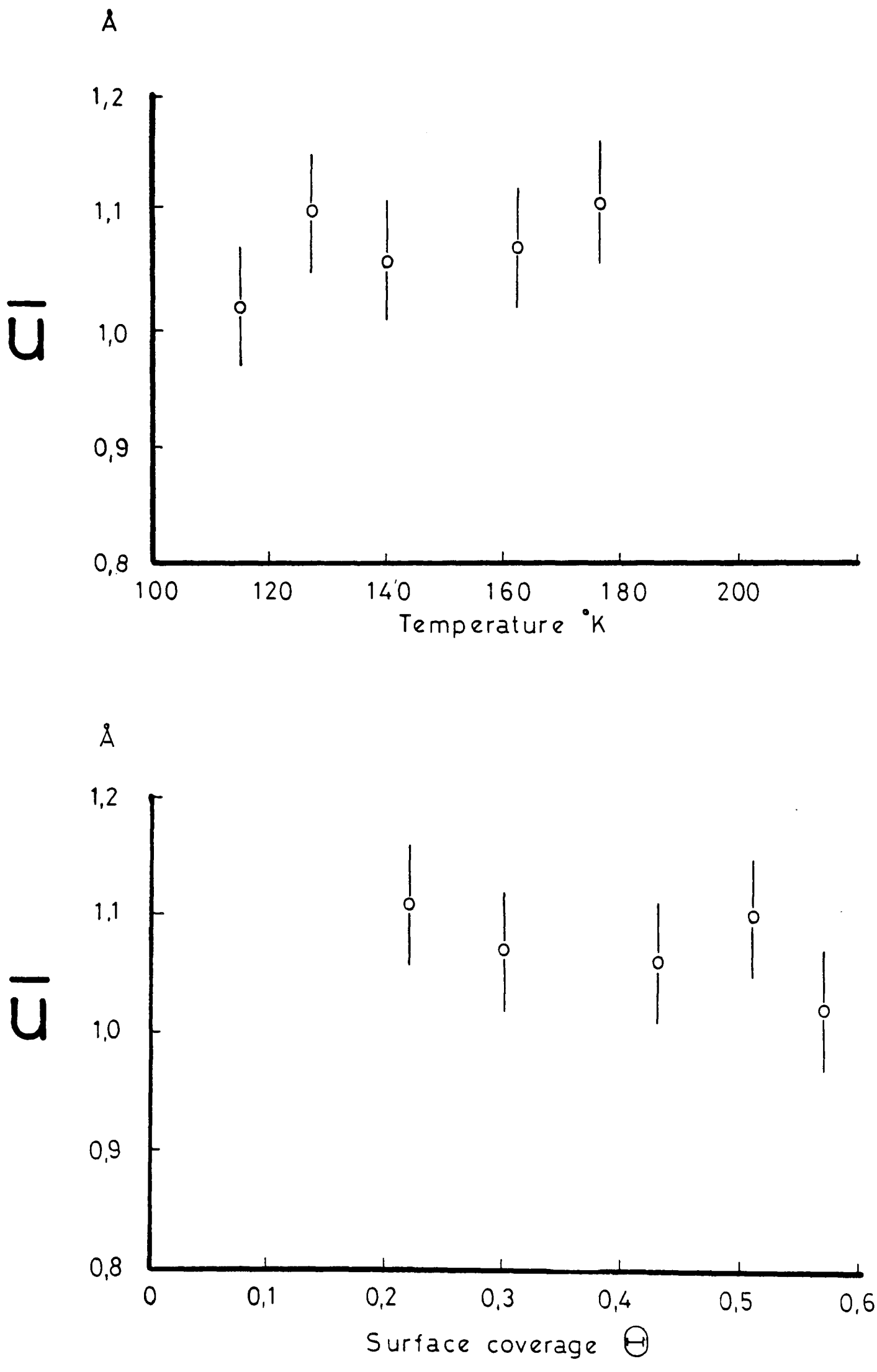

The inelastic time of flight spectrum for methane was simulated using the model of Dasannacharya (78) (See section 3.4). An example of a fit to the data is shown in figure 5.14. The prediction of the general form is good but agreement in detail is poor, particularly in the intensity scattered at small energy transfers. The calculation (78) has been found to be a good fit to the data for liquid methane (79). The extra intensity that is seen at low energy transfers could be due to the convoluted contribution of adsorbate-adsorbent vibrations in the rotational envelope.

Figure 5.15 plots the position of the observed inelastic maximum as a function of temperature. It is compared with the expected behaviour for liquid and gaseous methane. The different behaviour for the two phases is due to the distortion of the inelastic region in the gas spectrum that occurs when the "elastic" peak moves into the inelastic region as a result of the recoil. The behaviour for adsorbed methane is closer to that expected for liquid methane, though there does appear to be some distortion.

5.2.3 Translations of the adsorbed molecules

In line with the philosophy expressed in section 4.2.3, the shape dependence of the quasi elastic peak on κ^2 was initially investigated using a deconvolution method. Examples of the results obtained are shown in figure 5.16. The AREA and TABLE methods used in the DECONVOX routine (112) disagree significantly and systematically, and cannot be reconciled, for example by adjusting the background. The observation of a maximum in the ΔE vs κ^2 plot might arise from jump diffusion but it cannot be the case here as the plot is not oscillatory and there is apparently negligable broadening at the higher κ^2. As was stressed in section

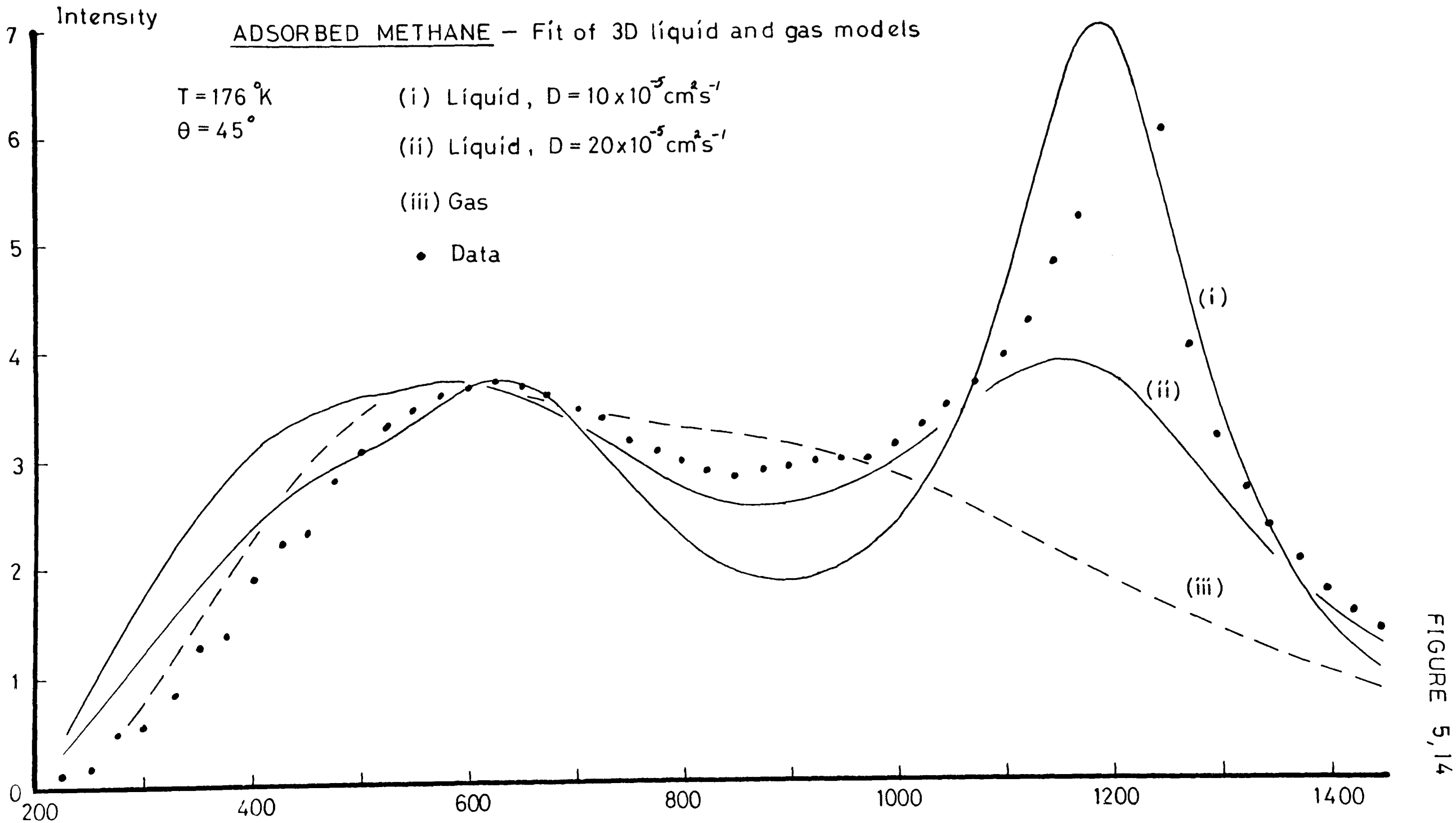
Intensity
ADSORBED METHANE – Fit of 3D liquid and gas models
T = 176 °K
θ = 45°
(i) Liquid, D = 10 x 10⁻⁵ cm²s⁻¹
(ii) Liquid, D = 20 x 10⁻⁵ cm²s⁻¹
(iii) Gas
• Data
(i)
(ii)
(iii)
0
1
2
3
4
5
6
7
200
400
600
800
1000
1200
1400

FIGURE 5,14

FIGURE 5,15

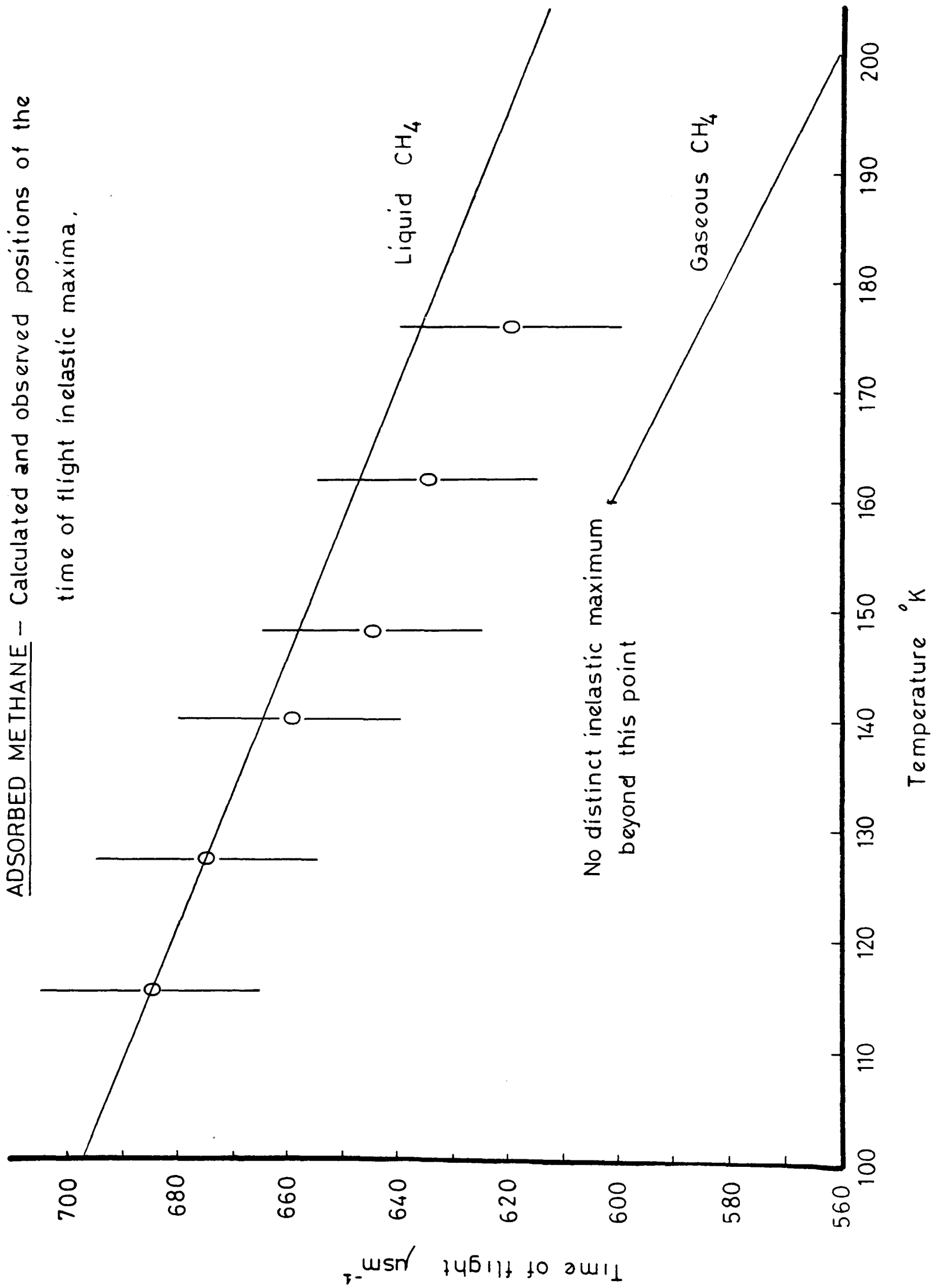
ADSORBED METHANE – Calculated and observed positions of the time of flight inelastic maxima.
Liquid CH_4
Gaseous CH_4
No distinct inelastic maximum beyond this point
Time of flight $\mu s m^{-\frac{1}{2}}$
Temperature °K
700
680
660
640
620
600
580
560
100
110
120
130
140
150
160
170
180
190
200

FIGURE 5,16

ADSORBED METHANE – Deconvolution of $S(k,\omega)$

∘ Area + Table

Temperature K

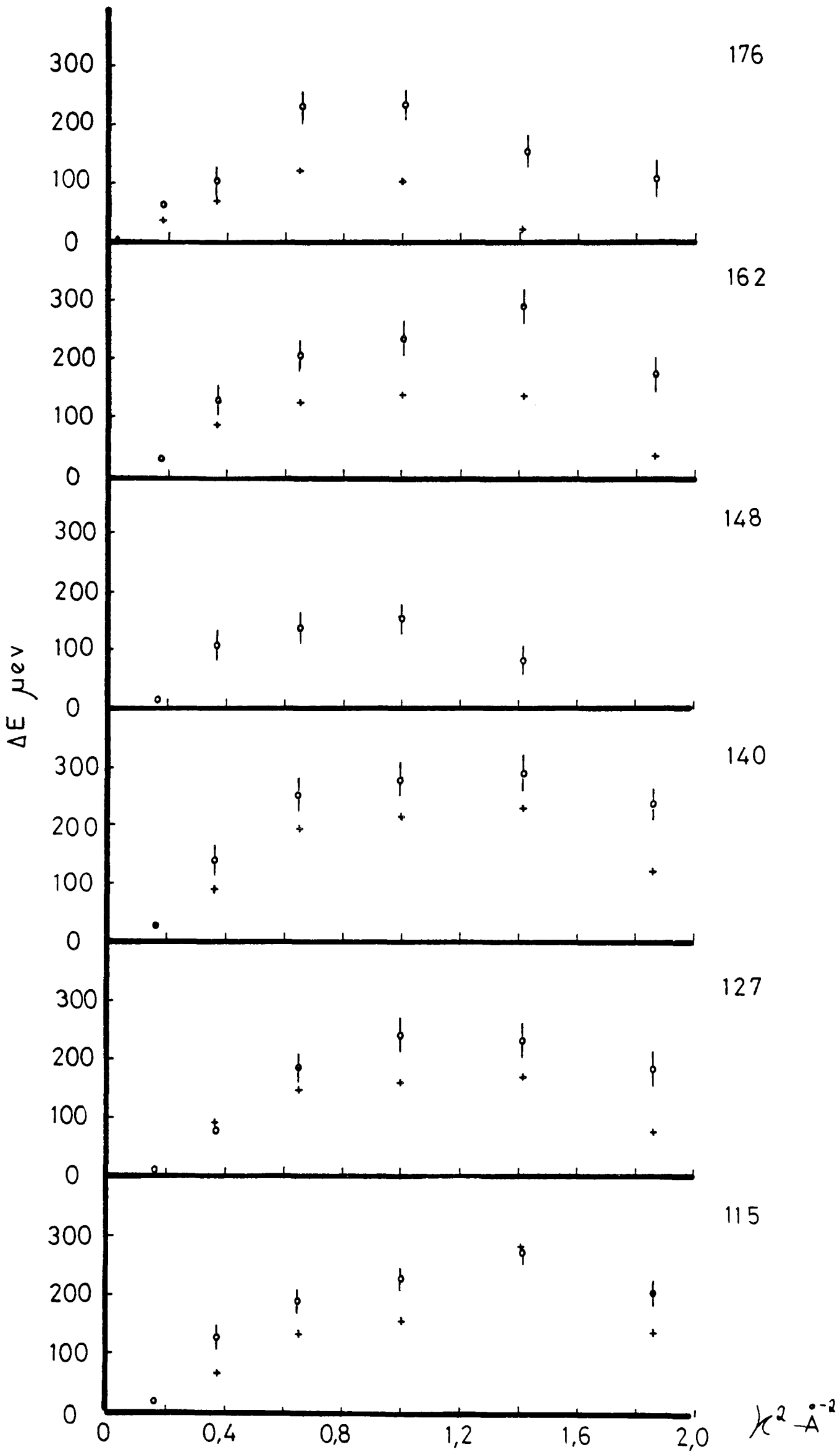

4.2.3 no conclusions can be drawn from this exercise, other than that the observed quasi elastic peak is the result of convoluting the machine gaussian resolution function with something other than a lorentzian sample spectrum.

At the temperatures of the measurements it is extremely unlikely that the adsorbed methane should be in a solid like phase. The shape of the inelastic envelope in the time of flight spectrum confirms this. A two dimensional gas or liquid phase is quite possible. The calculations and figures in section 3.11.1 show that a 2D gas, whilst retaining a maximum intensity at $S(\kappa,o)$, also develops an increasing asymmetry in $S(\kappa,w)$ as κ increases. Such asymmetry is not evident in the observed $S(\kappa,w)$ and attention has been focussed on the 2D liquid approach.

The programme ORIANA was used to generate scattering laws for randomly oriented two dimensional liquids with different diffusion coefficients. Multiple scattering corrections were applied and it was attempted to fit the $S(\kappa,w)$'s generated to those observed.

Analysis of the widths of the observed $S(\kappa,w)$ at chosen fractional heights was used to obtain the best fit value of the diffusion coefficient. Figure 5.17 shows how the predicted full width at the half maximum of the convoluted $S(\kappa,w)$ varies with diffusion coefficient and for selected values of κ^2. On these calculated lines are plotted the actual half widths of the convoluted scattering laws, the error bars reflect the error in the measurement of the FWHM. If the model is correct then the observed widths should occur at a constant value of D.

Examples of the observed $S(\kappa,w)$ and the best fits are shown in figures 5.18 to 5.20. Since the scattering law is symmetric in w, points on the energy gain side have been folded over onto the energy loss side. This is solely to improve the clarity of

FIGURE 5,17

ADSORBED METHANE – Determination of diffusion coefficient

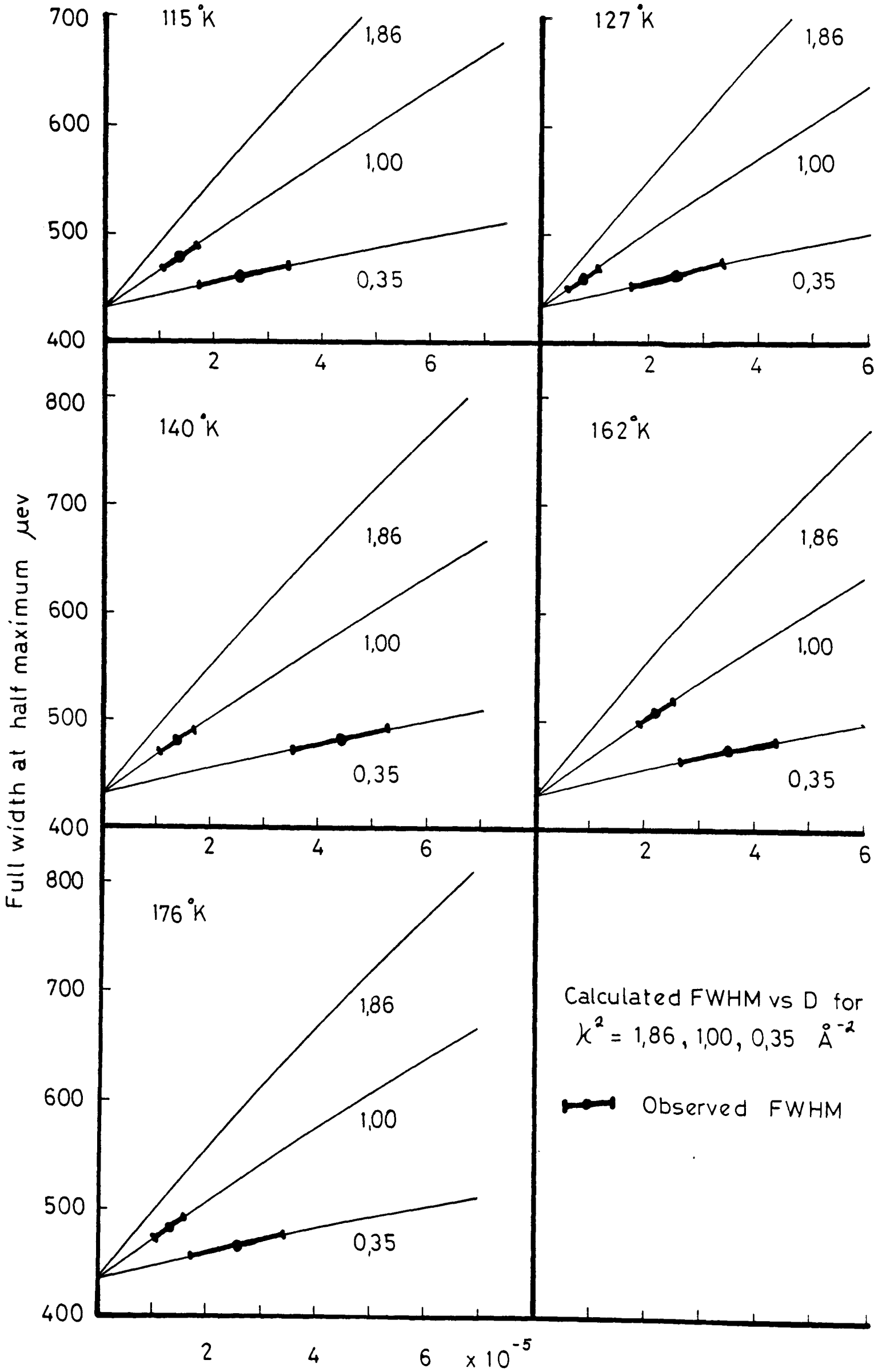

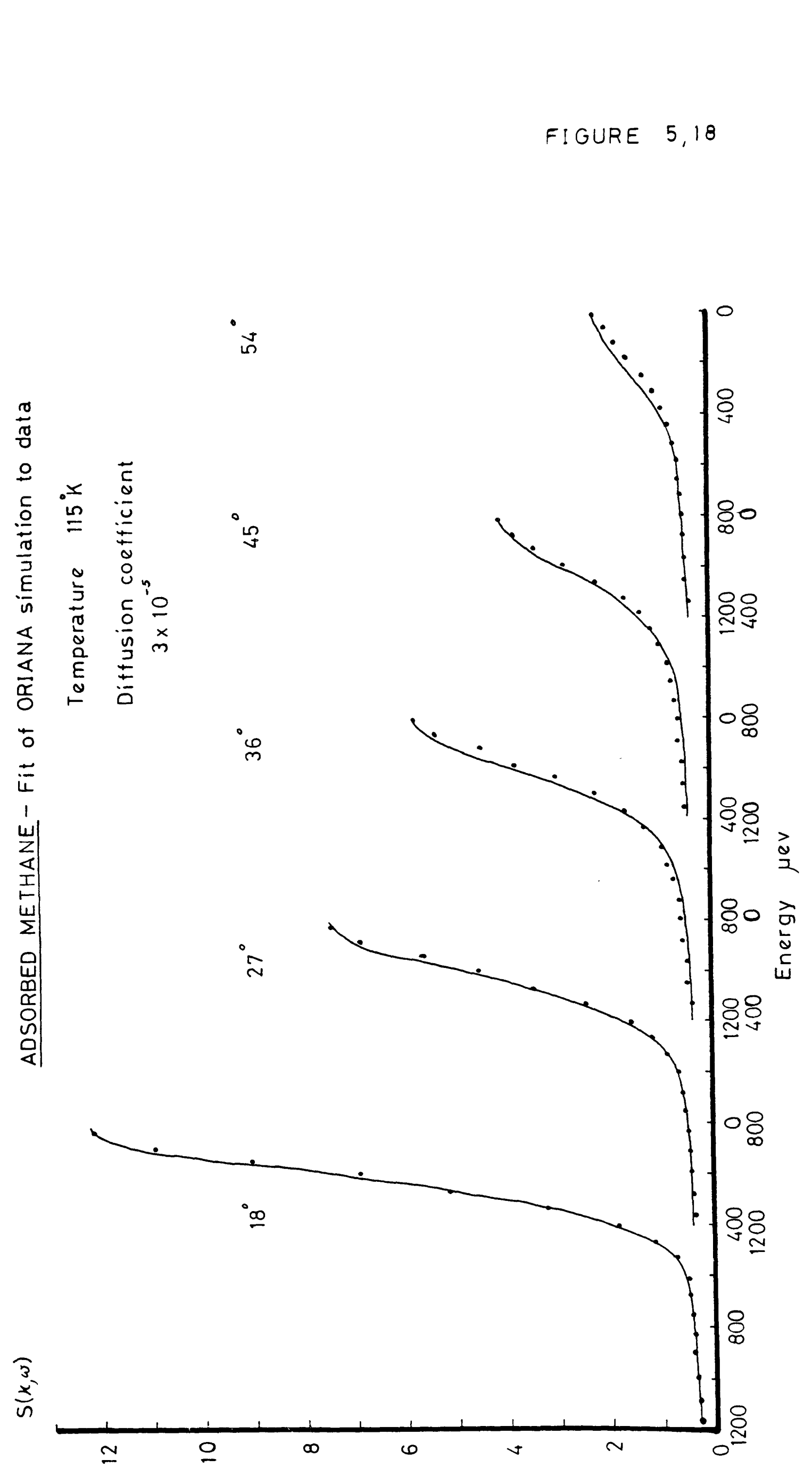
ADSORBED METHANE – Fit of ORIANA simulation to data
Temperature 115°K
Diffusion coefficient
3 x 10⁻⁵
S(κ,ω)
36°
45°
54°
27°
18°
12
10
8
6
4
2
0
1200
800
400
0
400
800
1200
0
800
400
0
400
800
1200
0
800
400
0
Energy μev

FIGURE 5,18

ADSORBED METHANE – Fit of ORIANA simulation to data

Temperature 127 °K

Diffusion coefficient

2×10^{-5}

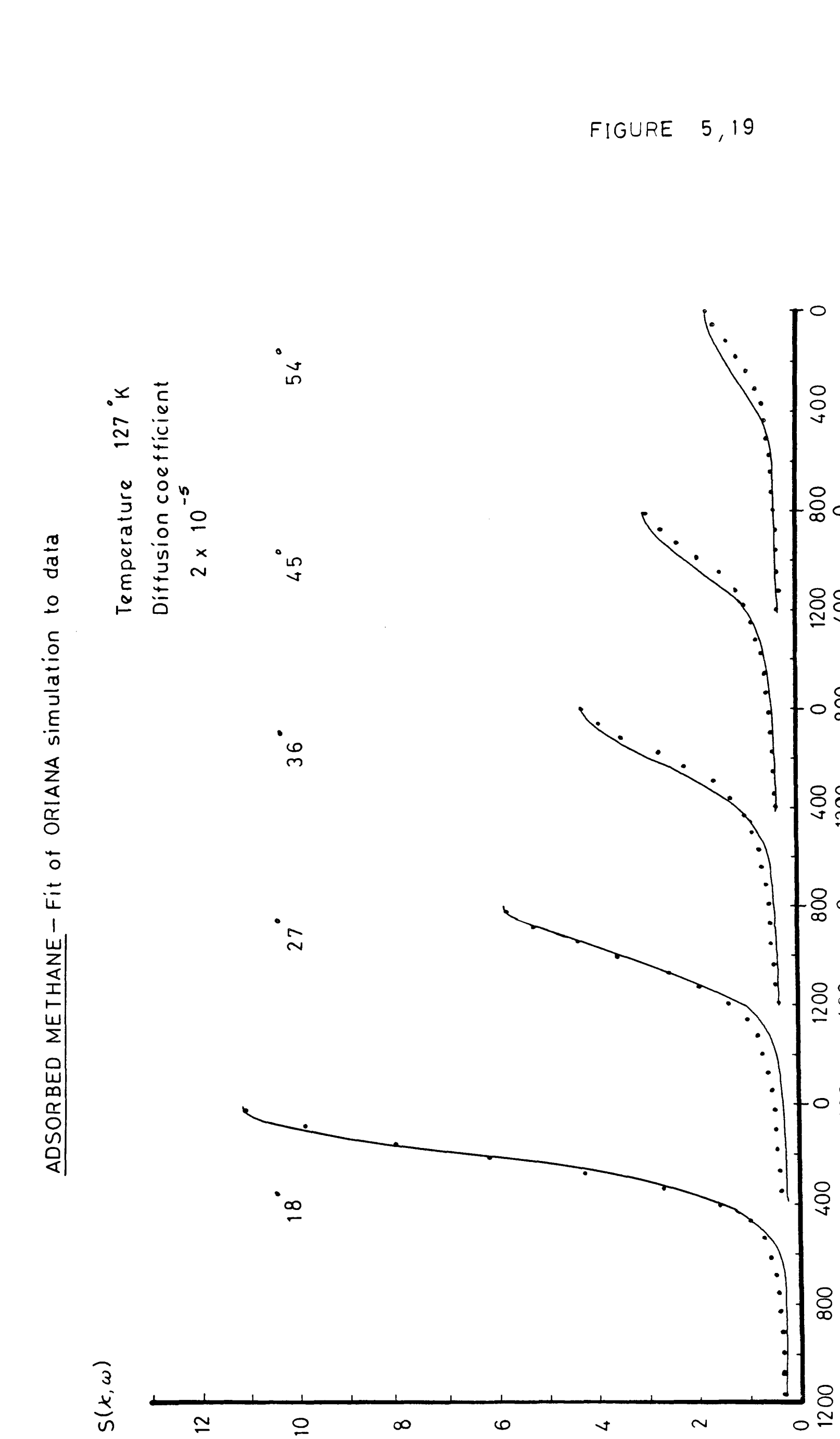

FIGURE 5,19

FIGURE 5,20

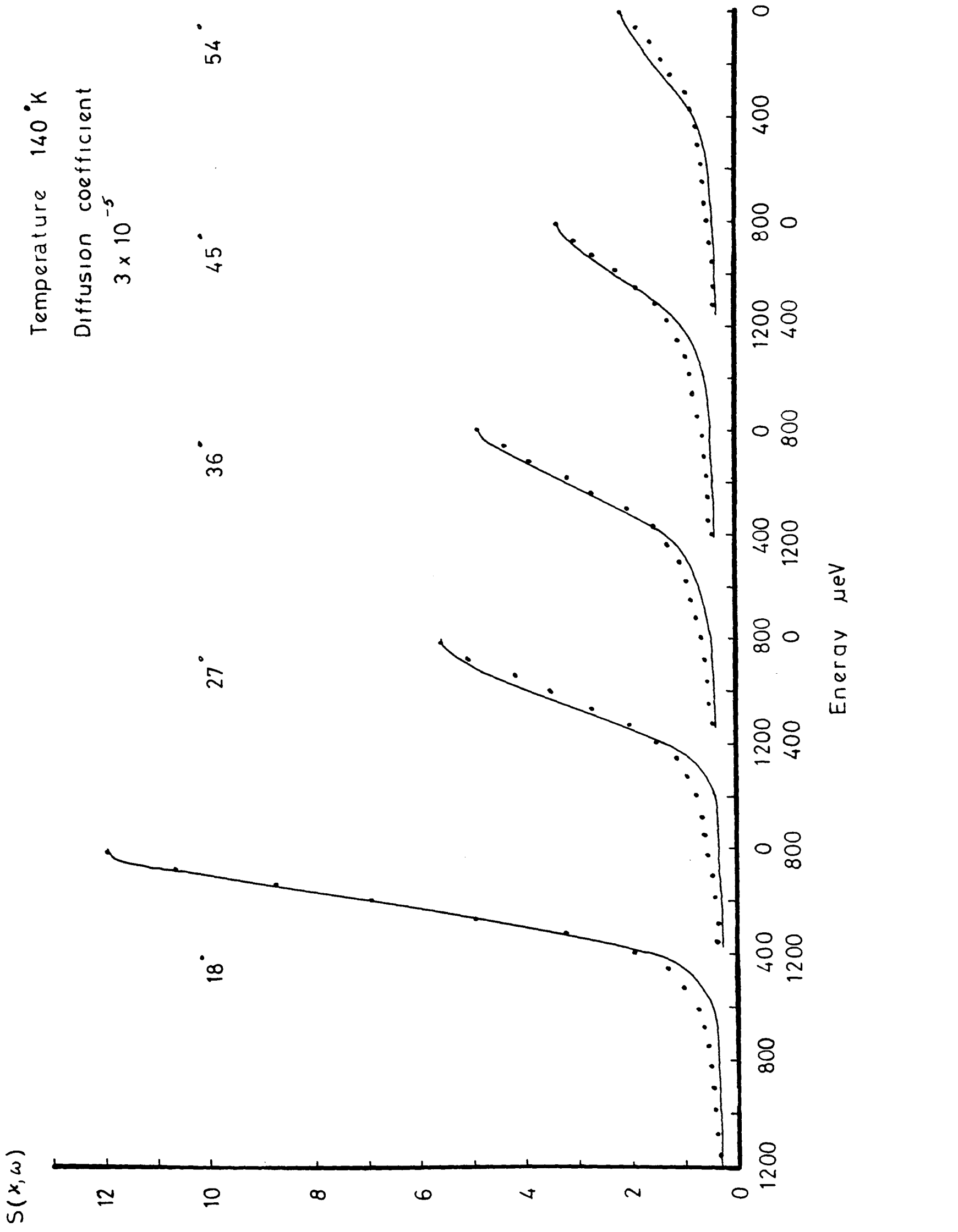
ADSORBED METHANE — Fit of ORIANA simulation to data
Temperature 140 °K
Diffusion coefficient
3 x 10⁻⁵
S(x, ω)
12
10
8
6
4
2
0
18°
27°
36°
45°
54°
1200
800
400
0
Energy μeV

presentation. The closeness of fit of the data to the model and to a voigt curve was checked using a crude χ^2 test (161). Some representative values are shown in table 5.2. It can be seen that the 2D liquid model is always a better fit than a voigt profile.

It can also be seen that the fit is reasonable at 115°K and 127°K but is much less satisfactory at higher temperatures. The lack of agreement could be due to a combination of real and apparent effects.

1) At the higher temperatures the concentration of adsorbed methane is small and there are likely to be large errors in subtracting out such a small contribution to the total scattering. The elastic scattering is by far the most intense feature of the graphon spectrum and it is possible that some of the intensity at w = o in the adsorbate spectrum arises from incomplete subtraction of the adsorbent spectrum. If this was the case then one might expect to see similar discontinuities in the inelastic region, arising from the graphon density of states and the c axis phonon. There is no evidence of this in figures 5.7 to 5.11.

2) The assignment of the background intensity becomes very much more difficult at the higher temperatures as the relative contribution from the inelastic scattering has increased and the quasi elastic scattering itself has become much broader. The original criteria adopted for selecting the background level may not now be applicable. It can be tested by considering the temperature dependence of the widths of $S(\kappa,w)$ at various fractional heights. For a Fickian liquid the unconvoluted widths should be a linear function of $^1/_T$, having the same slopes given by the activation energy for diffusion. The widths of the convoluted peaks will not give a linear variation with $^1/_T$ but would be expected to vary in some similar smooth fashion. If the background had been wrongly

assigned at higher temperatures then there may be a discontinuity in the curves for each fractional height.

Plots of widths against $^1/_T$ are shown in figure 5.21. The widths at $\frac{3}{4}$ and $\frac{1}{2}$ of the height of $S(\kappa,o)$ are virtually temperature independent. However the width at $\frac{1}{4}$ height does increase in temperature and in a fashion unrelated to the widths at $\frac{3}{4}$ and $\frac{1}{2}$ height. The possibility of a gross misalignment of the background can be ruled out.

The corrections used for multiple scattering were based on the predicted $S(\kappa,w)$ at one temperature. If the scattering law has significantly changed shape at the higher temperatures, due possibly to a change in dynamics, then the correction will not be so good. It is expected that this would be a minor change.

5.2.4 Discussion

The predicted scattering law for an isotropically dispersed, two dimensional liquid with a diffusion coefficient of 3×10^{-5} cm^2 s^{-1} agrees reasonably well with the observed spectrum of adsorbed methane at 115^oK and Ⓗ = 0.58. The agreement is considerably better than that obtained when trying to fit a Voigt profile.

With increasing temperature and decreasing surface coverage the agreement becomes quickly poorer and by 140^oK the predictions are clearly inadequate. The model cannot describe the sharpness of the central peak, nor the abrupt change to slowly decaying intensity in the wings of the function.

The method of angle averaging $S(\kappa,w)$ produces a sharply peaked scattering law more slowly varying in shape with κ than a three dimensional scattering law. Such behaviour is evident in the observed scattering laws and together with the partial success of the model in fitting the results it seems that the approach that ha been adopted is basically correct. The failure of the model in

Table 5.2

ADSORBED METHANE - Closeness of fit of 2D liquid model to the observed scattering law

Temperature ^{o}K	Angle of scatter	χ^2_ν	
		2D liquid profile	Voigt profile
127	27	13,112	16,341
	36	1,351	
	45	3,064	9,729
	54	2,667	
115	36	1,351	4,434
127	36	4,538	
162	36	1,492	

$$\chi^2_\nu = \frac{1}{N} \sum_i \frac{(\text{model}_i - \text{observed}_i)^2}{\sigma_i^2}$$

FIGURE 5, 21

ADSORBED METHANE – Widths at fractional heights

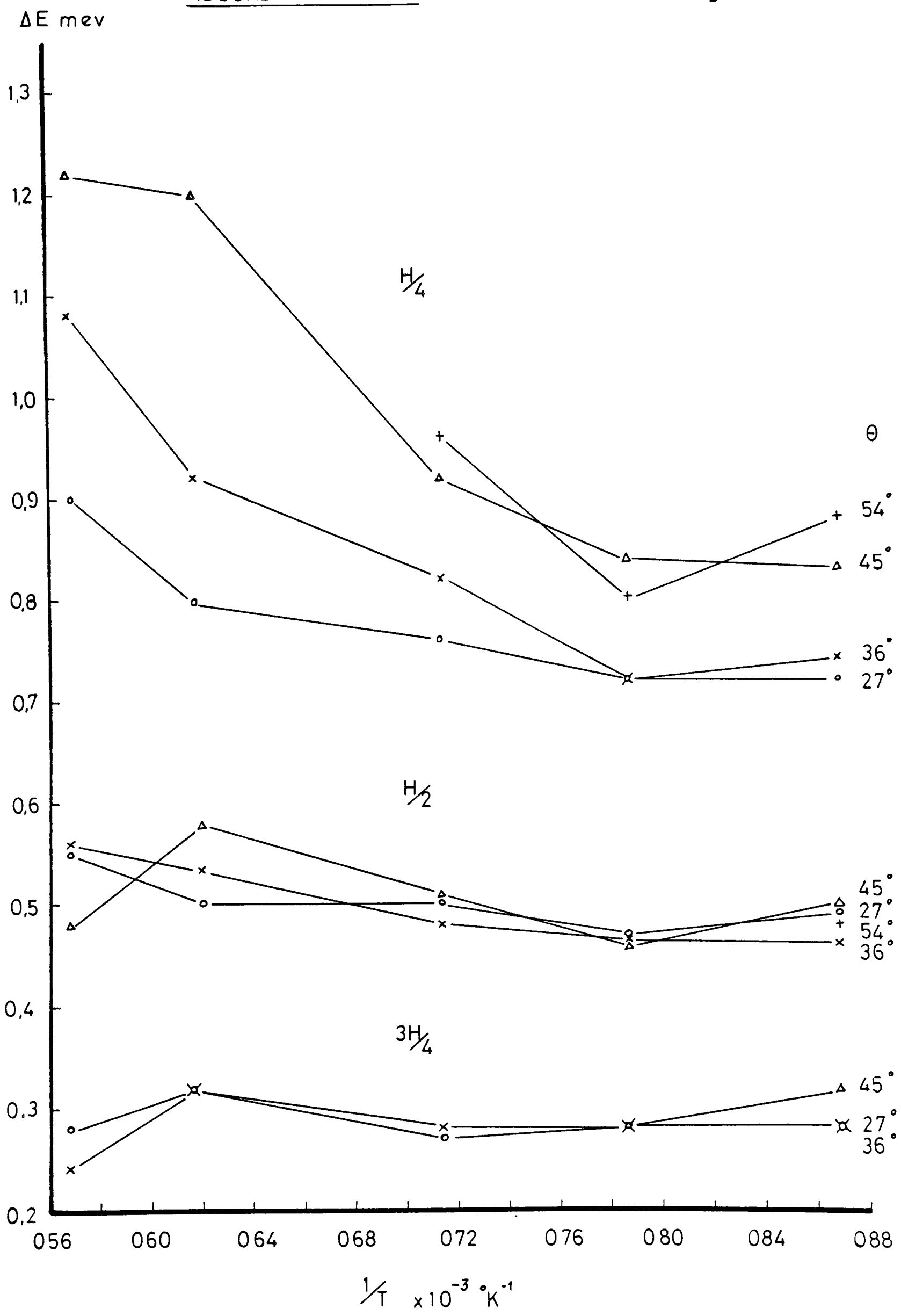

certain regimes is most likely due to the simplistic approach chosen to describe the dynamics of the adsorbate, rather than data handling errors.

At temperatures close to the bulk boiling point and with appreciable surface coverages, the methane-methane separation on the carbon surface is much smaller than in the bulk gas phase and may be similar to or slightly larger than in the bulk liquid phase. Thus a liquid like model of surface diffusion is a better approximation than gas like surface motion. With decreasing surface coverage and increasing temperature there is a steady increase in the ideal admolecule separations, to values which, though still much smaller than those in the bulk phase are now appreciably larger than the separations in the bulk liquid. This is possible as an admolecule experiences interactions with the adsorbent which compensate to some degree for the diminishing adsorbate-adsorbate interactions. As it is not possible to extract information from a scattered neutron spectrum in order to define a correlation function, but rather one tests a particular dynamical model against the actual data, it is not possible at this stage to define the translational motion of the adsorbed methane more closely. From the results obtained in this work it can only be concluded that in the range of T and Ⓗ studied the adsorbed methane passes from a two dimensional liquid like structure to a state which is neither liquid-like nor gas-like.

The κ^2 dependence of the quasi-elastic peak intensity changes slowly with T and Ⓗ and reinforces the supposition that the motion of the particle on the surface does not change abruptly. The values of the log (I) vs κ^2 plots are large, $\simeq 1$ Å, and in agreement with the small force constant and low vibration frequency that have been calculated for a methane-surface vibration. (See section 2.5.1 and (48)). Using the gross approximation of simple harmonic motion such

as amplitude of vibration for a particle with the mass of a methane molecule corresponds to a vibration frequency of 80 to 90 cm^{-1}.

5.3 Adsorbed Ethylene

5.3.1 Results

Neutron time of flight spectra were obtained from samples of ethylene adsorbed on graphon at the temperatures and surface coverages shown below. The experiments were carried out in the same way as for methane adsorbed on graphon so that temperature and surface coverage were not independent variables.

Pressure mm	Temperature	Ⓗ	Subtracted counts in the elastic channel θ = 45	Subtracted counts in the inelastic maximum θ = 45
760	175	2.1	20565	2625
	185	1.8	20640	3720
	195	1.3	10969	2142
	204	1.1	13138	2709
	215	1.0	11187	2625
	235	0.8	19349	1069

Examples of the adsorbate time of flight spectra are shown in figures 5.22 to 5.24. Subtraction of the graphon spectrum was carried out as described before. Results for $\kappa^2 > 1.6$ $\mathring{A}^{-2}$ have been disregarded due to the strong Bragg scatter from the graphon.

5.3.2 Vibrations of the adsorbed ethylene with respect to the surface

The time of flight spectra for adsorbed ethylene are qualitatively similar to the spectra of adsorbed methane. A quasi elastic peak is evident at all temperatures, diminishing in importance relative to the inelastic scattering as the temperature rises. For a given temperature the intensity of the quasi elastic peak decreases very rapidly with increasing momentum transfer.

The inelastic region shows a broad, featureless hump associated with rotational transitions. The maximum is less well

FIGURE 5,22

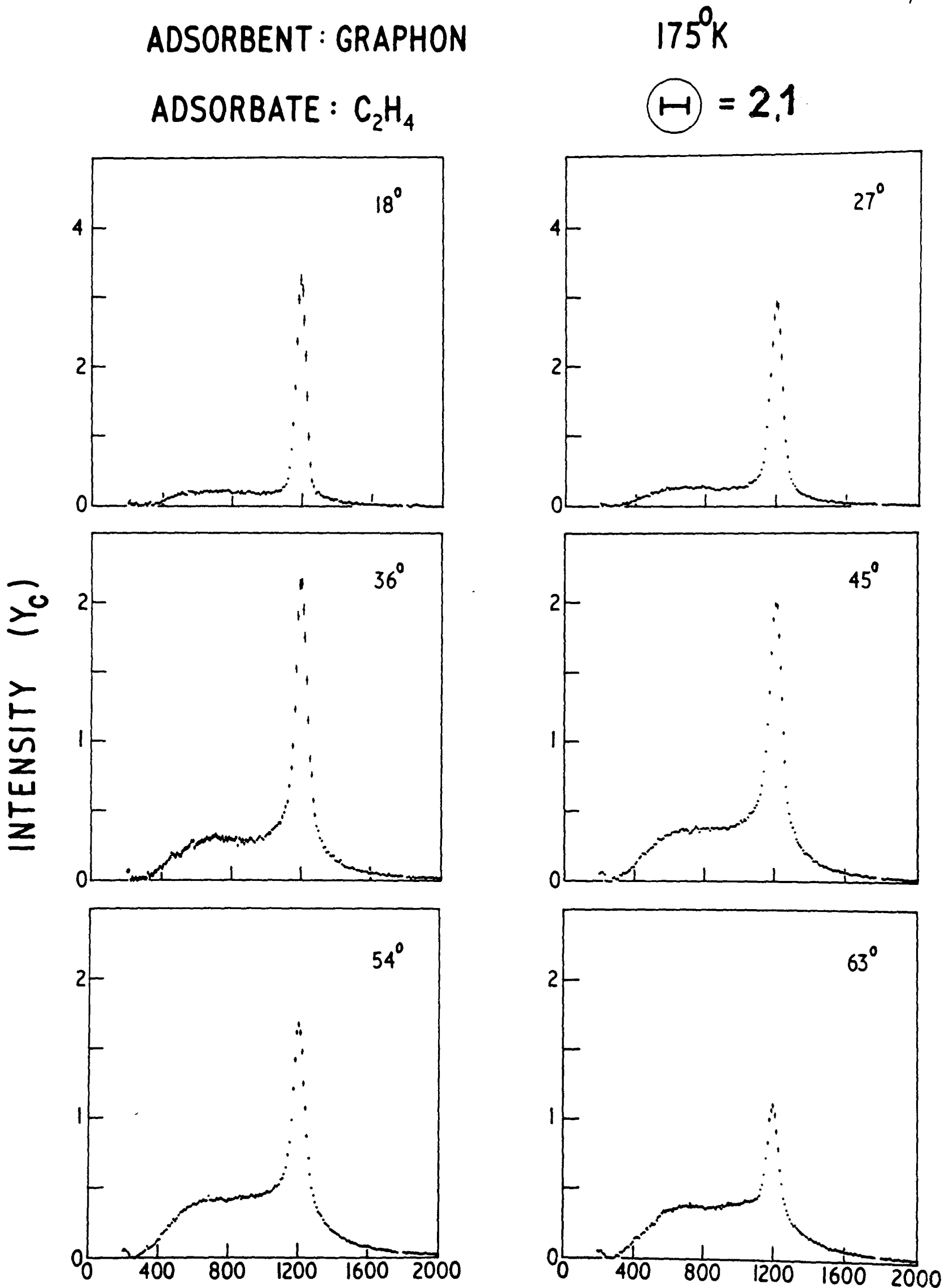
ADSORBENT : GRAPHON
ADSORBATE : C_2H_4
175°K
(H) = 2.1
18°
27°
36°
45°
54°
63°
INTENSITY (Yc)
TIME OF FLIGHT (μsm⁻¹)
ENERGY (cm⁻¹)
0
400
800
1200
1600
2000
1000
300
150
50
25

FIGURE 5,23

ADSORBENT : GRAPHON

ADSORBATE : C_2H_4

195^0K

(H) = 1,3

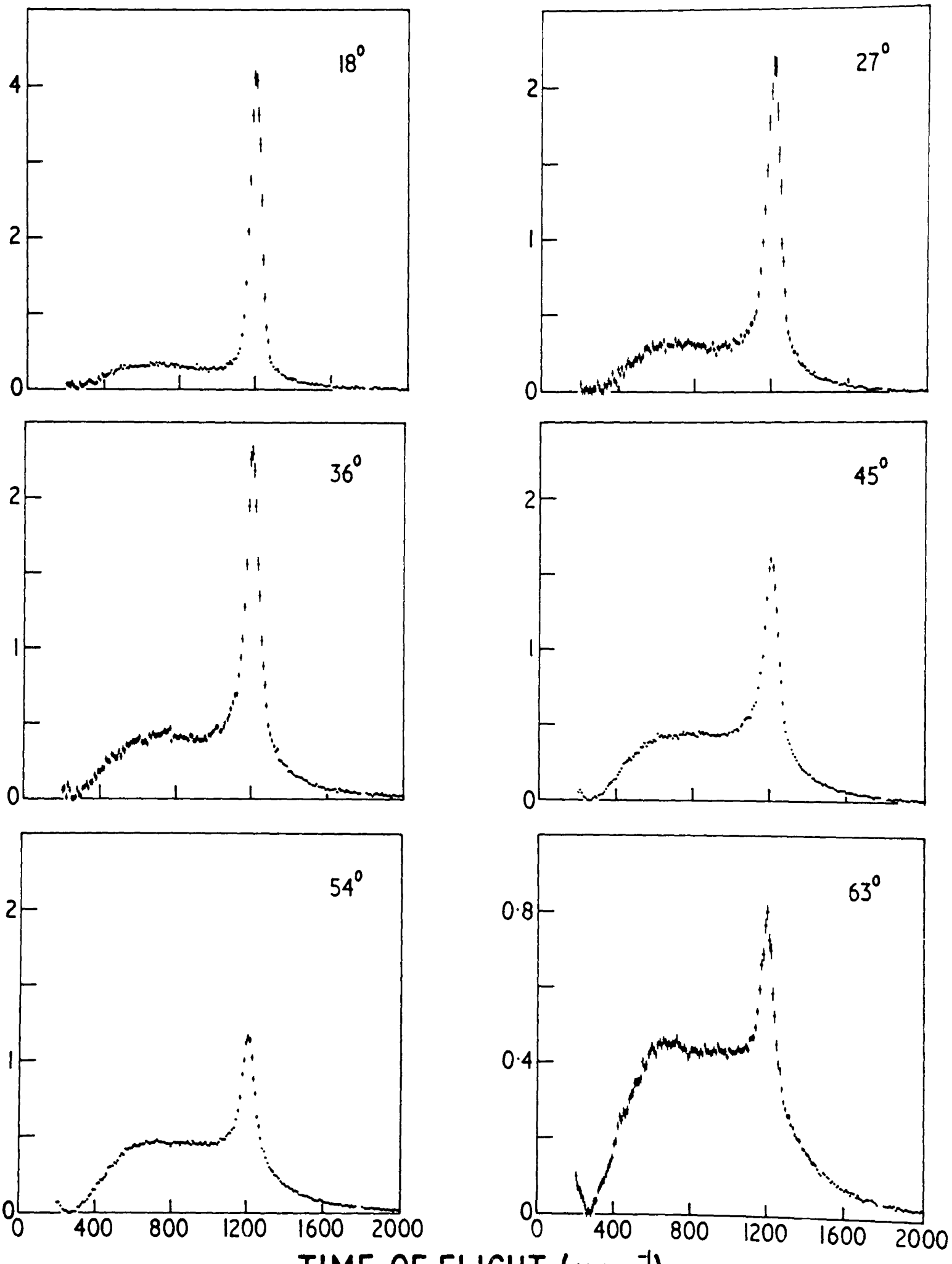

FIGURE 5,24

ADSORBENT: GRAPHON

ADSORBATE: C_2H_4

215^0K

(H) = 1,0

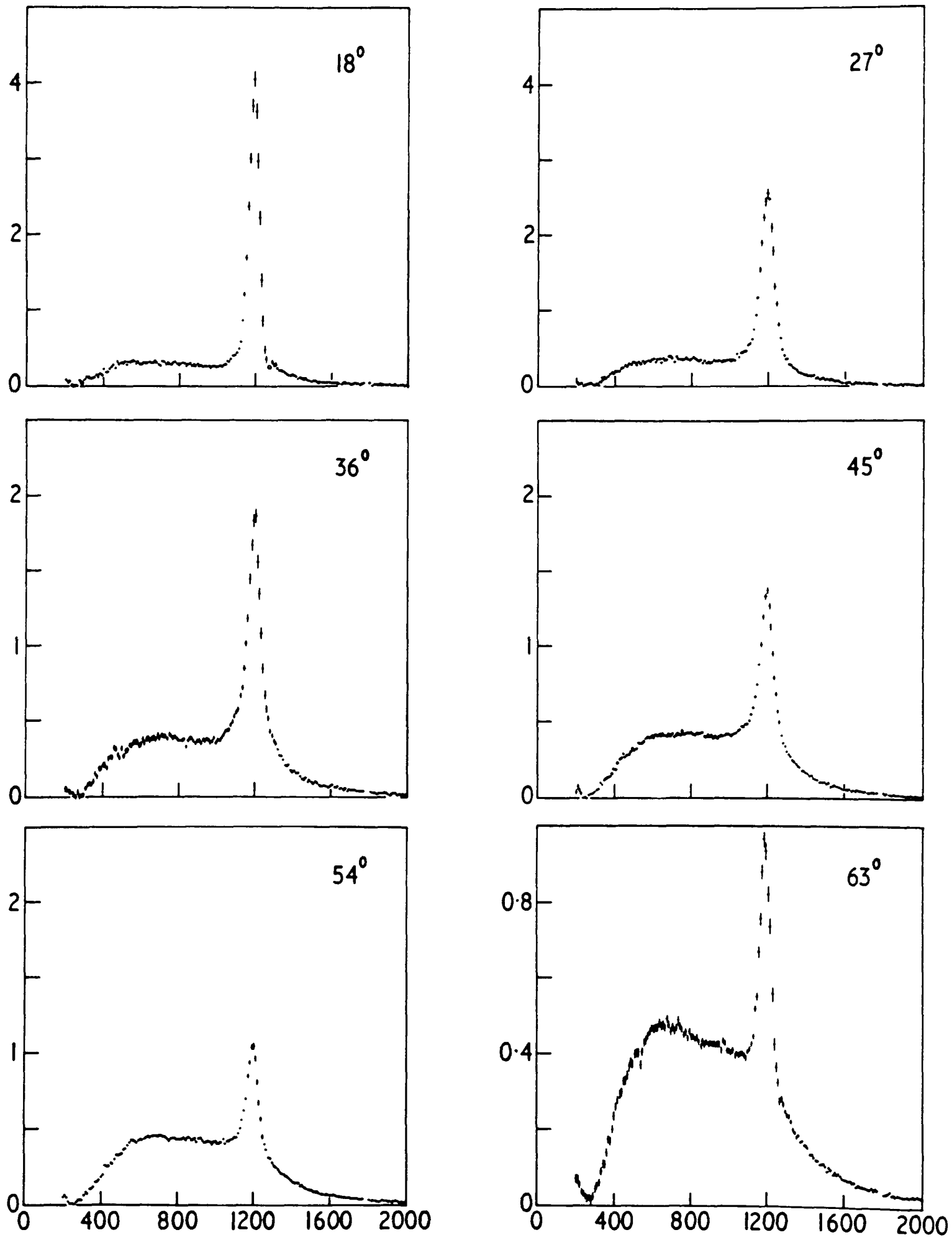

defined than for methane. At the higher temperatures and larger momentum transfers the inelastic and elastic scattering have merged and there is no minimum in the near elastic region. When the maximum is visible it is at lower energies than the maximum of the methane rotational envelope, in accord with the larger mass of the ethylene molecule.

The intensity variation of the quasi elastic peak is shown in figure 5.25. It can be seen that the plots of log(I) vs κ^2 are close to linear and as in the case of methane the data is parameterised by the gradient of these plots. Figure 5.26 shows the temperature and surface coverage variation of the parameter. It might have been expected that an asymmetric molecule such as ethylene would show a form factor with a Bessel function dependence, reflecting the contribution from rotational motions. However the data obtained can be adequately explained by a randomly moving particle scattering.

No features occur in the inelastic spectrum that can be directly attributed to scattered intensity from vibrations of the admolecule with respect to the carbon surface. Once again the high surface mobility rules out the possibility of observing discrete transitions. The asymmetry of the ethylene molecule has precluded any calculations of the neutron scattering spectrum to be expected from the bulk material. Neither have there been any published results for instruments of comparable resolution to 6H, so it is not possible to compare the shape of the inelastic spectrum for adsorbed ethylene with bulk ethylene as it was in the case of methane. Until high resolution measurements have been carried out on ethylene it is not possible to say if there is extra intensity in the near elastic scattering due to admolecule-surface vibrations.

FIGURE 5,25

ADSORBED ETHYLENE — Quasi elastic peak intensity vs χ^2

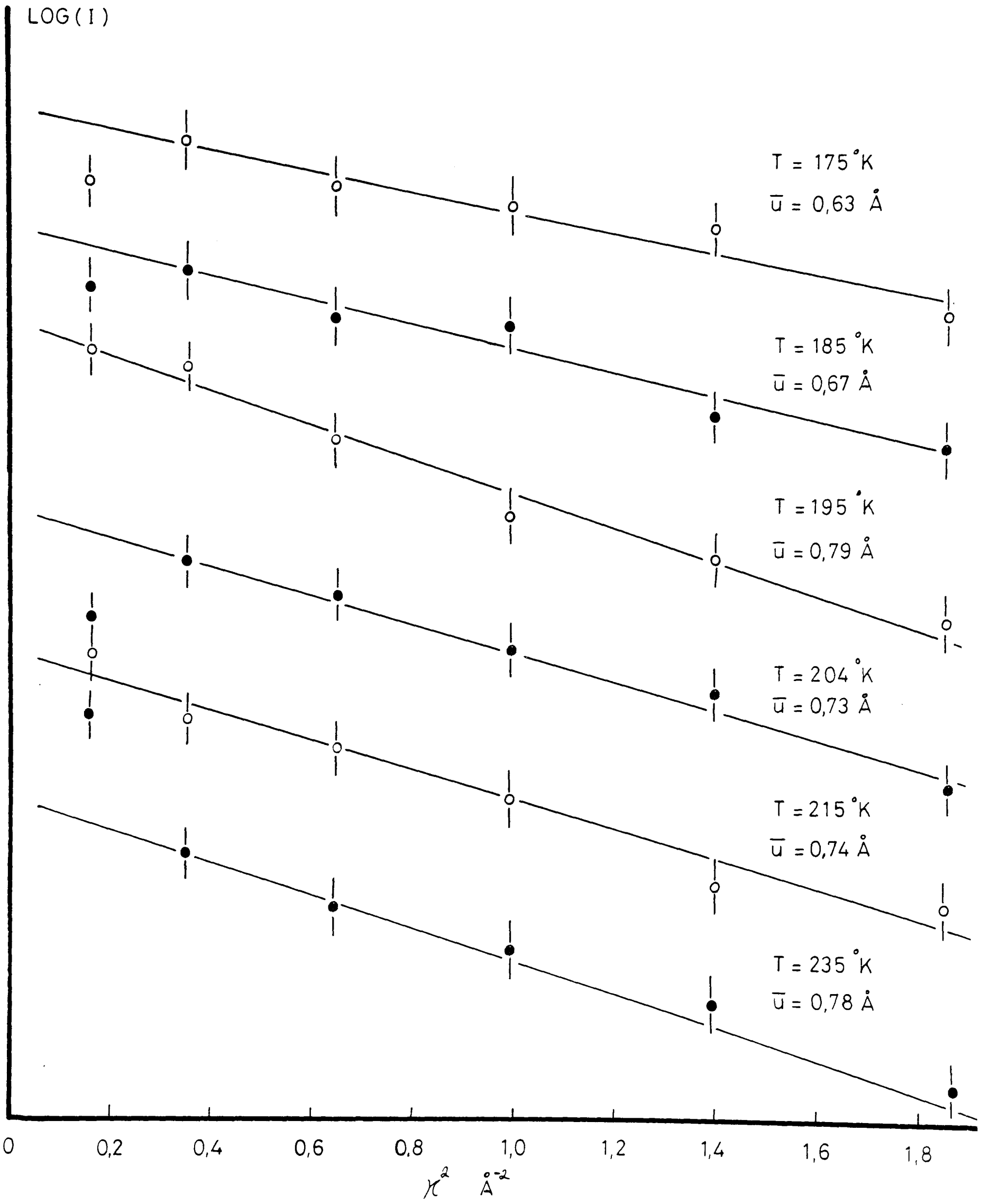

FIGURE 5,26

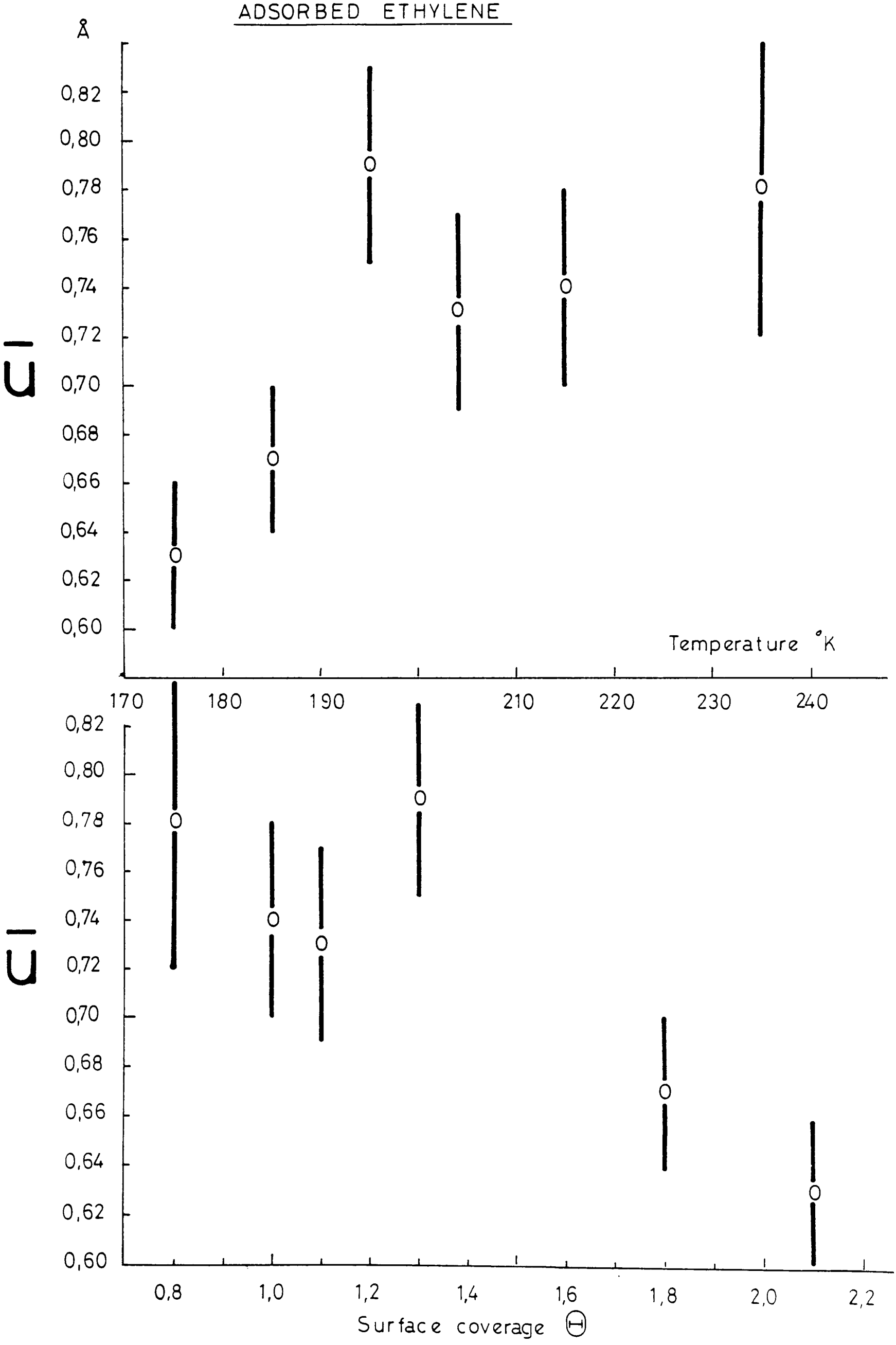
ADSORBED ETHYLENE
Å
0,82
0,80
0,78
0,76
0,74
0,72
0,70
0,68
0,66
0,64
0,62
0,60
Temperature °K
170
180
190
210
220
230
240
Surface coverage Θ
0,8
1,0
1,2
1,4
1,6
1,8
2,0
2,2

5.3.3 Translations of the adsorbed molecules

The results of attempting to analyse the shape dependence of the quasi elastic peak on κ^2 with the deconvolution method are shown in figure 5.27. It is clear that the approach is not satisfactory and that the sample scattering law is non-lorentzian. Following the same arguments as applied to adsorbed methane, scattering laws based on the 3D averaging of a 2D liquid model were generated by the ORIANA programme, convoluted with the machine resolution function and compared with the data.

The choice of diffusion coefficient for the calculation was made by an analysis of the widths of the observed $S(\kappa,w)$ at various fractional heights as a function of κ^2. Figure 5.28 shows the predicted widths as a function of the diffusion coefficient. On these graphs are plotted the observed widths which, if the model is correct, should occur at a constant value of D.

Examples of the observed $S(\kappa,w)$ and the best fits are shown in figures 5.29 to 5.32. It can be seen that the calculated scattering laws, based on the 3D averaged 2D liquid model, fit the observed scattering laws quite closely at all but the lowest temperatures. The closeness of fit of the different models to the data was checked using a crude χ^2 test and representative values of χ^2_ν are shown in table 5.3.

5.3.4 Discussion

The asymmetric shape of the ethylene molecule and its polarisability contrast with methane, and give rise to stronger adsorbate-adsorbate interactions when ethylene is adsorbed on graphon (91). If the enthalpy of interaction is sufficient to overcome the entropy of adsorption,i.e.the surface spreading pressure, then the adsorbate will form clusters on the surface and not be ideally dispersed. The translational scattering law observed

FIGURE 5,27

ADSORBED ETHYLENE — Deconvolution of $S(x,\omega)$

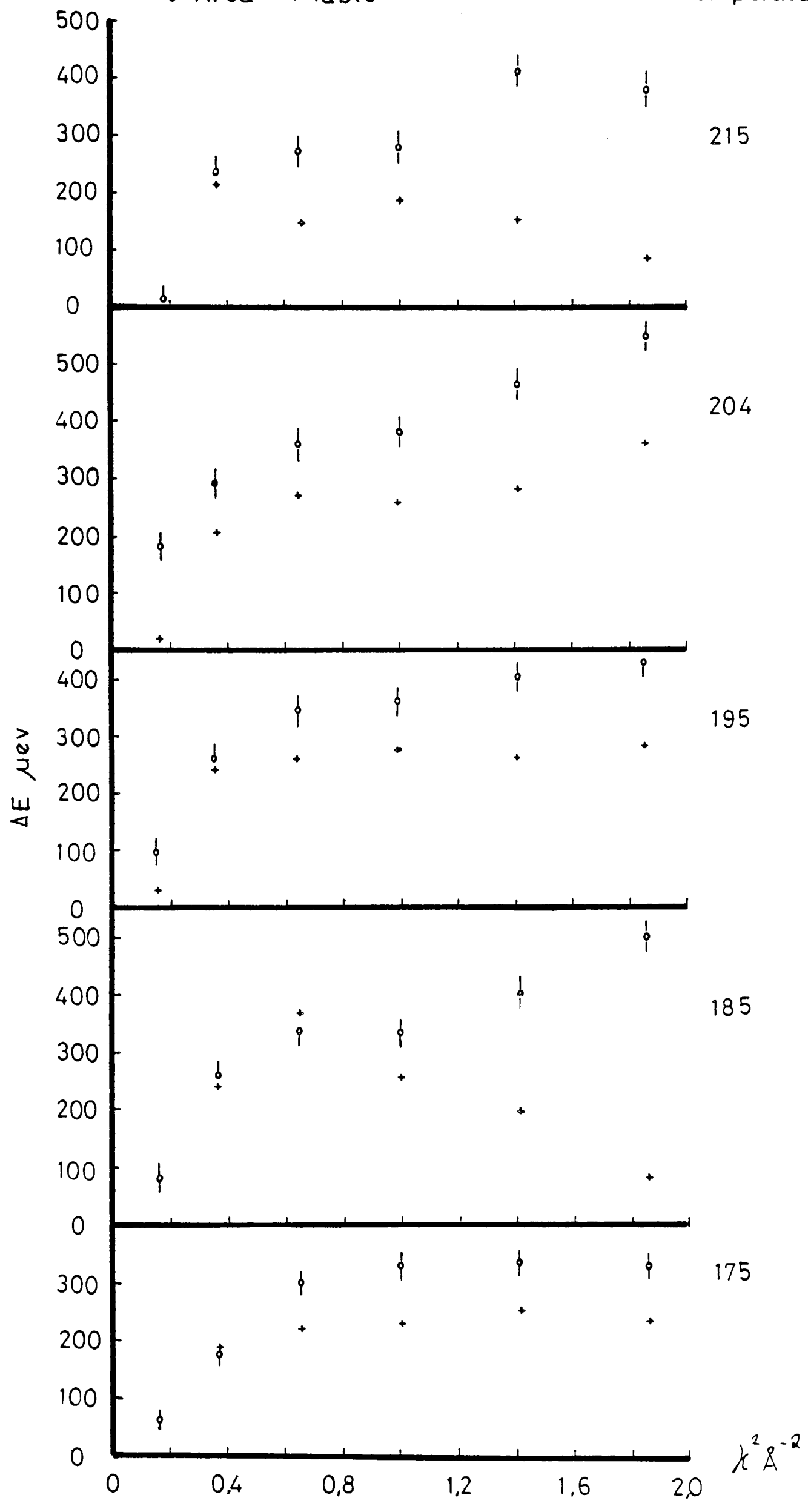

FIGURE 5,28

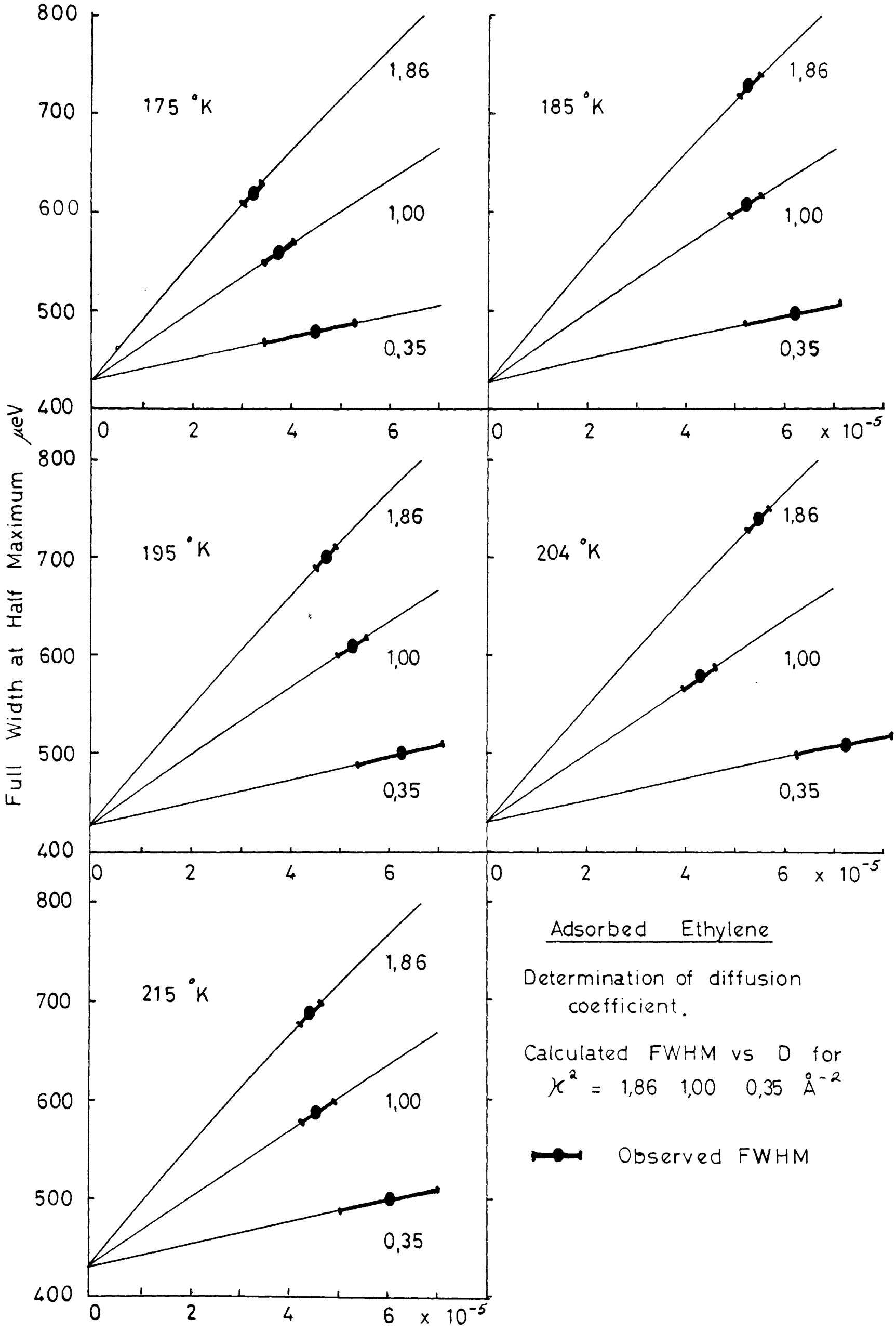

Adsorbed Ethylene

Determination of diffusion coefficient.

Calculated FWHM vs D for χ^2 = 1,86 1,00 0,35 Å^{-2}

Observed FWHM

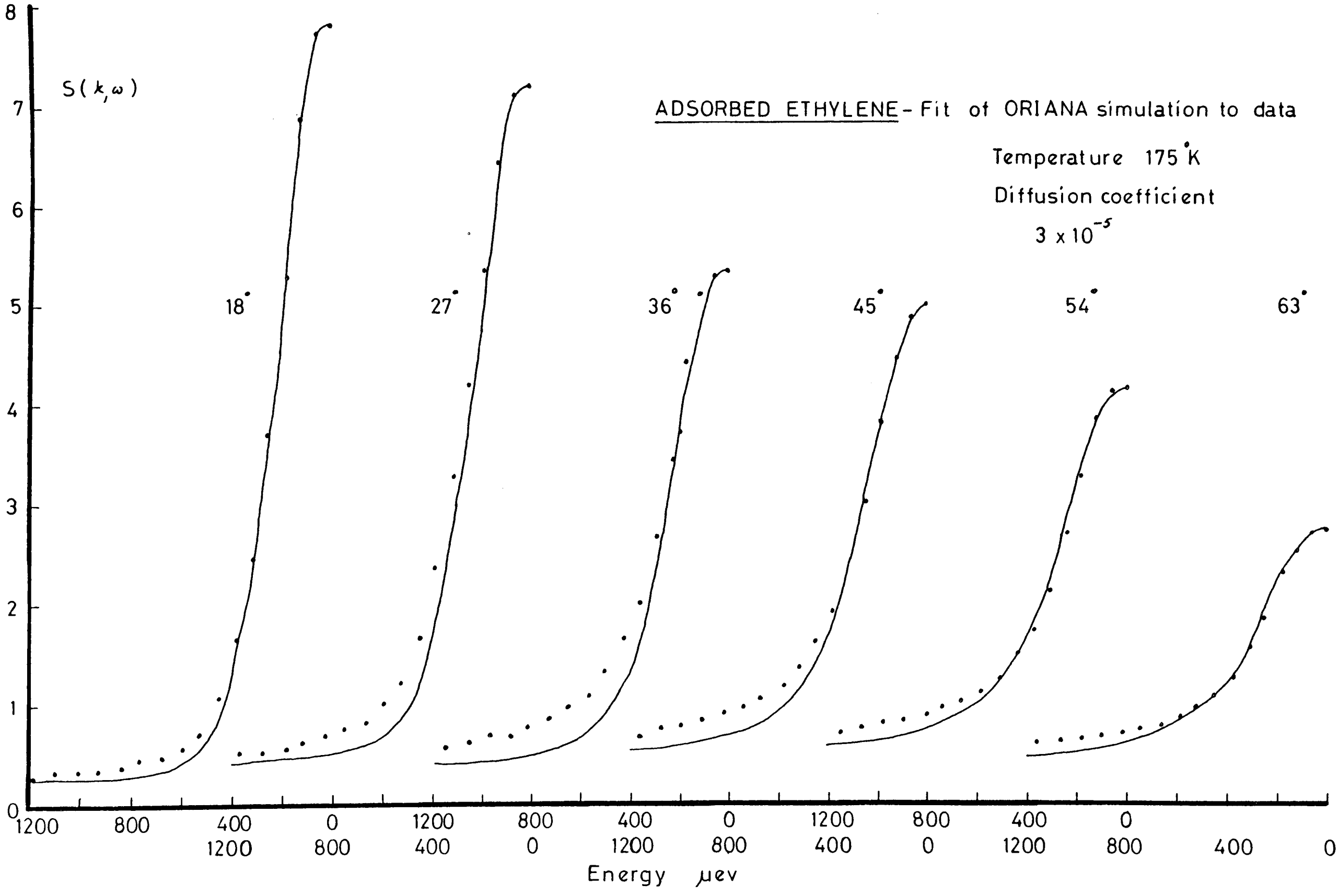
ADSORBED ETHYLENE - Fit of ORIANA simulation to data
Temperature 175 °K
Diffusion coefficient
3 x 10^-5
S(k,ω)
18°
27°
36°
45°
54°
63°
0
1
2
3
4
5
6
7
8
1200
800
400
0
Energy μev

FIGURE 5,29

ADSORBED ETHYLENE– Fit of ORIANA simulation to data

Temperature 185 °K

Diffusion coefficient

5×10^{-5}

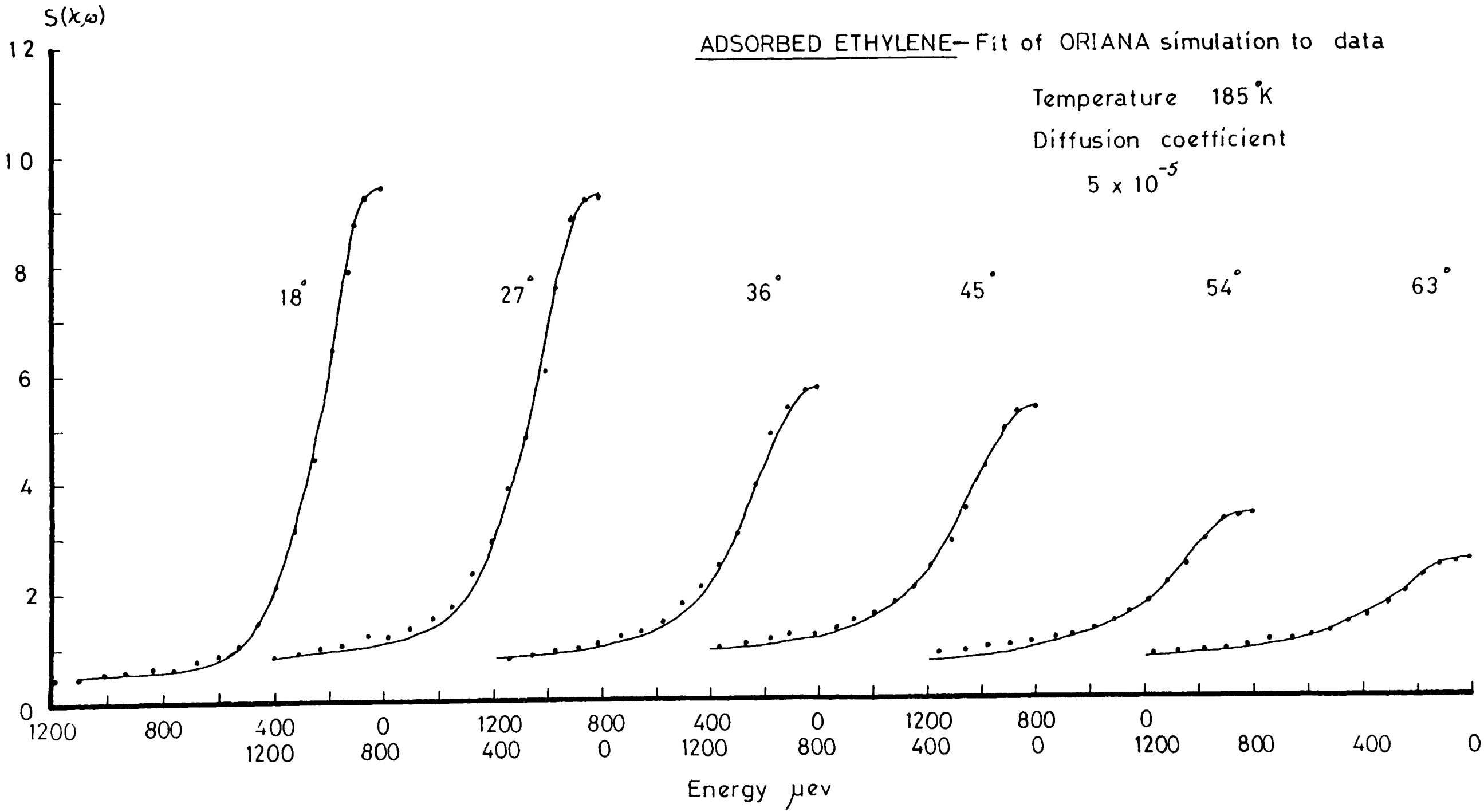

FIGURE 5,30

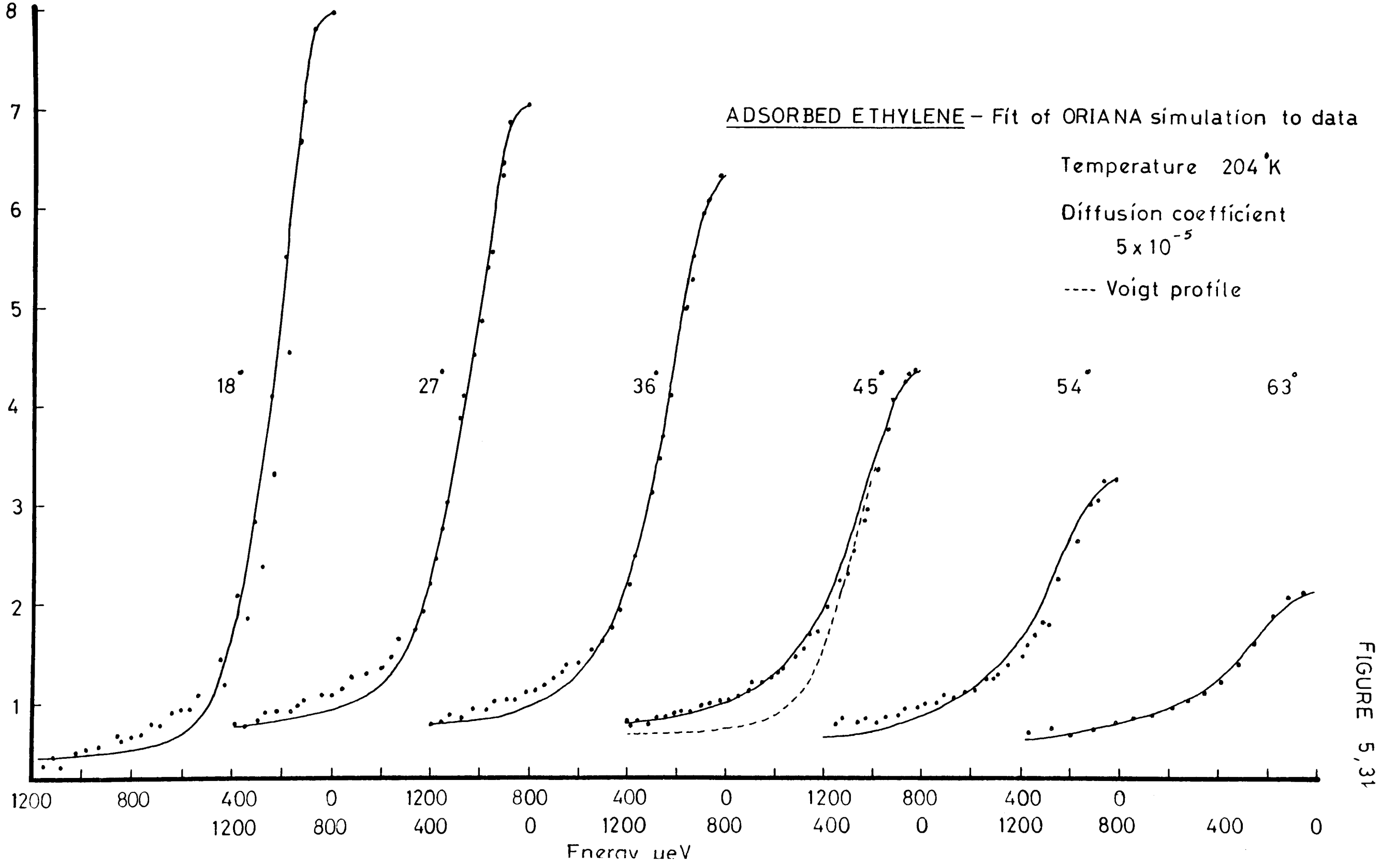
ADSORBED ETHYLENE – Fit of ORIANA simulation to data
Temperature 204 °K
Diffusion coefficient
5 x 10⁻⁵
---- Voigt profile
18°
27°
36°
45°
54°
63°
8
7
6
5
4
3
2
1
1200 800 400 0 1200 800 400 0 1200 800 400 0
1200 800 400 0 1200 800 400 0 1200 800 400 0
Energy ueV

FIGURE 5,31

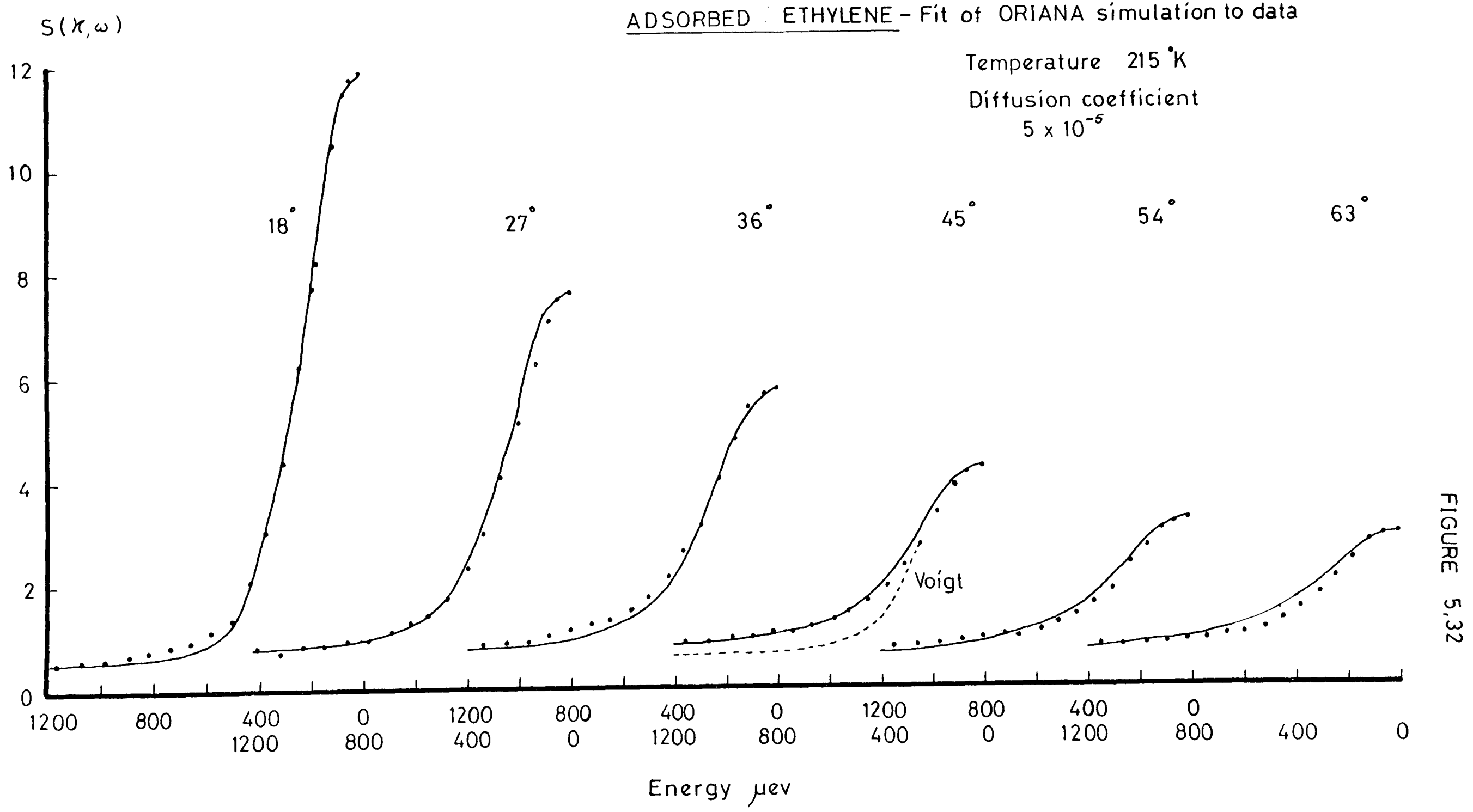
ADSORBED ETHYLENE – Fit of ORIANA simulation to data
Temperature 215 °K
Diffusion coefficient
5 x 10⁻⁵
S(κ,ω)
12
10
8
6
4
2
0
18°
27°
36°
45°
54°
63°
Voigt
1200
800
400
0
1200
800
400
0
1200
800
400
0
1200
800
400
0
1200
800
400
0
1200
800
400
0
Energy μev

FIGURE 5,32

by the neutron method would then be a composite of the diffusion of molecules in clusters and the very much faster diffusion of molecules between clusters. This does not seem to be occurring in the case of adsorbed ethylene as the simple 2D liquid model fits the observed data at several temperatures. The worsening fit that occurs at lower temperatures could be due to the increasing hinderance to rotational motion brought about by multilayer adsorption.

The change in shape of the calculated $S(\kappa,w)$ with the value of the diffusion coefficient input is small. Figure 5.33 shows the change in degree of goodness of fit to the data at 185°K when values of 4, 5 and 6 x 10^{-5} cm^2 sec^{-1} are used for the diffusion coefficient in the model. Though the statistics on the data points are good, and the worst error on a point is of the order of ± 10%, the insensitivity of the calculated scattering law to the value of the diffusion coefficient means that the value of D taken as the best fit cannot be quoted to better than ± 0.5cm^2 sec^{-1}.

The values of the diffusion coefficients determined hardly vary at all with temperature. It is possible that the imprecision of the analysis conceals a small temperature variation, such as would be expected if the activation energy for diffusion is small. Table 5.4 displays predicted diffusion coefficients over the temperature range of these experiments given that the diffusion coefficient at 195°K is 5 x 10^{-5} cm^2 sec^{-1} and the activation energy

ADSORBED ETHYLENE — Sensitivity of fit to choice of diffusion coefficient.

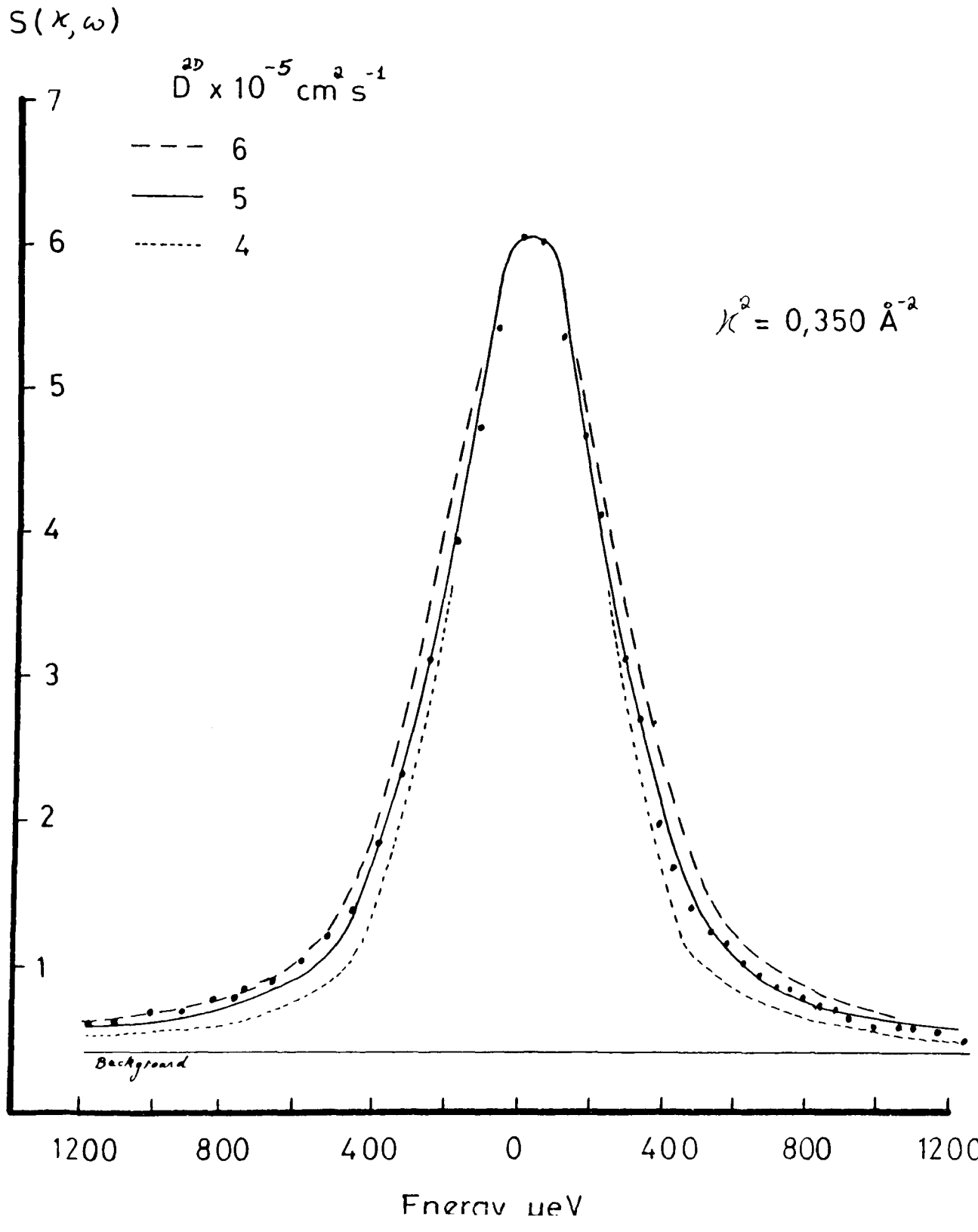

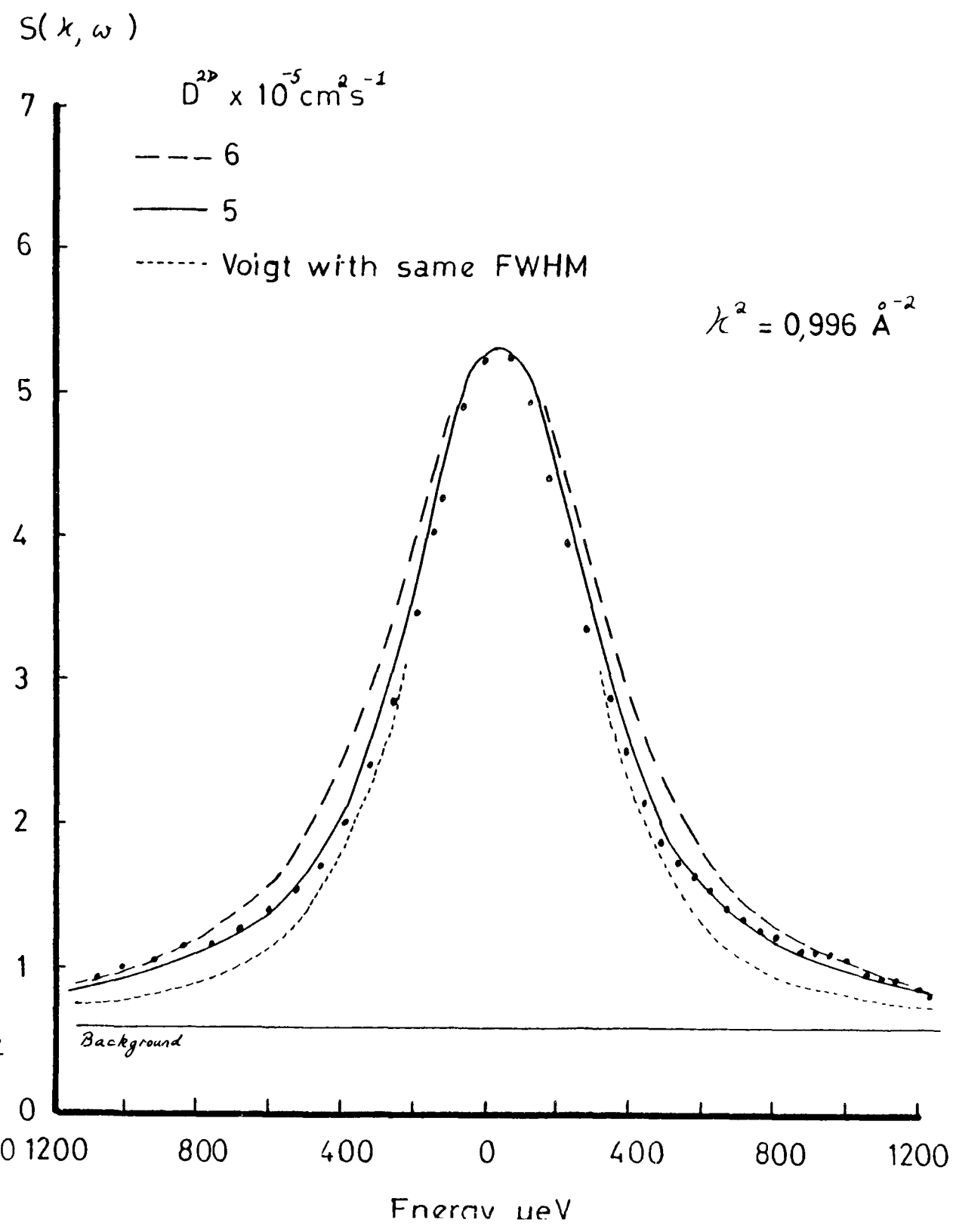

FIGURE 5,33

TABLE 5.3

ADSORBED ETHYLENE - Closeness of fit of 2D liquid model to the observed scattering law

Temperature °K	Angle of scatter	χ_ν^2	
		2D liquid profile	Voigt profile
175	18	6.765	
	27	7.156	
	36	9.351	
	45	4.319	9.723
	54	2.259	
	63	1.981	
185	18	0.562	
	27	0.863	
	36	0.627	4.697
175	36	9.351	
185	36	0.627	
195	36	0.721	3.314
204	36	0.615	
215	36	1.006	
185	27 D = 4E - 5	4.163	
	5E - 5	0.779	
	6E - 5	0.651	
	45 D = 5E - 5	0.246	
	6E - 5	1.476	
	Voigt		2.707

Table 5.4

Variation of Diffusion Coefficient with temperature

$$D = D_o \left(\exp - \left[E_A/RT\right]\right)$$

Assume $D = 5 \times 10^{-5}\ cm^2s^{-1}$ at 195^oK

E_A kcals/mole	TEMPERATURE ^oK					
	175	185	195	204	215	235
0.2	4.71	4.86	5.00	5.11	5.25	5.46
0.5	4.32	4.67	5.00	5.30	5.65	6.24
1.0	3.72	4.35	5.00	5.60	6.36	7.76
1.5	3.24	4.09	5.00	5.98	7.23	9.74
2.0	2.77	3.78	5.00	6.28	8.08	12.04

Values of diffusion coefficient in $10^{-5}\ cm^2s^{-1}$

for diffusion varies from 0.2 to 2 x $10^{-5}cm^2sec^{-1}$. It is clear that if $E_A \lesssim$ 0.5 kcals/mole any change in D will be undetectable. The problem is further compounded as the activation energy for diffusion undoubtedly depends on surface coverage, increasing as Ⓗ increases and the admolecule separation decreases. More measurements are required on a higher resolution instrument when the convolution of the sample scattering law with the machine resolution function will not produce such a diffuse observed spectrum, and so enable a more accurate determination of D at various temperatures.

A comparision of the log (I) vs K^2 plots for methane and ethylene shows that the gradients are significantly less in the case of ethylene. Interpreting the parameter in the gross approximation of simple harmonic motion leads to a vibration frequency in the range 110 to 120 cm^{-1}, higher than expected. If one considers the vibrations of the single molecule with respect to the surface, and assumes that the force constant for this motion will be the same for methane and ethylene then the vibration frequency for ethylene is calculated to be 20-30 cm^{-1}.

That a deviation to higher vibration frequency is observed, suggesting a larger force constant for the vibrations of ethylene with respect to the carbon surface, is in agreement with the liquid like behaviour of adsorbed ethylene, in constrast to the gas/liquid intermediate behaviour of methane. A further manifestation of the consequence of increased lateral interactions on the dynamics of the adsorbate layer.

5.4 Adsorbed Ammonia

5.4.1 Results

The scattered neutron time of flight spectrum of ammonia

adsorbed on graphon was obtained at the temperatures and surface coverages shown below. The same experimental apparatus was used as for the studies of adsorbed methane and ethylene. In this instance however it was possible to study a monolayer of adsorbed ammonia at various temperatures up to the point at which the monolayer melted. At higher temperatures experiments were conducted with an atmospheric pressure of ammonia vapour above the graphon and the temperature and surface coverage were now interdependent.

Temperature ^{o}K	Ⓗ	Subtracted counts in elastic channel $\theta = 45^{o}$	Subtracted counts in maximum of inelastic $\theta = 45^{o}$
145	0.90	71520	779
155	0.88	62961	778
168	0.93	66350	952
176	1.02	65476	995
186	1.04	51121	554
199	1.44	39653	2159
223	1.54	32174	3342
242	0.86	22935	4010
249	0.55	25988	3644
254	0.51	10123	2548
261	0.23	5545	1759

Examples of the time of flight spectra obtained are shown in figures 5.34 and 5.35. Figure 5.36 shows the change in inelastic scattering for close on monolayer coverage as the temperature varies.

5.42 Vibrations of adsorbed ammonia

The experiments cover a wide range of temperature, 261 to $145^{o}K$, and surface coverage, 0.2 to 1.8, and there are marked changes in the time of flight spectra, reflecting the changes in the dynamics of the adsorbate molecule. At high temperatures the inelastic region is a broad, featureless rotational envelope produced by the convolution of scattering laws for rotational

FIGURE 5,34

ADSORBENT : GRAPHON

ADSORBATE : NH_3

242^0K

(H) = 0·9

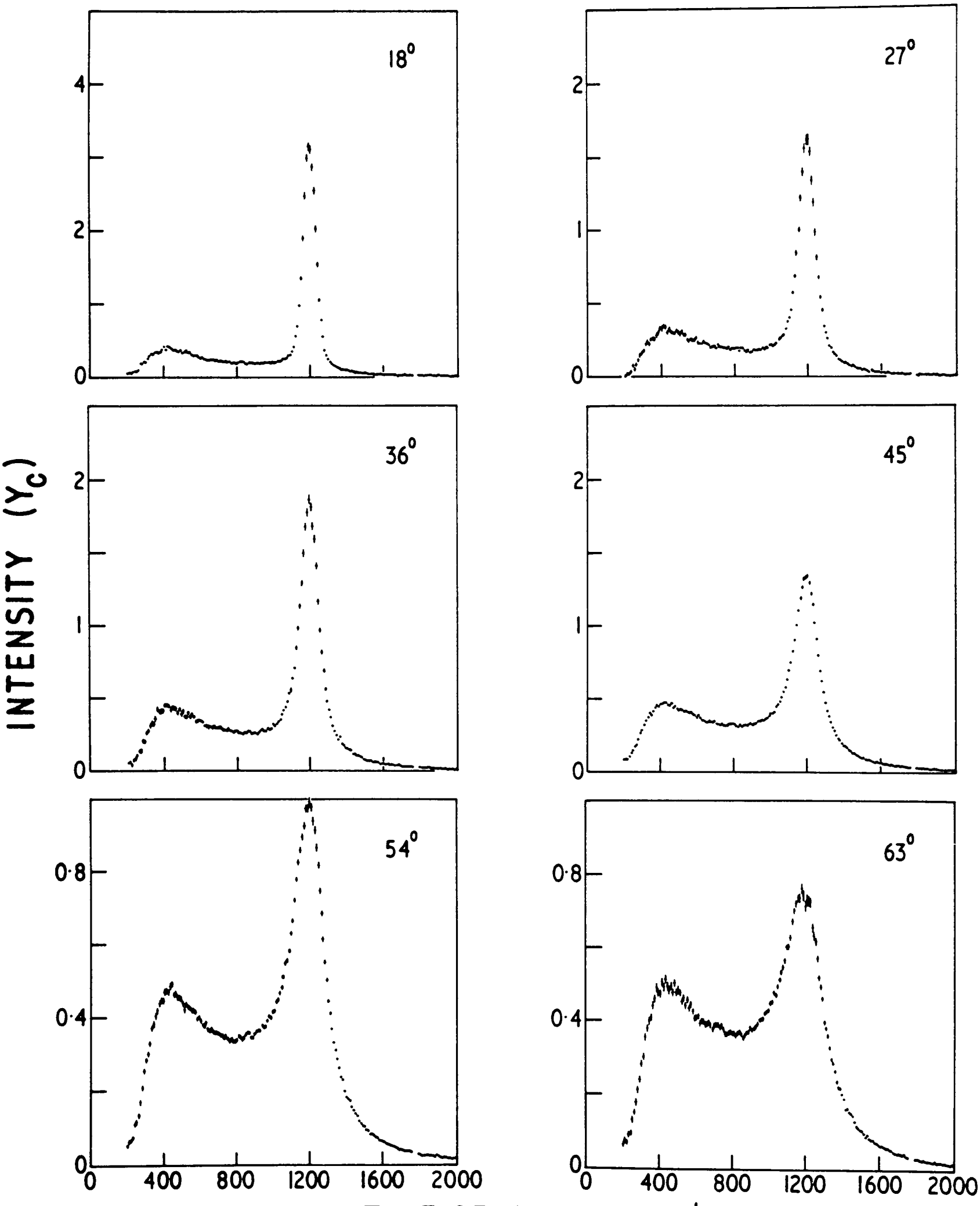

FIGURE 5,35

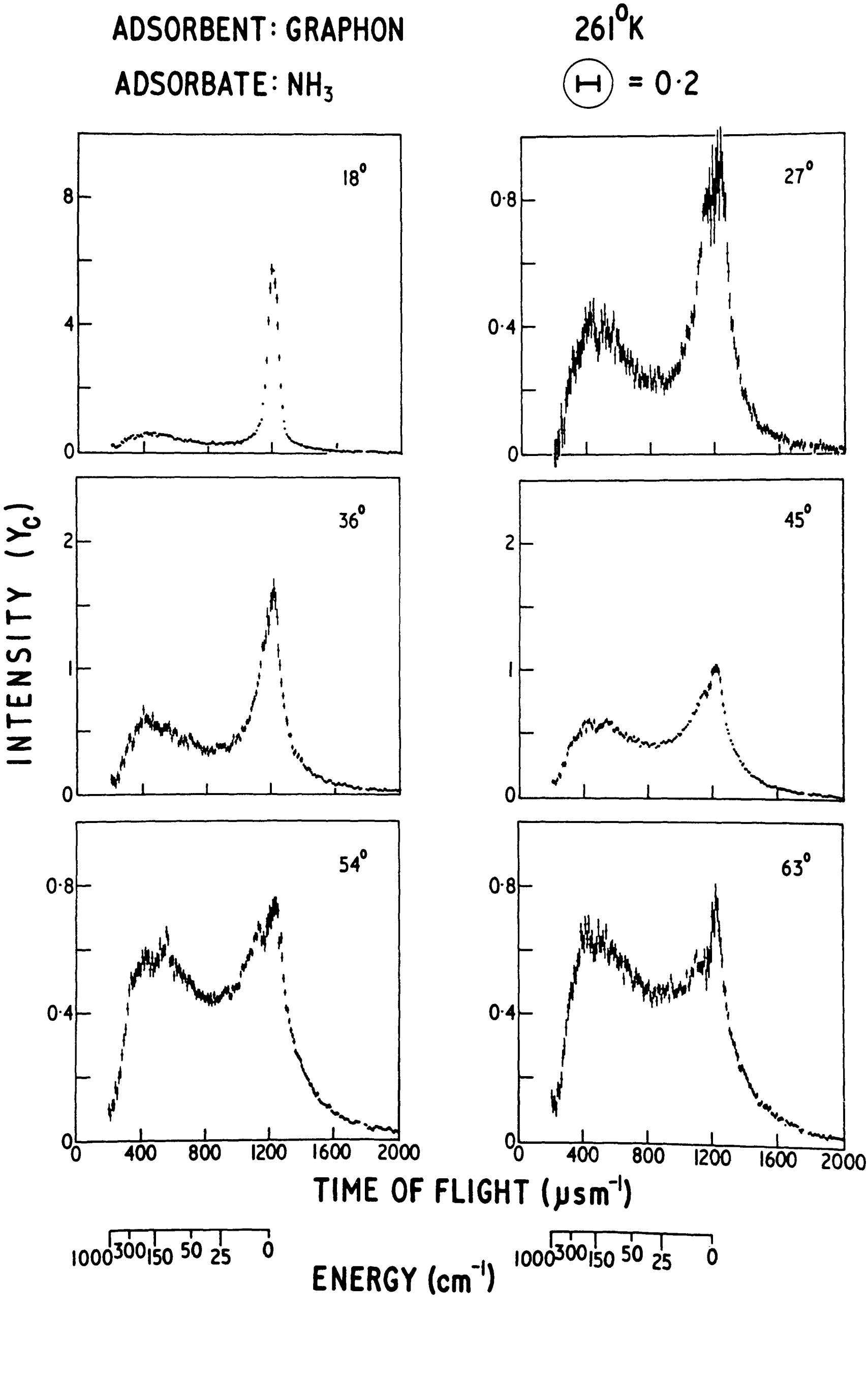
ADSORBENT: GRAPHON
ADSORBATE: NH_3
261°K
H = 0·2
18°
27°
36°
45°
54°
63°
INTENSITY (Yc)
TIME OF FLIGHT (μsm⁻¹)
ENERGY (cm⁻¹)
0
400
800
1200
1600
2000
1000
300
150
50
25
0

FIGURE 5,36

ADSORBENT: GRAPHON $\ominus = 72^0$

ADSORBATE: NH_3 $\Theta \simeq 1$

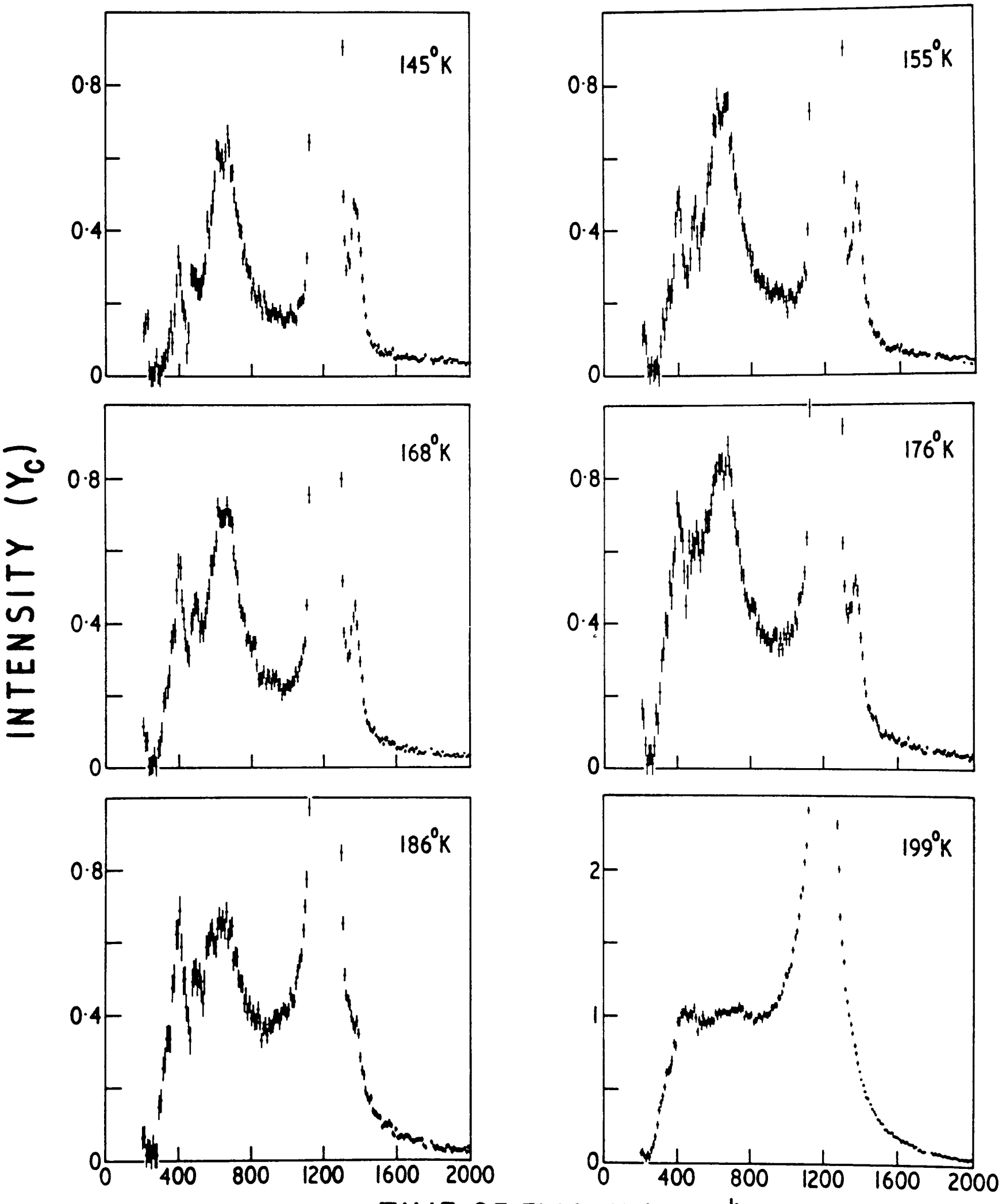

transitions and rapid surface diffusion. The quasi elastic peak broadens and drops in intensity very rapidly with momentum transfer.

Conversely at low temperatures and Ⓗ = 1.0, the inelastic region shows discrete transitions and the quasi elastic peak is only slightly broader than the machine resolution function. Since sharp features are present in the inelastic region it is certain that the scattering law for centre of mass motion is very sharp, implying none, or else very slow surface diffusion.

From the behaviour of the quasi elastic peak intensity with momentum transfer, it is possible to assess the amplitude of vibration of the molecule. Figure 5.37 shows plots of log(I) vs κ^2 for ammonia adsorbed on graphon. No data is shown for 261°K as it was impossible to achieve a good subtraction of the background scattering. This is clear in figure 5.35 where the break in the quasi elastic peak arises from subtracting off too much of the graphon spectrum.

The plots of log (I) vs κ^2 are close to linear and can be parameterised as before, by the slope of the least squares fitted straight line. Figure 5.38 plots this parameter as a function of temperature and surface coverage. The decrease in amplitude of motion of the adsorbate parallels the development of structure in the inelastic time of flight spectrum. It is first evident at 199°K and at the lower temperatures can readily be resolved into at least three peaks at times of flight 400, 500 and 650 $\mu s\ m^{-1}$. Time of flight spectra are not energy cuts at constant κ and the extrapolation procedure of Egalstaff (81) was used to construct the meaningful frequency distribution at zero momentum transfer, and to remove the distorting effect of temperature in the measured scattering law. Examples of the P(β) measured are shown in figure 5.39. The extrapolation technique is not very satisfactory and tends to obscure fine detail in S(κ,w). This is because of the few points

FIGURE 5,37

ADSORBED AMMONIA – Quasi elastic intensity vs χ^2

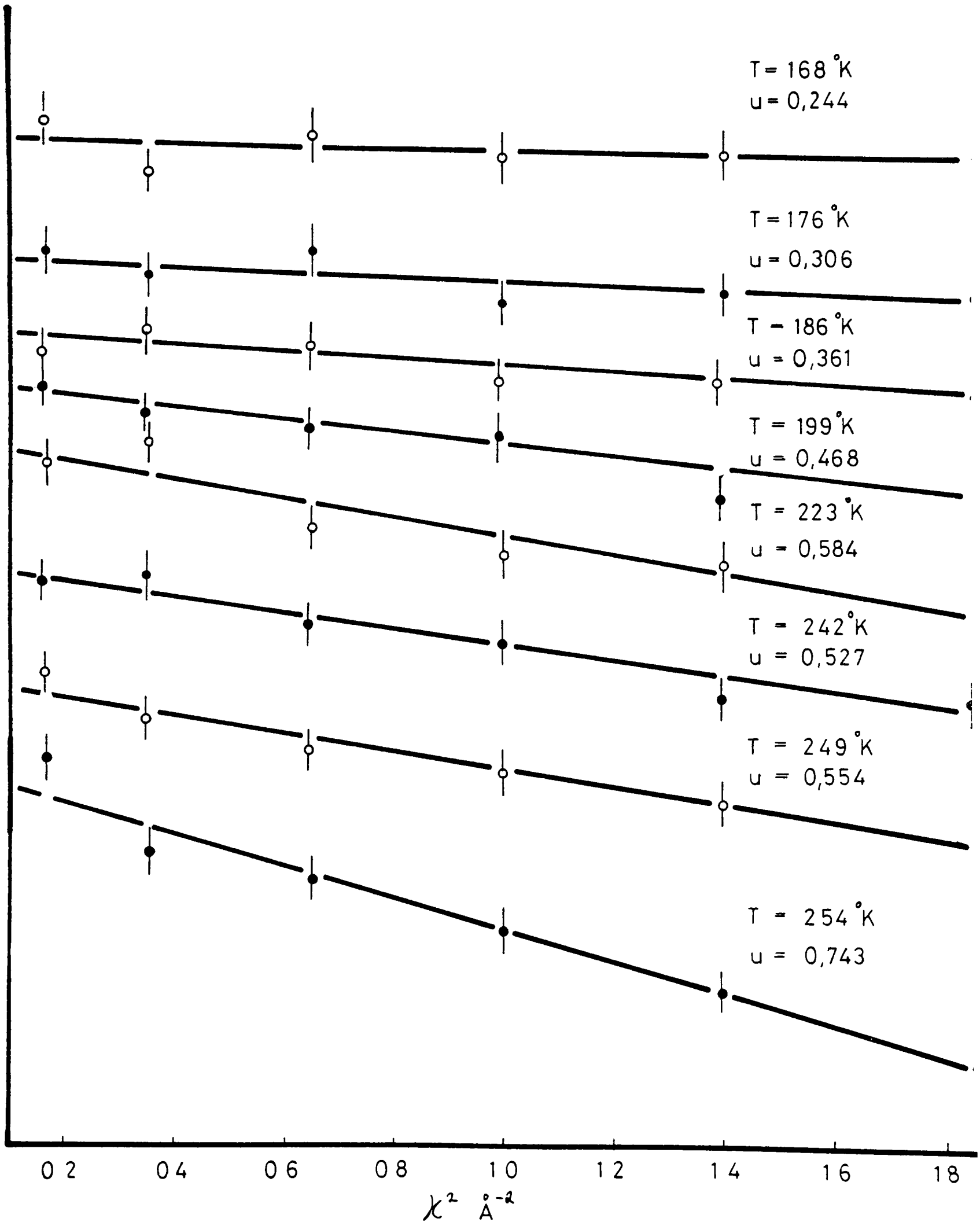

FIGURE 5,38

ADSORBED AMMONIA — Dependence of u on T & θ

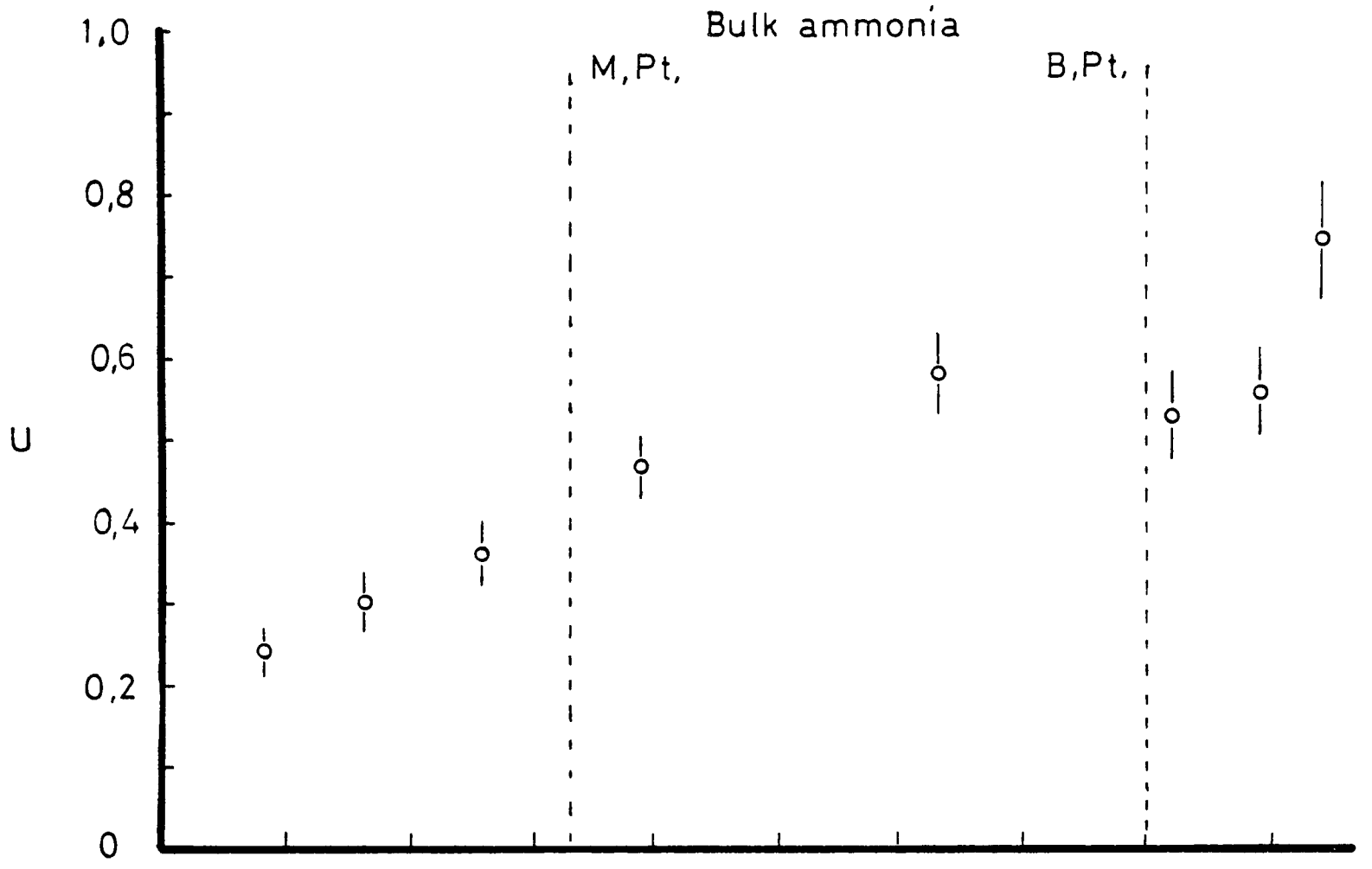

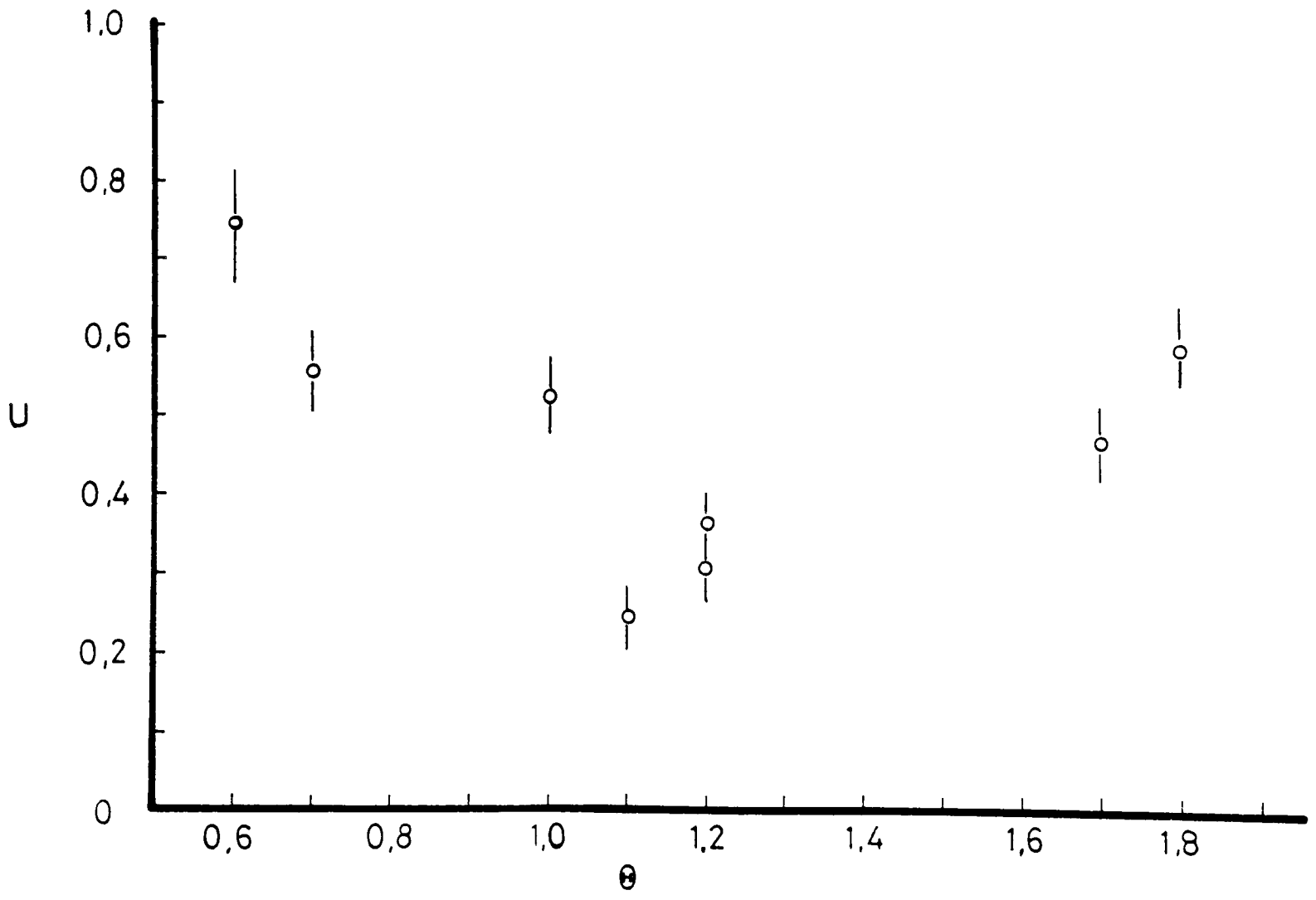

FIGURE 5,39

ADSORBED AMMONIA - $\rho(\beta)$ for $\theta \simeq 1$

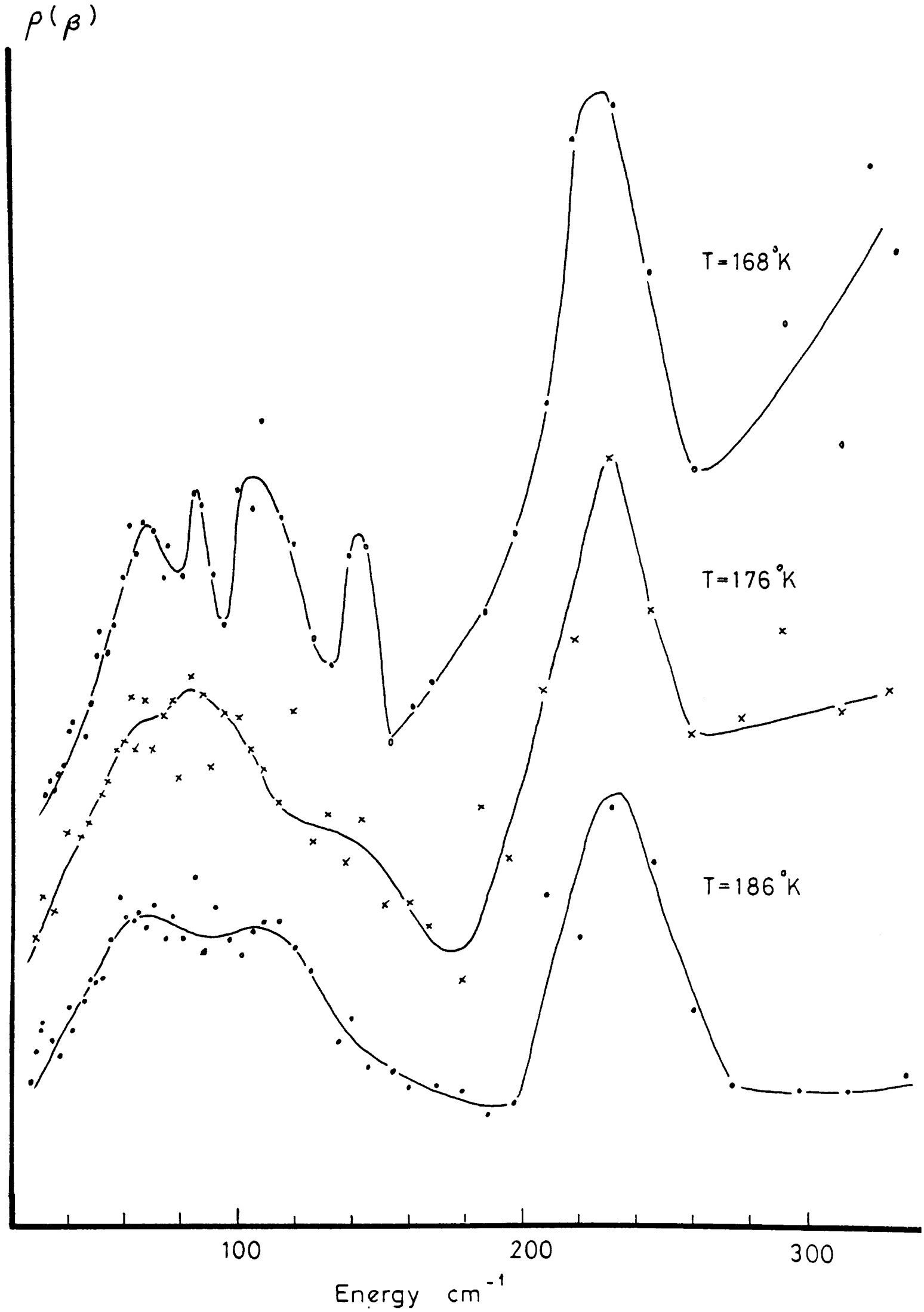

FIGURE 5,40

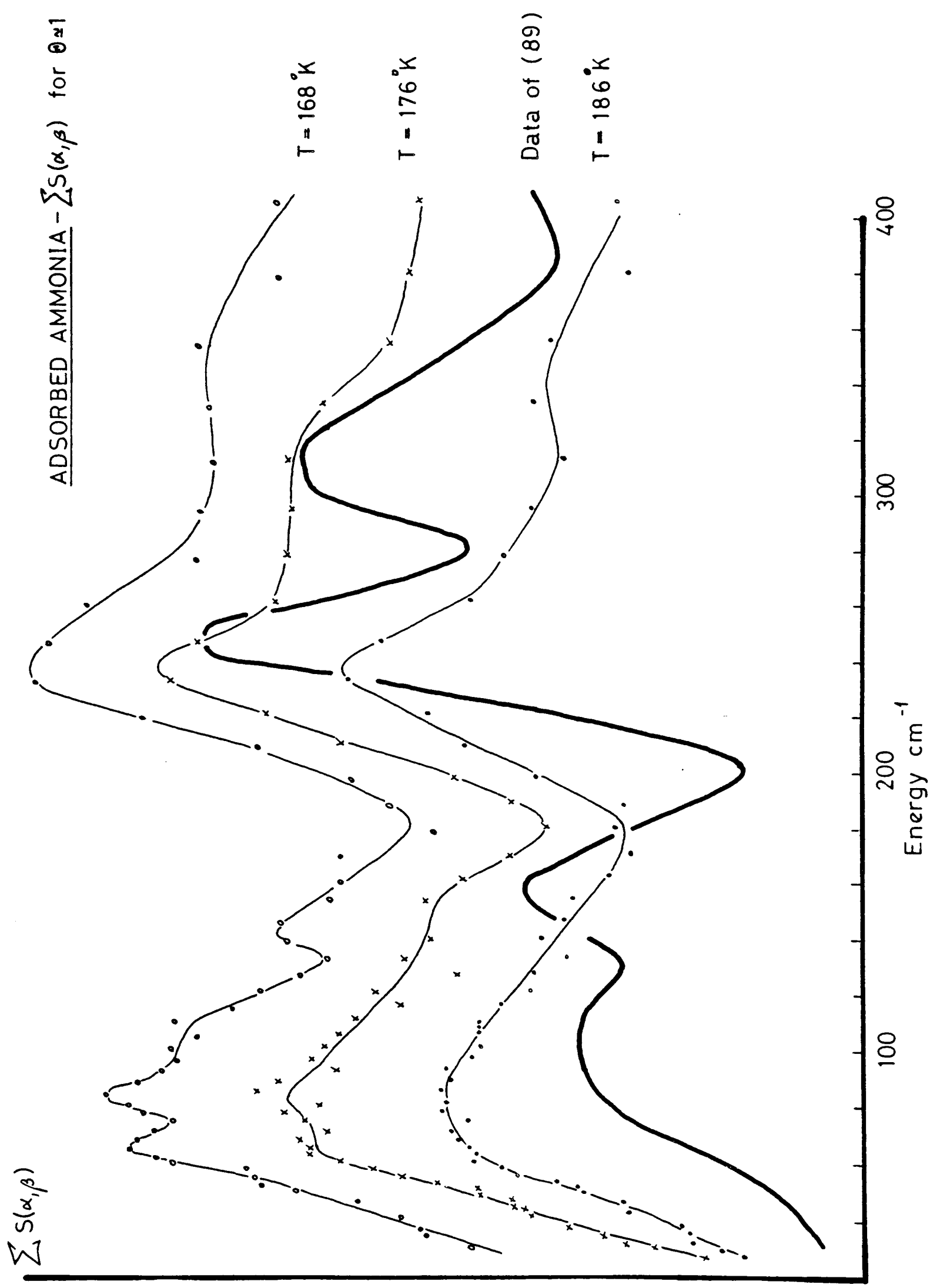
ADSORBED AMMONIA - $\sum S(\alpha,\beta)$ for $\theta \simeq 1$
T = 168°K
T = 176°K
Data of (89)
T = 186°K
$\sum S(\alpha,\beta)$
100
200
300
400
Energy cm^{-1}

available for extrapolation and the inherent curveature of the plot. If there are no features in the inelastic region whose positions are obviously κ dependent then it is reasonable to sum the scattered intensity at a given energy over all counters. The results are shown in figure 5.40. The apparent melting point of the adlayer is close to that of bulk ammonia (195°K) and the frequency distribution is not very different to that of bulk ammonia measured with neutron scattering by Goyal and Dasannacharya (89). Their result is shown on the figures for comparison. The sharp feature on the energy gain side of the quasi elastic peak in figure 5.36 is due to neutrons reflected from part of the sample can. As it does not occur for the blank can it could not be subtracted from the sample spectrum except by hand calculations.

5.4.3 Translations of the adsorbed ammonia

Figures 5.41 and 5.42 show the fit of the 3D averaged 2D ideal liquid model with diffusion coefficients of 4 x 10^{-5} and 9 x 10^{-5} cm^2sec^{-1} respectively. The fit is not good particularly at the higher angles of the data collected at 223°K, being unable to predict the observed broadening of the $S(\kappa,w)$ with increasing momentum transfer. By 242°K the fit is quite inadequate.

However the data collected from 199°K to 254°K (statistics at 261°K are too poor to allow quantitative treatment) can be well fitted as a Voigt profile. Accordingly it was attempted to deconvolute the gaussian machine resolution function to obtain the sample scattering law. The deconvolution method is only applicable if the profile is a Voigt and cannot otherwise be used as a diagnostic test. Figure 5.43 shows the linear dependence of the FWHM of the deconvoluted lorentzian as a function of κ^2. Such a dependence, together with the agreement between the two types of deconvolution method strengthens the description of the observed

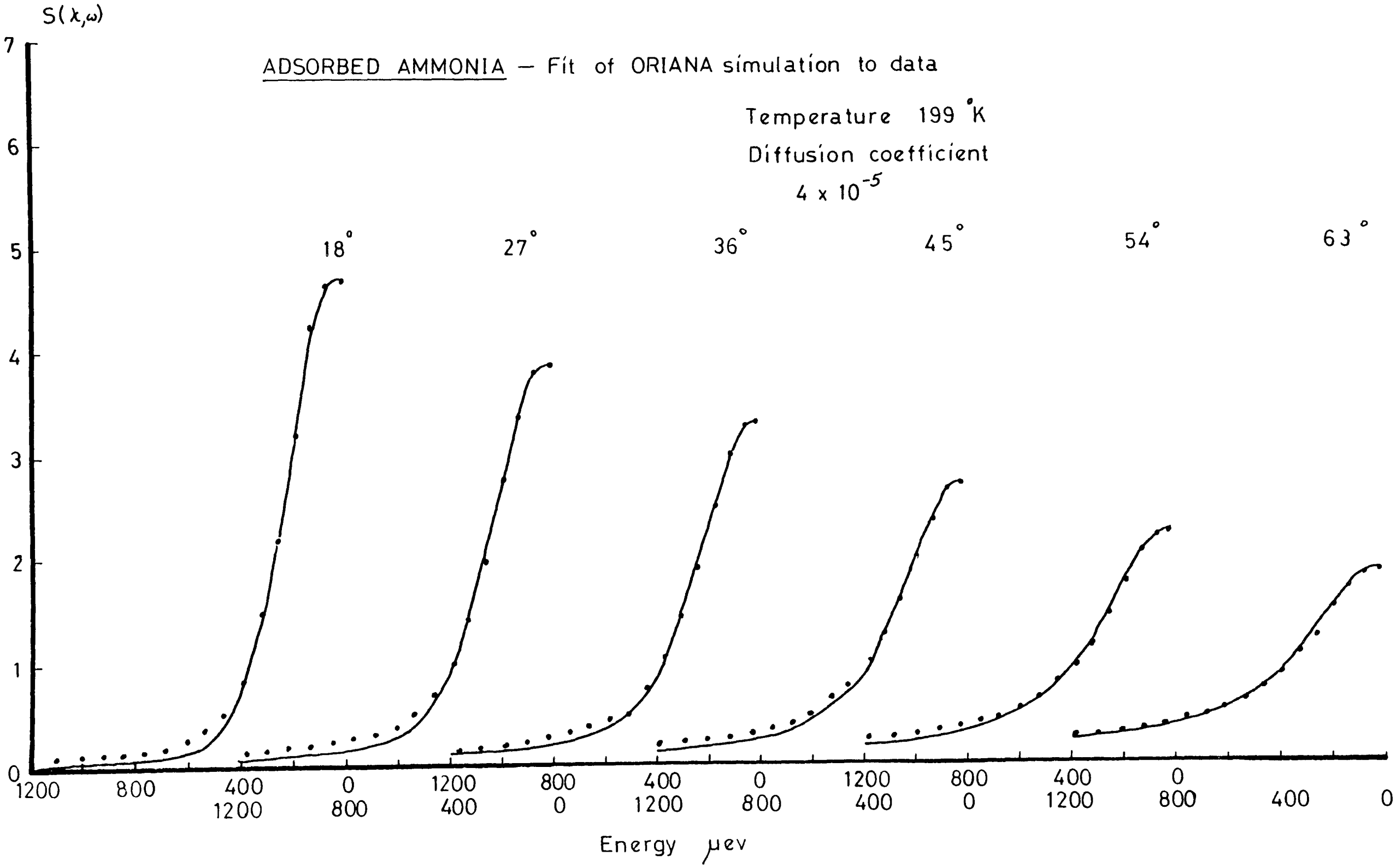
S(x,ω)
ADSORBED AMMONIA — Fit of ORIANA simulation to data
Temperature 199 °K
Diffusion coefficient
4 x 10^-5
18°
27°
36°
45°
54°
63°
7
6
5
4
3
2
1
0
1200
800
400
0
1200
800
400
0
1200
800
400
0
1200
800
400
0
1200
800
400
0
1200
800
400
0
Energy μev

FIGURE 5,41

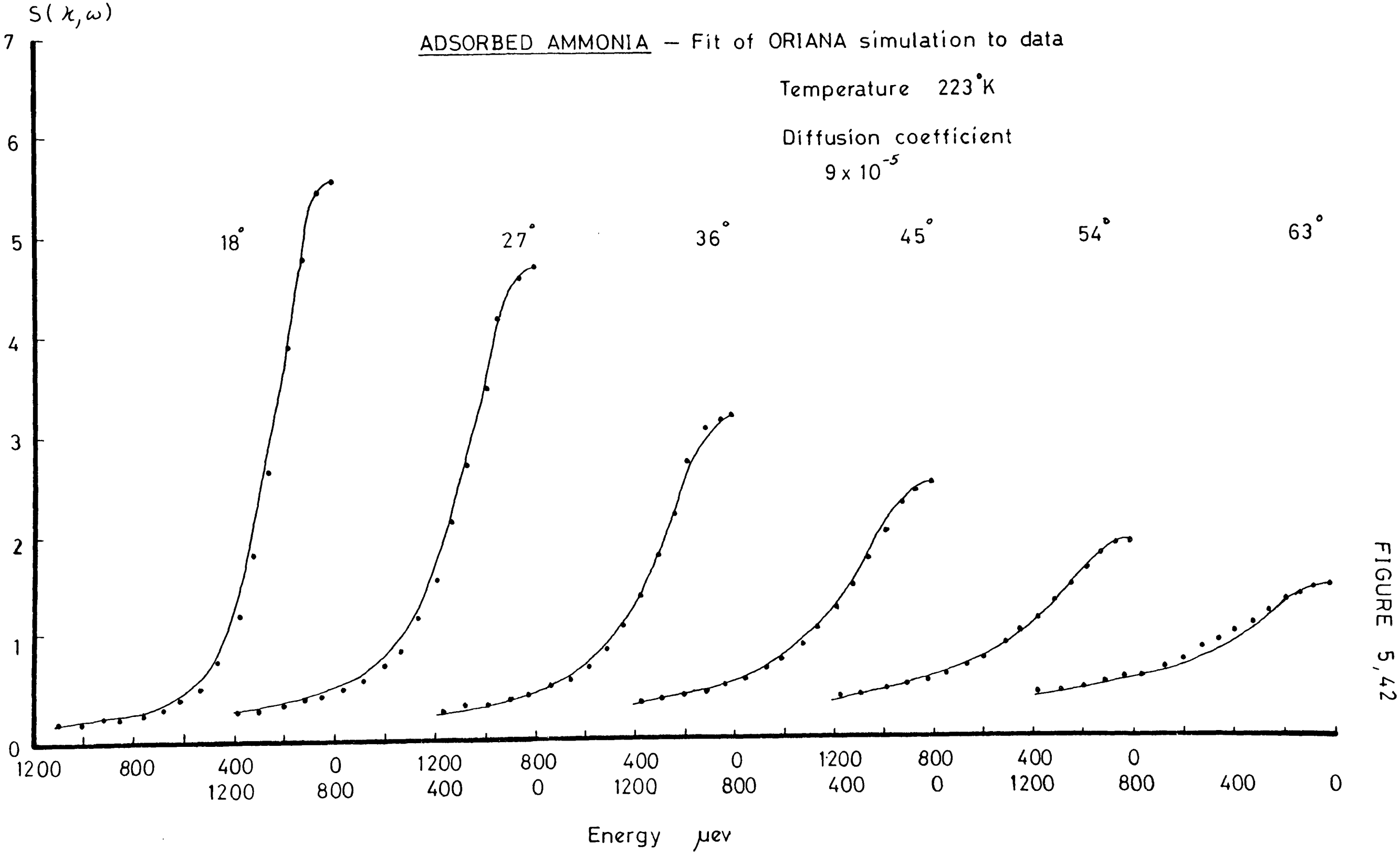
S(κ, ω)
ADSORBED AMMONIA — Fit of ORIANA simulation to data
Temperature 223°K
Diffusion coefficient
9 x 10^-5
18°
27°
36°
45°
54°
63°
7
6
5
4
3
2
1
0
1200
800
400
0
1200
800
400
0
1200
800
400
0
1200
800
400
0
1200
800
400
0
1200
800
400
0
Energy μev

FIGURE 5,42

FIGURE 5,43

ADSORBED AMMONIA – Deconvoluted FWHM vs χ^2

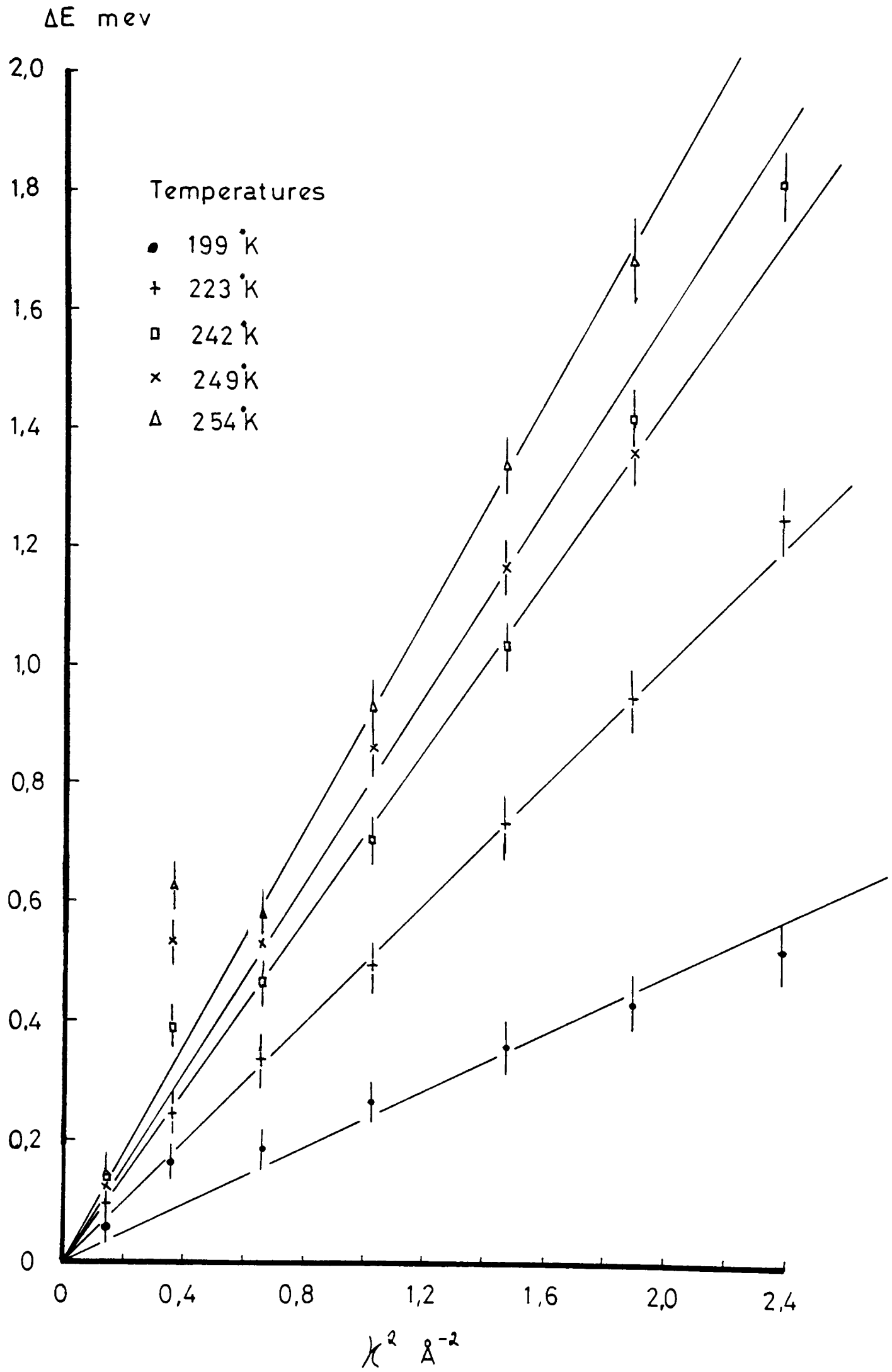

curve as a Voigt profile.

At temperatures below 199°K the quasi elastic peak shows only small broadenings, and these only slightly dependent on the momentum transfer. None of the 3D averaged models of 2D behaviour, not the simple 3D liquid or gas models fit the observed curves. Figure 5.44 shows the widths of the convoluted sample spectrum, together with the machine resolution widths. Figure 5.45 shows the results of attempting to deconvolute the machine resolution function. The different deconvolution methods give different results, and the broadening is small compared to the machine resolution so that errors in the deconvoluted "half widths" are large. Also included in the figures are the deconvoluted results for 199°K to emphasise the gradual change in the "broadening" plots from flat with a finite intercept and poor agreement between the methods of deconvolution, to a well defined straight line passing through the origin.

As no discontinuities occur in the subtracted inelastic spectrum at energies corresponding to transitions in the graphon density of states, one can be confident that the correct self attenuation factors were calculated and no residual scattering from the adsorbent remains in the adsorbate spectrum. The choice of background level was tested by plotting the temperature dependence of the full widths of $S(\kappa,w)$ at fractional heights of $\frac{1}{4}$, $\frac{1}{2}$ and $\frac{3}{4}$ of $S(\kappa,o)$. These are shown in figure 5.46. In contrast to the cases of adsorbed methane and ethylene the plots for ammonia show finite slopes and these slopes increase with increasing momentum transfer.

5.4.4 Discussion

The results will be considered in two parts, those for temperatures greater than 199°K and those for lower temperatures. Close to 199°K there appears to be a transition from a phase with a

FIGURE 5,44

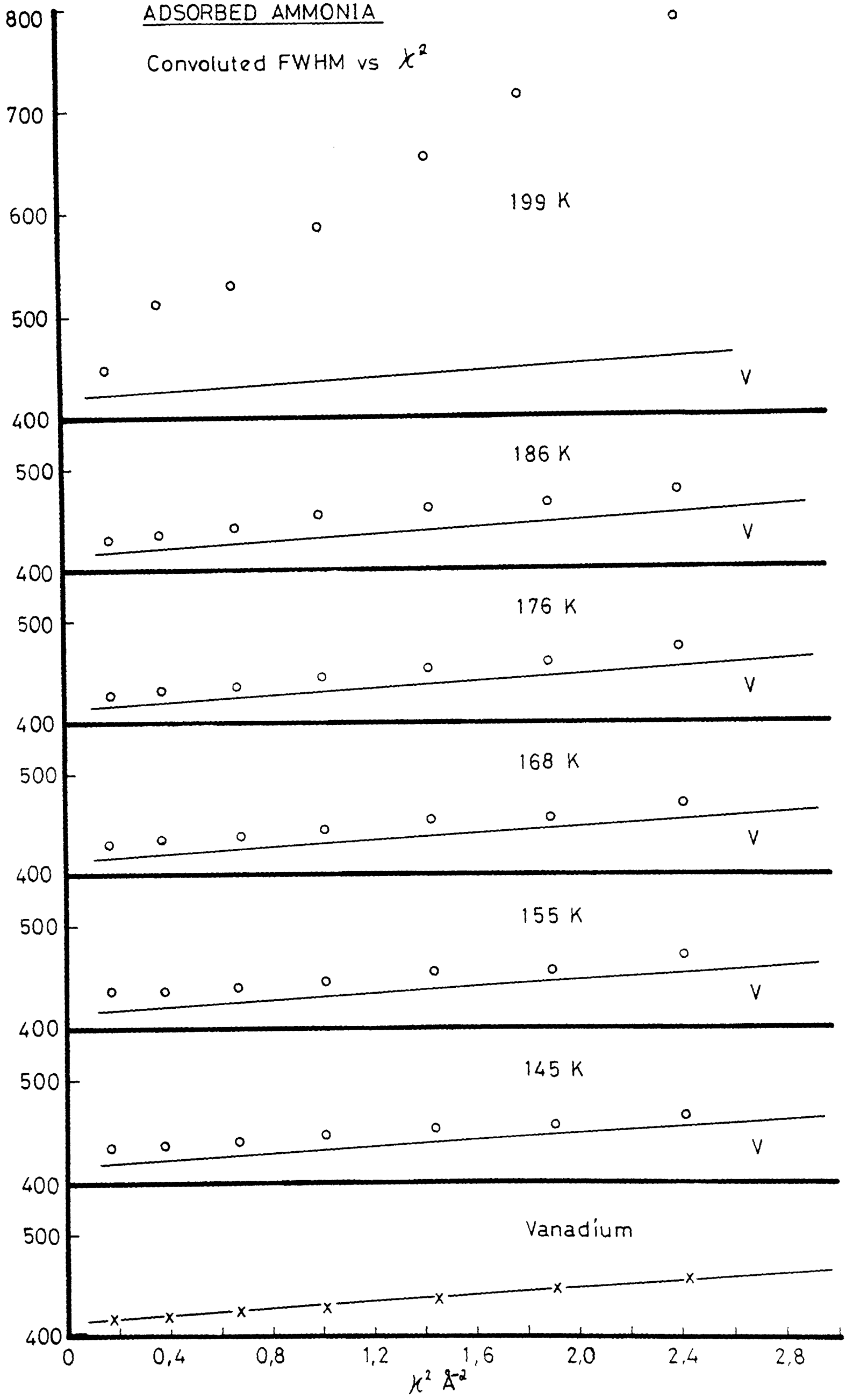
ADSORBED AMMONIA
Convoluted FWHM vs k^2
800
700
600
500
400
199 K
V
500
400
186 K
V
500
400
176 K
V
500
400
168 K
V
500
400
155 K
V
500
400
145 K
V
500
400
Vanadium
0
0,4
0,8
1,2
1,6
2,0
2,4
2,8
k^2 Å^{-2}

FIGURE 5,45

ADSORBED AMMONIA – Deconvoluted FWHM vs κ^2

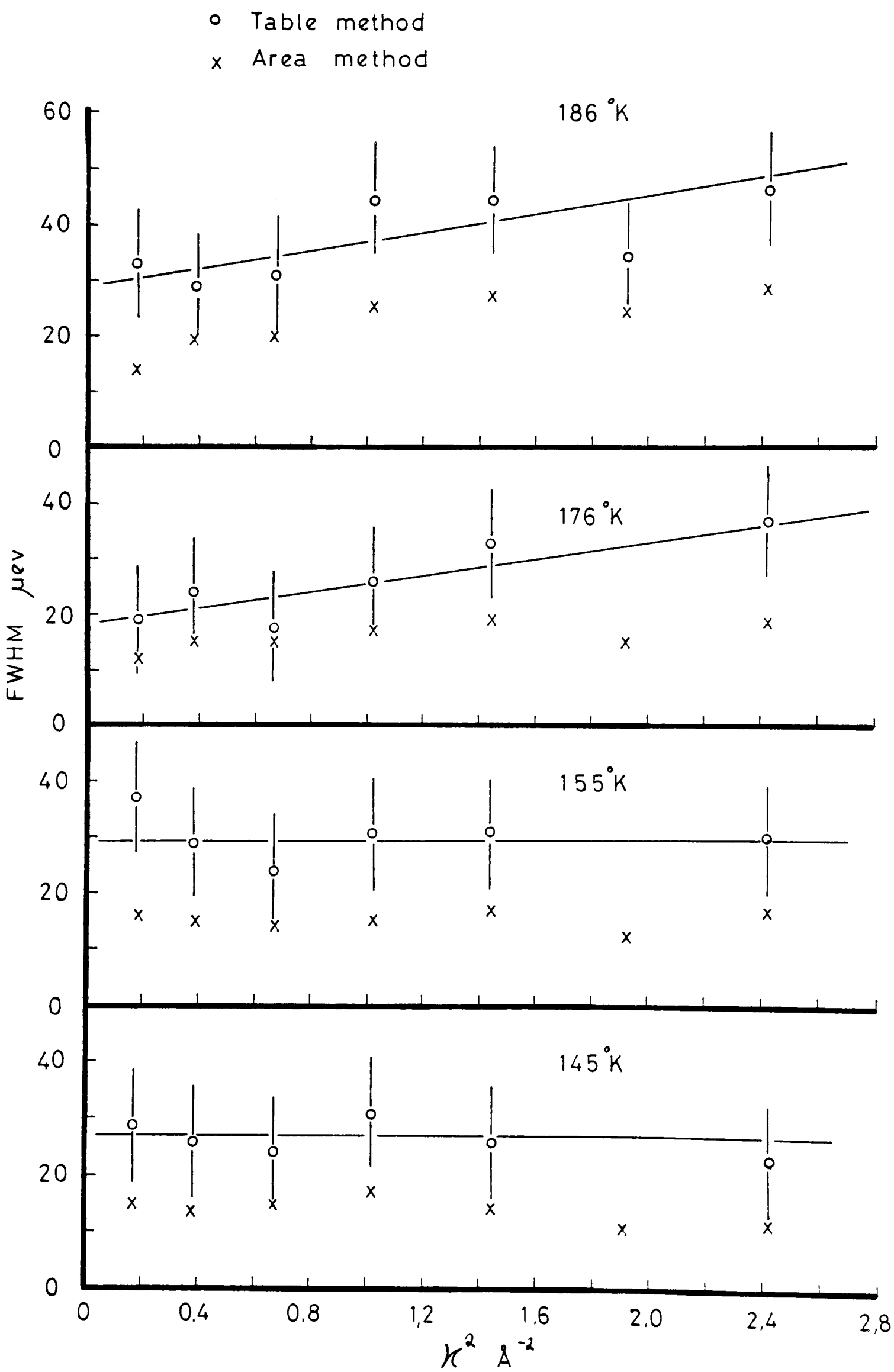

FIGURE 5,46

ADSORBED AMMONIA - Widths at fractional heights

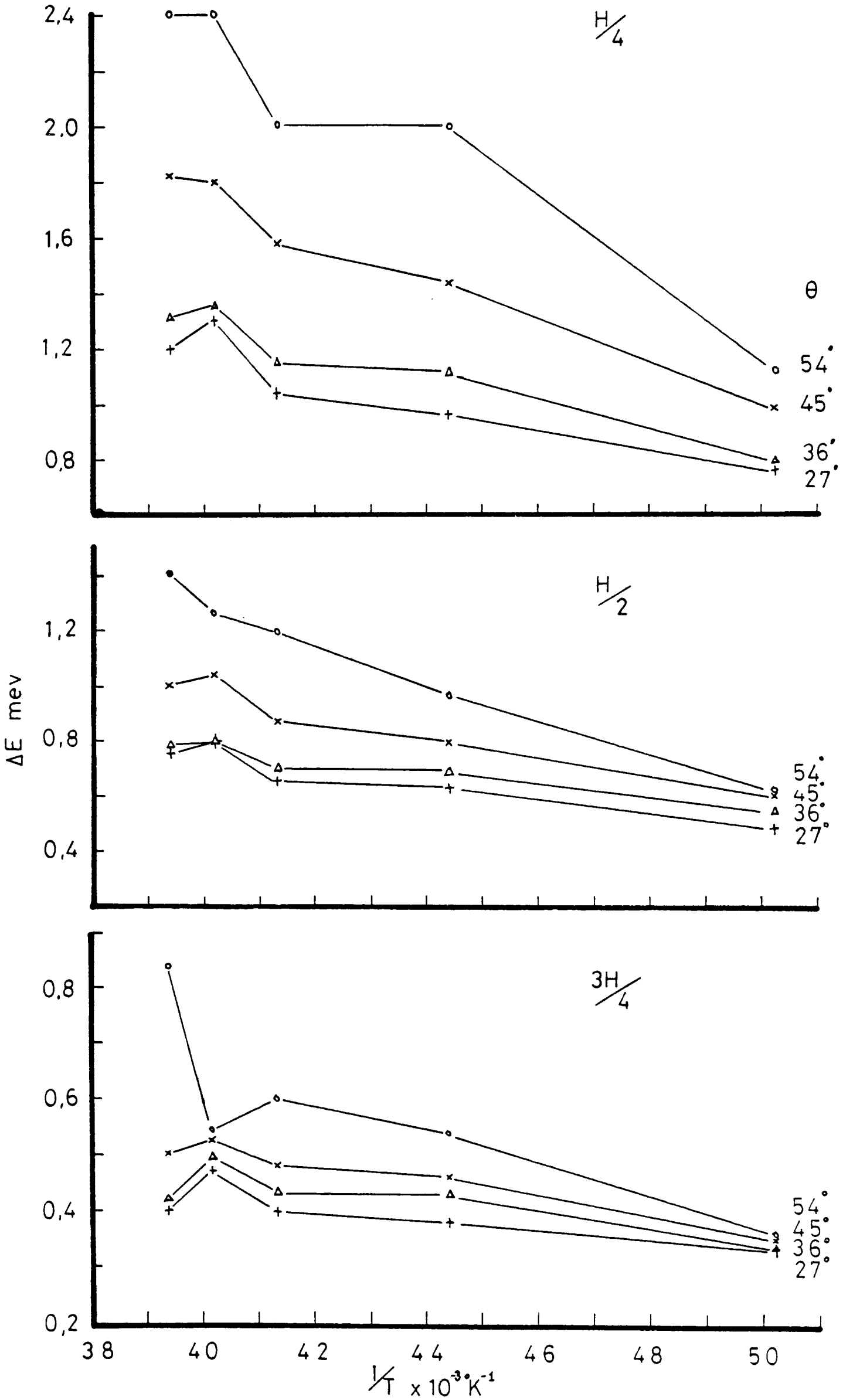

high surface mobility to a phase with a low, possibly non-existent surface mobility.

High Surface Mobility 199°K-261°K

In view of the success of the 3D averaged 2D liquid model for adsorbed methane and ethylene it is surprising at first sight that it should not apply to adsorbed ammonia. The observed scattering law is a good lorentzian and does not show any of the sharpness associated with the 3D averaging procedure. It seems likely that there is not true 2D motion on the poly-crystalline adsorbent. This could arise if there is appreciable motion of the ammonia molecule perpendicular to the adsorbent surface, or if the ammonia has not dispersed evenly about the carbon surface but has formed clusters of essentially bulk material. The latter case arises if the enthalpy of interaction is sufficiently strong to overcome the entropy of adsorption.

It is clear from the results that the adsorbate is not behaving in an identical fashion with bulk liquid ammonia. For example the data at 254°K, 249°K and 242°K, that is 14, 9 and 2 degrees above the bulk boiling point, nonetheless shows lorentzian scattering laws and nothing like the expected scattering law for bulk gaseous ammonia. Similarily the data at 199°K, 5 degrees above the bulk melting point, has clear evidence of discrete modes in the rotational envelope, so that at least some of the adsorbed ammonia has lost an appreciable amount of translational freedom.

However the observation of the lorentzian scattering law remains and requires explanation. In the 3D averaging of the 2D scattering laws it was assumed that the only motion perpendicular to the adsorbent surface was a simple harmonic vibration, i.e., in the case of a 2D liquid $D_{\perp} = 0$. If the adsorbed ammonia has not been evenly distributed across the graphon surface but has formed multi-layer patches, then this assumption is not true and there may well be diffusion perpendicular to the surface.

Dianoux and Volino (85) have developed the Stockmeyer (28) treatment to consider the motions of anisotropic molecules in liquid crystals. There are very different diffusion coefficients parallel and perpendicular to the long molecular axis. They find that if $D_{\parallel} \gtrsim D_{\perp}$ then the angle averaging as shown below

$$S(\kappa,w) = \tfrac{1}{2} \int_0^{\pi} \sin\phi d\phi \; \frac{(D_{\parallel} \cos^2\phi + D_{\perp}\sin^2\phi)\kappa^2}{(D_{\parallel} \cos^2\phi + D_{\perp}\sin^2\phi)^2\kappa^4 + w^2}$$

produces a scattering law which is very close to the lorentzian in shape having a full width at half maximum of

$$\Delta = 2\bar{\hbar}\, \overline{D}\, \kappa^2$$

where

$$\overline{D} = \frac{D_{\perp}\sqrt{(D_{\parallel} - D_{\perp}) / D_{\perp}}}{\arctan\sqrt{(D_{\parallel} - D_{\perp}) / D_{\perp}}}$$

If such a model is applicable then the neutron measurement is of $\overline{D}$ and no information is directly available on $D_{\perp}$ or $D_{\parallel}$. One possibility is to assume that as the 3D averaged 2D liquid model gives a reasonable fit at 199°K, the $D_{\perp} = 0$ at 199°K and the fitted diffusion coefficient of $4 \times 10^{-5} cm^2 sec^{-1}$ is equal to $D_{\parallel}$. Taking a reasonable value for the activation energy of diffusion the expected values of $D_{\parallel}$ can be calculated for the higher temperatures, and taking the measured D values as $\overline{D}$ one can obtain an estimate of $D_{\perp}$. The values obtained are shown in Table 5.4. The assumptions involved in such a treatment are gross and the conclusions can only be taken as indicative.

Independent of the absolute values of the diffusion coefficients employed their temperature dependence will give an activation energy for diffusion. Figure 5.47 shows this and the value of E_A determined from the plot is 2.4 kcals/mole, not very different to the value for

FIGURE 5,47

ADSORBED AMMONIA – Activation energy for diffusion

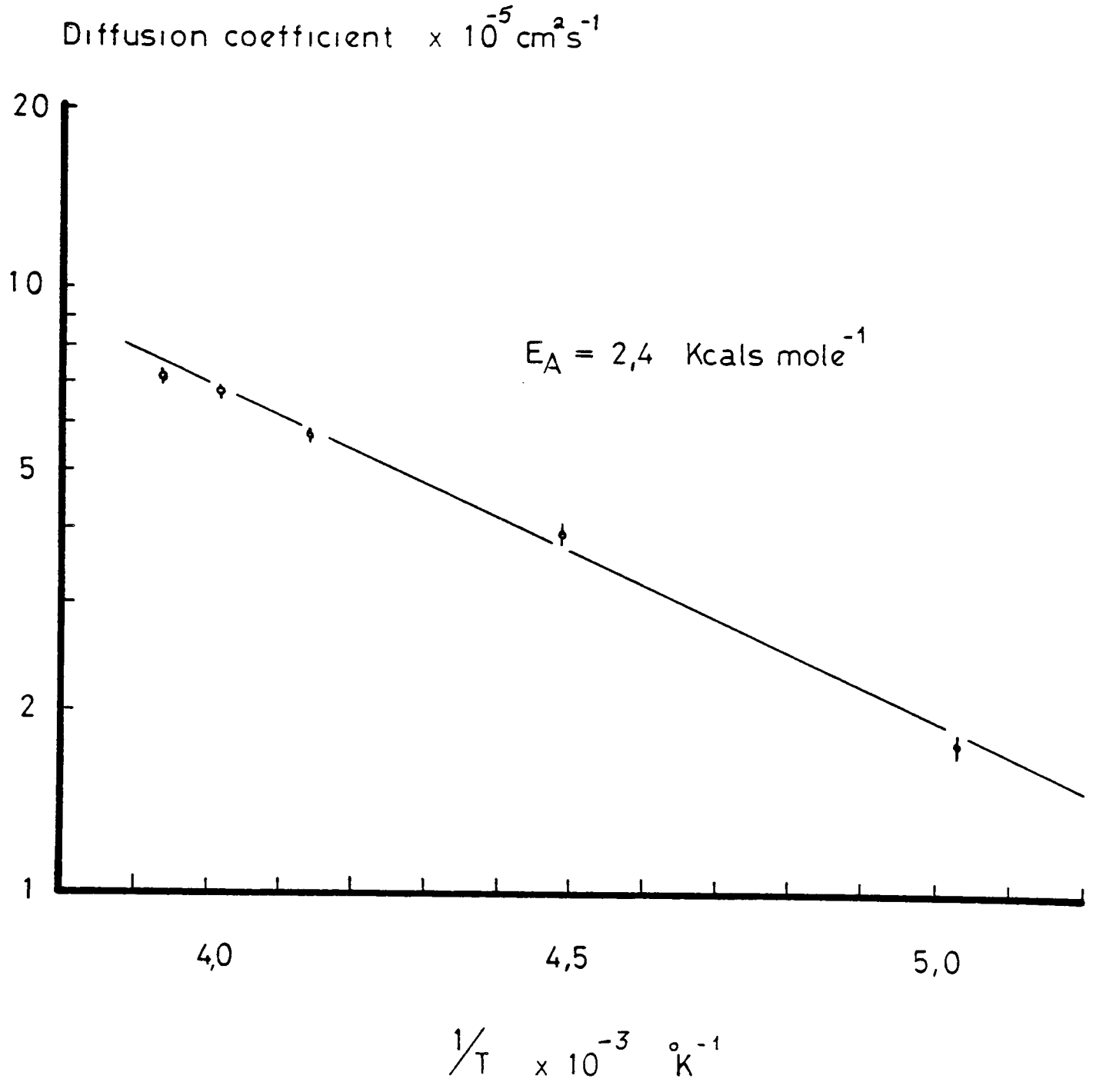

bulk liquid ammonia of 2.06 kcals/mole measured by NMR pulse echo (137). Table 5.4 also contains the diffusion coefficients calculated for liquid ammonia using the equation derived by (137). The expression is applicable to the range of temperatures for which ammonia is liquid, but one can calculate a hypothetical diffusion coefficient for the liquid at temperatures above the bulk boiling point and these values are entered in brackets. The agreement with the measured $\overline{D}$ values is remarkable, the $\overline{D}$ values being consistently slightly smaller than the calculated value.

The diffusion of ammonia across a microporous membrane has been studied by Ash et al (138). Figure 5.48 shows the measured surface diffusion coefficients as a function of surface coverage. From the graph can be obtained the surface diffusion coefficients at the same temperatures and surface coverages employed in the neutron scattering experiments. These values are also shown in Table 5.4

The values are signficantly lower than any of the other tabulated values and must rule out the possibility that the ammonia in the neutron experiment is adsorbed in micropores on the graphon surface. It is significant to note that the surface diffusion coefficient can be as low as 2×10^{-5} cm^2sec^{-1} at 273^oK, 33 degrees above the bulk melting point and it suggests that the restricted mobility for ammonia on graphon at high temperatures may be occurring in islands or pockets of condensed adsorbate.

The dynamics of the ammonia molecule within one of these islands must be very similar to that of an ammonia molecule in the bulk fluid. The interpretation of $\overline{D}$ in terms of dissimilar $D_{\perp}$ and $D_{\parallel}$'s has little supporting evidence, other than the success of the 3D averaged 2D liquid model at 199^oK and 223^oK. The NMR work does however give a prediction of the diffusion coefficients of "liquid" ammonia as a function of temperature which are surprisingly close to those observed for adsorbed ammonia.

FIGURE 5,48

ADSORBED AMMONIA — Surface fluxes

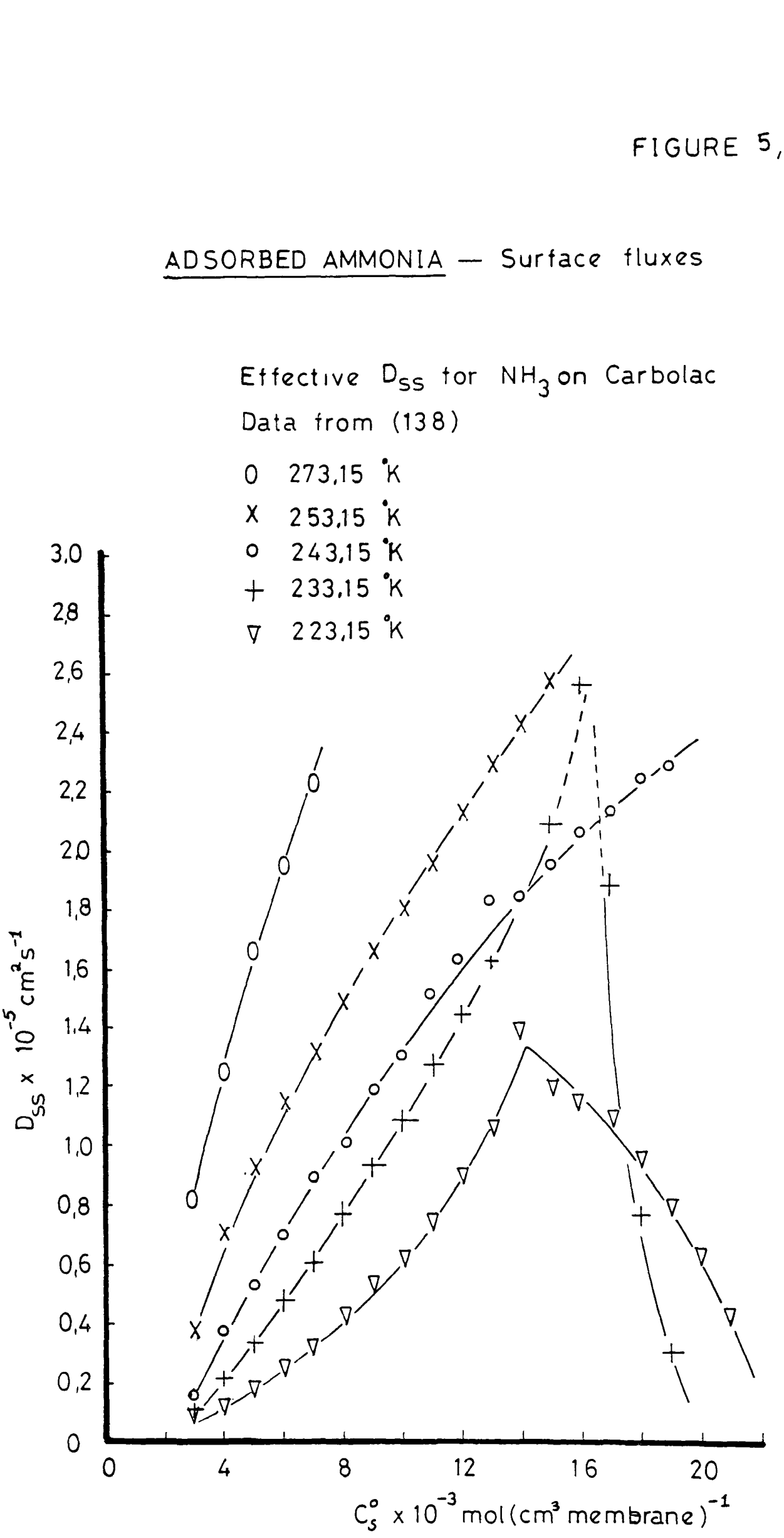

Surface area of Carbolac 950 $m^2 (cm^3 membrane)^{-1}$

2) Low surface mobility < 199°K

The similarity of the properties of the adsorbed ammonia to those of bulk ammonia can also be seen in the low temperature regime. The observed frequency distribution has a similar form to that of bulk ammonia at 106°K (89) although on close inspection there are differences. The frequency distribution of solid ammonia splits into two groups, the lower energy group arising from hindered molecular translations within the unit cell, the other group from hindered molecular rotations. Figures 5.39 and 5.40 include the neutron scattering data of (89) which is in good agreement with the raman measurements of Pine et al (139). The extrapolation of time of flight spectra to $\kappa = o$ is not precise over about 300 cm^{-1} but the data does show that the higher peak present in Goyal's data at 305 cm^{-1} is not present in the case of adsorbed ammonia when the temperature is higher than about 176°K. There is also a shift to lower energies of between 15 and 20 cm^{-1} for the transitions of adsorbed ammonia. A splitting is observed in the lowest energy translational group of adsorbed NH_3 and the splitting becomes more pronounced at the lower temperatures. No such splitting has been observed in the raman spectra of solid ammonia and it is unlikely that it is a crystal field splitting as there should be evidence of this in the other transitions and there is none. A possible assignment for one of these transitions could be to the perpendicular vibration of the ammonia molecule with respect to the carbon surface. The energy of 70 cm^{-1} is of the order of magnitude calculated for the energy of the methane-surface vibration (see section 2.5.1). It is only visible at the lowest temperatures as the rotational and translational scattering laws in the scattering law convolution are now quite sharp, due to the loss of motion.

The loss of translational motion shows up in the sharpness of the quasi elastic peak. The constant broadening observed probably

arises from residual rotational motion of the adsorbed ammonia, either as rotational diffusion or as a jump diffusion between fixed orientations of the admolecule which do not change the centre of mass position. Further work on a higher resolution instrument is necessary to quantify the observed broadening sufficiently well to distinguish and parameterise the correct model.

The results indicate that adsorbed ammonia is not evenly distributed on the graphon surface, but that it clusters into islands of adsorbate that have properties quite close to those of the bulk material. An unusual feature is that the islands of ammonia display these properties outside the expected temperature ranges of the phases corresponding to bulk ammonia. It may be due to the thermodynamic consequences of small particle growth or formation. Whether the clustering is due to imperfect outgassing of the graphon surface or to the strength of the adsorbate-adsorbate interaction remains to be discovered.

Table 5.4

Diffusion coefficients of Ammonia and Ammonia adsorbed on Graphon

TEMPERATURE ^{o}K	(a D_{LIQ} $x10^{-5}$	(b D^{2D} $x10^{-5}$	(c $\overline{D}$ $x10^{-5}$	(d $D_{\parallel}$ $x10^{-5}$	(e $D_{\perp}$ $x10^{-5}$	(f D^{SS} $x10^{-5}$
199	2.40	4.0	1.77	4.0		
223	4.22	9.0	3.88	7.01	2.80	1.1
242	(6.08)	-	5.63	10.10	4.00	1.3
249	(6.86)	-	6.70	11.40	4.40	1.1
254	(7.45)	-	7.09	12.38	5.00	1.2
261	(8.32)	-	-	-	-	-

Bulk melting point of ammonia 195°K, boiling point 240°K

a) D_{LIQ} calculated from $D = 4.4 * 10^{-3} \exp(-1038/T)$ (137)

b) D^{2D} value of diffusion coefficient used in the 3D averaging of the 2D liquid model

c) $\overline{D}$ value of the diffusion coefficient obtained from the ΔE vs κ^2 plot for the deconvoluted scattering law.

d) $D_{\parallel}$ and e) $D_{\perp}$ parallel and perpendicular components assuming that at 199°K $D_{\parallel} = 4 \times 10^{-5}$ $cm^2 s^{-1}$ and $D_{\perp} = 0$. The activation energy for diffusion was taken as 2.06 kcals/mole.

f) D_{SS} surface diffusion coefficient measured by Ash (138) for ammonia adsorbed on carbolac I, a microporous carbon of surface area 950 m^2 g^{-1}, of which an area of 686 m^2 g^{-1} is due to pores.

CHAPTER 6: ABSORPTION IN LA-Y ZEOLITE

6.1 Molecular Sieves as Absorbents

In contrast to the carbons, zeolites are a sorbent system of immense complexity (140).

a) Sorption takes place on internal surfaces rather than on external, well characterised, single crystal planes. These internal surfaces although quite regular, present a range of possible site absorption energies and geometries.

b) The sorption site may be a 'mobile' metal cation so that absorption causes structural changes in the zeolite. A characterisation of the absorption site in an outgassed absorbent may not then provide useful information for probing the mechanism of the absorption process. In the extreme case the absorbate may react irreversibly with the surface and become incorporated into the structure.

c) Absorption on an interior surface is subject to geometric constraints. Is the absorbate molecule of a size and shape such that it can readily penetrate and leave the absorbent? Once absorbed one would anticipate that the dynamics of the absorbate will be dependent on the relationship between the absorbate molecular geometry and the zeolite pore size, shape and interconnections. The lateral interactions in the absorbate layer will be modified compared to those existing in flat adlayers for now there is marked curveature and finite boundaries to the adlayer.

d) There is a great variety of zeolite structures, and within each class the absorption properties may be subtly altered by

i) Exchanging the metal cation over all concentration ranges.

ii) Altering the SiO_2/Al_2O_3 ratio within set limits - so as not to take the structure into another class. As a result

information and parameters obtained from particular absorbate/zeolite systems are highly specific and may not necessarily be transferable to another zeolite system. Naturally the range of adjustable parameters enables a molecular sieve to be tailored to suit a particular need, and molecular sieve zeolites have found widespread application in the chemical industry. (141)

6.1.1 Absorption properties and surface characteristics of Y-type zeolites

The molecular sieve absorbent used in this work is a Lanthanum exchanged Y-type zeolite (La-Y). There are several reasons why this particular system was chosen.

1) The 'surface area' is large, the void fraction of a Y-type zeolite is 0.35 cm^3gm^{-1} (142), and can be reproducibly obtained without unnecessarily stringent control of the outgassing conditions.

2) The small, tripositively charged cation confers great stability on the aluminosilicate lattice as the waters of hydration are removed during outgassing. This enables one to heat to high temperatures under vacuum and so produce a surface with a low concentration of hydroxyl groups (140a). Figure 6.1 shows the result of Differential Thermal Analysis of a Y-type zeolite (140a). Loss of water commences at just over room temperature, reaches a maximum at 510°K and is not complete until about 620°K. The loss of water does not lead to a collapse of the lattice until 1060°K as shown by the exothermic peak, when an amorphous residue is obtained.

3) The structure of the Y-type zeolite is well known (143). The pores form interconnecting, three dimensional channels with a pore diameter of some 13 Å and a pore window of 7 Å width. Most absorption is expected to take place here though small molecules may be able to penetrate into the β cages of the overlying sodalite cagework, where the pore window width is 2.2 Å and the internal diameter 6.6 Å. See figure 6.2.

FIGURE 6,1

X&Y TYPE ZEOLITES – Differential thermal analysis

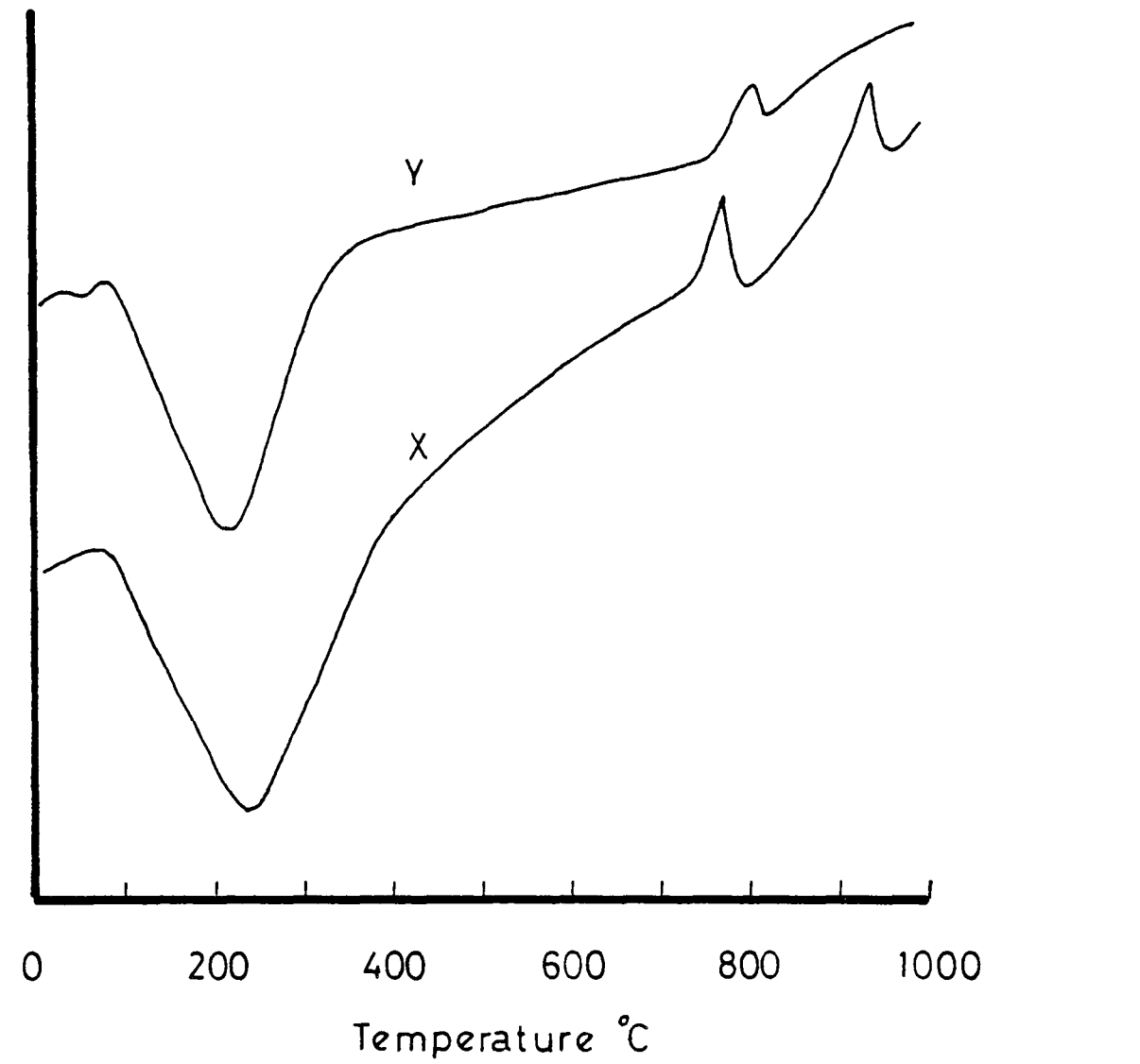

FIGURE 6,2

Y TYPE ZEOLITE – Framework structure

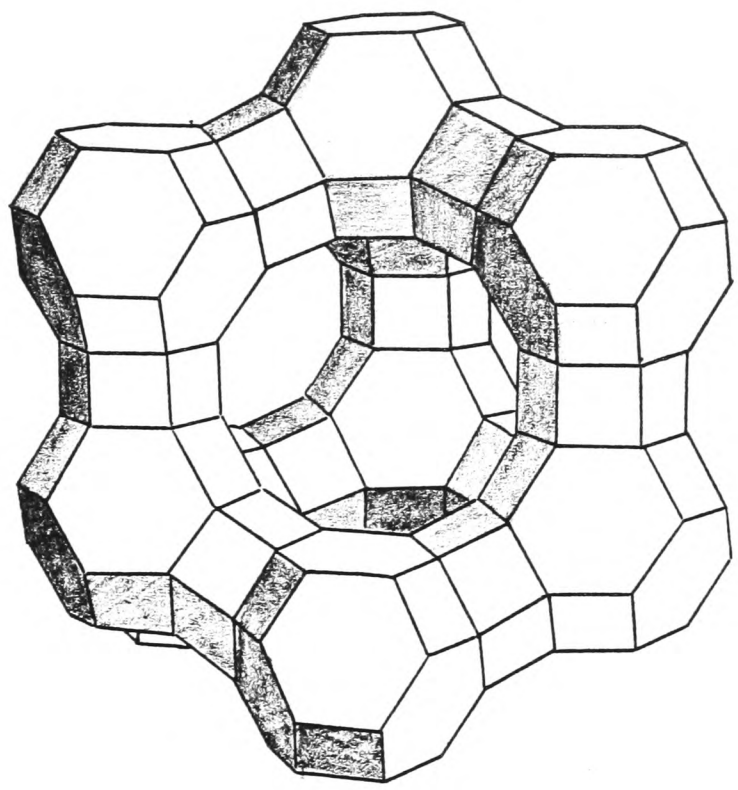

Tetrahedrally coordinated, truncated cubo-octahedra

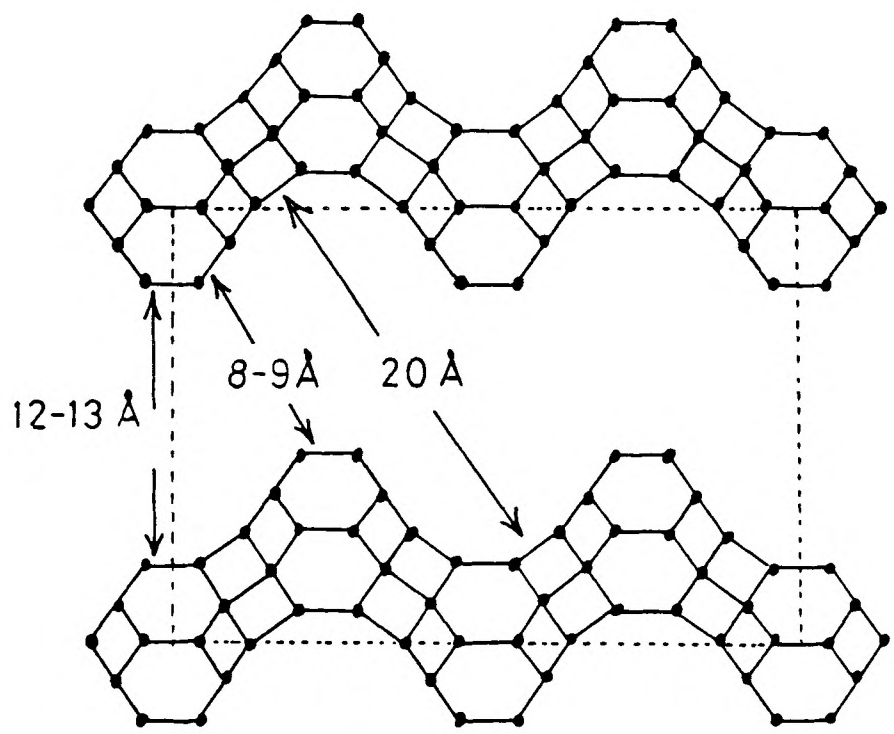

(011) projection of (Al+Si) atoms of cubo octahedral cages centred on this plane. From (140a).

6.2 Neutron Scattering from La-Y

In the same way as for graphon, the molecular sieve absorbent was characterised by several neutron scattering techniques. The purpose being to define operating conditions so that interference from scattering by the absorbent can be minimised. The structure and lattice dynamics of a zeolite are complex and a quantitative study of these properties was not undertaken.

6.2.1 Elastic scattering

Conventional powder diffraction patterns were obtained using the BADGER II machine at Harwell and the D1B multidetector instrument at the ILL. Samples of outgassed and unoutgassed La-Y were studied. The patterns are shown in figure 6.3 and the data condensed in table 6.1. The peak positions are in good agreement with the x-ray measurements. As would be expected the unoutgassed sample has a high background due to the incoherent scattering from the protons of absorbed water molecules.

The coherent scattering from the absorbent will affect the incoherent quasi elastic peak measurements on the absorbate by increasing the difficulty of background subtraction. The positions of these Bragg points in the (κ,w) space of the 4H5 time of flight spectrometer are shown in figure 6.4 together with the cuts that the fixed counter bank gives for incident wavelengths of 4.2 $\mathring{A}$ and 4.8 $\mathring{A}$.

Figure 6.12 shows the elastic peak intensity dependence on κ^2 determined from the time of flight measurements. The coherent scattering produces an irregular variation of scattered intensity, distorting the linear dependence of the In(I) vs κ^2 plot that would be expected. Knowing the κ values for the coherent scattering from the diffraction pattern enables the distorted data to be recognised and discarded and the value of $\langle u^2 \rangle$ determined from the slope of the

Table 6.1

Diffraction Data for Y-type Zeolites

(hkl)	X-ray data Na-Y wet d Å (a)	Neutron Data	
		La-Y 'wet' d Å	La-Y 'dry' d Å
111	14.29	14.08	14.08
220	8.75	-	8.75
311	7.46	-	7.45
331	5.68	5.69	5.59
333	4.76	4.77	4.70
511	-	-	-
440	4.38	-	4.32
620	3.91	-	-
533	3.775	3.73	3.73
444	3.573	-	-
711	3.466	-	-
551	-	-	-
642	3.308	3.32	3.32
731	3.222	-	-
553	-	-	-
733	3.042	-	-
822	2.917	-	-
660	-	-	-
751	2.858	-	2.86
555	-	-	-
840	2.767	-	-
911	2.717	-	-
753	-	-	-
664	2.638	-	-
931	2.595	-	-

a) Data from reference 140 a)

FIGURE 6,3

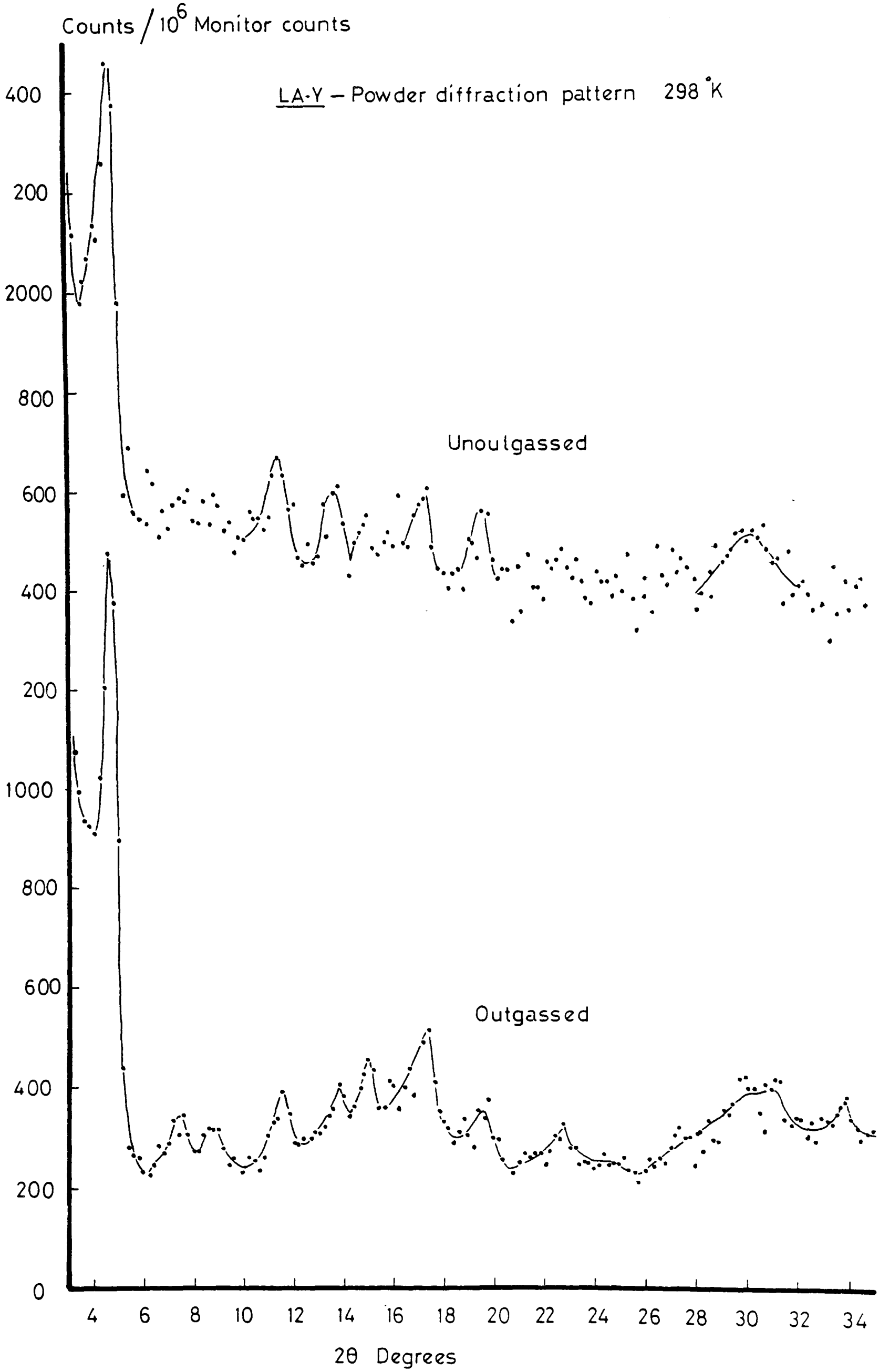
Counts / 10^6 Monitor counts
LA-Y – Powder diffraction pattern 298 °K
Unoutgassed
Outgassed
400
200
2000
800
600
400
200
1000
800
600
400
200
0
4
6
8
10
12
14
16
18
20
22
24
26
28
30
32
34
2θ Degrees

FIGURE 6,4

LA-Y – Coherent scattering

Choice of spectrometer wavelength

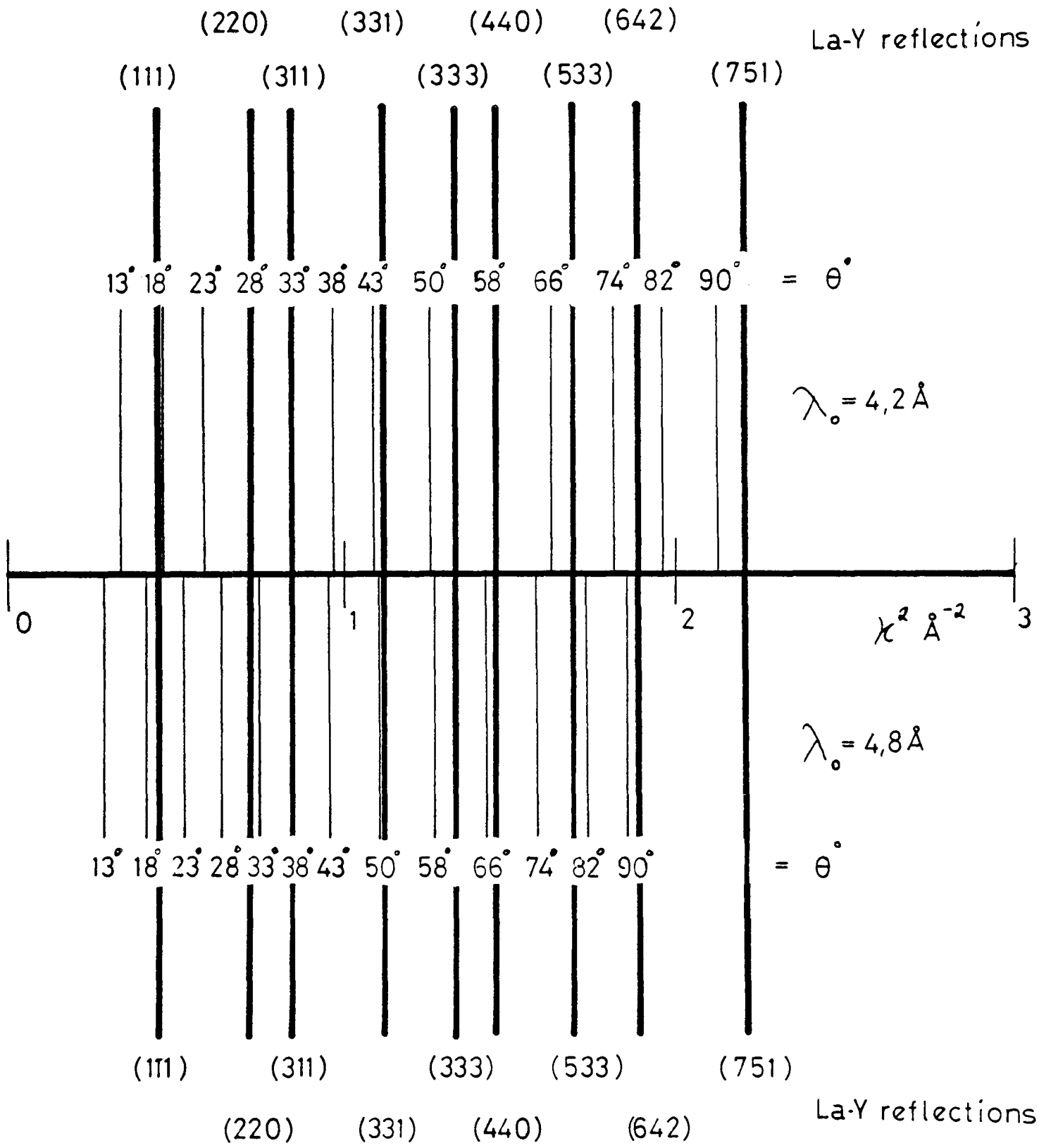

line shown. As an aluminosilicate lattice is rigid the small value of 0.193 $\mathring{A}^2$ is much as expected.

In contrast to the coherent scattering from graphon, the diffraction peaks for La-Y are not broadened but have the machine resolution width. Similarily the distortion of the Debye Waller plot by coherent scattering from one Bragg peak does not extend over several counters as it does for the graphon (0002) reflection. The lack of broadening implies that crystallite sizes in the aluminosilicate must therefore extend over several thousand angstroms.

The small angle scattering from unoutgassed La-Y zeolite was measured on the D11 spectrometer at the ILL. The ranges of κ space scanned are shown in the table below.

λ $\mathring{A}$	Sample to detector distance cm	κ range $\mathring{A}$
6	66	0.09 → 0.500
6	236	0.02 → 0.150
12	236	0.01 → 0.075

The curves of scattered intensity versus κ^2 are shown in figure 6.5, together with the low κ range of the powder diffraction pattern measured on D1B. The coherent scattering from the (111) plane is evident in the small angle scattering. As the D11 instrument is not optimised for this relatively large κ region, the poor resolution in κ space and the high sloping background produce a poor correspondence with the powder diffraction peak.

As in the case of graphon the In(I) VS κ^2 plots are sharply curved, probably because of interference effects as well as a distribution of particle sizes. The limiting slope of the curve as κ^2 tends to zero gives a value of R = 71 ± 2 $\mathring{A}$, though the physical significance of the parameter, about three times the unit cell length, is not obvious.

FIGURE 6,5

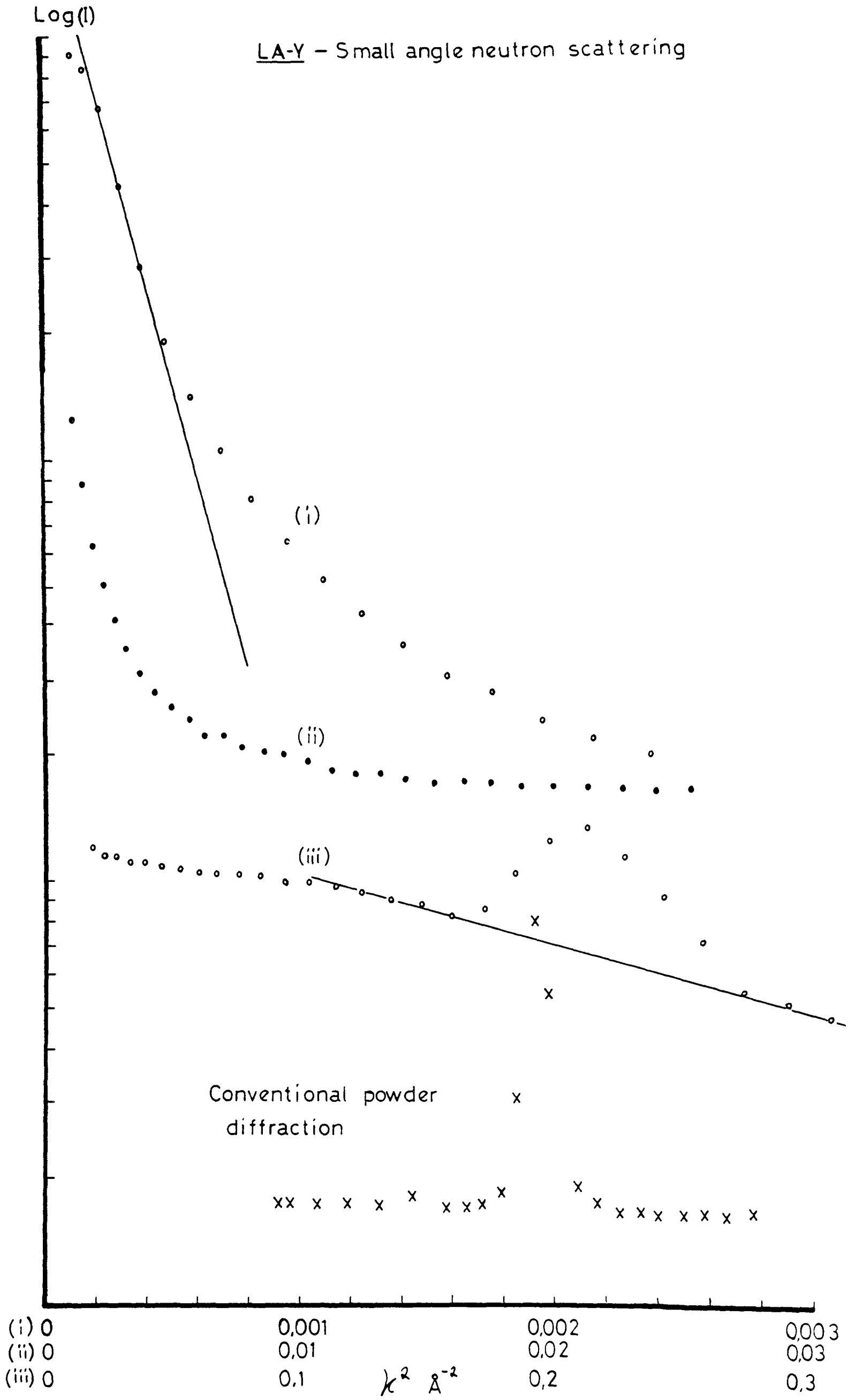
Log(I)
LA-Y – Small angle neutron scattering
(i)
(ii)
(iii)
Conventional powder diffraction
(i) 0
(ii) 0
(iii) 0
0,001
0,01
0,1
0,002
0,02
0,2
0,003
0,03
0,3
k^2 Å^{-2}

6.2.2 Inelastic Scattering

The incoherent cross sections for Si, O and Al are small compared to ^{1}H. The inelastic time of flight spectrum for unoutgassed La-Y zeolite arises solely from the rotational and vibrational density of states for water absorbed from the atmosphere. As the amount of water present is removed by outgassing so the inelastic scattering diminishes in intensity rapidly, eventually becoming comparable with the scattering from the magnalloy sample can. See figure 6.6.

In the spectrum of the 'wet'zeolite a sharp peak is evident at 440-480 cm^{-1} arising from the torsional oscillations of absorbed water. The observed spectrum shows a significant difference to the spectrum for bulk water in the reduced scattering intensity at energies below 150 cm^{-1} and in the apparent absence of any quasi elastic peak broadening. A similar behaviour has been seen for water absorbed in lamellar clays (30c). The loss of intensity in the low energy region reflects the loss of intermolecular vibrations and rotations that are possible in the bulk liquid. In a zeolite the water molecules are probably more widely separated with fewer and weaker water-water interactions but correspondingly more water-zeolite interactions. These will be stronger interactions and lead to a shift of intensity to higher energies. The stronger interactions together with the geometrical constraints on the motion of a water molecule inside a zeolite cavity, reduce the centre of mass motion considerably and there is no translational diffusion broadening of the quasi elastic peak. It is likely that broadening due to rotational or jump diffusion is present but concealed by the low resolution of the Harwell Instrument.

The Beryllium filter spectrum of an unoutgassed zeolite is shown in figure 6.7. The sample was at $77^{o}K$ so the molecular modes are sharpened but the intermolecular modes at lower energies are

FIGURE 6,6

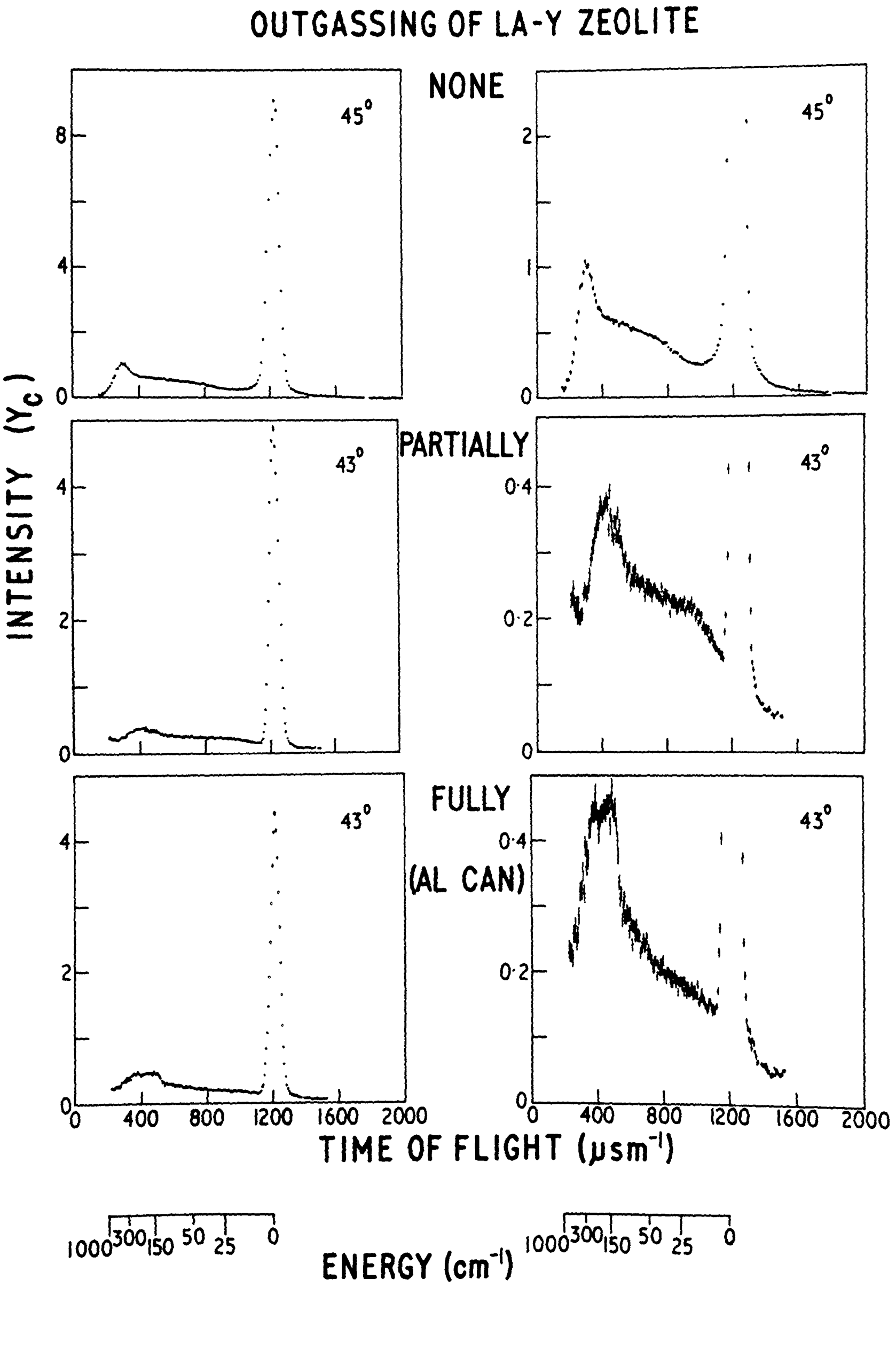
OUTGASSING OF LA-Y ZEOLITE
NONE
PARTIALLY
FULLY
(AL CAN)
45°
43°
INTENSITY (Yc)
TIME OF FLIGHT (μsm⁻¹)
ENERGY (cm⁻¹)
0
400
800
1200
1600
2000
1000
300
150
50
25

FIGURE 6,7

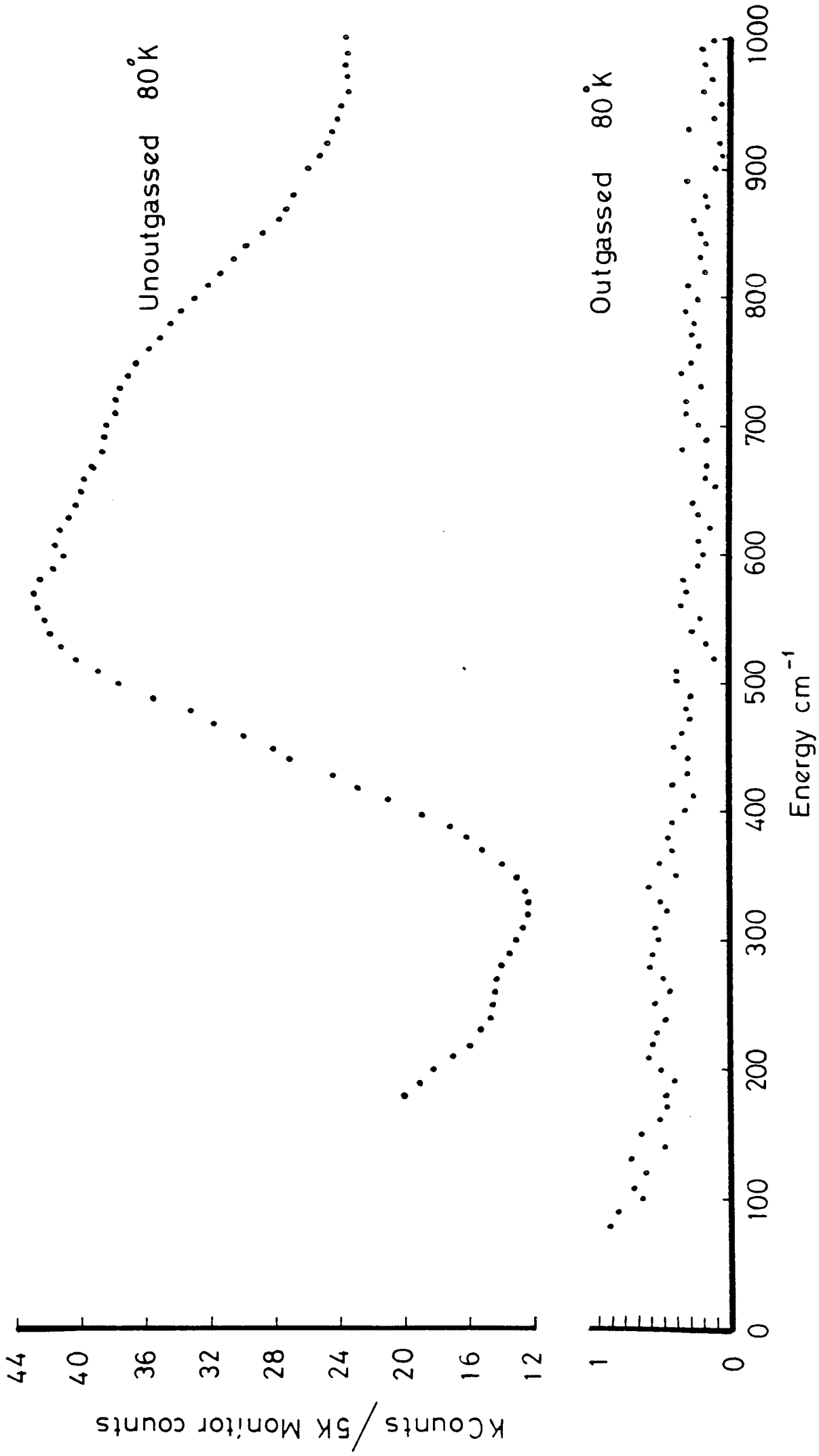
LA-Y — Beryllium filter spectrum
Unoutgassed 80°K
Outgassed 80°K
kCounts / 5K Monitor counts
44
40
36
32
28
24
20
16
12
1
0
0
100
200
300
400
500
600
700
800
900
1000
Energy cm⁻¹

substantially modified as a consequence of the 'freezing' of the included water.

The second spectrum in figure 6.6 is for a sample of La-Y zeolite heated to 520°K for 24 hours to a vacuum of 10^{-4} τ. The main peak is now shifted to 280-320 cm^{-1} and the scattering envelope at low energies has changed. The partial outgassing will have reduced the water content substantially but had little effect on the surface hydroxyl group concentration. The observed spectrum is now weighted towards the density of states for the distribution of bound hydroxyl groups.

Outgassing at 780°K for 48 hours to a vacuum of 10^{-5} τ removes nearly all of the water and substantially reduces the surface hydroxyl concentration. The choice of the La^{3+} cation ensures the stability of the aluminosilicate lattice under these conditions as has been shown by x-ray diffraction studies (143). The inelastic neutron scattering is now very small, appearing as an increased background and slight broadening of the inelastic features of the magnalloy can spectrum. Figure 6.7 shows the beryllium filter spectrum for a sample of outgassed La-Y and further demonstrates the reduction in scattered intensity that outgassing produces.

6.3 Absorption of Methane in La-Y

6.3.1 Results

The scattered neutron time of flight spectrum was obtained for samples of methane absorbed in an outgassed La-Y zeolite at the temperatures and concentrations shown below. In contrast to the experiments with graphon the La-Y was outgassed, allowed to cool under an atmosphere of helium gas; the helium gas pumped off when the sample was cool; the sample then equilibrated with methane gas at ambient temperature and pressure, and finally the system sealed for the duration of the measurements. The partial pressure of the methane gas above the absorbent thus varied with the temperature of the experiment.

Temperature ^{o}K	Number of CH_4 molecules per cavity	Subtracted counts in	
		Elastic channel $\theta = 74^{o}$	Inelastic maximum $\theta = 74^{o}$
160	1.4 ± 0.15	10799	1628
190	1.32 ± 0.12	9630	2029
213	1.11 ± 0.10	8597	1872
245	0.58 ± 0.07	8400	1582

Efficiency of Outgassing

An estimate of the residual water concentration in the La-Y zeolite after outgassing can be made from the observed % scatter from the blank La-Y zeolite.

The composition of the La-Y unit cell is

$$La_{28,6}\ (AlO_2)_{86}\ (SiO_2)_{106}\ x\ H_2O$$

$$MW = (22161 + 18x)$$

The % scatter from one gram of the sample is given by

$$T = \frac{3.31}{(22161 + 18x)} \left\{ (28.6\,\sigma_{LA}) + (86\,\sigma_{AL}) + (106\,\sigma_{SI}) + (384 + x)\sigma_{O} + (2x)\sigma_{H} \right\}$$

$$T = 3.31 \quad \frac{(2261 + 166.4x)}{(22161 + 18x)} \qquad \% \text{ per gm}$$

Now the weight of La-Y in the beam was 7.5 gms and the observed % scatter was 4.52% i.e. 0.6% per gram. Solving the above equation with T = 0.6 gives x = 10.7, i.e. about 4% of the water remains, probably as surface hydroxyl groups.

Absorbate concentration

In contrast with graphon La-Y is an absorbent and the parameter void fraction now assumes the role of available surface area. The void fraction for a Y-type zeolite is 0.35 cm^3gm^{-1}; the volume of the unit cell, determined from the powder diffraction experiments is 15050 $\mathring{A}^3$, and each unit cell contains eight pores (140a). The % scatter from the absorbed methane gives the methane concentration in a known weight of sample, and hence the average number of molecules in a single absorption cavity.

Temperature ^oK	% scatter CH_4 ABS	N x 10^{20}	Number of cavities in 7.5 gm La-Y	Number of CH_4 molecules per cavity
160	3.39	18.75		1.40
190	3.31	17.65		1.32
213	2.68	14.89	13.4 x 10^{20}	1.11
245	1.39	7.71		0.58
295	0.60	3.32		0.25

Figure 6.8 shows the variation of the number of CH_4 molecules per cavity with temperature. The number is smaller than expected,

ABSORBED METHANE – Cavity concentration

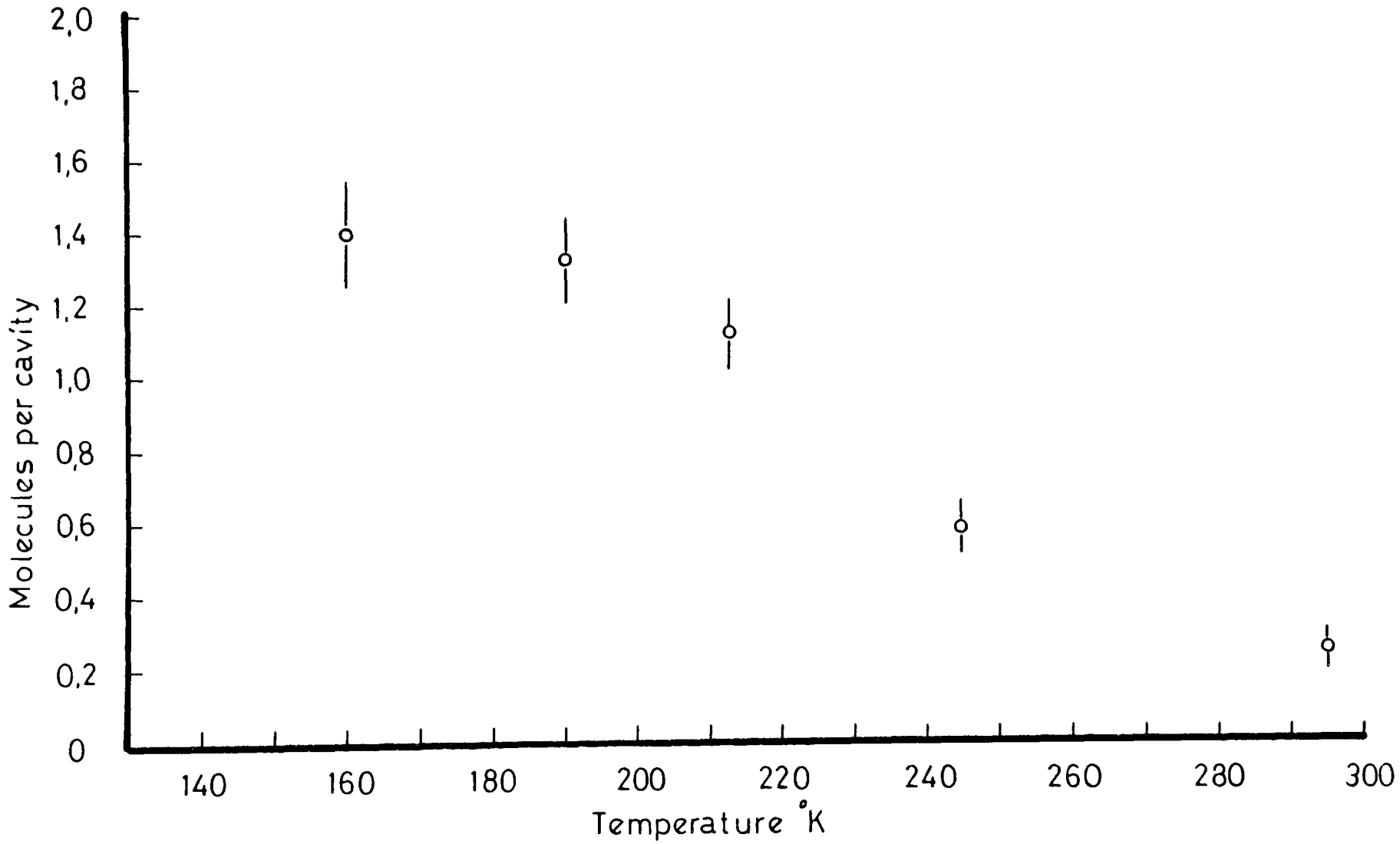

FIGURE 6,8

at saturation each cavity of a Y-type zeolite contains thirty three molecules of water. It is possible that not all the Helium gas was removed from the cooled sample before admitting methane, in which case the partial pressure of methane was less than intended.

Examples of the time of flight spectra obtained are shown in figures 6.9 to 6.11. The absorbent spectrum has been subtracted in each case

6.3.2 Vibrations and rotations of the absorbate within the cavity

The time of flight spectra for methane absorbed in an La-Y zeolite are significantly different to those for methane adsorbed on a graphon surface. The elastic peak is much narrower, more intense relative to the inelastic region, and shows no signs of increasing width with κ^2. A transition is visible in the low energy inelastic region superimposed on the broad rotational envelope seen for adsorbed methane on graphon. The apparent intensity of the transition decreases both with increasing temperature and increasing momentum transfer.

The intensity variation of the elastic peak is shown in figure 6.12. Subtraction of the absorbent spectrum can be checked by these plots and it is clear that there are still contributions to the absorbate elastic scattering at angles 18°, 50° and 58° from the absorbent coherent scattering. The difficulties of subtraction have been dealt with in general terms for the graphon experiments. In the case of the zeolite there are particular problems.

1) The structure factor of the zeolite may be significantly altered by the presence of the included methane. If this is the case then not only do the absolute intensities vary but so also do the relative intensities of the coherent scattering. The work of (23) has shown that the adsorption of nitrogen or argon on grafoil can lead to intensity changes in the (0002) reflection of the

FIGURE 6,9

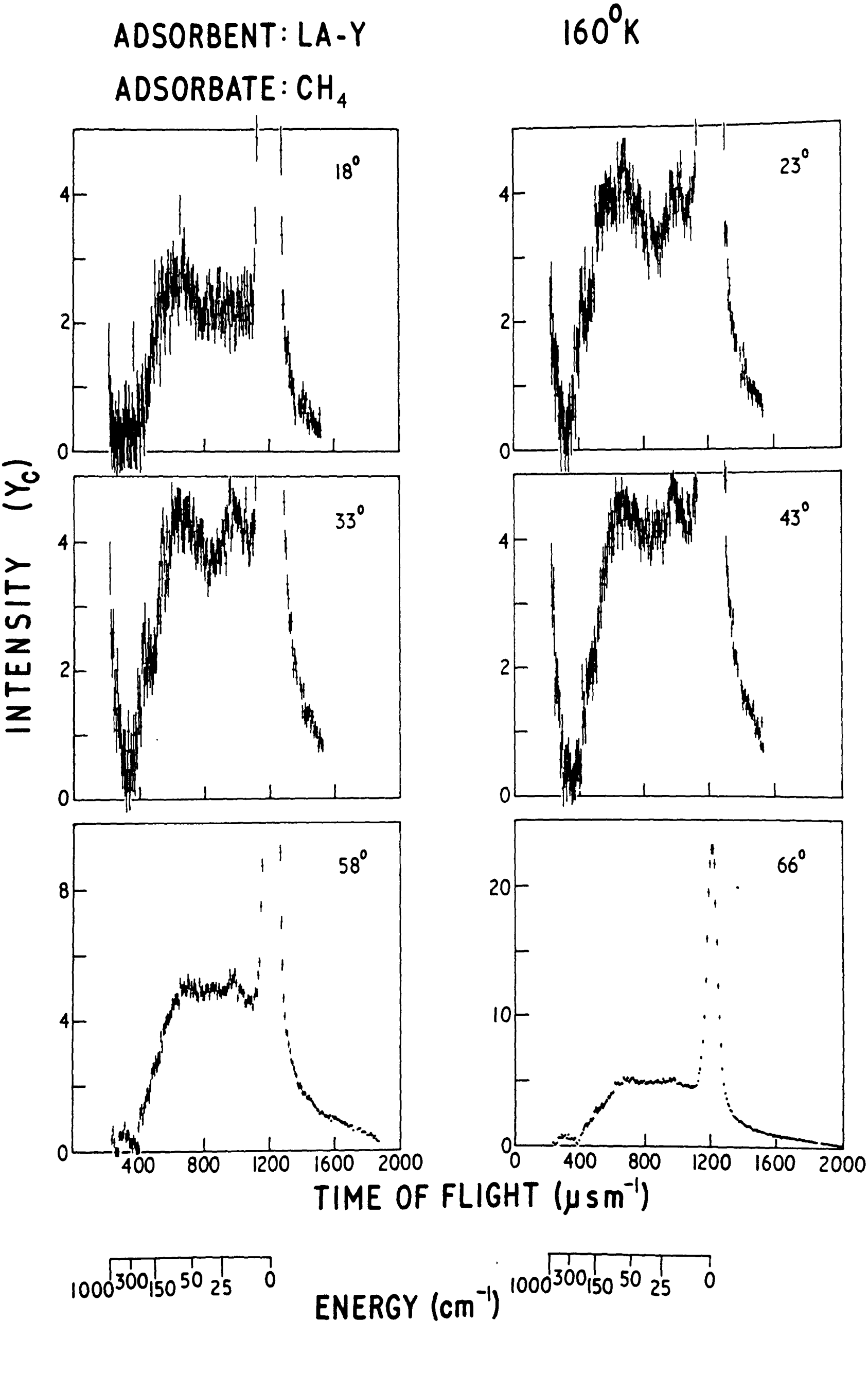
ADSORBENT: LA-Y
ADSORBATE: CH_4
160°K
18°
23°
33°
43°
58°
66°
INTENSITY (Yc)
TIME OF FLIGHT (μsm⁻¹)
ENERGY (cm⁻¹)
1000 300 150 50 25 0

FIGURE 6,10

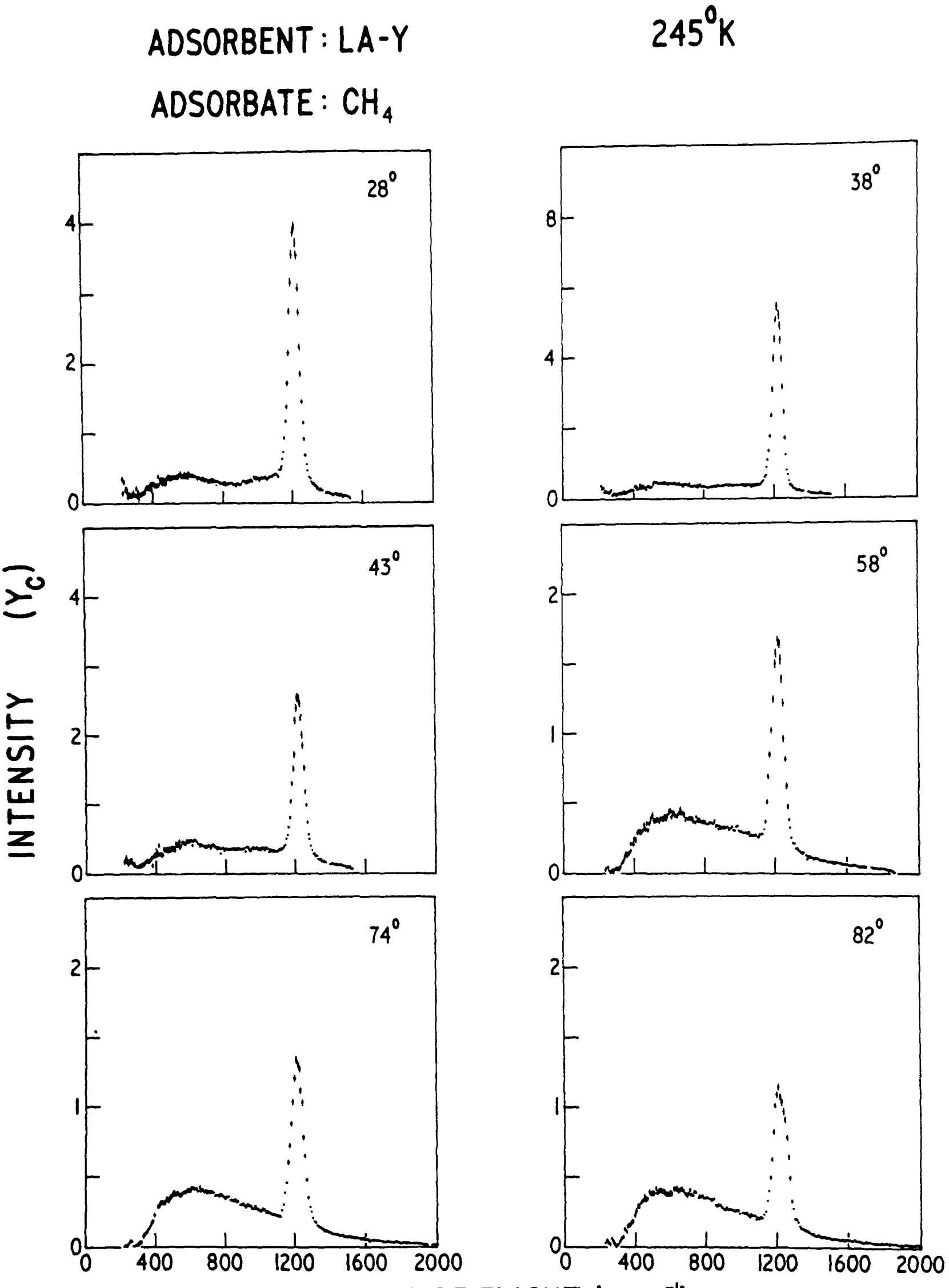
ADSORBENT : LA-Y
ADSORBATE : CH_4
245°K
28°
38°
43°
58°
74°
82°
INTENSITY (Yc)
TIME OF FLIGHT (μsm⁻¹)
ENERGY (cm⁻¹)
1000 300 150 50 25 0
0 400 800 1200 1600 2000

FIGURE 6,11

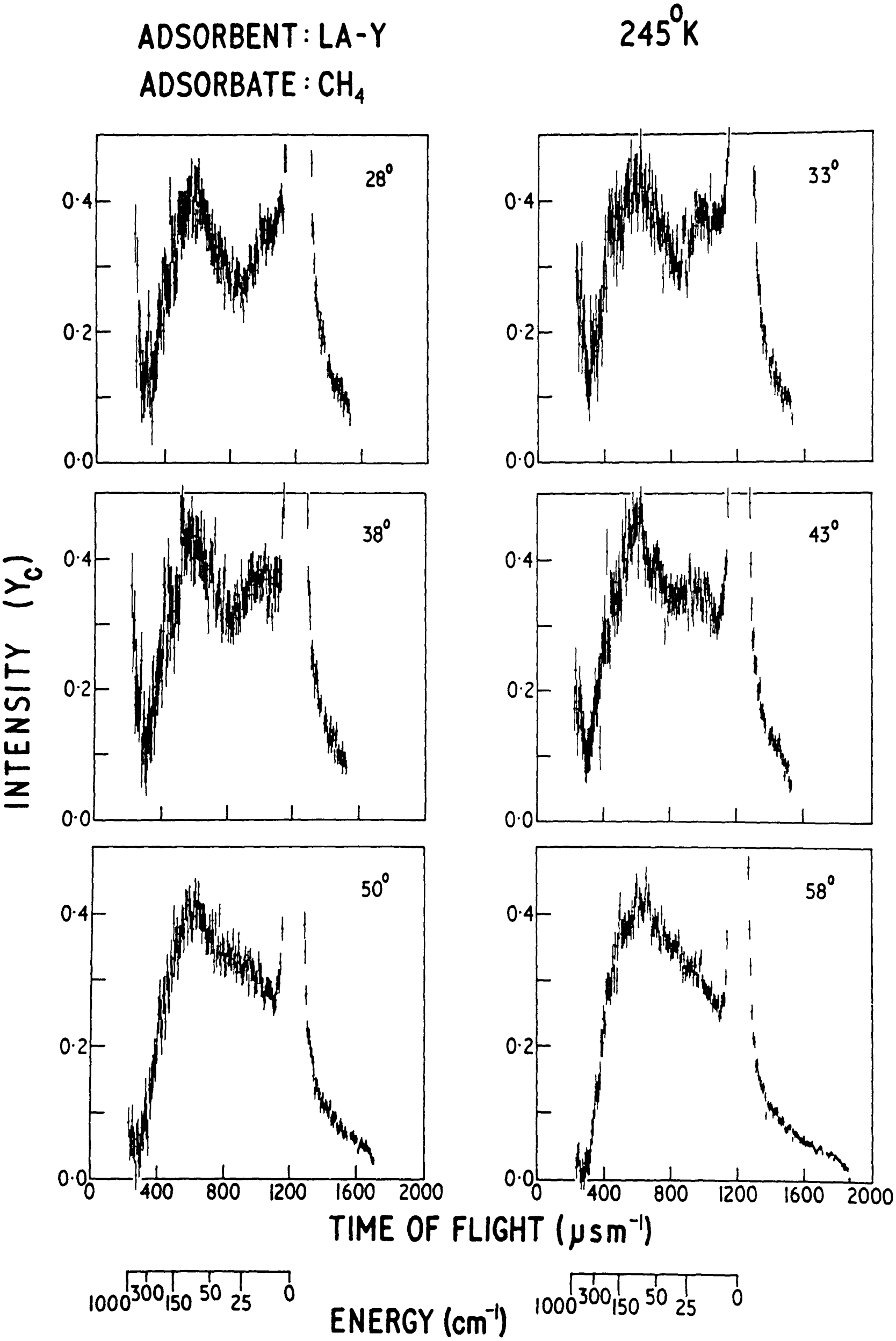
ADSORBENT : LA-Y
ADSORBATE : CH_4
245°K
28°
33°
38°
43°
50°
58°
0·0
0·2
0·4
INTENSITY (Y_c)
0
400
800
1200
1600
2000
TIME OF FLIGHT ($\mu s m^{-1}$)
1000
300
150
50
25
0
ENERGY (cm^{-1})

adsorbent and it is surmised that this is because the adlayer/surface distance is close to the basal plane spacing of the adsorbent. No diffraction experiments were carried out for adsorbed CH_4 on La-Y in this work so the question cannot be resolved.

2) There may be reaction between the methane and the surface leading to the formation of surface fragments, eg. -OH, $-O-CH_3$ etc. The effect would be expected to be greatest at the higher temperatures. Not only does this alter the scattering intensity from the support material but it also raises the question of multi-component absorbate spectra with the relative contributions to the final spectrum varying with temperature.

With these extra difficulties further complicating the subtraction problem it was decided to disregard the elastic peak data at angles of scatter where coherent effects occurred. The graphs of figure 6.12 are parameterised by their slopes and the results shown in table 6.2.

Table 6.2

Temperature Dependence of slope parameter $\bar{u}$ for absorbed methane

Temperature ^{o}K	160	190	213	245	La-Y
$\bar{u}$ Å	0.83	0.86	0.87	(0.72)	0.44
Number of molecules in cavity	1.40	1.32	1.12	0.58	-

The inelastic spectrum shows a weak peak at about 20 cm^{-1} in addition to the methane rotational envelope. See figure 6.9 and 6.11. The peak is most obvious at small κs and cannot be easily distinguished at angles of scatter greater than 50°. The disappearance of the transition is most likely that the increasing intensity of the rotational envelope, coupled with the increasing width of the

FIGURE 6,12

ABSORBED METHANE – Quasi-elastic intensity vs k^2

LOG(I)

Diffraction peak positions & relative intensities,

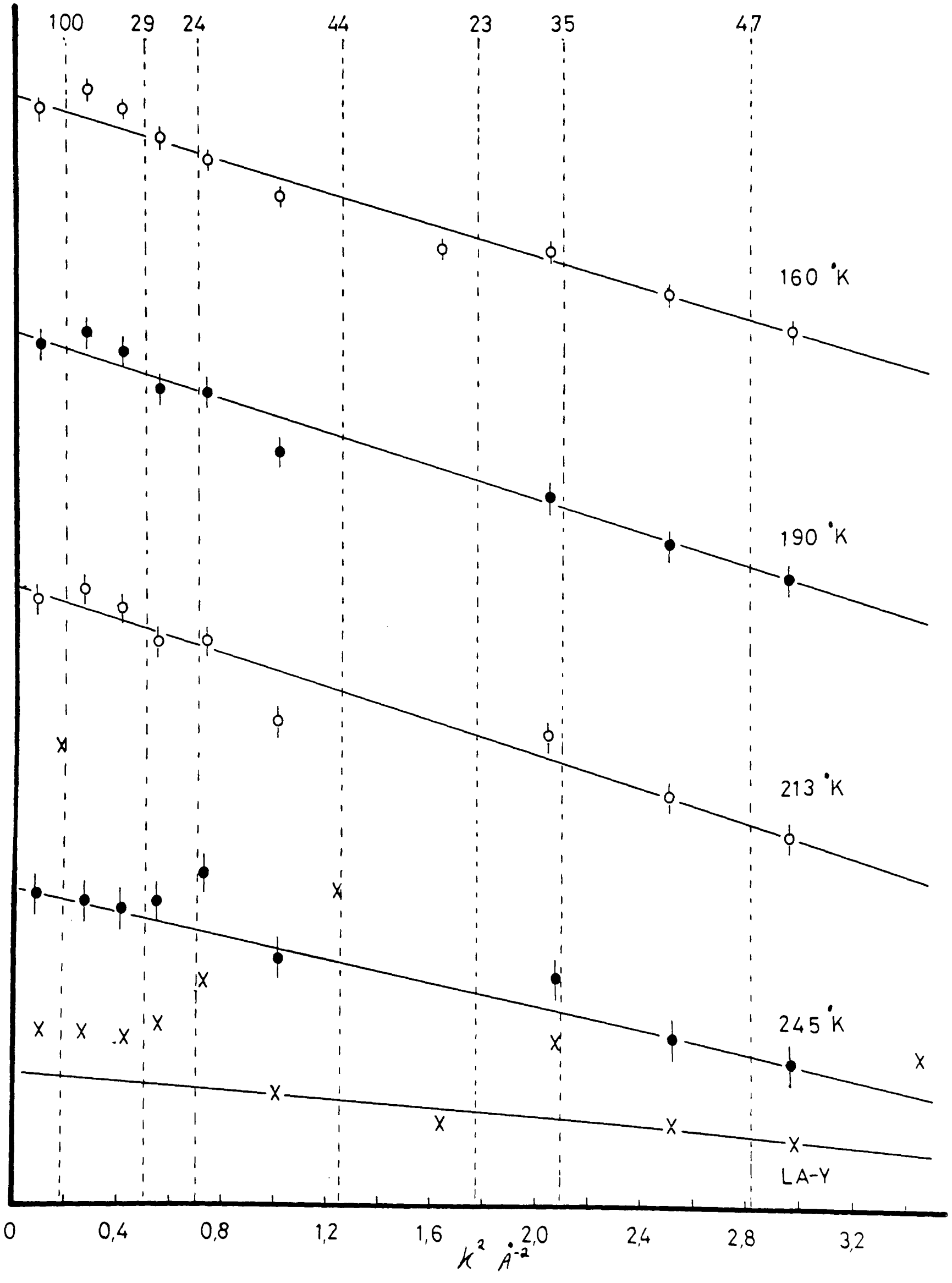

peak (both increasing with κ^2) make it difficult to pick out within the given error bars. Temperature does not have a marked effect, producing only a slight broadening of the peak. These observations are not readily quantifiable in view of the low intensity and consequently poor statistics.

The rotational envelope for physisorbed methane would not be expected to be greatly perturbed on moving from a graphon adsorbent to an La-Y absorbent, given similar conditions of temperature and momentum transfer. Figure 6.13 shows the inelastic spectrum resulting when the spectrum of methane adsorbed on graphon at $162^{o}K$ is subtracted from the spectrum of methane absorbed in La-Y at the $160^{o}K$. The propogation of errors produces very poor statistics but it is clear that there is a residual peak centred at 19 cm^{-1} and that the peak is wider than the machine resolution function. The sharp drop for times of flight greater than 1050 μsm^{-1} is a consequence of the long tail of the broadened QEP for adsorbed methane, which is not present for absorbed methane, extending into the inelastic region.

Apart from the scattering at low energy transfers the inelastic scattering is very closely approximated by the CHARLOTTE simulation. Figure 6.14 gives a comparison between the observed and predicted time of flight spectrum. In figure 6.15 is plotted the calculated and observed position of the inelastic maximum as a function of temperature. The shift to shorter times of flight with increasing temperature is due to the increased population of the higher rotational energy levels of the methane rotor. Also shown is the plot for the maximum of the inelastic scattering for an ideal gas of mass 16. The different position of the maximum in this instance is due to the recoil of the scattering nucleus which moves the psuedo elastic peak (i.e. the $J = 0 \rightarrow 0$ transition) into the inelastic region and so distorts the inelastic envelope.

FIGURE 6,13

ABSORBED METHANE – Difference spectrum

CH_4/La-Y — CH_4/C

T	160 °K	162 °K
θ	28°	27°
λ	4,8 Å	4,8 Å

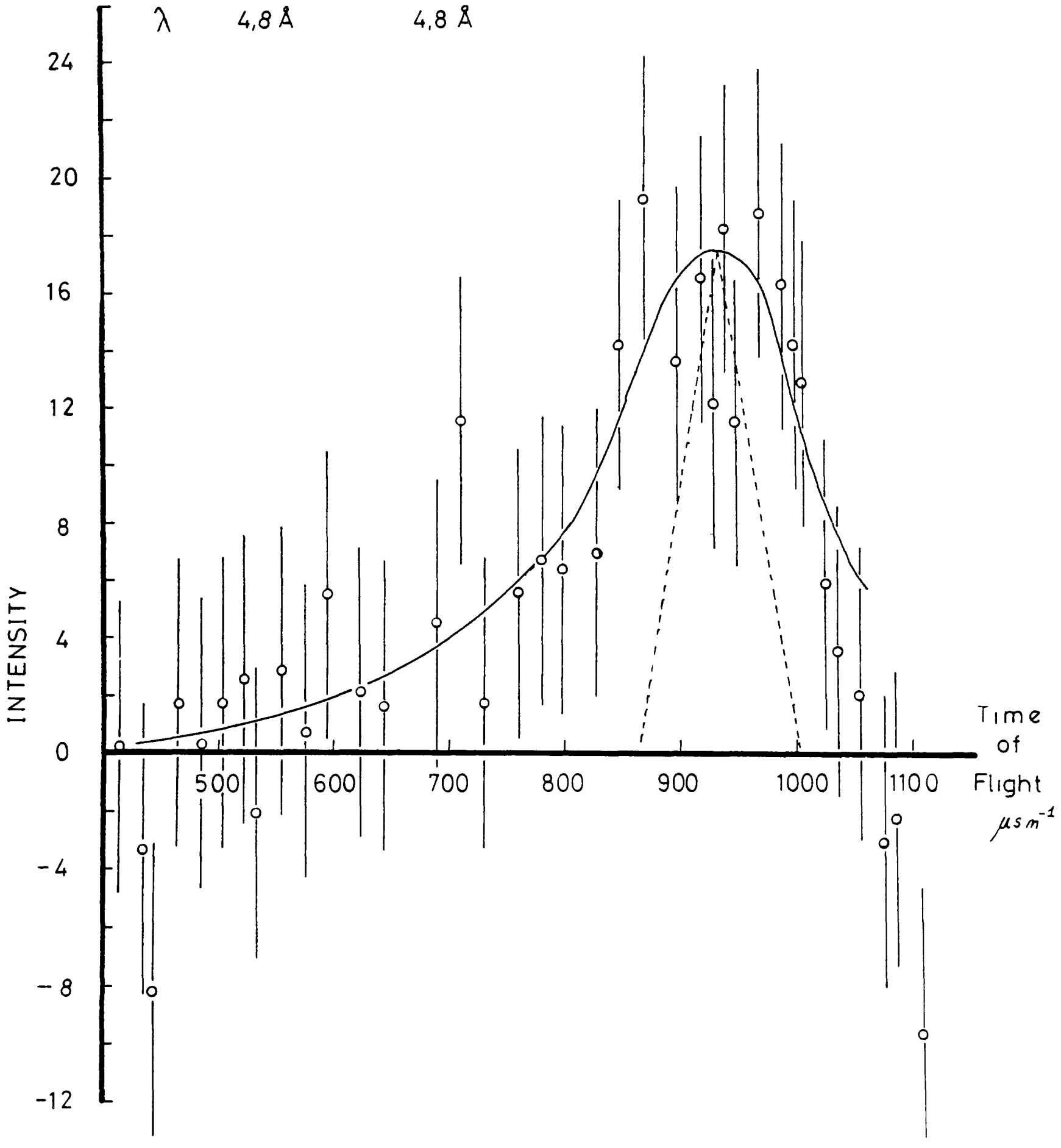

FIGURE 6,14

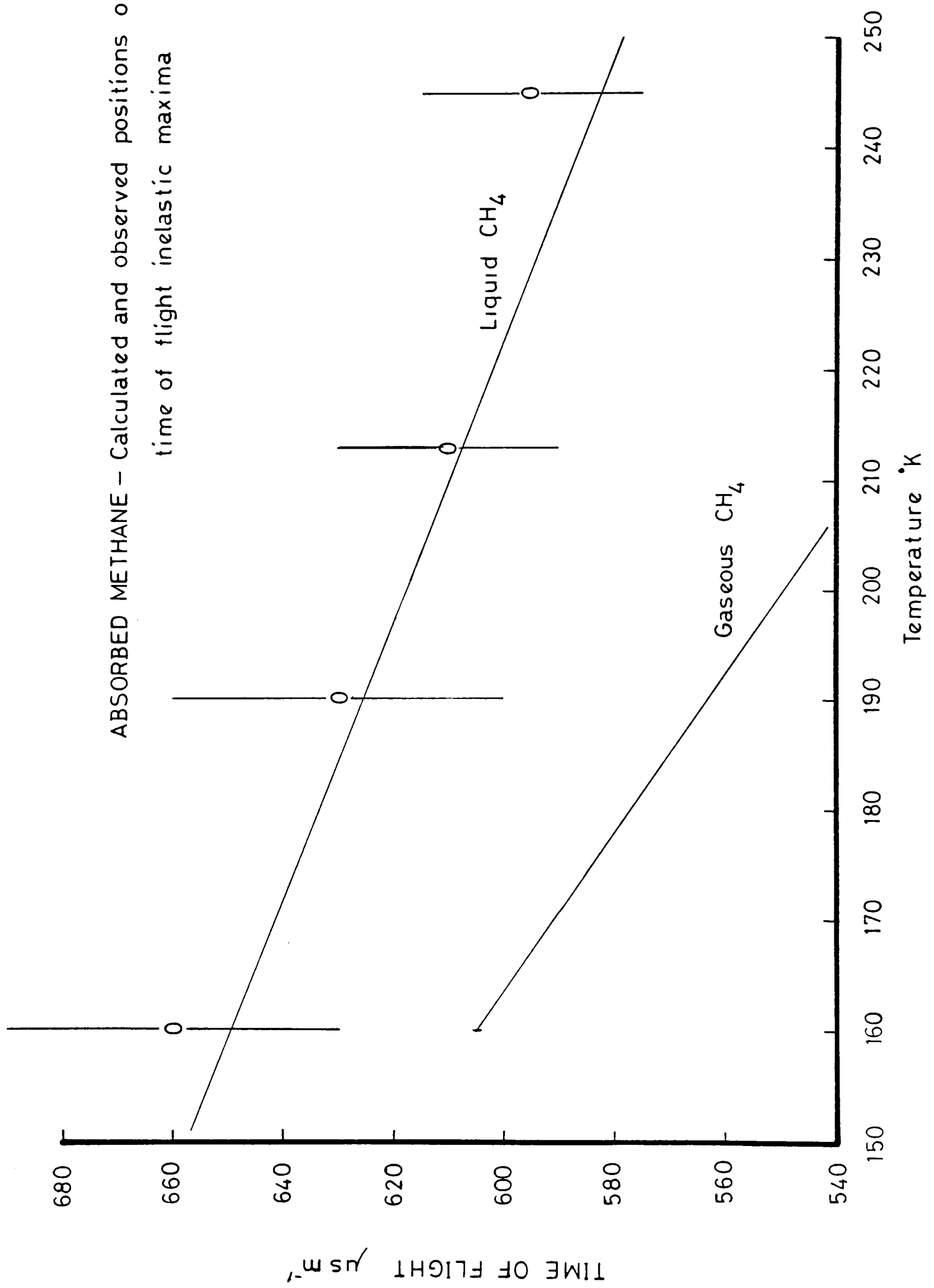
ABSORBED METHANE – Calculated and observed positions of the time of flight inelastic maxima
Liquid CH_4
Gaseous CH_4
TIME OF FLIGHT $\mu s\ m^{-1}$
Temperature °K
680
660
640
620
600
580
560
540
150
160
170
180
190
200
210
220
230
240
250

FIGURE 6.15

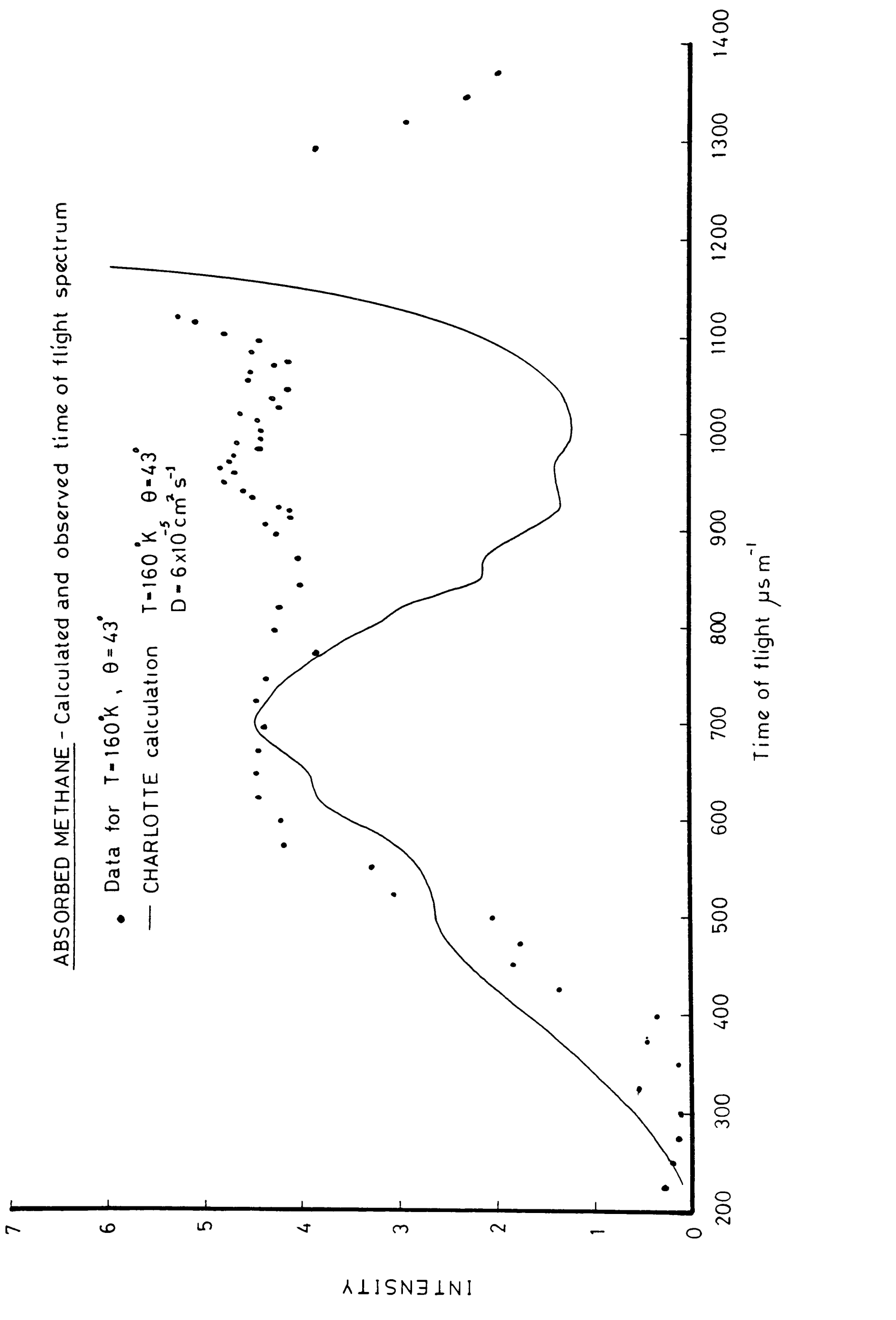
ABSORBED METHANE - Calculated and observed time of flight spectrum
• Data for T=160°K, θ=43°
— CHARLOTTE calculation T=160°K θ=43°
D=6x10⁻⁵cm²s⁻¹
INTENSITY
Time of flight μs m⁻¹
0
1
2
3
4
5
6
7
200
300
400
500
600
700
800
900
1000
1100
1200
1300
1400

The data for absorbed methane follows the predicted behaviour closely. Contrasting with adsorbed methane which shows a perturbation of the maximum inelastic intensity that increases with temperature

6.3.3 Translations of the Absorbed Molecule

The elastic peak shows only slight broadening irrespective of temperature or angle of scatter. At all times the width of the elastic peak is close to that of the machine resolution. Figure 6.16 shows the variations of the observed peak full width at half maximum as a function of κ^2, together with the FWHM for vanadium. There does appear to be a small broadening but the instrument resolution is inadequate for a detailed analysis. Figure 6.17 shows the result of fitting a gaussian to the observed data at conditions of temperature and momentum transfer where the broadening might be expected to be greatest. The disagreement in the wings of the function could be due to multiple scattering, poor choice of background level, or a real effect due to a contribution to the total scattering law from rotational diffusion. Further work on a higher resolution instrument will be necessary to answer this question.

6.3.4 Discussion

It is remarkable that the inelastic spectrum of methane absorbed in La-Y zeolite at $245^{o}K$ corresponds closely to the calculated rotational envelope for methane at that temperature. There is no sign of the distortions which might be expected if

1) The methane molecule was in the gas phase and could undergo recoil on scattering.

2) The methane molecule was in the liquid phase and performed rotational diffusion.

The sharp quasi elastic peak which is so prominent, even at these relatively high temperatures is also unexpected. (Boiling point of CH_4 = $105^{o}K$).

ABSORBED METHANE – Quasi elastic peak broadening vs χ^2

Convoluted FWHM x CH_4 La-Y 245°K

Δ CH_4 La-Y 160°K

• Vanadium

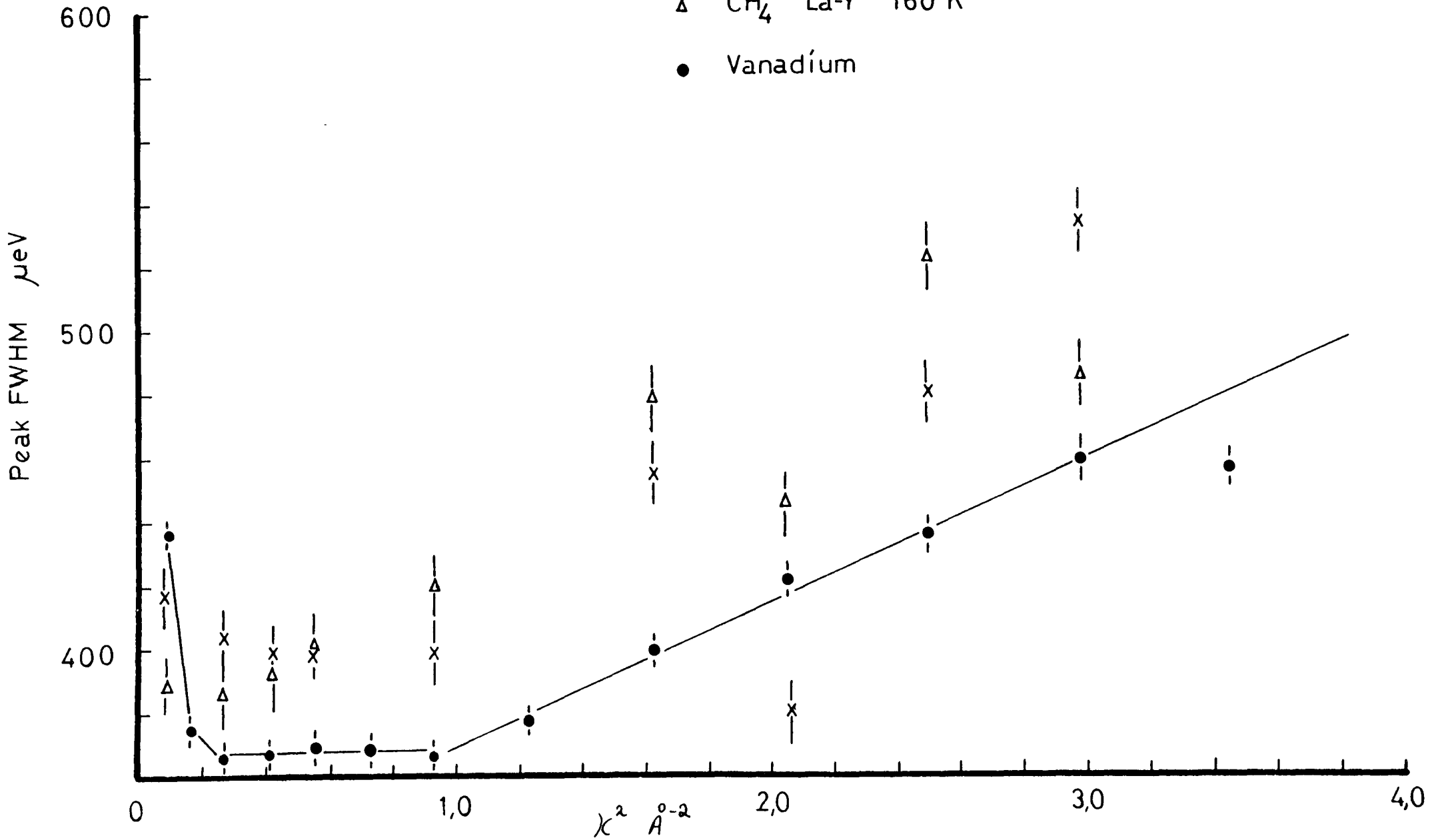

FIGURE 6,16

FIGURE 6,17

ABSORBED METHANE – Fit of gaussian to QEP data

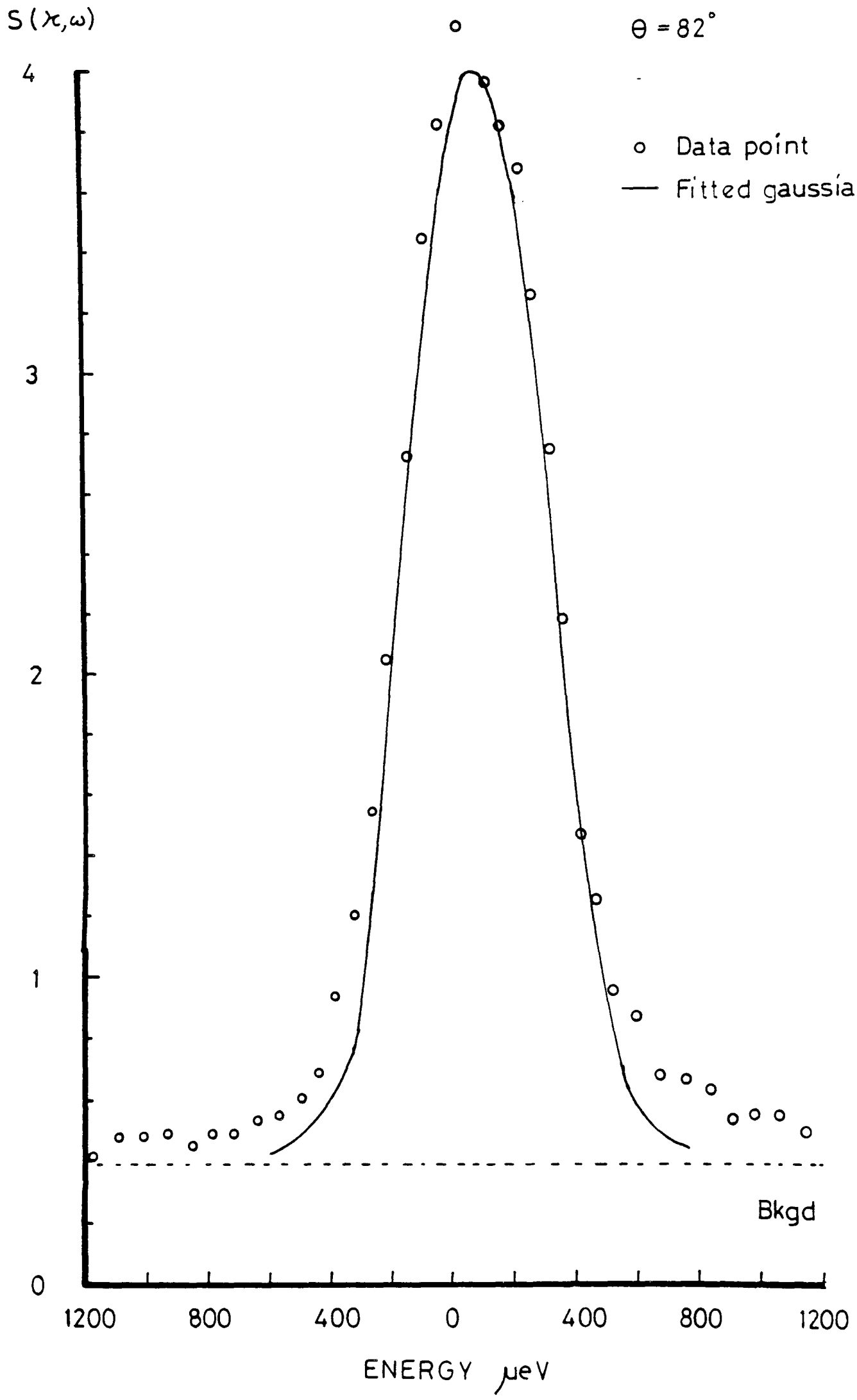

As discussed earlier in section 3.4 the total scattering law is derived from the convolution of the scattering laws for the individual degrees of freedom.

$$S_{TOTAL} = S_{TRANS} * S_{ROT} * S_{VIB}$$

The scattering laws for rotations and vibrations generally consist of a series of delta functions whilst the scattering law for translational motion may be gaussian, lorentzian or a combination of these functions. For a liquid with a finite translational diffusion coefficient, the height of the QEP diminsihes rapidly with increasing κ^2, (QEP area goes as $A = Ao \exp(-\kappa^2 u^2)$ but $\Delta E = 2\hbar D\kappa^2$), and with rising temperature, $D = Do \exp(-EA/RT)$. Similarily any details in S_{ROT} or S_{VIB} are submerged on convolution with S_{TRANS}, if S_{TRANS} is a broad function.

Not only is the QEP for methane absorbed in La-Y intense and unbroadened 140° above the boiling point of bulk methane but there is also a discrete inelastic transition. It would seem that the absorbed molecule has low translational freedom and S_{TRANS} is narrow in relation to the energy response of the spectrometer. It was suggested earlier that the observed spectrum may be composite, derived from the sum of the scattering laws from different types of scattering centre formed by reaction of the absorbed methane with the surface. The close correspondence between the observed and the calculated rotational envelope seems to rule out that possibility, so the narrow QEP is probably a true reflection of the scattering from a single type of absorbate molecule with low translational freedom.

The implication of these results is that the methane molecule is trapped in a zeolite cage where it can perform virtually free rotation but has no translational motion. The translational degrees of freedom will be replaced by vibrations of the methane molecule within the confines of the pore. In the case of the methane molecule

adsorbed on a carbon surface the parameter <u> is large, ≃ 1 Å, and was taken to indicate a large amplitude of vibration of the adsorbed molecule. For absorbed methane <u> is smaller, ≃ 0.7 Å, though still relatively large, and shows only a small temperature dependence. Such a change is what would be expected on going from a flat adsorption surface to the confines of an absorption cavity. Because of the high surface mobility there was no evidence for an admolecule/surface vibration when methane was adsorbed on graphon. For methane absorbed in La-Y it seems likely that the translational motion is slow, so the absorbate/surface vibration should be visible. The question arises whether the transition at 19 cm^{-1} can be so attributed.

There are several possible causes of the peak.

1) Instrumental anomaly. This is unlikely in view of the gradual change in the transition intensity with temperature and its non appearance in the spectrum of the blank La-Y zeolite.

2) Bad subtraction. For the transition to be an artefact of the subtraction procedure the scattering from the La-Y zeolite must show either a peak or a trough at about 20 cm^{-1}. This is not the case. The background to be subtracted is flat across the energy range of the transition and a poor subtraction will only alter the relative intensity and not the final shape of the spectrum.

3) Enhancement of a lattice vibration. The aluminosilicate framework atoms have small neutron scattering cross sections. If, however, an atom or molecule with a high cross section is strongly bound to the lattice then the lattice density of states will appear in the observed spectrum with enhanced intensity. There is no indication in the raman (144a), IR (144b), or neutron spectra of La-Y of a lattice mode at the required energy and the possibility of the 19 cm^{-1} transition arising this way must be discounted.

4) Phonon scattering. Extremely unlikely in view of the cross sections involved and the lack of any κ dependence for the observed peak.

5) Rotational transitions of the absorbed methane. The rotational transitions in solid methane have been measured by (87a). At the temperature of the measurement there is hinderance to rotation and the energy levels are shifted to lower values than expected.

$J = 0 \rightarrow 1$	$8.54\ cm^{-1}$	(10)
$J = 1 \rightarrow 2$	$14.52\ cm^{-1}$	(20)
$J = 0 \rightarrow 2$	$22.58\ cm^{-1}$	(30)

One might suppose that the observed transition at 19 cm^{-1} is therefore due to the $J = 0 \rightarrow 2$ transition. However there is no evidence for the other transitions, particularly the $J = 1 \rightarrow 3$ transition, which should be clearly visible at shorter times of flight the intensity increased by the $(2J + 1)^2$ weighting factor. For the $J = 0 \rightarrow 2$ transition, the intensity goes as $j_2{}^2(\kappa r)$, which with the known value of r and the given κ range should show a small but steady increase with κ. The observed transition shows a decrease in intensity with κ. The relative intensity of the observed transition to the inelastic maximum is too high for it to be a rotational transition of methane and it is concluded that the true rotational transitions are present underneath the transition at 19 cm^{-1}.

6) Vibrations of the absorbed CH_4 in the cavity. The frequency of vibration of an adsorbed methane molecule perpendicular to a carbon surface was calculated to be 80 cm^{-1}. The potential energy well for a methane molecule inside a zeolite pore is most difficult to calculate but it is clear that the vibrational frequency should be substantially lower than 80 cm^{-1}. Suppose the methane molecule was trapped between two infinite, parallel sheets of graphite. The total interaction potential would be the sum of the adsorption potentials

for the methane molecule on each surface (neglecting the penetration of the potential energy surface by the admolecule wave function). As a result the interaction potential starts off as a double well at large separation of the graphite sheets, and as these are brought closer together, the flatter becomes the minima of the wells,i.e. the lower the force constant, and the lower the vibrational frequency of the molecule in that well. For the absorbed molecule in an La-Y zeolite pore if the mean absorbate/surface separation is 3.3 $\mathring{A}$, then the methane molecule is moving in a spherical potential energy well of 6.4 $\mathring{A}$ diameter. The potential is not isotropic within the well being more positive at the centre. Such a potential well would be markedly anharmonic and one would expect to see a distribution of vibration frequencies. The observed transition at 19cm^{-1} is broader than the machine resolution, in agreement with this supposition. An increase in temperature of the system should lead to a further broadening of the transition as a result of the anharmonicity, and it has been noted that the observed transition is harder to distinguish at higher temperatures.

Measurements of the scattered neutron spectra from CH_4 included in xenon and argon matrices (145) show effects due to the localisation of the scattering molecule by the surrounding lattice, similar to those seen for absorbed methane in this work. There is no evidence for discrete rotational transitions, possibly because of rotational diffusion and the poor resolution of the instrument. Neither is there any indication of an absorbate/absorbent vibration as the containing lattice of inert gas atoms prevents such a motion.

It would seem that the observed transition has the right energy and the expected temperature and momentum transfer dependence for it to be assigned to a vibration of the methane molecule within the zeolite pore.

The picture that emerges is of a small number of methane molecules

in a zeolite cavity, transferring from that cavity only at a slow rate, unquantifiable on the neutron scattering time scale. Rotational motion of the molecule is virtually unhindered and the molecule vibrates against the pore wall with a frequency of 19 ± 1 cm^{-1}.

CHAPTER 7: INELASTIC NEUTRON SCATTERING FROM SIMPLE MOLECULES ABSORBED ON CATALYST SURFACES

7.1 Introduction

The underlying questions of any investigation of a sorbate/surface system are:-

1) What is the nature and strength of the sorbate/surface interaction? Is it strong enough to lead to an electronic re-arrangement in the sorbate molecule and the surface band structure? Is it a weak specific interaction such as a hydrogen bond with a surface hydroxyl group? Or possibly a weak, non specific interaction such as occurs in physisorption?

2) What can be learnt about the surface sorption site? Is there indeed a specific sorption site? If so, what is the geometry of the surface atoms at the site and how is the sorbate molecule aligned with respect to these atoms? Is there more than one kind of site and how do their structures relate to the bulk structure?

Answers to these kinds of questions are of fundamental importance when it comes to understanding the mechanism whereby a given reaction undergoes heterogeneous catalysis. Spectroscopic methods, recording the electronic, vibrational and rotational densities of states, have a particularly high information yield, if they can be applied to the chosen sorbate/surface system. (1a) Each spectroscopic method has its drawbacks and limited range of application.

i) In Photoelectron Spectroscopy, with UV or x-ray exciting radiation, the interaction of the scatterer and the radiation is so great that penetration of the sample is limited to 10-40 Å and the technique is highly surface specific (1). However the very strength of the interaction limits the method to systems where the sorbate atom is strongly bound to the surface. Generally only information on the electronic and vibrational densities of states is available, but

with careful use of the conservation of momentum requirement, manifested as an angular distribution of scattered photoelectrons, together with low incident energies, it is possible to get information on the alignment of the sorbate molecule with respect to the surface.

ii) With optical spectroscopy the interaction between the exciting radiation and the scatterer is less and the surface specificity disappears. Use of grazing incidence and multiple reflection spectroscopy overcomes the problem to some extent. The situation can be further improved by picking a probe molecule with an intense scattering cross section, e.g. carbon monoxide for infra red spectroscopy or dye molecules for ultra violet spectroscopy, which makes subtraction of the underlying substrate spectrum correspondingly easier (146). Optical spectroscopy can equally be hampered by the requirements of the selection rules.

Much more of a problem may arise from the scattering by the bulk material e.g. the fluoresence that can arise in laser raman scattering which swamps the sorbate spectrum (147).

With the complement of UV, IR and Raman spectroscopy it is possible to study the lower energy electronic transitions, vibrational and rotational transitions of a sorbed molecule. (Though not necessarily the same molecule over the complete range of energy). However the intermolecular motions of sorbed molecules occurring as they do at low energies viz 0-500 cm^{-1} are not amenable to study by optical spectroscopy, generally because of the intense absorption of the incident radiation by the bulk material.

iii) The particular attractions and demerits of using neutron spectroscopy for studying a sorbate/surface system have been dealt with in section 1.2.1. The most important features when it comes to studying molecules sorbed on catalyst surfaces can be summarised as follows:-

a) Particular sensitivity to the contribution that hydrogen nuclei motions make to the density of vibrational and rotational states. An overwhelming number of catalytic reactions involve the making or breaking of bonds to hydrogen atoms. Changes that should be quite evident in the scattered neutron spectrum

b) The lack of optical selection rules means that transitions which are extremely weak in optical spectroscopy can be observed quite clearly in neutron scattering. Examples that are pertinent to the study of sorbates on catalysts include modes associated with hydrogen bonds (either between sorbate molecules or between sorbate and surface), and modes arising from relative motion between the sorbate and surface.

c) Distortions and difficulties of subtraction with the sorbate spectrum do not arise if the catalyst chosen has a small neutron scattering cross section.

d) The neutron technique for inelastic scattering has its greatest sensitivity and highest resolution at low energy transfers, $<300\ cm^{-1}$. The method is particularly suited for studying intermolecular modes and providing information on the surface structure adopted by the sorbed molecules. The value of this feature is most evident when the sorbate/surface interaction is weak, < 20 kcals/mole, and there are no detectable changes in the sorbate molecule intramolecular modes. The weak surface bonding is nonetheless reflected in the structure of the sorbed phase which is in turn apparent in the intermolecular motions and hence detectable by the neutron experiment.

The main drawbacks to the use of neutron scattering spectroscopy for this application are the low sensitivity and poor resolution in comparison to optical spectroscopy.

A series of spectra from different sorbate/catalyst systems have been measured on the Beryllium Filter spectrometer at AERE

Harwell. They demonstrate how the neutron scattering technique can give information on systems where the sorbate/surface interaction varies from very weak to quite strong. The spectrometer is described in section 4.2.2 and the sample preparation in section 4.5.

7.2 The Sorption of Formic Acid on La-Y zeolite and on γ-Alumina

It is known that formic acid may undergo decomposition by two different routes depending on the choice of catalyst.

On metal oxide catalysts, such as alumina, the reaction products are water and carbon monoxide

$$HCOOH \rightleftharpoons H_2O + CO$$

The alumina/formic acid system has been studied by infra red spectroscopy. At low surface coverages it is not clear whether the formic acid is adsorbed undissociatively, as it is in the case of silica(148), or whether formate anions are produced. (149). It is certain that at higher surface coverages the formic acid is only physisorbed.

On metals such as Palladium, Platinum and Ruthenium a rapid decomposition takes place to give hydrogen and carbon dioxide. The reaction is less fast on, for example, iron, nickel, silver or gold.

$$HCOOH \rightleftharpoons H_2 + CO_2$$

There is evidence from infra red spectroscopy and kinetic studies that an intermediate formate ion is formed during the second process. (150). The structure has not been confirmed but (I) is more likely than (II) as the surface species is known to involve a hydrogen atom.

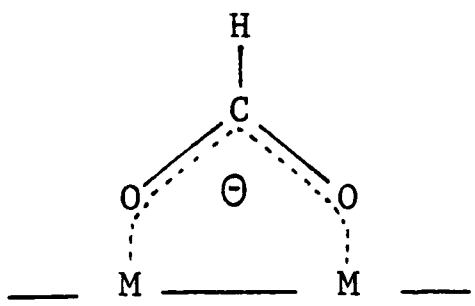

(I)

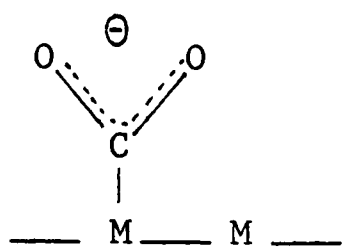

(II)

The different intermediates that must be formed during the two types of decomposition, decarboxylation or dehydration, are directly attributable to the very different surface chemistrys of the two classes of catalysts. An attempt was made using inelastic neutron scattering to indentify the intermediates that are formed in the reactions.

Formic acid was absorbed from the vapour phase on to

i) Outgassed γ-alumina with a quoted surface area of 300 m^2g^{-1}, to give a surface coverage of about $\Theta = 2$

ii) Outgassed La-Y zeolite with a surface area of about 500 m^2g^{-1}, to give a surface coverage of about $\Theta = 3$, i.e. about 30 molecules of HCOOH per cavity.

The absorption took place at 308-313°K and when the required surface coverage had been attained the sample tube was flooded with helium gas and the sample cooled to 80°K for the measurement of the neutron spectrum.

The spectra obtained are shown in figure 7.1 together with the spectrum of formic acid obtained by (151) on the same instrument. The inelastic spectra of both La-Y and γ-alumina are flat over this energy range and of very low intensity. Their contribution has been subtracted from the sorbate spectra shown in figure 7.1.

Discussion

Table 7.1 summarises the information available on the mode frequencies of formic acid together with the results for formic acid adsorbed on La-Y and γ-Al_2o_3. The intense peak at 517 cm^{-1} observed in the neutron spectrum by (151) has not been assigned. It is suggested that it may arise from a γ(COO) mode, the variation in bond angle causing a large amplitude of motion for the hydrogen atom in the hydrogen bond and so giving the mode a high intensity in the scattered neutron spectrum. Recent work by (159) casts doubt on this interpretation and indicates that the mode might arise from water

ABSORBED FORMIC ACID 80°K

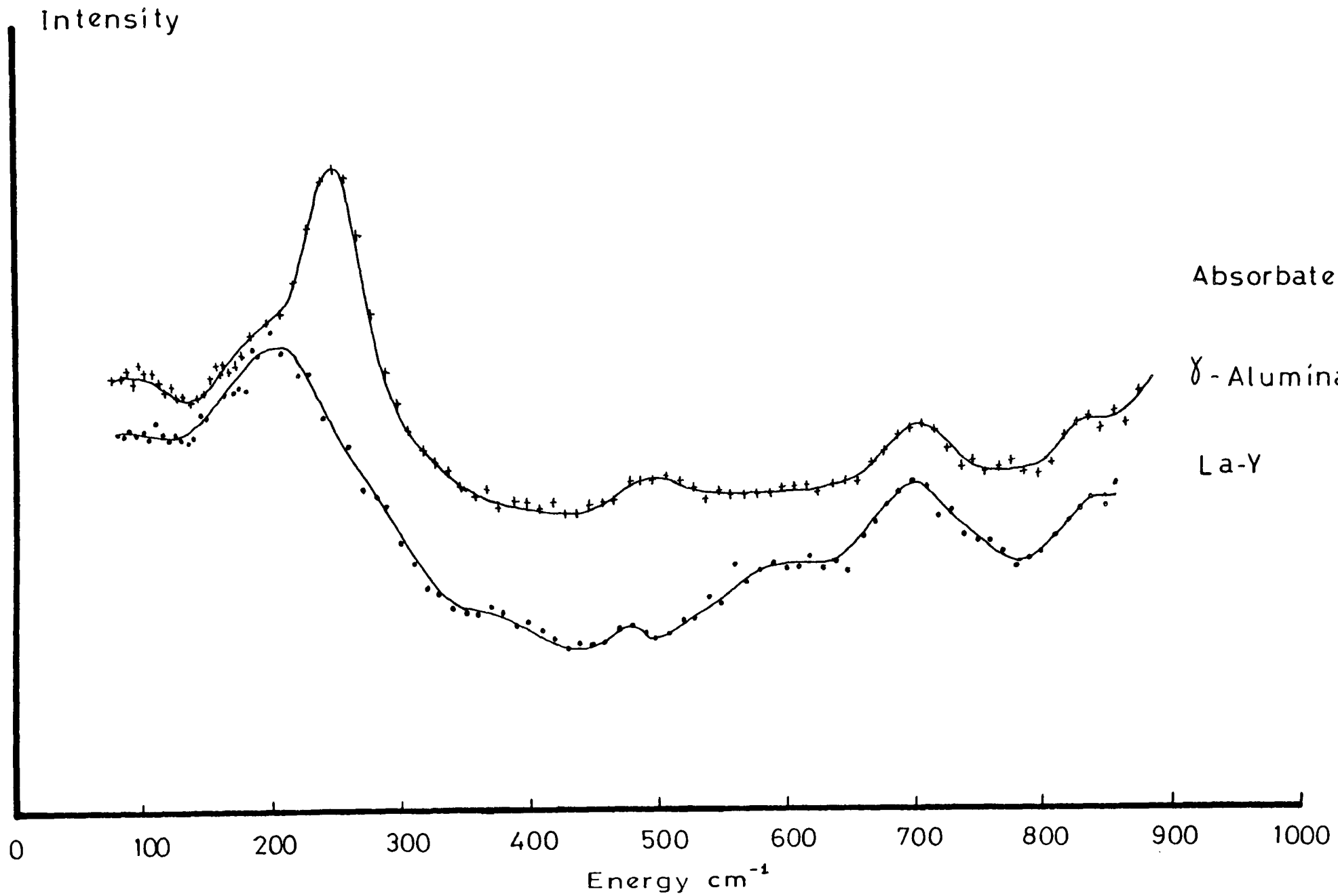

FIGURE 7,1

contaminating the formic acid. The situation is not yet resolved.

The crystalline phase of formic acid consists of a hydrogen bonded polymeric chain, whereas in the liquid phase various polymers exist, with the dimer predominating. The possibility of sorbed formic acid being present in a monomeric, gas like state can be ruled out immediately. The γ(OCO) mode appears in the spectra of formic acid on both surfaces, very similar in intensity and width with an energy of 710 cm^{-1}. For the monomer the transition is at 625 cm^{-1}, in the dimer 676-697 cm^{-1}, and (151) with a crystalline sample observed a frequency of 717 cm^{-1}.

The energy range which is particularly interesting is that below 400 cm^{-1}, where occur the frequencies associated with the vibrations and torsions of the hydrogen bonds. These are summarised in Table 7.1. In the glassy phase the hydrogen bond stretching vibration γ(OH..O) occurs at 249 cm^{-1}, the out of plane bend γ(OH...O) at 193 cm^{-1} and the twisting of the chains at 111 cm^{-1}. The beryllium filter spectrum of HCOOH on La-Y shows a broad peak centred at 190 ± 5 cm^{-1} with a width of about 100 cm^{-1}.

It appears that the spectrum of HCOOH sorbed on γ-Al_2O_3 is practically identical with that of the bulk polycrystalline formic acid glass. If the peak at 250 cm^{-1} had arisen from surface contamination, such as water or hydroxyl groups remaining after poor outgassing, then there should have been contributions from these extra species to the spectrum at higher energies. Similarily if the transition arose from a formic acid fragment formed by reaction at the surface. None are visible in the energy range covered.

The absence of the peak at 250 cm^{-1} from the spectrum of HCOOH sorbed on La-Y suggests that the hydrogen bonding is substantially altered in this sytem. The presence of a weak, broad peak at 600 cm^{-1} and a weak peak at 475 cm^{-1} (of 510 cm^{-1} for HCOOH on γ-Al_2O_3)

Table 7.1

Mode Frequencies of Formic Acid (157)

Formic Acid Monomer

Mode Number ν	Coordinate	Observed Energy cm^{-1}	
		Raman	IR
1	q (OH)	3566	3570
2	q (CH)	2945	2943
3	Q (C = O)		1770
4	β (OCH)	1345	1387
5	β (COH) Q(C-O)		1229
6	Q (C-O) β(COH)		1105
7	P_{CH}		1033
8	γ (OCO)		625
9	P_{OH}		638

Formic Acid Dimer

1	q (OH)	3162	
17	q (OH)		3110
18	q (CH)		2957
2	q (CH)	2957	
19	Q (C = O)		1754
3	Q (C = O)	1672	
20	β (OCH)		1450
4	β (OCH)	1395	
21	β (COH)		1365
5	β (COH)	1350	
22	Q (CO)		1218
6	Q (CO)	1204	
14	P_{CH}	1057	
10	P_{CH}		~ 1050
15	P_{OH}	919	
11	P_{OH}		917
23	γ (OCO)		697
7	γ (OCO)	676	
24	q (O...H)		248
8	q (O...H)	232	
12	p O...H		161
9	∝ (OH...O)	(116)	
16			
13	Ring bending		68

Table 7.1

Hydrogen bond frequencies of formic acid

Cyclic dimer (158)

Mode	Energy cm^{-1} (IR)		
	Calculated	Gas	Solution
γ (OH...O) out of plane bend	260		
ν (OH...O) stretch	249	248	248
ν (OH...O) stretch sym	224		
γ (OH...O) in plane bend	167	169	173
β (OH...O) in plane	91		
γ (twist)	68	68	

Linear Polymer	Glass	α-Crystal	β-Crystal
γ (OH...O) out of plane bend	-	280	271
ν (OH...O) stretch asym	249	239	232
ν (OH...O) stretch sym	-	-	-
γ (OH...O) in plane bend	193	200	-
β (OH...O) in plane	-	-	-
γ (twist)	111	92	88

Table 7.1 continued

Observed energies for formic acid

Adsorbent	Energy cm^{-1}
La-Y	190 ± 5 strong, broad
	475 ± 10 weak
	590 ± 10 broad
	700 ± 10 strong
γ-Al_2O_3	190 ± 5 shoulder
	250 ± 6 strong
	500 ± 8 medium
	710 ± 10 strong
	850 ± 10 weak

further distinguishes the two spectra. The alteration in the hydrogen bonding characteristics could possibly be due to

1) The stereo chemical constraints of sorption in an La-Y zeolite cavity compared to sorption on the surface of γ-Al_2O_3.

2) A specific interaction with the La^{3+} cation, possibly a formate anion.

3) The formation of hydrogen bonds to the zeolite surface rather than to other HCOOH molecules.

A firm conclusion cannot be reached without further experiments, for example

i) Sorption of HCOOD or DCOOH to look for isotope effects in the spectrum or isotope exchange reactions at the surface.

ii) Sorption of metal exchanged zeolites e.g. Na, Ag or Ni to test for a specific metal- HCOOH interaction.

7.3 The Sorption of CH_2CL_2 and CH_3CN on La-Y zeolite

Methyl cyanide and dichloromethane were chosen as probe molecules for investigating the structure of sorbed phases. The characteristics of these molecules which make them suitable for such a study can be summarised as follows:-

1) The hydrogen atoms in the probe molecules weight the scattered neutron intensity in favour of the sorbate molecule. Moreover as the hydrogen atoms in each molecule are in equivalent positions the neutron spectra are considerably simplified.

2) The bulk phases of the probe molecules have a small number of sharp, well defined intermolecular modes, giving a clear "fingerprint" of the bulk structure, and which will show up any changes on sorption quite clearly.

3) The intramolecular modes in the energy range scanned are few and well separated from the intermolecular modes. If there are reactions between the sorbate molecule and the surface then changes

in the intramolecular modes will show it. With this check it will be possible to say with certainty whether any changes in the intermolecular modes result from structural changes or if the change in the low energy modes is a consequence of the formation of new molecular species by reaction at the sorbent surface.

4) Neither of the probe molecules would be expected to react with or to form strong hydrogen bonds with the surface. They are molecules of fairly similar size though with quite different polarities, the dipole moment of methyl cyanide is 4D, that of dichloromethane 1.6D. For a given surface the choice of these molecules might be expected to show the balance between the relative strengths of sorbate-surface and sorbate-sorbate interactions.

La-Y zeolite was chosen as the sorbent since sorption on, or in a molecular sieve would be expected to have a marked effect on the molecular alignment in the sorbate phase.

Methyl cyanide was absorbed from the vapour phase at 308-313°C onto a sample of outgassed La-Y zeolite with a surface area of about 500 m^2g^{-1}, to give a surface concentration of Ⓗ ≃ 1.2, that is about 15 molecules per cavity.

Dichloromethane was similarily absorbed from the vapour phase to give a surface concentration of Ⓗ ≃ 1.3, that is about 19 molecules in each zeolite cavity.

The spectra of the absorbed molecules are shown in figures 7.2 and 7.3 together with the beryllium filter spectra of the bulk probe molecules at the same temperature. The spectrum of the absorbent has been subtracted in each case.

Discussion

7.3.1 Absorbed methyl cyanide

Table 7.2 summarises the available data on the mode frequencies of methyl cyanide in the gas, liquid and two possible solid phases.

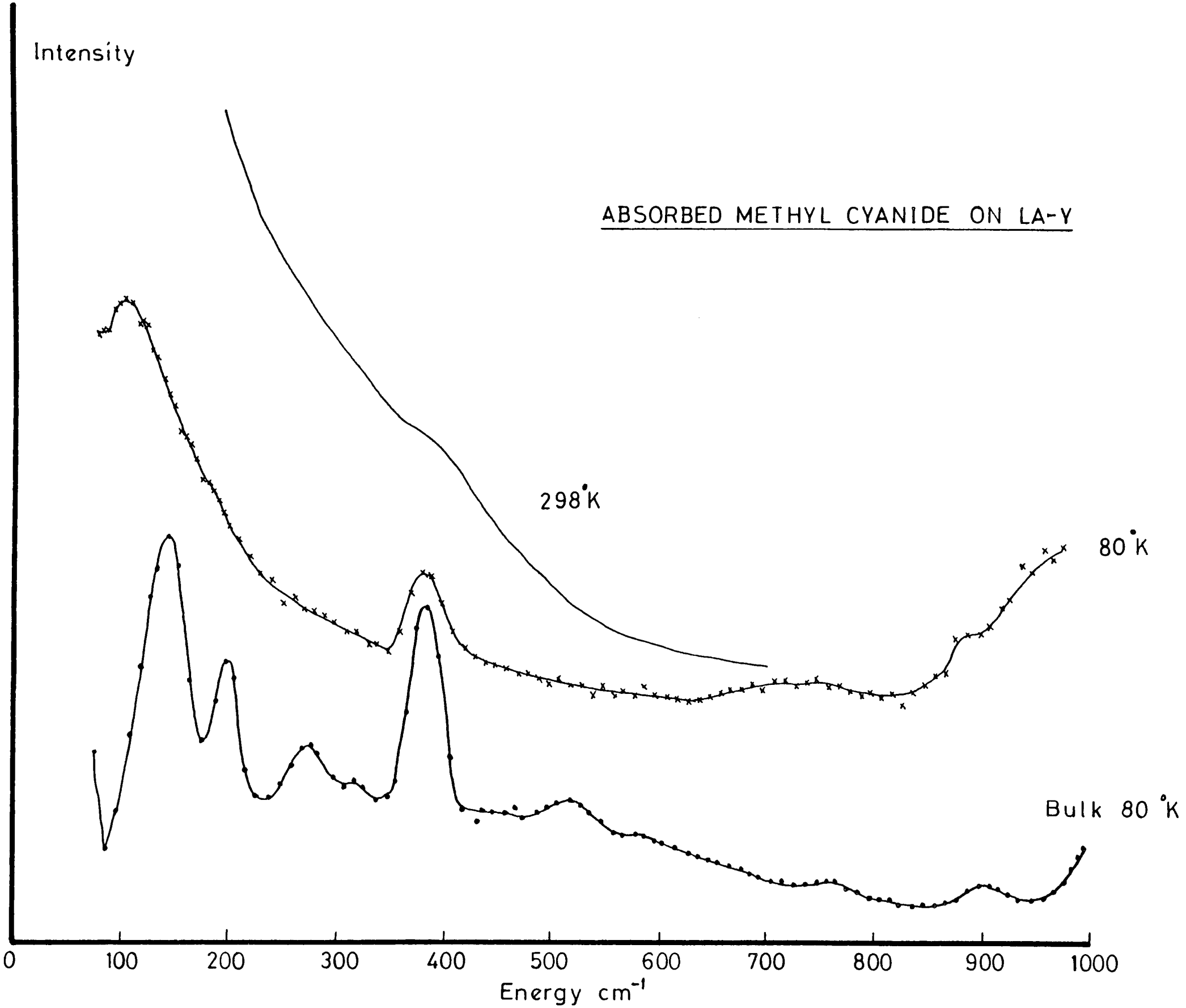
Intensity
ABSORBED METHYL CYANIDE ON LA-Y
298°K
80°K
Bulk 80 °K
0
100
200
300
400
500
600
700
800
900
1000
Energy cm⁻¹

FIGURE 7,2

FIGURE 7, 3

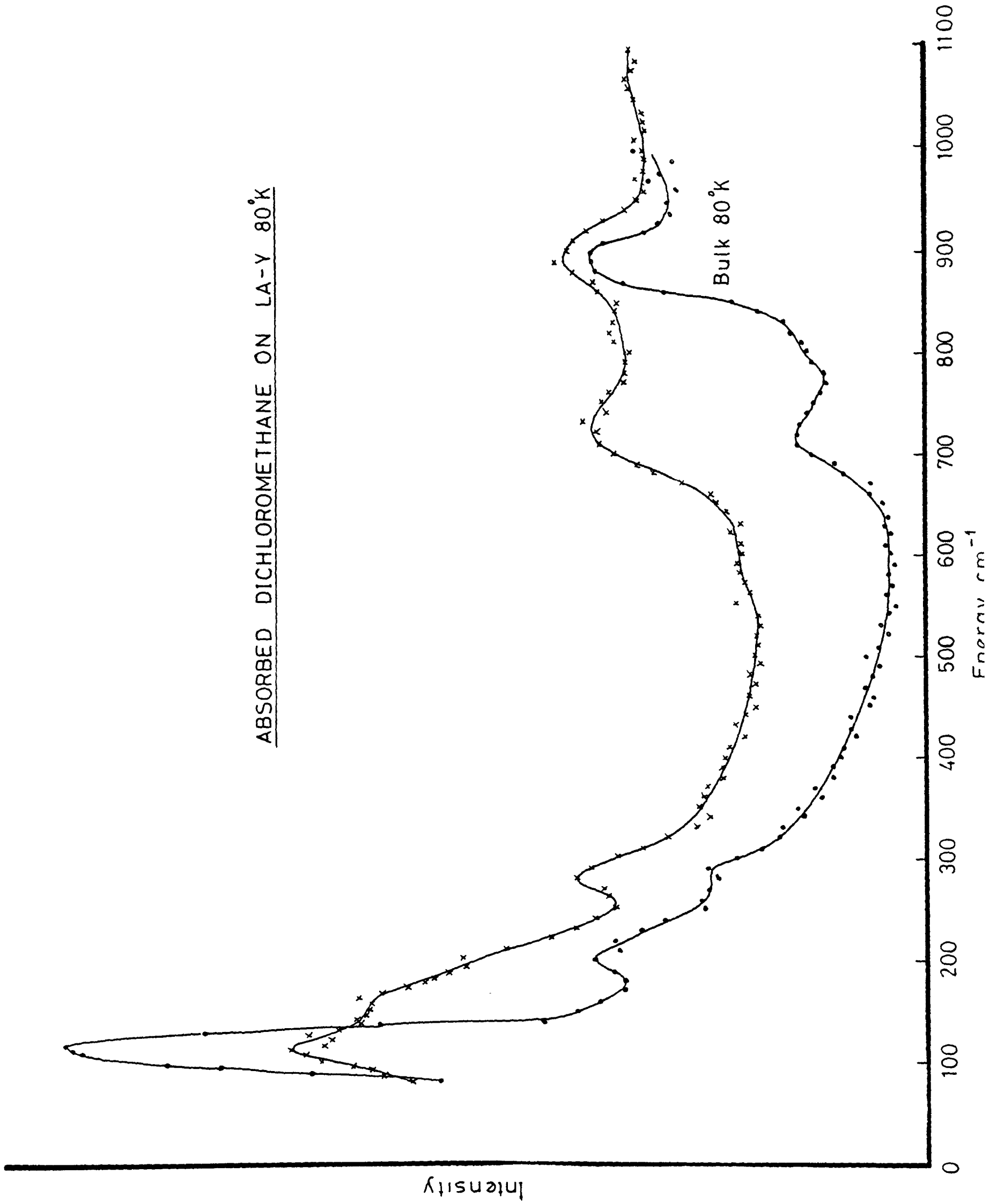
ABSORBED DICHLOROMETHANE ON LA-Y 80°K
Bulk 80°K
Intensity
Energy cm⁻¹
0
100
200
300
400
500
600
700
800
900
1000
1100

Two intramolecular modes appear in the energy range scanned, the γ(C-C≡N) asymmetric bend at 390 cm^{-1}, and the Q'(C-C) symmetric stretch at 918 cm^{-1}. At low temperatures in the α phase these transitions are further split due to the site symmetry. (152). The space group is inferred to be either D_{2h}^{1} (Pmmm) or D_{2h}^{9} (P_{bam}) with eight molecules in the unit cell. There does not appear to have been any study done of the intermolecular modes at lower energies.

The beryllium filter spectrum of methyl cyanide at 80°K shows the expected intramolecular modes at 385 ± 10 cm^{-1} and 905 ± 15 cm^{-1}. The hydrogen amplitude weighting of the scattered neutron intensity is clearly demonstrated. The γ(C-C≡N) mode 'wags' the methyl group producing a large displacement of the hydrogen atoms and giving the transition a high intensity. The Q'(C-C) mode, however, only produces a slight displacement of the hydrogens and as a result its intensity is much weaker. An intense transition is seen at 137 ± 5 cm^{-1} and progressively smaller peaks occur at 187 ± 8, 265 ± 8, 515 ± 10 and 750 ± 15 cm^{-1}. It seems likely that these are the harmonics of two series

Observed		Expected	
ν_0 = 137 ± 5			
ν_1 = 265 ± 8		$2\nu_0$ = 274 ± 10	
ν_2 = ?		$3\nu_0$ = 411 ± 15	
ν_3 = 515 ± 10		$4\nu_0$ = 548 ± 20	
ν_4 = ?		$5\nu_0$ = 685 ± 25	
ν_0^1 = 187 ± 8			
ν_1^1 = ?		$2\nu_0^1$ = 374 ± 16	
ν_2^1 = 590 ± 10 (?)		$3\nu_0^1$ = 561 ± 24	
ν_3^1 = 760 ± 15		$4\nu_0^1$ = 748 ± 32	

Table 7.2

Mode Frequencies of Methyl Cyanide

Gaseous (157)

Mode number ν	Coordinate	Observed energy cm^{-1}	
		Raman	IR
5	q (CH)	3001	3009.6
1	q (CH)	2941	2954
2	Q (C≡N), Q'(C-C)	2248	2267
6	α (HCH) β (CCH)	1443	1412.6
3	Q'(CC) α (HCH) β (CCH)	1371	1388
7	β (CCH) γ (CCN)		1059
4	Q'(CC)	919	918
8	γ (CCN)	378	

Solid (152)

Coordinate	Solid $77^{o}K$	α Crystal		
		$81^{o}K$	$158^{o}K$	$208^{o}K$
γ-(CCN) Asym. Bend	388 397	391.7 396.5 400.5	390.1 296.9	388 393.4
Q' (C-C) Sym. stretch	917.8	915.4 919.0 920.5	919.1	918.9

Inelastic Neutron scattering results

Solid CH_3CN $80^{o}K$ Energy cm^{-1}		Adsorbed on La-Y $80^{o}K$ Energy cm^{-1}	
137 ± 5	Very strong	85 ± 5	strong broad
187 ± 8	strong		
265 ± 8	weak		
385 ± 5	strong	380 ± 5	medium
515 ± 10	weak		
590 ± 10	weak		
760 ± 15	weak	730 ± 15	weak broad
905 ± 15	medium	880 ± 10	weak

The origin of the transitions at 137 ± 5 and 187 ± 8 cm^{-1} is not clear. They are both of high intensity and this suggests that they could be the results of torsions of the methyl group. In solid methyl cyanide there are two possible alignments of the molecules. Either methyl group end on to nitrile group (M-N) or methyl group end on to methyl group (M-M).

viz

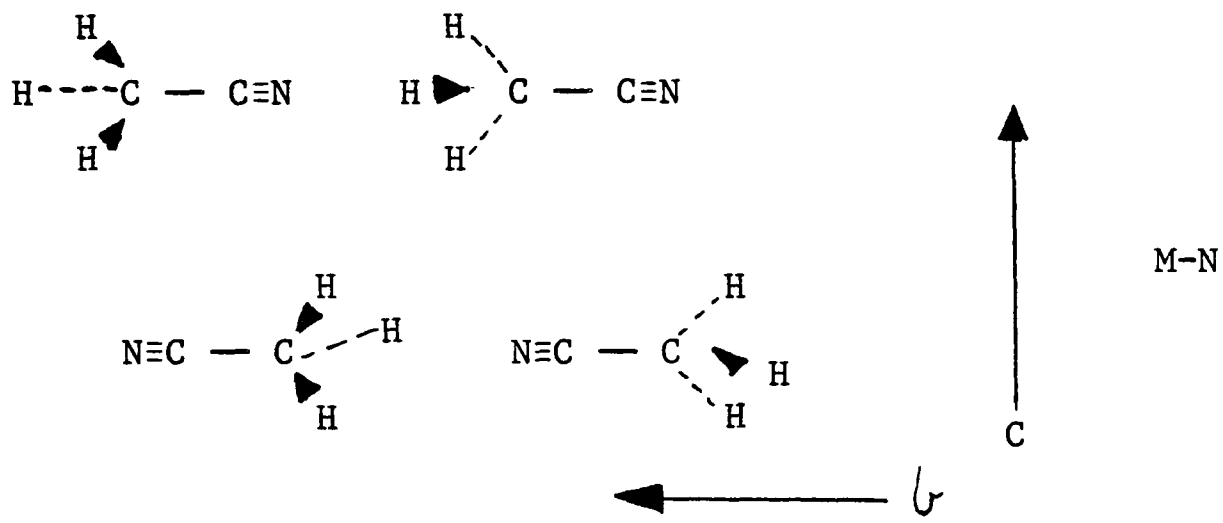

or

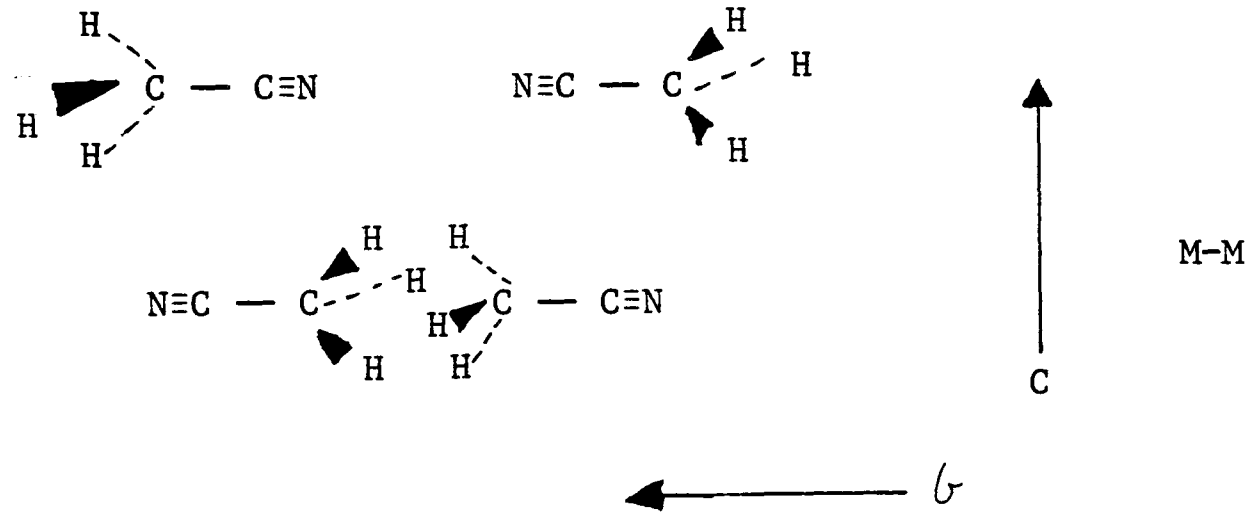

One would expect the steric hinderance to rotation of the methyl groups in the MM structure to be higher than in th e MN structure, and as a consequence the methyl group torsion frequency to be greater. It is possible that the polycrystalline sample of CH_3CN from which the spectrum was obtained, was a mixture of phases showing both possible structures. In which case the series with ν_o = 137 ± 5 cm^{-1} would correspond to the methyl group torsion in the M-N structure,whilst the series with $\nu_o{}^1$ = 187 cm^{-1} would be due to the methyl group torsion in the MM structure.

When methyl cyanide is sorbed on La-Y zeolite the scattered neutron spectrum undergoes an abrupt change. At 80°K the intramolecular modes are still present at 380 cm^{-1} and 880 cm^{-1}, the latter peak position distorted by a steeply rising background. The transition due to the $\gamma(C-C\equiv N)$ bend is less prominent than in the bulk solid and has a full width at half maximum of 45 cm^{-1} compared to 35 cm^{-1}.

If the temperature of the sample is increased to 298°K, then the only visible feature is a point of inflection occurring at 340-360 cm^{-1} in a steeply falling curve.

These observations might be explained if the methyl cyanide has not formed a definite structure on the zeolite surface within the cavity, or possibly if the structure adopted is expanded relative to the bulk structure so that hinderance to methyl group rotation is substantially reduced. At room temperatures rotation is essentially free, there is probably rapid translation of the sorbed molecules so that the inelastic spectrum is extensively broadened. (153). At 80°K the broadening is reduced though still detectable as a slightly increased width of the intramolecular modes, and in the presence of a broad peak at low energies attributed to the methyl group rotation in the sorbed layer.

7.3.2. Absorbed Dichloromethane

Table 7.3 summarises the data available on the mode frequencies of gas, liquid and solid dichloromethane. Davydov splittings are seen in the spectrum of solid CH_2CL_2 and transitions due to lattice modes are seen at 71, 95 and 113 cm^{-1}, though no assignments are given (154).

The beryllium filter spectrum of CH_2CL_2 at 80°K shows the expected intramolecular modes and the relative intensities reflect the amplitudes of motion of the hydrogen atoms in each of these modes viz

TABLE 7.3 Mode Frequencies of Dichloromethane

Assignment	Liquid		Crystal 77°K	
	IR cm^{-1}	RAMAN cm^{-1}	IR cm^{-1}	RAMAN cm^{-1}
Lattice Modes				71 95 113
ν_4 (A_1)		285	284 287 290.5	285
ν_3 (A_1)	707	701	681 684 687 699 702.5 704.5 707	701 706
ν_9 (B_2)	739	737	711 713 715 726 737 742 747	731 752
ν_7 (B_1)	896	896	888.5 893.4	
ν_5 (A_2)	1156	1153	1164	1162
ν_8 (B_2)	1265		1257.5 1259 1277	
ν_2 (A_1)	1426	1419	1404 1410	1409
ν_1 (A_1)	2986	2986	2983.5	2982
ν_6 (B_1)	3049	3048	3041.0 3053.5	3053

Mode Frequencies of Dichloromethane

measured by inelastic Neutron Scattering

BULK 80°K	ADSORBED 80°K	ASSIGNMENT
106 ± 5 187 ± 5	95 ± 5 142 ± 5	Lattice modes
285 ± 10	270 ± 7	ν_4 (A_1) CCL_2 scissors
720 ± 12	725 ± 15	ν_3 (A_1) & ν_9 (B_2) CCL_2 stretch
890 ± 15	890 ± 15	ν_7 (B_1) CH_2 rock

$$\nu_7(CH_2 \text{ rock}) > \left.\begin{matrix}\nu_3 \text{ sym} \\ \nu_9 \text{ asym}\end{matrix}\right\} CCL_2 \text{ stretch} > \nu_4 \; CCL_2 \text{ scissors}$$

A very intense peak is seen at 106 ± 5 cm^{-1} with a smaller peak at 187 cm^{-1}, probably the second harmonic of the first peak. It seems plausible that the transition arises from a methylene group torsion as this motion gives a large displacement to the hydrogen atoms.

When CH_2CL_2 is sorbed in La-Y at 80°K the intramolecular modes are again visible though noticeably broadened compared to the same transitions observed for the bulk sorbate. As in the case of methyl cyanide it is again the intermolecular modes which are more noticeably changed on sorption, though less so in the case of dichloromethane. A broad peak centred at 95 ± 5 cm^{-1} and a shoulder at 142 ± 5 cm^{-1} remains, suggesting that the environment of the CH_2CL_2 molecule is not dramatically changed on sorption. The peak considered to arise from a methylene torsion has shifted to a lower frequency, and the spectrum shows a universal increase in the width of the peaks, suggesting that barriers to rotation have diminished slightly, though not as much as in the case of sorbed methyl cyanide.

In conclusion the results indicate that when methyl cyanide is sorbed in La-Y zeolite, the sorbate-sorbent interaction is strong enough to overcome sorbate-sorbate interactions, and the 'structure' imposed on the sorbed layer by the surface is quite different to that of bulk methyl cyanide. Dichloromethane on the other hand has a weaker interaction with the surface and the 'structure' of the sorbed layer is only slightly perturbed from the structure of the bulk sorbate at that temperature. Such behaviour is not unexpected in view of the charge separation known to take place on the surface of molecular sieves.

7.4 The Sorption of Hydrogen and Methane on La-Y zeolite

The interactions of hydrogen and methane with La-Y zeolite are small and might be expected to be representative of physisorption on

zeolite surfaces. Beryllium filter spectra were recorded at 80°K and 298°K and the results are shown in figures 7.4 and 7.5. The spectrum of the sorbent has been subtracted in each instance. Accurate measurements of dosage could not be made with the apparatus used, but from the percentage scatter observed the concentrations of the sorbed gases was estimated to be between $\frac{1}{4}$ and $\frac{1}{2}$ cavity saturation.

Discussion

7.4.1 Sorption of Hydrogen

The hydrogen molecule does not have any intramolecular modes in the energy range scanned. The rotational transitions however, occur at intervals of 120 cm^{-1}, the large value of B a consequence of the small mass of the hydrogen atom. The J = 0→1 transition has been detected in the inelastic neutron spectra of both liquid and solid hydrogen (155).

The spectrum of sorbed hydrogen at 80°K does not show any sign of these rotational transitions. The reasons for this could be :-

1) The hydrogen molecule has been dissociatively absorbed to give a hydrogen atom bound to the lattice. In which case the lattice modes of the molecular sieve would be enhanced by the hydrogen amplitude weighting (28). There is no evidence of this in the spectrum obtained.

2) The hydrogen molecule has reacted at the surface to give surface hydroxyls or water. The newly formed species would be expected to give rise to characteristic transitions (eg. see section 6.2.2 for the beryllium filter spectrum of unoutgassed La-Y zeolite), and once again nothing is visible in the spectrum obtained.

3) The hydrogen molecule interacts so weakly with the zeolite surface that it maintains a high degree of translational motion in the physisorbed state. The scattering law for translational motion

FIGURE 7,4

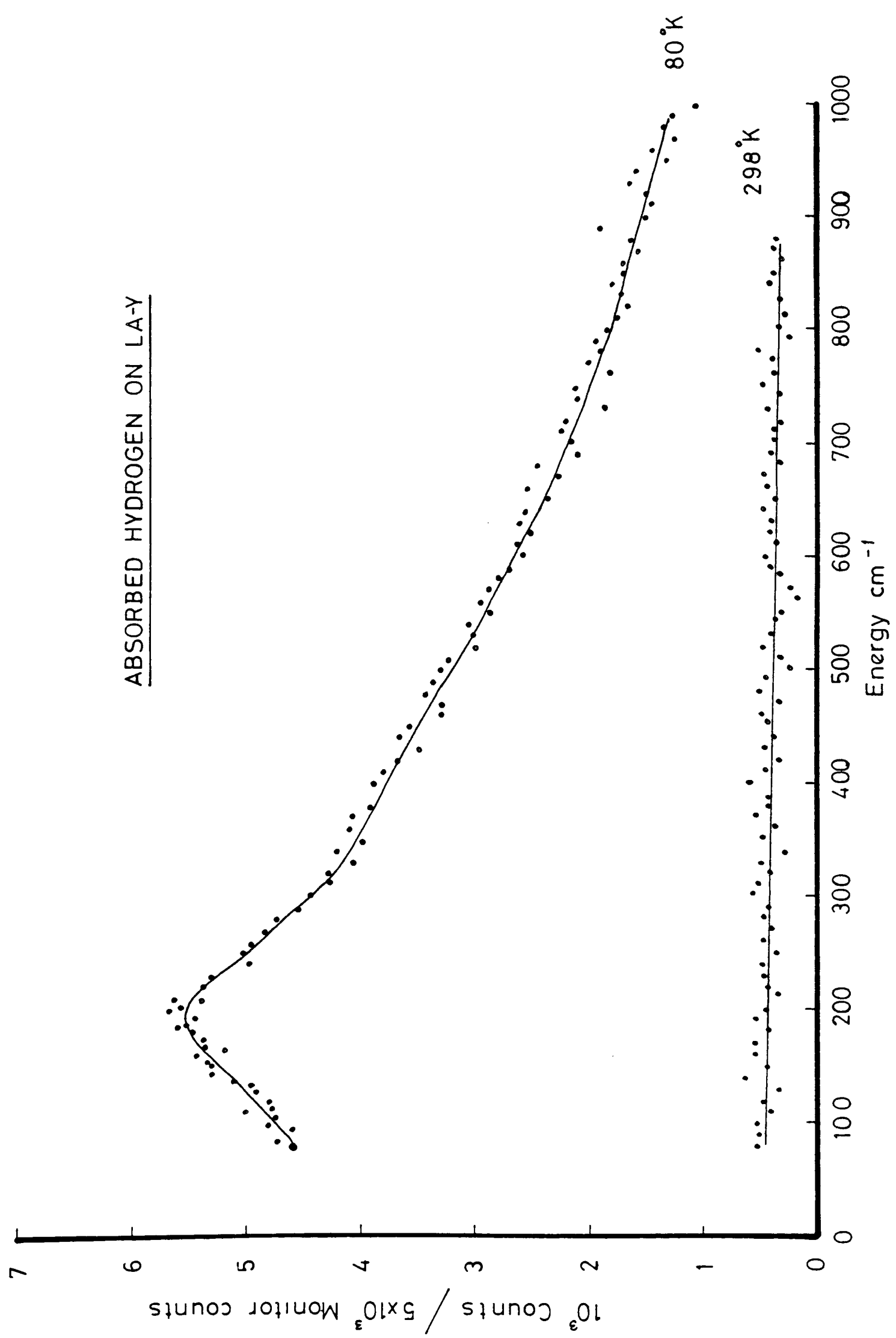
ABSORBED HYDROGEN ON LA-Y
80°K
298°K
10^3 Counts / $5x10^3$ Monitor counts
Energy cm^{-1}
0
1
2
3
4
5
6
7
100
200
300
400
500
600
700
800
900
1000

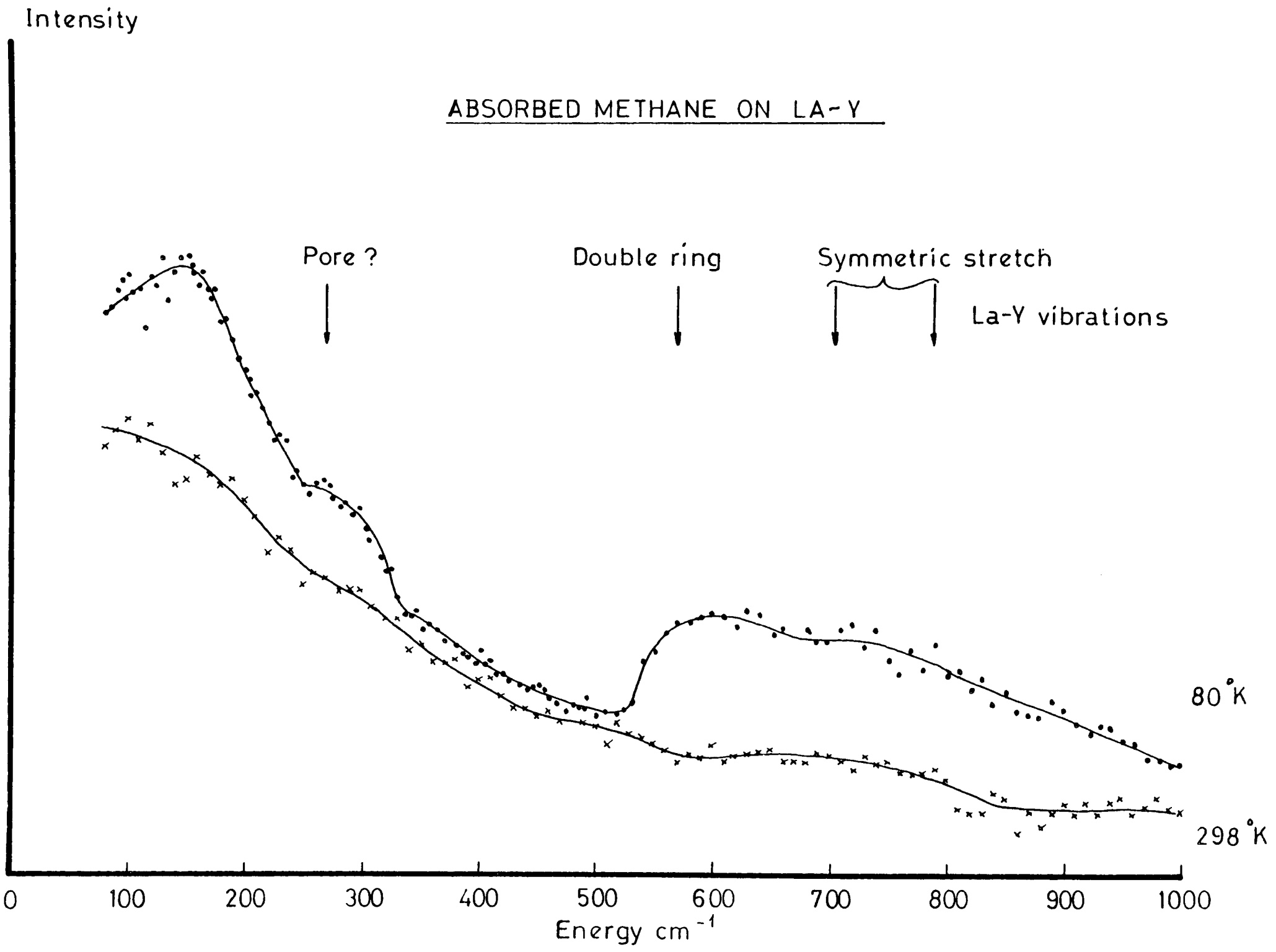
Intensity
ABSORBED METHANE ON LA-Y
Pore ?
Double ring
Symmetric stretch
La-Y vibrations
80 °K
298 °K
0
100
200
300
400
500
600
700
800
900
1000
Energy cm -1

FIGURE 7.5

FIGURE 7,6

ABSORBED GASES - Beryllium filter spectroscopy

Enhancement of intensity at low energies.

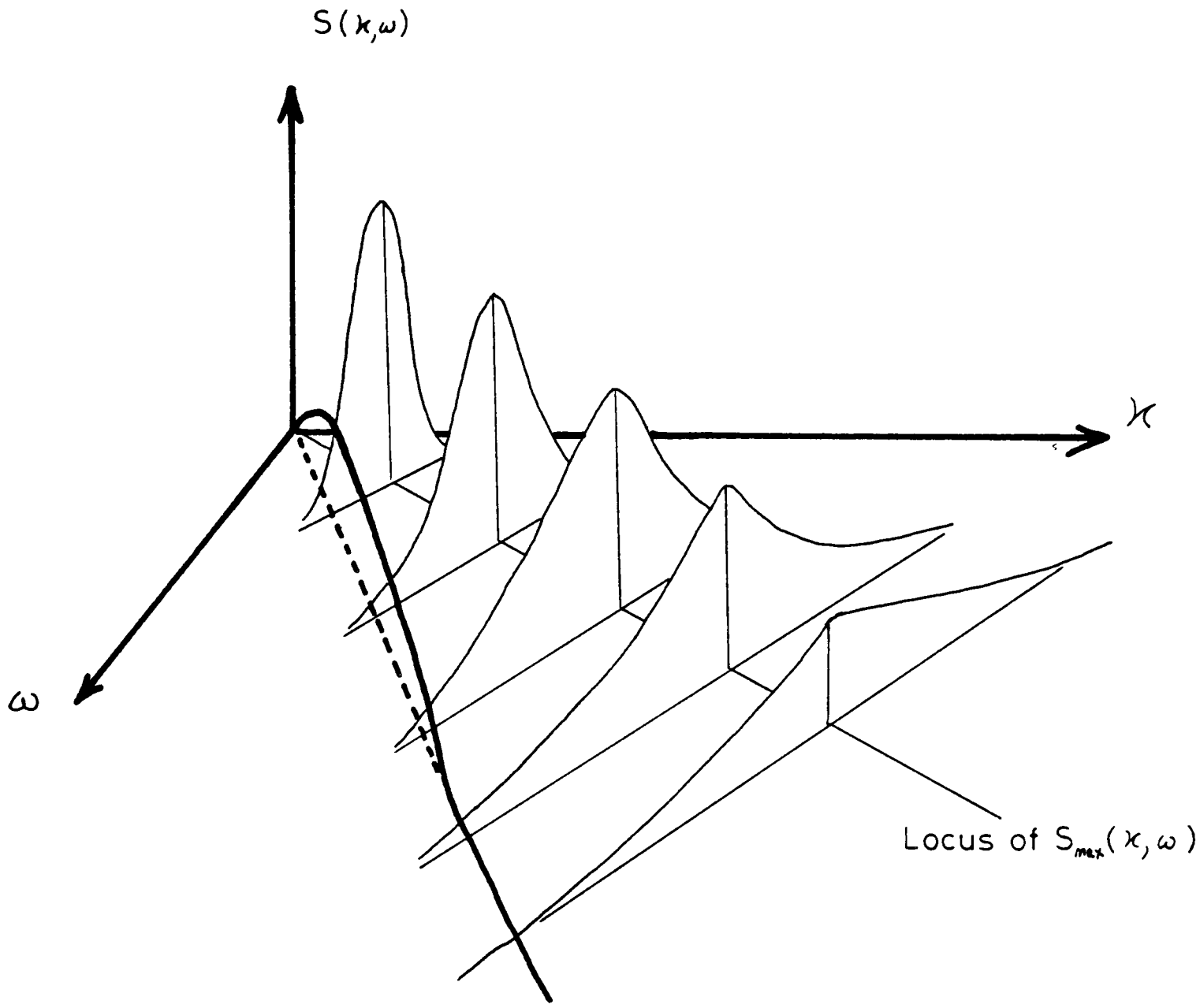

Cut taken by spectrometer

is thus very broad and when convoluted with the scattering law for the rotational degrees of freedom, the final scattering law is broad and featureless (see section 3.9.3).

Of these possibilities the presence of a physisorbed molecule with mobility seems the most likely. The observed spectrum at 80°K does show what appears to be a broad weak peak centred at about 200 cm^{-1} with a full width at half maximum of about 80 cm^{-1}. The most likely explanation for a "peak", in a system with high translational mobility, is that it is an artefact of the instrumental method.

The Beryllium Filter spectrometer takes a very close to straight cut through (κ^2,w) space (see section 4.2.2.)

$$\kappa^2 = \frac{2m}{\hbar^2} (E_i + E_f - 2\sqrt{E_i E_f} \cos\alpha) \qquad (7.1)$$

where $E_{i,f}$ are the incident and final neutron energies, $0<E_f<42$ cm^{-1} and α is the detector to sample angle, generally 90°.

Figure 7.6 shows the (κ^2,w) surface for a 3D and 2D gas with a mass of 16. For hydrogen, mass 2, the surface will be similar though the lighter mass will mean that the recoil of the scattering centre is greater and the peak maximum will move out into the inelastic region faster with κ^2. The peak will also broaden more rapidly with increasing κ^2.

Super position of the (κ^2,w) cut taken by the beryllium filter instrument upon the (κ^2,w) surface for hydrogen gas shows how a 'peak' might arise. Figure 7.6 shows this diagrammatically, the slope of the cut taken by the instrument is about $\frac{1}{2}$ that of the slope of the locus of the gas scattering peak maximum as the mass of the neutron is about $\frac{1}{2}$ that of the hydrogen molecule. An enhancement of intensity occurs at the lower energies when the instrument (κ^2,w) cut takes an oblique section through the intensity contours of the gas scattering.

Insufficient hydrogen is absorbed by the zeolite at 298°K for a spectrum to be detected.

7.4.2 The Sorption of Methane

As with hydrogen there are no intramolecular modes of methane within the energy range studied. The increased mass of the molecule reduces the energies of the rotational transitions and these occur at intervals of about 10 cm^{-1}. In the time of flight spectrum of absorbed methane, the rotational envelope of these transitions is clearly visible, (see section 6.2.2), but the maximum intensity of the envelope is at too low an energy to appear in the beryllium filter spectrum.

The spectrum of sorbed methane at 298°K shows a steady fall in scattered intensity with increasing energy. At this temperature one would expect that the absorbed molecule is performing fast translational motion on the surface, i.e. a 2D gas, and the broad scattering law for this motion is convoluted with the delta functions of the scattering law for rotational motions to produce the total scattering law as discussed in section 3.9.3. The greater mass of the methane molecule compared to the hydrogen molecule leads to less recoil during the scattering event than in the case of the hydrogen molecule. This observation taken in conjunction with the presence of a broad rotational envelope makes it unsurprising that the single cut through (κ^2,w) space by the instrument has produced such a featureless spectrum.

What is remarkable is that cooling the specimen down to 80°K produces an altogether different spectrum for the absorbed methane with evidence for discrete, though broad, transitions. The features are present on top of a spectrum similar to that of sorbed hydrogen at the same temperature, though the broad, low energy maximum now occurs at 150 cm^{-1} rather than 200 cm^{-1} as in the case of hydrogen. The conclusion is that the spectrum is composite and derives from two or more species on the surface of the zeolite, one of which is still physisorbed and behaving like a 2D gas, the other component deriving from localised methane or methane fragments.

Identification of the nature of the localised methane species is not possible from so few, broad transitions. However it is significant that the extra intensity occurs at energies associated with vibrations of the alumino silicate lattice measured by IR spectroscopy (156). The frequencies observed and their assignments are shown on the figure. It is suggested that the methane molecule has reacted at the surface to give strongly bound molecular fragments, and that the hydrogen atoms in the fragments are "riding" on the alumino silicate lattice vibrations. (28). The neutron scattering intensity of these modes is greatly enhanced as a consequence. The greater intensity of the transitions in the energy range 500-800 cm^{-1} would be due to these modes of vibration disturbing more hydrogen atoms than the pore breathing mode at 270-300 cm^{-1}.

7.5 Summary

Inelastic Neutron Spectroscopy has been shown to be an adequate qualitative tool for studying simple molecules absorbed on catalytic surfaces.

It has been used to show the presence of different surface species when formic acid is sorbed on γ-Al_2O_3 or La-Y zeolite. Whilst the changes in the spectrum certainly indicate different hydrogen bonding in the two systems, it is not possible to positively identify the presence of a formate anion on La-Y without further experiments.

Changes in intermolecular modes are detected when dichloromethane and methyl cyanide are absorbed on La-Y zeolite. A reduction in the hinderance to molecular rotations appears to be occurring on sorption relative to the bulk sorbate at the same temperature. This is not unequivocal as the observed peak broadenings could have their origin in the heterogeneity of the surface and a resulting distribution of torsion frequencies.

Little information is forthcoming from using the technique to

study the physisorption of hydrogen and methane on La-Y zeolite. It is remarkable however that methane appears to react with the zeolite at low temperatures yielding unidentifiable fragments strongly bound to the alumino silicate lattice.

The application of inelastic neutron spectroscopy to these studies is hampered by the low resolution, poor sensitivity and narrow energy window of the technique. With heterogenous catalyst surfaces one would anticipate a broad distribution of sorbate frequencies, producing, because of the low resolution, a broad spread of intensity over several tens of wave numbers which cannot be attributed to any specific mode. More success is likely to be achieved if catalysts with homogeneous surfaces are used as sorbents and extremely simple hydrogenous molecules such as H_2, $CHCl_3$ are absorbed thereupon.

REFERENCES

1 a) INFRA-RED SPECTROSCOPY
L H Little "Infrared Spectra of Adsorbed Molecules"
Academic Press 1966

b) RAMAN SPECTROSCOPY
P J Hendra p 80 "Chemisorption and Catalysis"
Ed. Hepple 1971

c) ELECTRON SPIN RESONANCE
B D Flockhart "ESR of Adsorbed Species"
ch. 3 of "Surface and Defect Properties of Solids" Vol 2

d) NUCLEAR MAGNETIC RESONANCE
H A Resing "NMR Relaxation of Molecules Adsorbed on Surfaces"
Adv. Mol. Relaxation Processes 1 109 (1967)

e) ULTRA VIOLET PHOTOELECTRON SPECTROSCOPY (UPS)
C R Brundle J. Vac. Sci. Tech. 11 212 (1974)

f) X-RAY PHOTOELECTRON SPECTROSCOPY (XPS)
C R Brundle J. Electron Spec. Relat. Phenom. 5 291 (1974)
G Ertl J Kuppers "Low Energy Electrons and Surface Chemistry"
Verlag Chemie Weinheim 1974

g) AUGER ELECTRON SPECTROSCOPY (AES)
C R Brundle Proc. Soc. Anal. Chem. 10 194 (1973)

h) SECONDARY ION MASS SPECTROMETRY (SIMS)
J M Morabito Proc. Symp. Mat. Sci. Aspects Thin Films
99 (1974) NITS Springfield Va.

i) LOW ENERGY ELECTRON DIFFRACTION (LEED)
R W Joyner G A Somorjai "Recent Trends in the Application
LEED" Ch. 1 of "Surface and Defect Properties of
Solids" Vol.2

j) ELECTRON MICROSCOPY
J Bagg H Jaeger J V Sanders J. Catalysis 2 449 (1963)

2 a) ADSORPTION ISOTHERM MEASUREMENT
"Solid Surfaces and the Gas Solid Interface"
Adv. Chem. Ser. 33

b) HEAT CAPACITY MEASUREMENTS
M Bretz J G Dash D C Hickernell E O McLean O E Vilches
Phys. Rev A 8 (3) 1589 (1973)

c) CHROMATOGRAPHY MEASUREMENTS
A V Kiselev Adv. Chromatog. 4 113 (1967)

3 C R Brundle A F Carley Chem. Phys. Lett. 31 423 (1975)

4 J E Demuth D E Eastman Phys. Rev. Lett 32 1123 (1974)

5 J J Lander J Morrison Sur. Sci 6 1 (1967)

6 P J Page D L Trimm P M Williams JCSFT (1) 70 1769 (1974)

7 "Monolayer and Submonolayer Films" Ed. J G Daunt E Lerner Plenum NY 1973

8 a) N D Mermin The Physical Review 176 (1) 250 (1968)

b) J G Dash M Bretz J Low Temp. Phys. 9 291 (1972)

9 a) Grafoil is the trademark of a product marketed by Union Carbide Products Division New York

b) S Ross Progr. Sur. Membrane Science 4 377 (1971)

10 A Thorny X Duval J. Chim. Phys. 67 1101 (1970)

11 a) R F Steiger J M Morabito G A Somorjai R H Muller Sur. Sci 14 274 (1969)

b) C Marti P Thorel Colloq. Int. Sur. Brest May 1975

12 J B Forsyth P J Brown "The Crystal Structure of Solids" 1974

13 J W White IAEA Conference Vienna 1972 p 315

14 T Springer "Quasi elastic Neutron Scattering for the Investigation of Diffusive Motions in Solids and Liquids" Springer Tracts in Modern Physics 64 (1972)

15 a) G A Somorjai H H Farrell Adv. Chem.Phys. 20 215 (1971)

b) M M Traum N V Smith F J Disalvo Phys. Rev. Lett 32 1241 (1974)

16 a) N Sheppard D J C Yates Proc.Roy.Soc. 238A 69 (1956)

b) P J Hendra J R Horder E J Loader J.Chem Soc A 1766 (1971)

17 K J Packer Prog. NMR. Spectroscopy Vol.3

18 R M Barrer T Gabor Proc.Roy.Soc. 256A 267 (1960)

19 J W White in "Chemical Applications of Neutron Scattering" ed B T M Willis OUP (1972)

20 B Feuerbacher M R Adriens Sur.Sci. 45 553 (1974)

21 L Genzel in "Excitations of Surfaces and Adsorbed Molecules" Farad. Div. Meeting July 1975 Oxford.

22 W Marshall S W Lovesey "Theory of Thermal Neutron Scattering" Clarendon Press, Oxford 1971

23 J K Kjerns L Passell H Taub J G Dash Phys. Rev. Lett. 32 724 (1974)

24 H Taub L Passell J K Kjerns K Carneiro J P McTague J G Dash Phys. Rev. Lett. 34 654 (1975)

25 M Nielsen in "Excitations of Surfaces and Adsorbed Molecules" Farad. Div. Meeting July 1975 Oxford

26 A Bourdon C Marti P Thorel *Phys. Rev. Lett. Awaiting publication.*

27 M Nielsen Ris Progress Report March 1975

28 a) R Stockmeyer KFA Jülich 1162 February 1975

b) R Stockmeyer H M Conrad A Renouprez P Fouillouz Sur. Sci. 49 549 (1975)

29 R E Ghosh R Stockmeyer in "Excitations of Surfaces and Adsorbed Molecules" Farad. Div. Meeting July 1975 Oxford

30 a) P A Egelstaff J S Downes J W White SCI Special Publication "Molecular Sieves" (1967) p 306

b) J S Downes J W White P A Egelstaff V Rainey Phys Rev Lett 17 542 (1966)

c) S Olejnik G C Stirling J W White Spec.Disc. Farad. Soc. No 1 (1970)

d) S Olejnik J W White Nature Phys. Sci. 236 15 (1972)

31 a) C J Wright in "Molecular Spectroscopy and Neutron Scattering" IOP/CS Meeting April 1975 Durham

b) C J Wright AERE MPD Research Reports September 1974

32 R G W Anderson DPhil Thesis Oxford 1974

33 S Todireanu Phys.Lett. 24A 544 1967

34 G Verdan Helv. Phys. Acta 41 533 1968

35 a) J H de Boer "The Dynamical Character of Adsorption" Clarendon Press Oxford (1953)

b) A Clark "The Theory of Adsorption" Academic Press New York (1970)

c) J H Thomas W J Thomas "An Introduction to the Principles of Heterogeneous Catalysis" Academic Press New York (1974)

36 F London Z Phys. Chem.B11 222 (1930)

37 a) A V Kiselev Adv.Chromat. 4 113 (1967)

b) A V Kiselev Disc. Farad. Soc. 40 205 (1965)

38 W A Steele R Karl J. Coll. Int. Sci. 28 397 (1968)

39 A L Myers J M Prausnitz Trans. Farad. Soc. 61 755 (1965)

40 a) Y Nardon Y Larher Sur. Sci. 42 299 (1974)

b) Y Larher J.Coll.Int.Sci. 37 836 (1971)

c) Y Larher CEN Saclay (1973) CEA-N-1574

d) Y Nardon CEN Saclay (1971) CEA-R-4089

41 a) J W Riehl K Koch J.Chem.Phys. 57 2199 (1972)

b) J W Riehl C J Fisher J.Chem.Phys. 59 4336 (1973)

42 J K Thompson J J Krebs H A Resing J.Chem.Phys. 43 3853 (1965)

43 a) D E Woessner J.Chem.Phys. 39 2783 (1963)

b) V E Kvlividze Dokl.Akad.Nauk. SSSR 157 158 (1964)

44 D E Woessner J. Phys.Chem. 70 1217 (1966)

45 H A Resing J K Thompson J.Chem.Phys. 46 2786 (1967)

46 a) Q R Stottlemeyer G R Murray J G Aston
J.Am.Chem.Soc. 82 1284 (1960)

b) J G Aston H W Bernard J.Am.Chem.Soc. 85 1573 (1963)

47 N N Avgul A V Kiselev Chem.Phys.Carbon 6 1 (1970)

48 S Ross J P Oliver "On Physical Adsorption"
Interscience 1964

49 M M Dubinin B P Bering V P Serpinskii
Prog.Sur.Sci. 2 1 (1964)

50 J Mahanty B Ninham JCS FT (II) 70 637 (1974)

51 C H Anderson E S Sabisky Phys. Rev. Lett. 24 1049 (1970)

52 R M Barrer Proc. Roy. Soc. 161A 476 (1937)

53 N N Avgul I A Lygina A V Kiselev Trans. Farad. Soc. 59 2113
(1963)

54 a) J G Kirkwood Phys.Z. 33 57 (1932)

b) A Müller Proc. Roy. Soc. 154A 624 (1936)

55 A D Crowell R B Steele J.Chem.Phys. 34 1347 (1961)

56 N N Avgul A V Kiselev I A Lygina
Bull. Acad. Sci. USSR Div.Chem.Sci. 1264 1271 (1962)

57 P H Gamlen O U Neutron Scattering Group Program Suite
Users Handbook (1973)

58 A I Kitaigorodskii K V Mirskaya
Sov. Phys. Cryst. 6 409 (1961)
Sov. Phys. Cryst. 9 137 (1964)

59 D E Williams J.Chem.Phys. 43 4424 (1965)
J.Chem.Phys. 45 3770 (1966)
J.Chem.Phys. 47 4680 (1967)

60 a) G S Pawley Phys. Stat. Sol. 20 347 (1967)

b) G S Pawley E A Yeats Sol. Stat. Comm. 7 385 (1969)

61 J O Hirschfelder C F Curtiss R B Bird
"Molecular Theory of Gases and Liquids" Wiley (1954)

62 P A Reynolds DPhil Thesis Oxford 1972

63 J F Twistleton J W White "Chemistry of the Organic
Solid State" Third Int. Symp. Glasgow September 1972

64 a) J K Kjerms P A Reynolds J W White
IAEA Conference Grenoble 1972 p 195

b) P A Reynolds J K Kjerms J W White J.Chem.Phys. 60 824 (1974)

65 M Lal D Spencer JCS FT (II) 910 (1974)

66 G E Bacon Acta Cryst 5 492 (1952)

67 J F Twistleton DPhil Thesis Oxford 1974

68 R K Thomas Phys.Chem.Lab. Oxford Private Communication

69 a) W Press A Huller H Stiller W Stirling R Currat
Phys. Rev. Lett. 32 1354 (1974)

b) W Press A Kollmar KFA Jühlich Private Communication

70 A G Bezus A V Kiselev V P Dreving
Zh.Fiz.Khim 38 947 (1964)

71 G Constabaris J R Sams G D Halsey
J. Phys. Chem. 65 367 (1961)

72 a) W Marshall S W Lovesey "Theory of Thermal Neutron Scattering"
Clarendon Press Oxford 1971

b) I I Gurevich L V Tarasov "Low Energy Neutron Physics"
North Holland 1968

c) "Chemical Applications of Neutron Scattering" Ed. B T M Willis
OUP 1972

d) G Allen J S Higgins Rep.Prog.Phys. 36 (9) 1073 (1973)

73 L Van Hove Phys.Rev. 95 249 (1954)
Physica 24 404 (1958)

74 For example see E Merzbacher "Quantum Mechanics"
Wiley 1970

75 For example see ref 22

76 G W Griffing Phys. Rev 124 1489 (1961)

77 F J Webb Proc. Phys. Soc. 89 379 (1966)
92 912 (1967)

78 B A Dasannacharya G Venkataraman Phys. Rev 156 196 (1967)

79 A K Agrawal S Yip J.Chem.Phys. 46 1999 (1967)

80 V F Sears Canad. J. Phys. 45 237 (1967)

81 "Thermal Neutron Scattering" Ed. P A Egelstaff Academic Press 1965

82 R E Ghosh "Computer Programs for Analysis of Neutron Time of Flight Data" AERE - USS/P19 July 1971

83 a) B K Aldred D. Phil. Thesis Oxford 1971

b) N F Hall O U Neutron Scattering Group Program Suite Users Handbook (1973)

84 A J Leadbetter F P Temme A Heidemann W S Howells
Chem. Phys. Lett. 34 363 (1975)

85 A J Dianoux F Volino H Hervet
Mol. Phys. 30 1181 (1975)

86 K Sköld G Nelin J. Phys. Chem. Solids 28 2369 (1967)

87 a) H Kapulla W Gläser IAEA Conference Grenoble 1974 p 841

b) See reference 69 a)

88 C L Thaper B A Dassannacharya P S Goyal
Pramana 2 148 (1974)

89 P S Goyal B A Dasannacharya C L Thaper P K Iyengar
Proc.Nuc.Phys.Sol.Stat.Phys.Symp. V3 457 (1970)

90 B A Dasannacharya C L Thaper P S Goyal
IAEA Conference Vienna 1972 p 477

91 A G Bezus V P Dreving A V Kiselev
Russ. J.Phys.Chem 38 511 (1964)

92 M B M Harryman J B Hayter AERE-USS/P23 October 1972

93 C T Chudley R J Elliott Proc.Phys.Soc.77 353 (1961)

94 W Gissler H Rother Physica 50 380 (1970)

95 K S Singwi A Sjölander Phys. Rev. 126 986 (1962)

96 G E Bacon "Neutron Diffraction" OUP

97 F A Wedgewood AERE R5802 1968

98 "Neutron Beam Facilities Available for University Users at AERE Harwell and AWRE Aldermaston" Science Research Council 1973

99 P Convert ILL Internal Report on DIB

100 W Schmatz T Springer J Schelten K Ibel
J.Appl.Cryst 7 96 (1974)

101 K Ibel ILL Internal Report on D11

102 E B Wilson J C Decius P C Cross "Molecular Vibrations" 1955

103 P H Gamlen N F Hall A D Taylor AERE-USS/P29 September 1974

104 M F Collins B C Haywood G C Stirling
J.Chem.Phys. 52 1828 (1970)

105 J R D Copley S Lovesey Rep.Prog.Phys. 38 (4) 451 (1975)

106 L J Bunce D H C Harris G C Stirling AERE R6246 (1970)

107 a) M F Collins B C Haywood J.Chem.Phys. 52 5740 (1970)

b) B C Haywood M F Collins R D Lowde AERE PR/MPD/1 (1970)

108 S H Chen S Yip "Neutron Scattering In Chemistry"
NSF Symposium MIT May 1975

109 J J Rush Crit.Eval.Chem.Phys.Structure Inf. (1974) NAS

110 C Carlile Rutherford High Energy Laboratory RL-74-103 (1974)

111 J Tudor Davies J M Vaughan
Astrophysics Journal 137 1302 (1963)

112 M B M Harryman J B Hayter OU Neutron Scattering Group
Program Suite Users Handbook 1973

113 A D Taylor DPhil Thesis Oxford 1976

114 A G Dianoux R E Ghosh C H Hervet R E Lechner
ILL-ITR 75D16T

115 P N Brier J S Higgins IAEA Conference Grenoble 1972

116 M W Johnson AERE R7682 March 1974

117 a) T Trewern Part II Thesis Oxford 1975

b) S Raddats Part II Thesis Oxford 1975

c) A D Taylor R K Thomas T Trewern J W White Awaiting
publication

118 a) A J Leadbetter M W Stringfellow IAEA Conference Grenoble 1972

b) See also reference 103

119 P H Gamlen Part II Thesis Oxford 1972

120 R A Beebe J Biscoe W R Smith G B Wendell
J.Am.Chem.Soc. 69 95 (1947)

121 Sample of Graphon obtained from The School of Chemistry, Bristol University. Provided by R Brown

122 a) A G Bezus V P Dreving A V Kiselev
Russ. J. Phys. Chem. 38 1589 (1964)

b) A G Bezus V P Dreving A V Kiselev
Russ. J. Phys. Chem. 41 1568 (1967)

123 a) See reference 122 b)

b) A G Bezus V P Dreving A V Kiselev
Russ. J. Phys. Chem. 38 511 (1964)

124 a) R A Beebe A V Kiselev N B Kovaleva R F S Tyson J M Holmes
Russ. J. Phys. Chem. 38 372 (1964)

b) R A Beebe A V Kiselev N B Kovaleva J M Holmes M E R Camplin
Russ. J. Phys . Chem. 38 506 (1964)

125 Handbook of Chemistry and Physics 54th Edition 1973-74
CRC Press

126 P H Gamlen J W White JSC FT (II) 72 446 (1976)

127 Use of Sartorius 1400 microbalance kindly provided by Chemistry Division, AERE Harwell. Acknowledgements to A J Tench, J Kibblewhite and J Winter for assistance

128 a) R A Beebe J Biscoe W R Smith C B Wendell
J. Am. Chem.Soc. 69 95 (1947)

b) M H Polley W D Schaeffer W R Smith
J.Phys.Chem 57 469 (1953)

129 J Biscoe B E Warren J.App.Phys. 13 364 (1942)

130 A Guinier G Fournet "Small Angle Scattering of X-Rays"
Wiley (1955)

131 D Graham W S Kay J.Coll.Sci 16 182 (1961)

132 a) See reference 103

b) D K Ross J.Phys.C(Sol.Stat.Phys) 6 3525 (1973)

133 G Dolling B N Brockhouse Phys.Rev. 128 1120 (1962)

134 J A Young J U Koppel J.Chem.Phys. 42 357 (1965)

135 R Nicklow N Wakabayashi H G Smith
Phys. Rev. 5 4951 (1972)

136 a) P A Egelstaff S J Cocking IAEA Conference Vienna 1960 p 569

b) B C Haywood I M Thorsen IAEA Conference Chalk River 1962 p 111

c) D I Page IAEA Conference Copenhagen 1968 p 325

d) P A Egelstaff D H C Harris Phys. Lett. 7 220 (1963)

137 D W McCall D C Douglas E W Anderson
Phys. Fluids 4 1317 (1961)

138 R Ash R M Barrer R T Lowson Trans. Farad. Soc. 69 2166 (1973)

139 A S Pine C J Glassbrenner G Dresselhaus
Phonons Proc. Int. Conf. (1971) p 258

140 a) D W Breck "Zeolite Molecular Sieves, Chemistry and Use"
Wiley

b) R M Barrer in "Non Stoichiometric Compounds"
Ed. L. Mandlecorn.

c) "Molecular Sieve Zeolites" Adv. Chem.Series 101 and 102 (1971)

141 "Molecular Sieves" Adv.Chem.Series 121 (1973)

142 D W Breck J.Chem.Ed. 41 (12) 678 (1964)

143 J M Bennett J V Smith
Mat. Res. Bull. 3 633 (1968)
Mat. Res. Bull. 3 865 (1968)
Mat. Res. Bull. 3 933 (1968)
Mat. Res. Bull. 4 7 (1969)

144 a) C L Angell J.Phys.Chem. 77 222 (1973)

b) See reference 140 c)

145 a) A Cabana G B Savitsky D F Hornig
J. Chem. Phys. 39 2942 (1963)

b) P Eder P A Egelstaff IAEA Conference Copenhagen 1968 p 223

c) P Eder S H Chen P A Egelstaff Proc. Phys. Soc. 89 833 (1966)

146 H F Leftin M C Robson Adv. Catal. 14 115 (1963)

147 P J Hendra J R Horder E J Loader J.Chem. Soc A 1766 (1971)

148 K Hirota K Fueki T Sakai
Bull. Chem. Soc. Japan 35 1545 (1962)

149 K Hirota K Fueki K Shindo Y Nakai
Bull. Chem. Soc. Japan 32 1261 (1959)

150 P Mars J J F Scholten P Zwietering
"Advances in Catalysis" 14 35 (1963)

151 M F Collins B C Haywood J.Chem.Phys. 52 5740 (1970)

152 E L Pace L J Noe J.Chem.Phys. 49 5317 (1968)

153 A N Brown J W White Spectrochimica Acta 30A 1665 (1974)

154 M P Mazoocchi P Manzelli J.Chem.Phys. 52 2630 (1970)

155 P A Egelstaff B C Haywood F J Webb
Proc. Phys. Soc. 90 681 (1967)

156 Flanigen Grose Article 16 in "Molecular Sieve Zeolites"
Adv. Chem.Series 101 (1971)

157 L M Sverdlov M A Kovner E P Krainov
"Vibrational Spectra of Polyatomic Molecules"
Halsted Press

158 R J Jakorsen Spectrochimica Acta 23A 2199 (1967)

159 C V Berney NSF Conference March 1975 MIT
"Neutrons in Chemistry"

160 A V Kiselev D P Poshkus Russ. J. Phys. Chem. 39 204 (1965)

161 P R Bevington "Data Reduction and Error Analysis in the
Physical Sciences"
McGraw-Hill 1969

ABSTRACT

The advantages and limitations of applying cold neutron scattering to the study of sorbed molecules are presented. Although restricted by the lack of surface sensitivity to high surface area sorbents and hydrogenous sorbates the method is capable of providing information about three important aspects of the gas/solid interface.

1) Determination of the structure of the sorbed layer by neutron diffraction

2) Measurement of the extent and nature of rotational and translational freedom possessed by the sorbed molecule, from the quasi elastic scattering

3) Determination of the frequency of sorbate vibrations with respect to the sorbent surface by inelastic neutron scattering.

An atom-atom pair calculation has been carried out to determine the interaction energy of a single methane and a single hydrogen molecule with a graphite basal plane. The most energetically favourable position for a methane molecule is found to be a stable tripod position at a centre to centre distance of 3.30 $\mathring{A}$ above the centre of a surface carbon hexagon. The energy of interaction is calculated to be -2.97 kcals/mole, the force constant of the sorbate-sorbent bond 7.39×10^3 dynes cm^{-1}. The hydrogen molecule achieves a maximum interaction with the surface with the long axis of the molecule parallel to the surface at a centre to centre distance of 2.9 $\mathring{A}$ above the centre of a surface carbon hexagon. The energy of interaction is calculated to be -1.11 kcals/mole, the force constant of the sorbate-sorbent bond 3.17×10^3 dynes cm^{-1}, and the sorbate-sorbent perpendicular vibration frequency 163 cm^{-1}.

Barriers to rotation of the methane and hydrogen molecules about axes parallel and perpendicular to the surface were calculated At the temperatures at which the neutron scattering experiments were performed the rotations of the molecules are expected to be

unhindered by the periodicity of the surface adsorption potential.

With this information simple scattering laws for two dimensional gaseous, liquid and solid phases are established. The two dimensional scattering laws are then averaged over three dimensions so as to be applicable to the dynamics of an admolecule on a powdered adsorbent. The final scattering laws produced are sharply peaked at w = o, because of the inability of the admolecule to recoil through the sorbent surface during the scattering event.

Neutron time of flight spectra are presented for simple molecules adsorbed on 'Graphon', a graphitised carbon black with a surface area of 86 m^2g^{-1} and a well characterised homogeneous surface.

i) Adsorbed methane in the temperature range 115°K to 176°K and surface coverages of 0.58 to 0.23

ii) Adsorbed ethylene in the temperature range 175°K to 235°K and surface coverages of 2.1 to 0.8

iii) Adsorbed ammonia in the temperature range 145°K to 261°K and surface coverages of 1.54 to 0.23

At low temperatures and high surface coverages adsorbed methane appears to be in the form of a two dimensional liquid with a measured diffusion coefficient of $3 \pm 0.5 \times 10^{-5} cm^2 s^{-1}$. Above 140°K the fit of the model to the data is inadequate and it appears that some kind of an expanded liquid is formed. The spectra of the adsorbed methane is not gas like even at 176°K.

Ethylene, in constrast, is two dimensional liquid like at high temperatures with a diffusion coefficient of $5 \pm 0.5 \times 10^{-5} cm^2 s^{-1}$. There is apparently little change in the diffusion coefficient with temperature. Decreasing temperatures produce progressively poorer fits of the data to the predictions of the two dimensional liquid model. Multilayer formation and stronger lateral interactions for adsorbed ethylene will lead to restricted rotations and translations of the sorbate molecule, and could be responsible for the deviations

from the predicted behaviour of the scattering law.

The observed scattering law for ammonia on 'Graphon' is in disagreement with scattering laws predicted for two dimensional phases. The results are Voigt profiles such as would be expected for a three dimensional liquid. Diffusion coefficients determined from the deconvoluted data range from $1.77 \pm 0.06 \times 10^{-5} cm^2 s^{-1}$ at 199^oK to $7.09 \pm 0.09 \times 10^{-5} cm^2 s^{-1}$ at 254^oK and give an activation energy for diffusion of 2.4 kcals/mole. It appears from these results that the sorbed ammonia molecules have not spread uniformly over the available carbon surface, but rather have clustered into three dimensional islands of liquid bulk ammonia, a consequence of the strong sorbate-sorbate dipolar interactions. At low temperatures the islands of bulk ammonia freeze to give solid ammonia crystallites. These are identified from their inelastic neutron spectrum at low temperatures.

The adsorption surfaces of 'Graphon' are wholly exterior but with molecular sieves sorption takes place on the interior surfaces of pores and this can have a profound effect on the translational and rotational freedom of the adsorbed molecule. Time of flight spectra were measured for methane absorbed in a lanthanum exchanged Y-type zeolite over the temperature range $160-245^oK$ when the number of methane molecules in the cavity varied from about 1.4 to about 0.6. The spectra show that the methane molecule has no or very little translational motion,but the molecular rotations are unhindered, and it suggests that the molecule is trapped in a cavity. A vibration frequency of $19 \pm 1 cm^{-1}$ is observed and this is ascribed to a vibration of the methane molecule within the cavity.

The absorption of simple molecules on catalytically active surfaces was investigated with beryllium filter spectroscopy. La-Y zeolite and γ alumina are found to sorb formic acid in different

forms. On γ alumina bulk polymeric formic acid is present, whilst an unidentifiable form, possibly a formate anion, exists on the La-Y surface.

The spectra obtained on the absorption of methyl cyanide and dichloromethane on La-Y zeolite demonstrate how the sorbate structure adopted is modified relative to the bulk phase. Methyl cyanide significantly, dichloromethane less so, reflecting the stronger interaction of the former molecule with the zeolite surface. A gain in rotational freedom takes place on sorption in both instances.

Absorbed hydrogen is shown to retain high, gas like mobility at temperatures from 298°K to 80°K and similar behaviour is observed for absorbed methane at 298°K. At 80°K however, the spectrum suggests that the methane has reacted with the surface to give bound molecular fragments, so that the spectrum obtained is a reflection of the absorbent density of states, enhanced by the hydrogen nuclei localised on the alumino silicate lattice.

ACKNOWLEDGEMENTS

It is with pleasure that I take this opportunity to acknowledge the assistance that a great many people have been kind enough to render me. Some help was of the hard, technical kind, some of a more philosophical character, yet both equally necessary to ensure the production of this thesis.

I have been fortunate to have Dr J W White for my supervisor. A believer in the value of Research for academic, cultural and personal development, he has been kind enough to provide me with opportunities to pursue all three aspects. His enthusiasm, drive and creativity have been an encouragement at all times. The hospitality of John and his wife, Ailsa, when I was doing experiments during unsociable hours in France and England, was generously given and is greatly appreciated. I am much in their debt.

The staff at AERE Harwell and the ILL, Grenoble, were most helpful in the provision of instrument time, laboratory and computing facilities. I wish to express my thanks to D H C Harris (University Support Group), G E Haines (DIDO Time of Flight Instruments) and J Milne (PLUTO Beryllium Filter Spectrometer). At the ILL the assistance of K Ibel (DII), P Convert (DIB) and G Stirling (Chemistry College) ensured that experiments ran smoothly.

The Oxford Neutron Scattering Group were always a source of stimulating discussion, informative comment and practical help. In particular I am indebted to Bob Thomas for reading the drafts of this thesis, and his comments and guidance are appreciated. John Hayter, Andrew Taylor, Martin Anderson, Nigel Hall, Graham Jenkin, Mike Mortimer and Mike Harriman are members of the Group who at one time or another have given more than a passing thought to the study of adsorbed molecules by neutron scattering. For those thoughts, thanks.

For assistance of a less technical nature I am firstly most grateful to St Johns College for supporting me with a Scholarship. Secondly it gives me much pleasure to acknowledge the assistance of many friends, in particular Neville Richardson, Jo Timmins, Ian and Mary Elson, and Val Heath.

The production of my thesis has been in the hands of Jane Waghorn and her work is greatly appreciated.